The Role of Glycolipids at the Interface of Plant-Microbe Interactions during Nodulation and Mycorrhiza Formation in *Lotus japonicus*

Dissertation

zur
Erlangung des Doktorgrades (Dr. rer. nat.)
der
Mathematisch-Naturwissenschaftlichen Fakultät
der
Rheinischen Friedrich-Wilhelms-Universität Bonn

vorgelegt von

Vera Wewer
aus
Essen

Bonn, Juli 2012

Angefertigt mit Genehmigung der Mathematisch-Naturwissenschaftlichen Fakultät der Rheinischen Friedrich-Wilhelms-Universität Bonn

1. Gutachter: Prof. Dr. Peter Dörmann

2. Gutachter: Prof. Dr. Lukas Schreiber

Tag der Promotion:

Erscheinungsjahr:

Table of Contents

Table of Figures

Abbreviations

ddH_20	double deionized water
DNA	deoxyribonucleic acid
dpi	days post infection
EDTA	ethylenediaminetetraacetic acid
e. g.	lat.: *exempli gratia* = for example
ER	endoplasmic reticulum
et al.	lat.: *et alii* = and others
FAME	fatty acid methyl ester
Fig	figure
FW	fresh weight
g	standard gravity (g = 9.81 m s^{-2})
Gal	galactose
GC FID	gas chromatograph with flame ionization detector
GC MS	gas chromatograph with mass spectrometer
GCS	glucosylceramide synthase
Glc	glucose
hrs	hours
HPLC	high pressure liquid chromatography
LB	lysogeny broth
min	minute
mol%	molar percentage
MS/MS	tandem mass spectrometry
m/z	mass to charge ratio
OD_{600}	optical density at a wavelength of 600 nm
oe	overexpression
OPA	o*rtho*-phthaldialdehyde
PCR	polymerase chain reaction
PBM	peribacteroid membrane
ppm	parts per million
Q-TOF MS	quadrupole time-of-flight mass spectrometer
RNA	ribonucleic acid
RNAi	RNA interference
RT	room temperature
RT-PCR	reverse transcriptase polymerase chain reaction
sec	second
SGT	sterol glucosyl transferase
sn	stereospecific numbering
SPE	solid phase extraction
TBE	Tris-boric acid-EDTA
TE	Tris-EDTA
TLC	thin layer chromatography
TY	tryptone yeast
UV	ultra violet
WT	wild type
YNB	yeast nitrogen base
% (v/v)	percent volume per volume (mL per 100 mL)
% (w/v)	percent weight per volume (g per 100 mL)

Abbreviations for Lipids

ASG	acylated sterol glucoside
Cer	ceramide
cFA	non-hydroxylated fatty acid
DAG	diacylglycerol
DGDG	digalactosyldiacylglycerol
FA	fatty acid
FS	free sterol
GIPC	glycosylinositolphosphorylceramide
GlcCer	glucosylceramide
hFA	hydroxylated fatty acid
MGDG	monogalactosyldiacylglycerol
LCB	long chain base
PA	phosphatidic acid
PC	phosphatidylcholine
PE	phosphatidylethanolamine
PS	phosphatidylserine
SG	sterol glucoside
SE	sterol ester
SQDG	sulfoquinovosyldiacylglycerol
TAG	triacylglycerol

Fatty acids are abbreviated X:Y, where X represents the number of carbon atoms, and Y represents the number of double bonds.

Sphingolipids are abbreviated dX:Y-x:y or tX:Y-x:y, where X represents the number of carbon atoms, Y represents the number of double bonds in the long chain base, x represents the number of carbon atoms, and Y represents the number of double bonds in the acyl chain. The prefix “d” or “t” depicts the degree of hydroxylation of the long chain base with two (d, dihydroxy) or three (t, trihydroxy) hydroxyl groups.

Note that β-sitosterol is abbreviated as sitosterol throughout the text.

1 Introduction

1.1 Lipids and Lipid Biosynthesis

Lipids show a great variety in their molecular structure and function. While exact definitions of the term can vary, there is a consensus on lipids being hydrophobic or amphipatic small molecules, which are derived from fatty acids or related compounds (Fahy *et al.*, 2005). This includes sterol lipids and other isoprenoid lipids, which unlike most lipids do not contain fatty acids but whose molecular structure is based on the condensation of isoprene units.

Plant lipids fulfill a diversity of functions, the most prominent ones being membrane formation and energy storage. Nonpolar lipids such as triacylglycerol (TAG) are a major form of energy and carbon storage. TAG is constituted of a glycerol backbone which is esterified to fatty acids at positions sn1 to sn3 and therefore does not contain any polar moieties. Due to this nonpolar nature, TAG does not localize to membranes, but accumulates in the cytosol in so-called oil bodies (oleosomes), where it is presumed to be associated with other non-polar lipids such as sterol esters (Kemp and Mercer, 1968; Zinser *et al.*, 1993). TAG as a source of carbon and energy storage accumulates during embryo development, where it constitutes the energy reserves required for subsequent germination of the seedling.

Amphipatic lipid molecules are required for the constitution of plant membranes. These lipids contain a hydrophobic tail and a hydrophilic head group, conferring the ability to spontaneously form lipid bilayers. There are three major lipid groups of different molecular structures in plants which can meet these requirements and are hence termed membrane lipids. The largest group is constituted by the glycerolipids. These are derived from a glycerol molecule, which is substituted with fatty acids at positions sn 1 and sn 2 and with a variety of polar head groups at sn 3. Depending on the structure of the head group, glycerolipids can be organized into phosphoglycerolipids, carrying phosphate containing head groups (e.g. phosphatidylcholine (PC), phosphatidylethanolamine (PE), phosphatidylinositol (PI) and phosphatigylglycerol (PG)) and glycoglycerolipids with sugar containing head groups (monogalactosyldiacylglcerol (MGDG), digalactosyldiacylglycerol (DGDG) and sulfoquinovosyldiacylglycerol (SQDG)). While the phosphoglycerolipids are mainly localized to the extraplastidial membranes, with the exception of PG, the glycoglycerolipids represent the most abundant constituents of the chloroplast membranes (Joyard *et al.*, 1994; Benning and Ohta, 2005).

In contrast to glycerolipids, sphingolipids do not contain glycerol but a long chain base (LCB) bound via an amide bond to a fatty acid, which is generally hydroxylated. This ceramide backbone may be substituted with a sugar moiety to form glycosylceramide. Glucosylinositolphosphorylceramides (GIPCs) are very complex sphingolipids, which can carry a large number of different substitutions containing sugar alcohols or sugar moieties bound to

phosphate. Sphingolipids can be found in extraplastidial membranes, such as the plasma membrane, the tonoplast, Golgi membranes and the ER (Markham *et al.*, 2006).

The third group of membrane lipids comprises the sterol lipids. There are three classes of sterol lipids in plant membranes, i.e. free sterols (FSs) containing a free hydroxyl group at C3, as well as conjugated sterols carrying a glucose residue at C3, which are called sterol glucosides (SGs). SGs can be further modified to form acylated sterol glucosides (ASGs), which are acylated at the C6 of the sugar residue. Another conjugated sterol lipid class, the sterol esters which are substituted with an acyl chain at C3, does not participate in membrane formation for lack of a polar head group.

While membrane formation and energy storage are very prominent examples of lipid functions in plants, there are a number of other processes in which various lipid classes are involved. For example, lipid molecules such as lyso-PC, PIP_2 and DAG serve as signaling molecules during various physiological processes (Meijer and Munnik, 2003; Drissner *et al.*, 2007). Furthermore, plant lipids can fulfill functions as pigments in photosynthesis (carotenoids, chlorophyll), as antioxidants (tocopherol), phytohormones (jasmonic acid), electron carriers (ubiquinone, plastoquinone, phylloquinone) or are involved in the formation of barriers against the environment, covering leaf and root surfaces (cutin, suberin, waxes).

1.1.1 Membrane Remodeling in Response to Phosphate Limitation

Within plant membranes, lipids do not only constitute mere building blocks, they are also involved in specific functions e.g. the activation of proteins by lipid-protein interactions. It is widely acknowledged that the lipid composition of membranes is closely related to their physiological function. Therefore, the lipid distribution varies greatly among the different intracellular membranes. For example, the galactolipid MGDG, which is absent from extraplastidial membranes, is abundant in the thylakoid membrane, where it plays a vital role in photosynthesis (Páli *et al.*, 2003; Botté *et al.*, 2005). Plants can also modify their membrane lipid constitution in response to biotic or abiotic stress. For example, unsaturated fatty acids are known to confer higher membrane fluidity than saturated fatty acids and therefore accumulate in membranes during cold acclimation.

Moreover, a very severe remodeling of the plasma membrane in response to abiotic stress can be observed during phosphate deprivation. Phosphate, next to nitrogen, is one of the most important macronutrients and often represents a growth limiting factor for plants (Abel, 2011). It is involved in many different cellular processes and can be found in nucleotides, sugar phosphates and phosphoproteins. During phosphate limitation, plants degrade phospholipids, releasing phosphate for other important cellular processes. To compensate for the loss of membrane lipids, galactolipids are synthesized by the transfer galactose from UDP-galactose

onto the diacylglycerol molecules which were previously released by degradation of phospholipids (Härtel *et al.*, 2000, 2001). Thus, MGDG is synthesized which is converted into DGDG by addition of another galactose. During phosphate deprivation, DGDG replaces up to 70 % of the total plasma membrane phosphoglycerolipids in oat shoots and roots (Andersson *et al.*, 2003). This increase in galactolipid biosynthesis is mediated by a strong upregulation of the gene expression of the MGDG synthase genes *MGD2* and *MGD3* and the DGDG synthases *DGD1* and *DGD2. MGD1* and *DGD1* are also expressed under phosphate replete conditions, but expression of the additional glycosyltransferase genes *in Arabidopsis* is restricted to phosphate limitation (Awai *et al.*, 2001; Kelly and Dörmann, 2002; Kelly *et al.*, 2003). While the accumulation of DGDG during phosphate deprivation is the most striking change in lipid composition, there are additional adaptations to phosphate limitation. For example, SQDG accumulates inside the plastids to replace phospholipids (Essigmann *et al.*, 1998). Studies in phosphate limited oat revealed acylated sterol glucosides (ASG) to replace phospholipids in the apoplastic leaflet of the plasma membrane, while the accumulation of DGDG was restricted to the cytosolic leaflet (Tjellström *et al.*, 2010). This regulation of membrane remodeling emphasizes the importance of membrane lipid composition for optimal membrane functionality.

1.1.2 Sterols

1.1.2.1 Sterol Biosynthesis

Sterols are isoprenoid lipids derived from squalene, consisting of a steroid backbone, substituted with an alkyl side chain at C17 and a hydroxyl group at C3. The C5 isoprene units IPP (isopentenyl diphosphate) and dimethylallyl diphosphate (DMAPP) are synthesized via the cytosolic mevalonate (MVA) pathway and via the plastidic 2-C-methyl-D-erythritol-4-phosphate (MEP) pathway (Benveniste, 2004). As sterols are produced at the ER, the MVA pathway represents the major route for isoprenoid units for sterol synthesis (Hartmann and Benveniste, 1987; Moreau *et al.*, 1998; Men *et al.*, 2008). Sterols do not accumulate at the ER but are transported via the Golgi apparatus to the plasma membrane, by a trafficking process which is yet to be characterized in detail (Grebe *et al.*, 2003).

Acetyl-CoA serves as a precursor for the biosynthesis of the steroid backbone in plants. It is converted via acetoacetyl-CoA into 3-hydroxy-3-methylglutaryl-CoA by the 3-hydroxy-3-methylglutaryl-CoA synthase (HMGS). The next step, the synthesis of mevalonate from 3-hydroxy-3-methylglutaryl-CoA by 3-hydroxy-3-methylglutaryl-CoA reductase (HMGR) has been postulated to be associated with sphingolipid biosynthesis in plants, as the activity of HMGR and the sterol content are reduced upon chemical inhibition of palmitoyltransferase, the first enzyme of sphingolipid biosynthesis (Nieto *et al.*, 2009). Indications for genetic interactions between the

sterol and sphingolipid biosynthesis pathways were also found in yeast, by analysis of various mutants affected in sphingolipid and sterol biosynthesis. In a recent study it was shown that mutants of *S. cerevisiae* affected in ergosterol synthesis react to the accumulation of sterol precursors by modifications of their sphingolipid content (Guan *et al.*, 2009). Mevalonate serves as a precursor for the synthesis of IPP via phosphomevalonate and diphosphomevalonate (Suzuki and Muranaka, 2007). IPP and DMAPP can be interconverted by IPP isomerase. Farnesyl diphosphate is formed by condensation of an IPP and a DMAPP molecule.

An overview of the final steps of sterol biosynthesis is depicted in Figure 1 (modified after Boutté and Grebe, 2009. The formation of squalene is catalyzed by squalene synthase in a condensation reaction of two farnesyl diphosphate molecules. In the following reactions 2,3-oxidosqualene is oxidized by squalene epoxidase, and is further processed by cyclization to cycloartenol by cycloartenol synthase. While the predominant proportion of 2,3-oxidosqualene is converted into cycloartenol, a small proportion is also used for the synthesis of lanosterol by lanosterol synthase. Cycloartenol is further processed in several steps to form obtusifoliol.

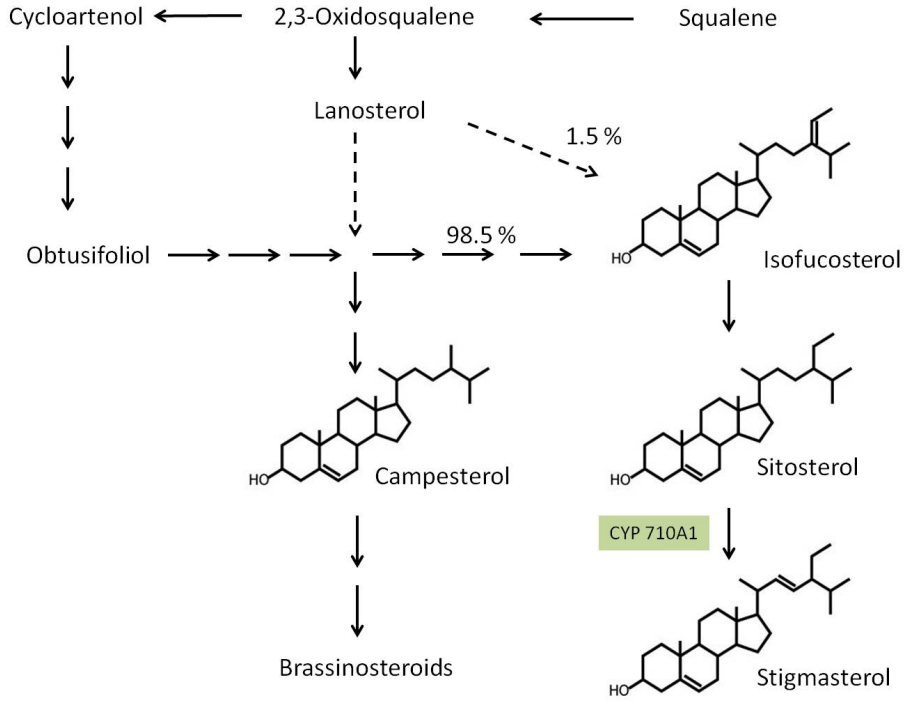

Figure 1: Sterol Biosynthesis in Plants (modified after Boutté and Grebe, 2009). The final steps of sterol biosynthesis in plants are shown. The predominant proportion of phytosterols is synthesized via the cycloartenol pathway, and only a minor proportion is synthesized via the lanosterol pathway. In contrast, the only pathway for the synthesis of sterols in mammals and fungi is via lanosterol. Campesterol is a precursor for brassinosteroid synthesis. The major phytosterol sitosterol can be converted into stigmasterol by the cytochrome P450 Δ22 desaturase CYP710A1 in *Arabidopsis*.

Biosynthesis of phytosterols is later divided into two pathways. The abundant phytosterols stigmasterol and sitosterol are synthesized from isofucosterol, which can be

derived from the lanosterol pathway and the cycloartenol pathway. In contrast to mammals and fungi, which exclusively utilize the lanosterol pathway for the biosynthesis of cholesterol or ergosterol, *Arabidopsis thaliana* synthesizes around 98.5 % of its total sterol content via the cycloartenol pathway and only a minor proportion (1.5 %) is derived from the lanosterol pathway. A role for the lanosterol pathway in steroid synthesis and during plant defense reactions is being discussed (Ohyama *et al.*, 2009). The synthesis of stigmasterol from sitosterol is synthesized by a Δ22 desaturase which introduces a double bond into the alkyl side chain of the sterol. A second pathway leads to the synthesis of campesterol, which is an important phytosterol and in addition serves as a precursor for the biosynthesis of brassinosteroids, a large group of phytohormones involved in plant growth and development (Fujioka *et al.*, 2002; Fujioka and Yokota, 2003).

1.1.2.2 Functions of Sterol Lipids in Plants

Sterol lipids are essential membrane compounds in all eukaryotes. While ergosterol is the most common sterol synthesized by fungi (see 1.3.2.1), most animals synthesize cholesterol. Insects are incapable of *de novo* sterol biosynthesis and are therefore dependent on dietary uptake of these essential lipids (Svoboda and Weirich, 1995). In plants, the phytosterols campesterol, stigmasterol and sitosterol generally present the most abundant sterols, with cholesterol being a minor compound (Nomura *et al.*, 1999; Schaeffer *et al.*, 2001).

As structural components of the plasma membrane, sterols regulate membrane stability and fluidity (Demel and De Kruyff, 1976; Schuler *et al.*, 1991). Furthermore, the interaction of sphingolipids and sterols has been demonstrated to play a vital role in the formation of membrane rafts (lipid rafts) in animals. Membrane rafts are defined as small heterogeneous domains which are enriched in sterols and sphingolipids. They are believed to have a function in the compartmentation of cellular processes by specifically binding proteins and enabling the formation of complex membrane structures (Pike, 2006; Zappel and Panstruga, 2008). *In vitro* experiments showed stigmasterol and sitosterol to promote domain formation and also revealed the addition of ceramide to be crucial for domain stability (Xu *et al.*, 2001). While a final proof for a function of phytosterols in plant membrane rafts is still missing, there is increasing evidence for such role, analogous to cholesterol in animal membranes (Mongrand *et al.*, 2004; Bhat and Panstruga, 2005; Borner *et al.*, 2005; Laloi *et al.*, 2007).

Among the different phytosterols, the function of campesterol, which is the precursor for brassinosteroid synthesis, has been studied in most detail (Fujioka and Yokota, 2003). Mutants affected in campesterol biosynthesis or in biosynthesis of brassinosteroids downstream of campesterol, show an inhibition in plant development and display dwarf phenotypes. The growth retardation and developmental defects of these mutants can be rescued by exogenous

application of brassinosteroids (Clouse, 2002) and references therein). While campesterol as a precursor for brassinosteroid synthesis plays a crucial role in plant development, there is evidence that sterols may also be directly involved in plant growth and development, independent of their role as precursors for brassinosteroid biosynthesis. Mutants affected in sterol C-14 reductase (*fackel*)(Jang *et al.*, 2000; Schrick *et al.*, 2000), sterol C-24 methyltransferase (*smt1*)(Diener *et al.*, 2000; Schrick *et al.*, 2002) and sterol C-8,7 isomerase (*hyd1*)(Schrick *et al.*, 2002; Souter *et al.*, 2002) show defects in cell division and embryonic patterning; phenotypes that cannot be rescued by application of brassinosteroids. It is a subject of debate, whether the observed phenotypes are caused by the lack of sterols essential for plant development or from the accumulation of sterol precursors (Benveniste, 2004). Another interpretation of these phenotypes suggests a role for sterols in auxin signaling by interactions of sterols with auxin carrier proteins (Lindsey *et al.*, 2003).

Only recently, a specific function in plant-pathogen interactions has been attributed to the phytosterol stigmasterol (Griebel and Zeier, 2010). Stigmasterol was shown to accumulate in plant membranes of *Arabidopsis* leaves after infection with the bacterial pathogen *Pseudomonas syringae*. Mutants in *CYP710A1* are affected in the cytochrome P450 sitosterol Δ22-desaturase, which catalyzes the conversion of sitosterol to stigmasterol (Morikawa *et al.*, 2006), and display a decreased accumulation of stigmasterol. Interestingly, the reduced increase of stigmasterol upon infection conferred enhanced resistance against *Pseudomonas syringae*. Furthermore, exogenous application of stigmasterol led to an increased susceptibility of the plant, representing further evidence of a specific function of this particular phytosterol in plant-pathogen interactions (Griebel and Zeier, 2010).

In addition to the various functions of the different molecular species of phytosterols, the role of conjugated sterols in plants has been subject to recent research. While the only conjugated sterols synthesized by animals are sterol esters (SE), sterols which are esterified to an acyl chain at the C3 position of the sterol backbone, plants do not only contain a larger diversity of phytosterols, they also possess a variety of conjugated sterols. In addition to the non-polar sterol esters, the major forms of conjugated sterols are sterol glucosides (SG) and acylated sterol glucosides (ASG). These membrane bound sterol lipids are less abundant than free sterols (FS) in *Arabidopsis thaliana*, but they can represent the predominant form of sterol lipids in other plants, e.g. in the *Solanaceae* (Duperon *et al.*, 1984; Palta *et al.*, 1993). The molecular structures of the different classes of conjugated sterols in plants are depicted in Figure 2.

In *Arabidopsis thaliana*, the synthesis of sterol esters is catalyzed by two acyltransferases, acyl-CoA:sterol acyltransferase (ASAT) and phospholipid:sterol acyltransferase (PSAT). The acyl donors for the esterification reactions are acyl-CoA and phosphoglycerolipids

such as PE, respectively (Banas *et al.*, 2005; Chen *et al.*, 2007). A mutant affected in PSAT displayed an early leaf senescence phenotype. Further characterization of this mutant revealed a function of this enzyme for lipid homeostasis, as the plants were incapable of regulating the amount of free sterols in plant membranes. Exogenous application of the sterol precursor squalene led to a strong increase of SEs in the wild type, while the mutant showed no accumulation of SEs, but rather displayed a significant increase of FSs, which appeared to cause leaf necrosis (Bouvier-Navé *et al.*, 2010). These findings confirm the previous assumption that the main function of SEs is that of a storage lipid, which regulates the pool of free sterols (Lewis *et al.*, 1987; Dyas and Goad, 1993; Sturley, 1997; Schaller, 2004). As SEs localize hardly to the membrane bilayer (Hamilton and Small, 1982), but are rather thought to form oil bodies in the cytoplasm in association with TAG, their formation can prevent excess accumulation of FSs in the membranes.

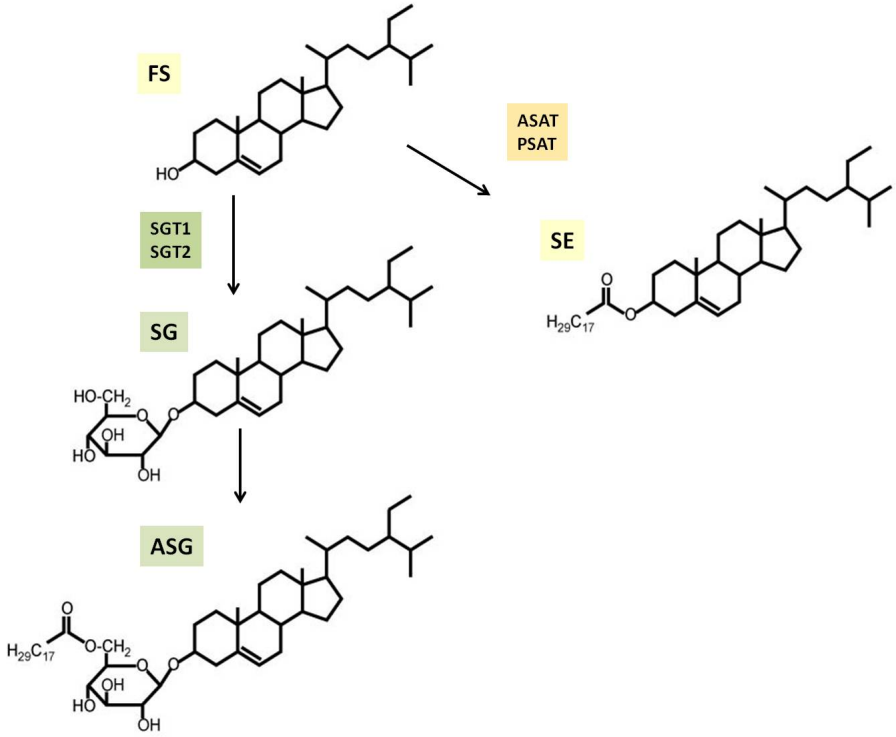

Figure 2: Biosynthesis of Conjugated Sterols in Plants. Free sterols are used as substrates for the synthesis of SG by SGT1 and SGT2 and for the synthesis of SEs by ASAT and PSAT. SGs are acylated by an unknown acyltransferase to form ASGs. The molecular structures of the predominant molecular species from *Arabidopsis* are displayed, i.e. sitosterol, sitosterol glucoside, 18:3-sitosterol and 18:3-sitosterol glucoside. ASAT: acyl-CoA:sterol acyltransferase, ASG: acylated sterol glucoside, FS: free sterol, PSAT: phospholipid:sterol acyltransferase, SE: sterol ester, SG: sterol glucoside, SGT: sterol glucoside transferase.

Sterol glucosides (SGs) constitute the second group of conjugated sterols in plants. They are synthesized by the enzyme sterol glucosyl transferase (SGT) which catalyzes the transfer of a glucose moiety from UDP-glucose to the hydroxyl group at the C3 position of a sterol molecule (Grunwald, 1971; Warnecke *et al.*, 1997). SGs serve as precursors for the synthesis of acylated sterol glucosides (ASGs) by an acyltransferase which remains unidentified to date. In *Arabidopsis*

two genes have been identified which encode for sterol glucosyl transferases: *UGT80B1* and *UGT80A2.* A double mutant of *Arabidopsis* T-DNA insertion lines for *UGT80B1* and *UGT80A2* showed a severe reduction of SG and ASG levels in leaves and siliques (DeBolt *et al.*, 2009) as well as in seeds (Schrick *et al.*, 2012). The mutant was viable, but displayed a slow growth phenotype and embryogenesis was affected. The plants showed a reduction in seed size and a loss of suberization in the seed, as well as a transparent testa phenotype. The suberization defect was suggested to be caused by a function of glycosylated sterols in lipid polyester precursor trafficking (DeBolt *et al.*, 2009). While gene expression of *UGT80A2* was increased in stomata and some reproductive organs, i.e. pollen, siliques and stamen by promoter::GUS studies, *UGT80B1* was more strongly expressed in leaves, seedlings, apical tips of cotelydons and in developing seeds (DeBolt *et al.*, 2009).

Previous studies also suggested a role for sitosterol glucoside as a primer for cellulose synthesis (Peng *et al.*, 2002). However, the amounts of cellulose or cell wall sugar in the *ugt80B1*/*ugt80A2* double mutants were not altered, when compared with the wild type (DeBolt *et al.*, 2009). It remains unclear whether the residual amounts of SG which were detected in the double mutant are sufficient for priming of cellulose synthesis. Furthermore, mutants affected in sterol biosynthesis such as *fackel, smt1 and hyd1* display symptoms of cellulose deficiency, which suggests an involvement of sterols in cellulose synthesis, although these observations do not provide evidence for a specific role of glycosylated sterols (Schrick *et al.*, 2004).

1.1.3 Sphingolipids

1.1.3.1 Structure and Biosynthesis

The common structure of all sphingolipids is an amino alcohol long chain base (LCB), a C18 chain, which is hydroxylated at C1 and C4 and carries an amine group at C2. In addition, the LCB can be hydroxylated at C3 and desaturated at C4 and C8 in *cis* or *trans* configuration. In all sphingolipids except in free LCBs and LCB-phosphate, the LCB is linked to a hydroxylated or non-hydroxylated C14 -26 fatty acid, via an amide bond (Sperling and Heinz, 2003; Lynch and Dunn, 2004). Substitution of this ceramide backbone with a sugar moiety such as glucose, results in the formation of glucosylceramide. More complex sphingolipids can carry a variety of different substitutions, containing inositol and several sugar moieties bound to phosphate and are hence called glucosylinositolphosphoceramides (GIPCs). The molecular structures of selected sphingolipids are depicted in Figure 3.

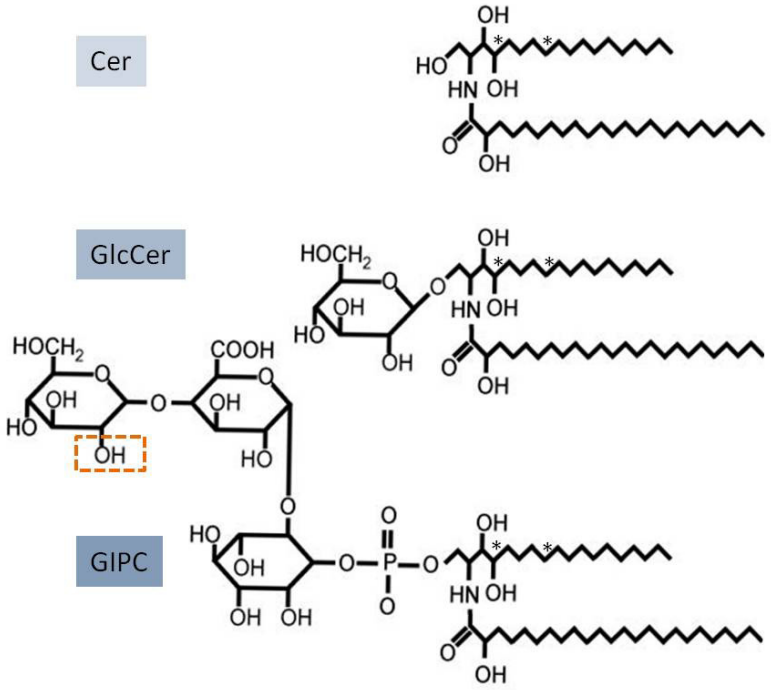

Figure 3: Molecular Structures of Selected Sphingolipids (modified after Markham *et al.*, 2006; Pata *et al.*, 2010) Ceramides are comprised of C14 –C26 fatty acids, which are usually hydroxylated, linked via an amide bond to a long chain base (LCB). LCBs contain 18 C atoms and can be modified by additional hydroxylation of C3, yielding a trihydroxy LCB. In plants, the LCB is usually desaturated at C8 (t18:1), however, additional double bonds at C4 are also found in dihydroxy LCBs (d18:2). Asterisks indicate the positions of double bonds at C4 and C8 of the LCB. Ceramides can be glucosylated by glucosylceramide synthase (GCS) to form glucosylceramide (GlcCer), or serve as substrates for IPC synthase, catalyzing the synthesis of the complex sphingolipid glucosylinositolphosphoceramide (GIPC). The head group structure of GIPCs can vary among plant species; depicted is the major form found in *Arabidopsis* containing glucose, glucuronic acid and inositol. The sugars are usually connected by α-glycosidic linkage (not shown). In tomato and soybean, the hydroxyl group at C2 of the glucose (highlighted in orange) is replaced by acetyl amine (Markham *et al.*, 2006).

In sphingolipid biosynthesis, palmitoyl-CoA and serine are condensed by serine palmitoyltransferase (*LCB1*, *LCB2*, *TSC3*) at the ER resulting in the formation of 3-ketosphinganine. After reduction, d18:0 LCB (sphinganine) is produced (Lynch and Fairfield, 1993; Chen *et al.*, 2006). Sphinganine can either directly serve as a substrate for ceramide synthesis by ceramide synthase (*LAC1*, *LAG1*), or can be hydroxylated to form t18:0 (phytosphingosine), which can also be accepted as a substrate by ceramide synthase (Wright *et al.*, 2003; Chen *et al.*, 2008). Acyl donors for the synthesis of ceramides in the acyl-CoA dependent pathway are C14 –C26 acyl-CoAs (Sperling and Heinz, 2003). Most ceramides in plants contain hydroxylated fatty acids, however, the ceramide synthase does not accept hydroxylated acyl-CoAs as a substrate (Lynch and Dunn, 2004). Therefore, fatty acid moieties are modified by an α-hydroxylation reaction following ceramide synthesis (Lynch and Alfred H. Merrill, 2000; Sperling and Heinz, 2003). Sphingolipid desaturases subsequently introduce double bonds at positions 4 and 8 in *cis* or *trans* configuration, giving rise to d18:1, t18:1 or d18:2 LCBs (Ternes *et al.*, 2002). Further processing of sphingolipids involves the glycosylation of ceramides which is catalyzed by the glucosylceramide synthase (GCS) (Warnecke and Heinz,

2003). In this step, a glucose moiety is transferred from UDP-glucose to ceramide to form a β-glycosidic linkage at C1, yielding glucosylceramide (GlcCer). While GlcCer synthesis takes place at the ER or at the plasma membrane, ceramide can likewise be exported to the Golgi apparatus, where it serves as a precursor for GIPC biosynthesis (Bromley *et al.*, 2003; Hillig *et al.*, 2003; Wang *et al.*, 2008). The phospholipid phosphatidylinositol (PI) serves as a donor of inositol phosphate, which is transferred to ceramide by the enzyme inositol phosphorylceramide (IPC) synthase (ERH1)(Wang *et al.*, 2008). Inositol phosphate is esterified to the hydroxy group at C1 of the ceramide by a phosphate ester linkage (Bromley *et al.*, 2003). Inositolphosphoceramide (IPC) can be further modified by addition of various complex sugar moieties, resulting in the formation of GIPCs. GIPCs from *Arabidopsis* were shown to contain mainly N-acetyl-glucosamine (α 1→4)-glucuronic acid (α1→2)-myo-inositol-1-O-phosphate, attached to t18:1 LCB containing ceramides (Kaul and Lester, 1978; Hsieh *et al.*, 1981; Pata *et al.*, 2010). An overview of the most important steps in the biosynthesis of complex sphingolipids from LCBs is given in Figure 4.

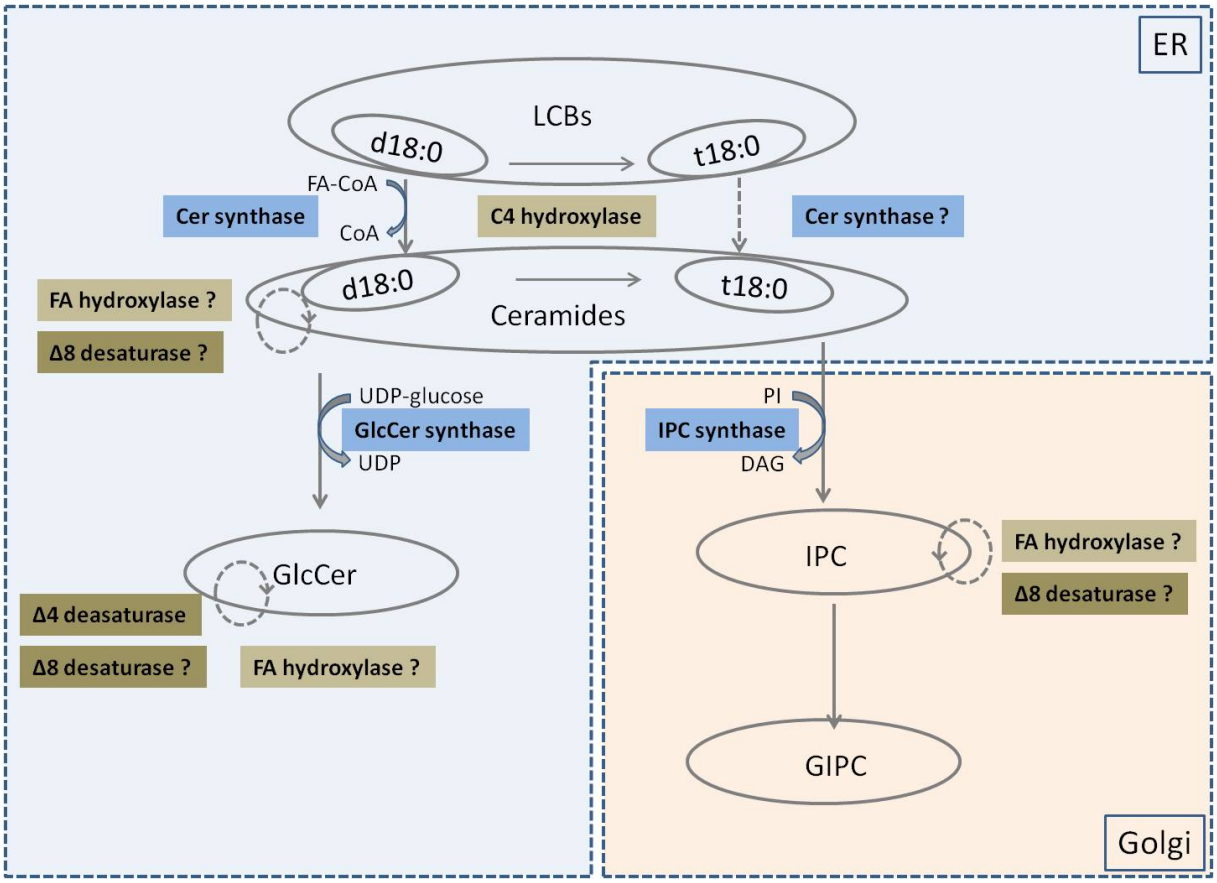

Figure 4: Sphingolipid Biosynthesis in Plants (modified after Pata *et al.*, 2010). Schematic overview of selected synthetic steps of sphingolipid biosynthesis from LCBs. Enzymes for ceramide and glucosylceramide synthesis are located at the ER. For IPC synthesis, ceramides are exported to the Golgi apparatus. Modifications of fatty acids and LCBs can take place at different steps during the biosynthesis of complex sphingolipids. Cer: ceramide; FA: fatty acid, GIPC: glucosylinositolphosphoceramide, GlcCer: glucosylceramide, IPC: inositolphospho-ceramide, LCB: long chain base

1.1.3.2 Functions of Sphingolipids in Plants

Sphingolipids show a great structural and functional diversity. Free LCBs, LCB phosphates and ceramides are known to play multiple roles in signaling (Sperling *et al.*, 2005; Pata *et al.*, 2010). In contrast to the more complex glycosylated sphingolipids, ceramides are present at minor concentrations in plant cells. They have been estimated to represent around 10 % of glycosylceramide content (Vesper *et al.*, 1999; Wang *et al.*, 2006). Ceramide can induce apoptosis in animals (Hannun and Obeid, 2008) and there is increasing evidence of a similar function in plants (Liang *et al.*, 2003). It could be shown that the accumulation of free LCBs leads to programmed cell death in plants (Wang *et al.*, 1996; Spassieva *et al.*, 2002; Takahashi *et al.*, 2008), which is a well-known reaction to pathogen attack; therefore, regulation of this process is likely to be relevant in plant-pathogen interactions. The presumed role of ceramide-phosphates in plant responses to pathogen attack is supported by the upregulation of a ceramide kinase after infection with a virulent strain of *Pseudomonas syringae* (Liang *et al.*, 2003).

Sphingolipids are known to be involved in stabilization of membrane integrity, e.g. of the ER and Golgi (Chen *et al.*, 2008). While glycosylceramides are found in most eukaryotes and even in a few bacteria (Warnecke and Heinz, 2003), GIPCs are restricted to plants and fungi. In comparison to GlcCer, the large sugar containing headgroup of GIPCs renders these molecules extremely polar. Specific functions in the membrane bilayer are associated with the high polarity of GIPCs. GPI-anchors contain a phosphatidylinositol moiety which serves as a membrane anchor for membrane proteins, which are also associated with membrane raft formation (see 1.1.2.2)(Bhat and Panstruga, 2005; Borner *et al.*, 2005). In yeast, the glycerol moiety of the GPI anchor can also be exchanged with ceramide, resulting in a GIPC-like lipid serving as a membrane anchor for proteins (Conzelmann *et al.*, 1992). The presence of GPI- anchors containing ceramides has also been demonstrated in plants (Svetek *et al.*, 1999; Sperling and Heinz, 2003). There also seems to be an important connection between the synthesis of GIPCs and the regulation of free ceramide content in plants. An *Arabidopsis* mutants affected in IPC synthase showed an accumulation of ceramides, which led to enhanced hypersensitive response (HR)-like cell death upon infection with powdery mildew (Wang *et al.*, 2008) GIPCs were also detected within the peribacteroid membrane of root nodules in pea, where their presence was restricted to early infection events (Perotto *et al.*, 1995). Interestingly, IPC activity was found to be especially active in the plant family of the *Fabaceae*, which are able to undergo root-nodule symbiosis with nitrogen fixing soil bacteria (see 1.3.1).

As important constituents of plant membranes, GlcCers are involved in the upkeep of membrane stability and the regulation of membrane permeability (Pata *et al.*, 2010). The great variety of different molecular species of GlcCer seems to confer specific membrane properties,

which can be vital for plant growth, e.g. during cold acclimation (Chen *et al.*, 2011). While chilling sensitive plants were shown to contain mainly GlcCer species with saturated fatty acids (Imai *et al.*, 1995), chilling resistant plants contained monounsaturated very long chain fatty acids (VLCFA), with a chain length of more than 20 carbon atoms (Cahoon and Lynch, 1991). Additionally, GlcCer have been suggested to play a role during drought tolerance (Warnecke and Heinz, 2003). In plant-pathogen interactions, fungal GlcCer have been implicated as targets for anti-fungal compounds (Ramamoorthy *et al.*, 2007; Rittenour *et al.*, 2011).

Despite of these findings, many functions of sphingolipids are yet to be determined. Further understanding of sphingolipid functions is believed to be facilitated by increased sphingolipidomics analysis, providing more information on the diversity of sphingolipid species and content in different plant species and tissues (Pata *et al.*, 2010).

1.2 Mass Spectrometry Approaches for Lipid Analysis

The understanding of lipid functions in plants is largely dependent on the ability to accurately quantify the different lipid classes. Adequate methods allow the monitoring of lipid changes e.g. during plant growth and development or as a response to biotic and abiotic stress. Various techniques can be employed for quantification of the different lipid classes. Classical methods include the quantification of glycerolipids by measurement of fatty acid methyl esters by GC-FID (Browse *et al.*, 1986). Sphingolipids can be analyzed by quantification of derivatized long chain base moieties by HPLC (Morrison and Hay, 1970; Merrill *et al.*, 1988; Sperling *et al.*, 1998). Sterol lipid analysis involves the measurement of the sterol moieties by GC-FID (DeBolt *et al.*, 2009; Bouvier-Navé *et al.*, 2010). These methods rely on the cleavage of complex lipids to lease fatty acids, long chain bases or sterol residues prior to analysis. Thus, information on the structure of the lipid molecular species is limited. Furthermore, these methods can suffer from low sensitivity and careful separation of the different lipid classes has to be achieved prior to analysis, for example by thin layer chromatography or solid phase extraction.

In the last years, a number of methods have been developed for the non-destructive measurement of lipids by mass spectrometry. Most lipids are not volatile and measurement by gas chromatography is restricted to small molecules such as free fatty acids or free sterols, after transmethylation or derivatization. However, recent development of liquid chromatography based techniques has allowed the direct measurement of more complex lipids by mass spectrometry.

Mass spectrometry analysis requires the ionization of lipids in the ion source, which can vary between instruments. One prominent example is electrospray ionization (ESI). Depending on the solvent and the ionization conditions, lipid molecules can be protonated, deprotonated or ionized by formation of adducts with salts, e.g. lithium, sodium, potassium or ammonium. Ions

with a specific mass to charge ratio (m/z) can be selected by the use of quadrupoles, consisting of four or more rod-shaped metal electrodes (Paul, 1953). Application of alternating and direct voltage guides the selected ions through the quadrupole while ions with a deviating m/z collide with the metal rods. A widely used variation of tandem mass spectrometry is carried out on triple quadrupole mass spectrometers. Here, several quadrupoles are used successively, which can be operated in different modes. In the so-called product ion scan, the desired lipids are selected by the first quadrupole, the ion-selecting cell, and fragmented by collision induced dissociation with an inert gas such as nitrogen or argon. The fragmentation takes place in a second quadrupole, the collision cell. The fragmented ions are detected by a third quadrupole, the mass analyzer. In precursor ion scan, all ions are allowed to pass the first quadrupole after scanning and are subsequently fragmented in the collision cell. The mass analyzer does not detect all ions but only fragments of a specific m/z. The information on the product ion is then correlated with the parent ion selected in the first quadrupole. In neutral loss scan, the first quadrupole is operated synchronously with the mass analyzer by scanning for molecules which show a specific m/z difference, the so-called neutral loss, after fragmentation in the collision cell.

In quadrupole time-of-flight (Q-TOF) mass spectrometers the third quadrupole is replaced with a time-of-flight mass analyzer. Lipid ions are accelerated by the pulser, after passing the first quadrupole and the collision cell, and enter the flight tube. A very high mass accuracy can be obtained by measuring the time the ions require to cover the distance between the pulser and the detector. Lipids with a high m/z require more time to cover the distance than small molecules. Similar to triple quadrupole mass spectrometers, lipids can be analyzed after collision induced dissociation with an inert gas. In Q-TOF MS/MS analysis precursor ion scan and neutral loss scan can be simulated by electronically extracting the signal intensities of fragmented parent ion spectra.

One example for the development of tandem mass spectrometry based analysis for the quantification of membrane lipids in plants was described by Welti *et al.*, (2002). Here, electrospray ionization tandem mass spectrometry (ESI-MS/MS) was employed for the analysis of phospho- and galactolipids in crude lipid extracts of *Arabidopsis*. In this approach, the lipids were directly infused to the mass spectrometer and measured after collision induced dissociation in the collision cell. Quantification was based on precursor or neutral loss scanning compared to internal standards.

Another mass spectrometry based method was described for the non-destructive measurement of sphingolipids by LC-MS (Markham *et al.*, 2006; Markham and Jaworski, 2007). A challenge in sphingolipid analysis was represented by the different polarity of sphingolipids, which required the development of novel extraction methods. Unlike phospho-and galactolipids, sphingolipids were separated by liquid chromatography prior to infusion to the MS and electrospray ionization. Multiple reaction monitoring allowed the identification of sphingolipid

molecular species based on their molecular mass, neutral loss of the fatty acid residue or the polar head group, respectively, and on the presence of the precursor long chain base.

Tandem mass spectrometry approaches for the quantification of sterol lipids have so far been limited to the analysis of cholesterol and ergosterol in animals and yeast (*Saccharomyces*), which only contain free sterols or sterol esters (Liebisch *et al.*, 2006; Honda *et al.*, 2008; Ejsing *et al.*, 2009). A comprehensive tandem mass spectrometry based method for the quantification of all sterol lipid classes in plants, including sterol glucosides (SG) and acylated sterol glucosides (ASG) has not been described to date.

The development of a tandem mass spectrometry based method for the quantification of sterol lipids, equivalent to the methods described for phospho-and galactolipids and sphingolipids, would considerably improve the possibilities to investigate the role of sterol lipids in plants.

1.3 Plant Microbe Interactions

1.3.1 Root-Nodule Symbiosis

Members of the plant family *Fabaceae* have the ability to undergo symbiotic interactions with nitrogen fixing soil bacteria (*Rhizobiaceae*). The resulting root nodule symbiosis is one of the agriculturally most important, beneficial plant microbe interactions, found in crop plants such as soybean, bean, pea, alfalfa and peanut (Popp and Ott, 2011). These plants are more commonly known as legumes and are characterized by their independence of nitrogen fertilization. While nitrogen, together with phosphate, represents the major growth limiting factor for most crop plants, legumes obtain reduced nitrogen from their symbiotic interaction partners (Udvardi and Day, 1997).

In root nodule symbiosis, rhizobial soil bacteria in the rhizosphere of the host plant exude signal molecules, the so called *Nod* factors which have been identified as lipochitooligosaccharides with strain-specific side chains (Denarie and Cullimore, 1993). These are detected by receptor-like kinases, the *Nod* factor receptors, a process which initiates specific physiological responses in the host plant, including the depolarization of the plasma membrane, alkalization of the rhizosphere and calcium spiking around the nucleus (Downie and Walker, 1999; Oldroyd and Downie, 2006). Subsequently, root hair curling is induced, resulting in the enclosure of bacteria which invade the root through an infection thread formed by the plant (Brewin, 2004; Yokota *et al.*, 2009). The bacteria enter the plant cell by invagination of the plant plasma membrane. This leads to the formation of symbiosomes, containing the rhizobial bacteroids surrounded by the plasma-membrane derived peribacteroid membrane (PBM)(Whitehead and Day, 1997). Within these symbiosomes, atmospheric nitrogen is reduced to ammonia by the rhizobia specific enzyme nitrogenase. The nitrogenase is extremely sensitive

to the presence of oxygen, therefore the symbiosomes present an oxygen-free environment optimized for nitrogen fixation. This is enabled by the presence of the oxygen-binding pigment leghemoglobin (Appleby, 1984; Ott *et al.*, 2005). In exchange for reduced nitrogen the bacteroids receive carbon derived from photosynthesis, e.g. in the form of malate, from the plant. Figure 5 provides a schematic overview of the initial infection events during root nodule symbiosis (adapted from Whitehead and Day, 1997; Jones *et al.*, 2007).

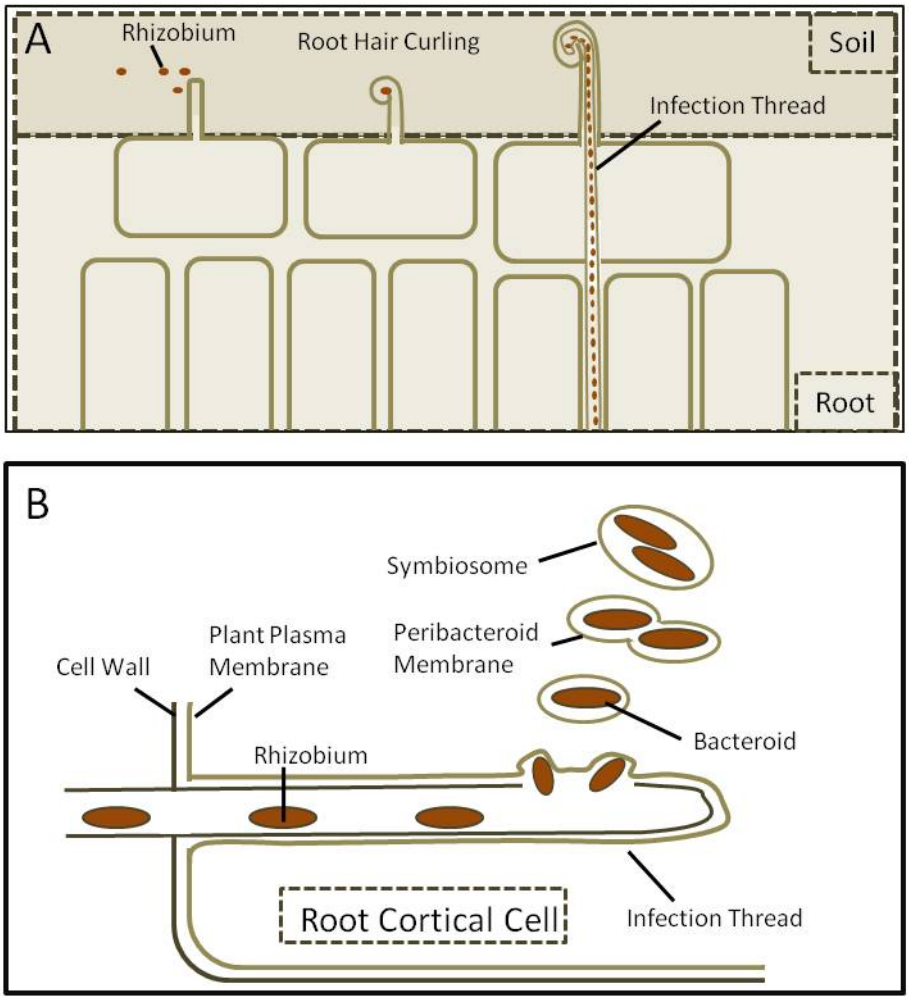

Figure 5: Invasion of a Legume Root by Rhizobia. **A** Upon detection of bacterial Nod factors, root hair curling is initiated (adapted from Jones *et al.*, 2007). Rhizobia are trapped in the root hairs and enter the root via an infection thread formed by the plant. **B** When the bacteria reach the root cortex they invade plant cells by endocytosis (adapted from Whitehead and Day, 1997). The bacteroids are then surrounded by the peribacteroid membrane, which is derived from the plant plasma membrane, and are hence termed symbiosomes.

The various members of the legume family capable of root nodule symbiosis have established specific interactions with certain members of the *Rhizobiaceae*. Soybean (*Glycine max*), which is widely employed for physiological studies enters symbiosis with *Bradyrhizobium japonicum*. The smaller, non-agricultural plants *Medicago truncatula* and *Lotus japonicus* undergo symbiotic relationships with *Sinorhizobium meliloti* and *Mesorhizobium loti*,

respectively (Sullivan *et al.*, 1995). These plants have been established as model plants for genetic and physiological studies of root nodule symbiosis (Handberg and Stougaard, 1992). Research is facilitated by the fact that the genomes of the two plants are diploid and have been fully sequenced and transformation protocols for the generation of transgenic plants and mutants are available (Handberg and Stougaard, 1992; Tirichine *et al.*, 2005). For *Lotus japonicus* a collection of ethyl methane-sulfonate (EMS) treated mutants has been made available, using a strategy called "targeted induced local lesions in genomes" (TILLING) for identification of mutated gene loci (Perry *et al.*, 2003).

The two model plants *Medicago truncatula* and *Lotus japonicus* display two different mechanisms with regard to nodule formation. *Medicago* forms indeterminate nodules, which contain a persistent meristem, ensuring that nodules are continuously infected. *Lotus* and soybean on the other hand produce determinate nodules which have a defined lifespan. Upon maturation, these nodules lose their meristem and are no longer infected by rhizobia (Popp and Ott, 2011).

1.3.1.1 Lipids in Root-Nodule Symbiosis

Root-nodule symbiosis has been the subject of extensive research in the last years. Great progress has been achieved by the characterization of mutants impaired in the regulation of nodule formation. Many genes have been identified which are involved in the complex signaling cascades involved in Nod factor perception and in regulation of infection thread formation and nodule infection (Popp and Ott, 2011). Furthermore, many transporters have been characterized which are responsible for the exchange of nutrients across the peribacteroid membrane (Udvardi and Day, 1997). However, only limited information is available about the lipid structure of the peribacteroid membrane and about the putative functions of the lipids involved in the setup of this membrane. Previous analyses of the lipid composition of the PBM in nodules of *Lotus* and soybean revealed the presence of the galactolipid DGDG (Gaude *et al.*, 2004). This galactolipid was initially believed to be restricted to plastidial membranes, except for the replacement of phospholipids in extraplastidial membranes during phosphate deprivation (see 1.1.1). Therefore, the discovery of substantial amounts of DGDG in the PBM, independent of phosphate deprivation, was novel. In the same study, PC, PE, PI and PG were found to be present in the PBM of soybean. In previous studies, the presence of phospholipids (PC, PE, PG and PI) and sterols had been reported (Hernández and Cooke, 1996; Whitehead and Day, 1997). Analysis of the PBM from pea revealed stigmasterol to be the major sterol, followed by sitosterol. However, no attempts were made to analyze conjugated sterols. In the same study, PE and PC were found to be the predominant phospholipids in pea PBM, while PI was not detected and PG was detected, but not quantified. This study represents the only one to reveal the

presence of sphingolipids in the PBM, but does not specify the nature of the detected sphingolipids.

Analysis of fatty acid distribution of the PBM revealed the presence of 16:0, 16:1, 18:0, 18:1, 18:2 and 18:3 fatty acids in soybean (Gaude *et al.*, 2004) and pea (Hernández and Cooke, 1996). In general, the lipid composition of the PBM in pea was found to be more similar to the lipid distribution in the microsomal fraction, enriched in ER membranes than to the plasma membrane (Hernández and Cooke, 1996).

1.3.2 Arbuscular Mycorrhiza

Glomus intraradices is an arbuscular mycorrhizal fungus which belongs to the phylum of the *Glomeromycota* (Schüßler *et al.*, 2001). These fungi undergo symbiotic interactions, the so called arbuscular mycorrhiza formation, with most land plants, including *Lotus japonicus*. This ancient and widespread symbiosis enables plants to prosper on soils, where nutrients such as phosphorus and nitrogen are not abundant and where water supply is limited. The extensive mycelium of the fungus enables an efficient uptake of water and nutrients, which are supplied to the host plant in exchange for photosynthetic products in the form of carbohydrates (Solaiman and Saito, 1997; Bago *et al.*, 2003; Finlay, 2008).

Symbiosis is regulated by different signaling molecules from both interaction partners (Bonfante and Requena, 2011). The plant roots exude plant hormones called strigolactones, which stimulate hyphal branching (Akiyama *et al.*, 2005). On the other hand, symbiotic root responses can be induced by the detection of fungal signaling molecules, the so called “Myc factors”, which show evolutionary homologies to the bacterial “Nod factors” found in root nodule symbiosis (Maillet *et al.*, 2011). Upon germination of a fungal spore, hyphal growth and branching is initiated. The fungus grows towards the root, following a chemical gradient of strigolactones exuded by the plant (Akiyama *et al.*, 2005). These events, which are initiated by strigolactone perception, are part of the so-called presymbiotic stage of arbuscular mycorrhiza formation. When the hyphae get into contact with the host root, the fungus forms a specialized appressorium, the hyphopodium on the root surface. This is followed by the active formation of a prepenetration apparatus by the plant, triggered by unknown signaling molecules and possibly by mechanical stimulation (Genre *et al.*, 2005). This plant derived structure, consisting of cytoskeletal compounds lined with ER membranes, is crucial for fungal penetration and presents a cytoplasmatic bridge across the vacuole of the plant cell. The fungal hyphae enter the root through the prepenetration apparatus and are guided to the cortex where they exit the plant cells and enter the apoplast (Genre *et al.*, 2005; Parniske, 2008). Subsequently, the branching hyphae grow along the root axis and finally enter inner cortical cells where they form arbuscules. These tree-shaped structures are characterized by repeated branching of the hyphae

within a plant cell, surrounded by a plant derived membrane, the so called periarbuscular membrane. The fungal plasma membrane and the periarbuscular membrane are separated by the periarbuscular space and constitute the site of nutrient and signal exchange between the fungus and the host plant. The fungal mycelium enables the efficient uptake of nutrients from the soil and provides the plant with minerals such as nitrogen, zink, copper and especially phosphate, which is often found in inorganic complexes in the soil (Harrison and van Buuren, 1995; Gonzalez-Guerrero *et al.*, 2005; Lopez-Pedrosa *et al.*, 2006). The fungus can release phosphate from these insoluble complexes and can mediate its transport to the host root in the form of polyphosphate granules. These negatively charged phosphate granules are believed to be transported together with arginine, which serves as a transport form of nitrogen, acquired by the fungus from organic material and delivered to the host root in the form of urea or ammonium (Govindarajulu *et al.*, 2005). Phosphate and ammonium are transported through the fungal plasma membrane, the periarbuscular space and the periarbuscular membrane into the plant cytoplasm. On the other hand, the plant provides carbohydrates, which are transported in the form of sucrose into the periarbuscular space. Here, cleavage of the disaccharide takes place and hexoses are transferred into the fungal cytoplasm by a fungal monosaccharide transporter (Schaarschmidt *et al.*, 2006). For long distance transport, the hexoses are converted into glycogen or triacylglycerol (TAG) (Pfeffer *et al.*, 1999). While glycogen is transported in the form of glycogen granules, TAGs accumulate and form lipid droplets, which are transported within the hyphal network as so-called vesicles (Bago *et al.*, 2002; Bago *et al.*, 2003). Figure 6 shows the process of mycorrhizal root invasion and microscopic photographs of mycorrhizal structures within the plant root. A schematic illustration of metabolite fluxes in arbuscules is shown in Figure 7.

Among the numerous advantages provided to the plant by arbuscular mycorrhiza formation, the improved phosphate supply to the host plant is the most important one (Javot *et al.*, 2007). This is expressed in the plant's ability to regulate arbuscule degradation depending on the efficiency of phosphate supply. While efficient arbuscules with a strong phosphate transport capacity are allowed to prosper, inefficient ones are prematurely degraded by the plant. The phospholipid lyso-phosphatidylcholine (LPC) has been suggested to serve as a signal molecule for the efficiency of phosphate transport in arbuscules (Drissner *et al.*, 2007; Parniske, 2008). Furthermore, high concentrations of P_i in the soil inhibit mycorrhiza formation (Olsson *et al.*, 2002).

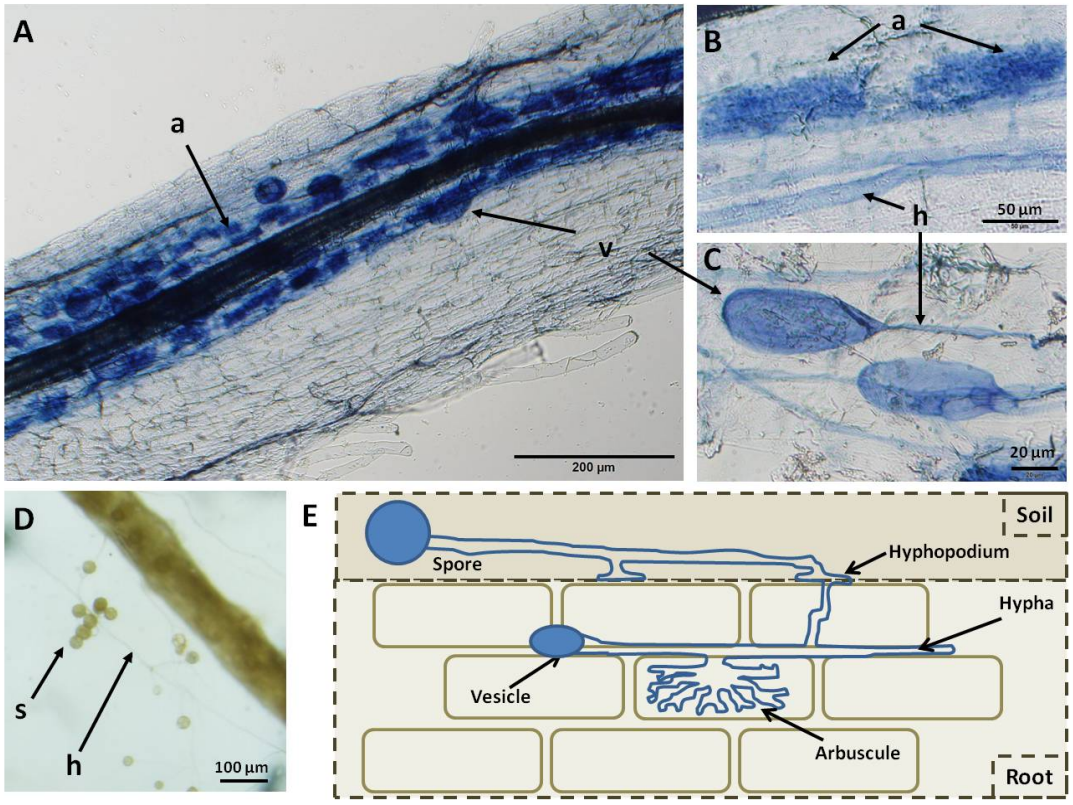

Figure 6: Arbuscular Mycorrhiza Colonization of Plant Roots. A: *Lotus japonicus* root with colonized with *Glomus intraradices*. Fungal structures were stained with ink and vinegar. **B**: Arbuscules **C**: Vesicles **D**: *Glomus intraradices* spores and hyphae in axenic root culture with *Agrobacterium rhizogenes* transformed chicory roots **E**: Schematic process of colonization (modified after Parniske 2008). *Glomus* spores germinate and hyphae grow towards the root after perception of strigolactones. The fungus forms hyphopodia on the root surface and invades the plant via rhizodermal cells. The hyphae enter the apoplast when they reach the root cortex and form arbuscules inside inner cortical cells. Vesicles are formed inside the apoplast. a: arbuscule, h: hypha, s: spore, v: vesicle. Sources of microscopic photos: this work.

1.3.2.1 Lipid Metabolism in the Arbuscular Mycorrhizal Fungus *Glomus intraradices*

Glomus intraradices has been shown to synthesize sterols that are usually associated with plants, i.e. predominantly campesterol and sitosterol (Fontaine *et al.*, 2001). In that regard it differs from most fungi, including *Saccharomyces cerevisiae,* where ergosterol is the major sterol. While earlier studies showed ergosterol to be present in mycelia of *Glomus* (Frey *et al.*, 1992), and it has even been proposed as a suitable biochemical marker for the estimation of mycorrhizal biomass (Hart and Reader, 2002), more recent studies have shown ergosterol to be absent from *Glomus* cultures when grown *in vitro* (Olsson *et al.*, 2003). The presence of ergosterol, which constitutes a pathogen associated molecular pattern (PAMP), can trigger plant defense reactions, as it is associated with pathogenic fungi. The evolutionary development of the biosynthetic pathways for campesterol and sitosterol presumably presents a prerequisite for the establishment of arbuscular mycorrhiza. Radioactive labeling experiments showed sterols to be present predominantly in the free form (60%) and as sterol esters (Fontaine *et al.*, 2001).

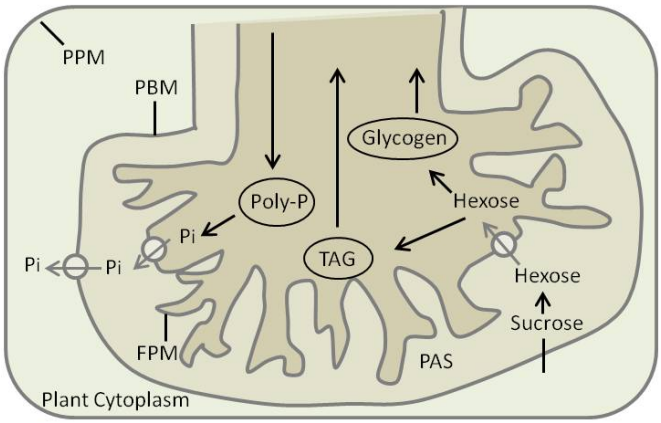

Figure 7: Exchange of Phosphate and Metabolites during Arbuscular Mycorrhiza Formation (modified after Parniske, 2008)**.** Schematic overview of carbon and phosphate fluxes between the host plant and the arbuscular mycorrhizal fungus. The arbuscule is surrounded by the periarbuscular space, which is separated from the plant cytoplasm by the periarbuscular membrane. Phosphate is transported from the soil through the fungal hyphal network in the form of poly-phosphate granules. P_i is released inside the arbuscules and is transported across the fungal plasma membrane and the periarbuscular membrane into the plant cytoplasm. In return, reduced carbon is delivered to the fungus in the form of hexoses, which are released from sucrose in the periarbuscular space and are subsequently transported across the fungal plasma membrane by a fungal hexose transporter. Hexoses are used for the synthesis of glycogen and triacylglycerol (TAG). PPM: plant plasma membrane, FPM: fungal plasma membrane, PAS: periarbuscular space, Pi: inorganic phosphate, Poly-P: phosphate granules, TAG: triacylglycerol

The non-polar lipid and phospholipid composition of hyphae and spores of *Glomus intraradices* has been previously analyzed (Olsson and Johansen, 2000). One of the major motivations for the analysis of the fatty acid profile was the quest for a reliable biochemical marker for fungal biomass determination. In addition to the membrane bound phospholipids, mycorrhiza fungi are known to comprise large amounts of non-polar lipids, mainly triacylglycerol (TAG), in the hyphae and spores (Jabaji-Hare *et al.*, 1984). Microscopic analysis of mycorrhized roots reveals a large number of vesicles surrounded by the periarbuscular membrane, which are considered to be a means of transport for TAG. Analysis of the fatty acid profile showed 16:1ω5 and 16:0 fatty acids to be predominant in the non-polar lipid fraction, whereas the phospholipids additionally contained 18:1ω7(Olsson and Johansen, 2000). In a different study, the phospholipid fraction was shown to contain considerable amounts of the polyunsaturated fatty acids 20:4 and 20:5 (Johansen *et al.*, 1996). In a recent gene expression profiling experiment of arbuscules and neighboring cells a strong upregulation of numerous genes involved in lipid metabolism was revealed. Among them was the gene encoding for a digalactosyldiacylglycerol synthase (DGD2), indicating a role for the glycolipid DGDG in arbuscule formation. This study provided increasing evidence for the importance of lipid biosynthesis in the formation of the extensive membrane system required for arbuscule generation; in particular for the synthesis of the periarbuscular membrane (Gaude *et al.*, 2012).

1.4 Aim

Lipids are involved in numerous important cellular processes including signalling, energy storage and membrane formation. Membrane properties in particular are of great importance for plant-microbe symbiosis, as membranes represent the interface of all interactions between the two partners. The galactolipid DGDG was previously shown to be involved in root nodule symbiosis, because it constitutes an important integral part of the peribacteroid membrane and is crucial for nodule formation during phosphate deprivation.

The aim of this work was the analysis of the putative functions of the glycolipids sterol glucoside and glucosylceramide during root-nodule symbiosis and arbuscular mycorrhiza formation in the model plant *Lotus japonicus*. To this end, comprehensive lipid profiles of *Lotus japonicus* roots and of the symbiotic tissues, nodules and mycorrhized roots, were to be generated, to monitor lipid changes during symbiosis. This strategy required the development of novel methods for lipid analysis to record lipid profiles from low amounts of plant tissue. Mass spectrometry based approaches for the quantification of glycerolipids and sphingolipids were to be adapted for the analysis of the samples at hand. For the quantification of free and conjugated sterols by mass spectrometry, no method has been described to date. Therefore, one focus of this work was the establishment of a novel Q-TOF MS based method for comprehensive quantification of free and conjugated sterols in plants. In addition, gene expression of glycosyltransferase genes was to be monitored during nodulation and mycorrhiza formation

In a second approach, transgenic *Lotus japonicus* plants and mutants affected in sterol glucoside and glucosylceramide biosynthesis were to be analyzed, to unravel putative functions of these lipids in nodulation and mycorrhiza formation. To this end, TILLING mutants should be obtained which carry point mutations in the SGT genes. In addition, transgenic *Lotus* RNAi plants were to be generated with a downregulated gene expression for the sterol glucosyltransferases *SGT1* and *SGT2* and for the glucosylceramide synthase *GCS*. In all plants, the glycolipid content was to be analyzed and plants with decreased amounts of sterol glucosides or glucosylceramides were to be characterized with regard to their ability to undergo symbiosis with *Mesorhizobium loti* and *Glomus intraradices*. To this end, nodulation and mycorrhization assays were to be performed, to determine, whether a decrease in glycolipid content affects symbiosis efficiency or causes changes in the symbiotic structures.

2 Materials and Methods

2.1 Materials

2.1.1 Equipment

Autoclave	Tuttnauer Systec, Kirchseeon-Buch (D)
Balance 770	Kern, Balingen-Frommern (D)
Balance PG503-S Delta Range	Mettler Toledo, Gießen (D)
Binocular microscope SZX16	Olympus, Hamburg (D)
Camera DP7Z for microscope	Olympus, Hamburg (D)
Centrifuge 5810 R	Eppendorf, Hamburg (D)
Centrifuge 5417R	Eppendorf, Hamburg (D)
Growing cabinet, Rumed	Rubarth Apparate GmbH (D)
Heating block	Bioer, Hangzhow (CHN)
Homogeniser Precellys®24	PeQlab, Erlangen (D)
Incubator, Kelvitron®t	Thermo Scientific Heraeus®, Waltham (USA)
Incubation shaker, Multitron 28570	INFORS, Einsbach (D)
Light microscope BH-2	Olympus, Hamburg (D)
Microtome Leica RM 2155	Leica Instruments GmbH, Nussloch (D)
Mixer mill MM400	Retsch, Haan (D)
Photometer, Specord 205	Analytik Jena, Jena (D)
Running chamber for gel electrophoresis	Cti, Idstein (D)
Sample concentrator	Techne (Bibby Scientific), Stone (UK)
Spectrophotometer Nanodrop 1000	PeQlab, Erlangen (D)
Sterile bench model 1.8	Holten Lamin Air, Allerød (DK)
Thermocycler Tpersonal	Biometra, Göttingen (D)
Vortex Cetromat® MV	Braun Biotech, Melsungen (D)
6530 Accurate-mass quadrupole time-of-flight (Q-TOF) LC/MS	Agilent, Böblingen (D)
7890 Gas chromatograph (GC) with flame ionization detector (FID)	Agilent, Böblingen (D)
7890 Gas chromatograph (GC) with mass spectrometer (MS)	Agilent, Böblingen (D)

2.1.2 Consumables

Coverslips, 24 mm x 60 mm	Marienfeld, Lauda Königshofen (D)
Glass pipettes	Brand, Wertheim (D)
Glass tubes, 8 mL	Fisher Scientific, Schwerte (D)
Glass tubes, 8 mL with 40 GL thread	Agilent, Böblingen (D)
Glass vials and inlets for sample analysis	Agilent, Böblingen (D)
Microliter pipette tips type 3 series 1700	Labomedic, Bonn (D)
Microscope slides, 76 x 26 x 1 mm	Marienfeld, Lauda Königshofen (D)
Petri dishes 94 x 16 mm	Greiner bio-One, Frickenhausen (D)
Petri dishes 145 x 20 mm	Greiner bio-One, Frickenhausen (D)
Pots for plant cultivation, 10 cm	Pöppelmann, Lohne (D)
Reaction tubes, 1.5 mL and 2 mL	Sarstedt, Nümbrecht (D)
Reaction tubes, 15 mL and 50 mL	Greiner bio-One Frickenhausen (D)

Screw caps with GL 14 threads	Agilent, Böblingen (D)
Silica sand, grain size 1.4 – 2.3 mm	Quarzwerke Witterschlick GmbH, Alfter (D)
Sodium methylate	Merck, Darmstadt (D)
Soil, type „Pikier“	Gebrüder Patzer, Sinntal-Jossa (D)
SPE silica columns, Strata Si-1 1 mL	Phenomenex, Aschaffenburg (D)
Sterile filters, 0.2 µm pore size	Schleicher und Schuell, Dassel (D)
Teflon septa for GL 14 screw caps	Schmidlin, Neuheim (CH)
TLC plates Si 250, with concentration zone	J.T. Baker, Phillipsburg, NJ (USA)
Trays for plant cultivation	Pöppelmann, Lohne (D)
Vermiculite, grain size 2-3 mm	Rolfs, Siegburg (D)

2.1.3 Chemicals

Acetic acid	AppliChem, Darmstadt (D)
Acetone	Prolabo VWR, Darmstadt (D)
Agarose	PeQlab, Erlangen (D)
Ammonium acetate	Sigma-Aldrich, Taufkirchen (D)
Ammonium sulfate	Sigma-Aldrich, Taufkirchen (D)
Bacto agar	Duchefa Biochemie, Haarlem (NL)
Bacto peptone	Duchefa Biochemie, Haarlem (NL
Barium hydroxide	Riedel-de Haën (Honeywell), Seelze (D)
Betaine hydrochloride	Sigma-Aldrich, Taufkirchen (D)
Boric acid	Grüssing, Filsum (D)
Butylated hydroxytoluene	Sigma-Aldrich, Taufkirchen (D)
Cadmium carbonate	Sigma-Aldrich, Taufkirchen (D)
Calcium chloride	Merck, Darmstadt (D)
Chloroform	Merck, Darmstadt (D)
Diethylether	Prolabo VWR, Darmstadt (D)
Drierite	Fluka, Sigma-Aldrich, Saint-Louis (USA)
1, 4-Dioxane	Grüssing, Filsum (D)
Dipotassiumhydrogenphosphate	AppliChem, Darmstadt (D)
Ethanol 99 %, technical grade with 1 % MEK	Hofmann
Ethanol, p.A.	Merck, Darmstadt (D)
Ethidium bromide	Serva, Heidelberg (D)
Ethylenediaminetetraacetic acid (EDTA)	Roth, Karlsruhe (D)
Formaldehyde	AppliChem, Darmstadt (D)
Formic Acid	VWR, Darmstadt (D)
Gamborg B5 basal salt mixture 1000 x	Duchefa Biochemie, Haarlem (NL
Gamborg B5 vitamins 1000 x	Duchefa Biochemie, Haarlem (NL)
Gelrite	Duchefa Biochemie, Haarlem (NL)
Glucopyranosyl bromide tetrabenzoate	Sigma-Aldrich, Taufkirchen (D)
Glutaraldehyde	Sigma-Aldrich, Taufkirchen (D)
Glycerol	AppliChem, Darmstadt (D)
Hexane	Merck, Darmstadt (D)
Ink, “Quink” black	Parker, Saint Herblain (F)
Iodine	AppliChem, Darmstadt (D)
Iron-Ethylenediaminetetraacetic acid (Fe-EDTA)	Sigma-Aldrich, Taufkirchen (D)
Isopropanol	AppliChem, Darmstadt (D)
Magnesium chloride	AppliChem, Darmstadt (D)
Magnesium sulfate	Duchefa Biochemie, Haarlem (NL)
β-Mercaptoethanol	Sigma-Aldrich, Taufkirchen (D)

Methanol	J.T. Baker, Phillipsburg (USA)
Methanolic hydrochloric acid (3N)	Sigma-Aldrich, Taufkirchen (D)
Methylene chloride	AppliChem, Darmstadt (D)
Molybdenumtrioxide ammoniumtetrahydrate	Sigma-Aldrich, Taufkirchen (D)
α-Naphthol	Merck, Darmstadt (D)
N-methyl-N-(trimethylsilyl)-trifluoroacetamide (MSTFA)	AppliChem, Darmstadt (D)
3-(N-morpholino)propanesulfonic acid (MOPS)	AppliChem, Darmstadt (D)
ortho-Phthaldialdehyde (OPA)	Sigma-Aldrich, Taufkirchen (D)
Oxalyl chloride	Sigma-Aldrich, Taufkirchen (D)
Phosphoric acid	AppliChem, Darmstadt (D)
Potassium chloride	Merck, Darmstadt (D)
Potassium dihydrogenphosphate	Merck, Darmstadt (D)
Potassium hydroxide	Merck, Darmstadt (D)
Potassium nitrate	Grüssing, Filsum (D)
Pyridine	AppliChem, Darmstadt (D)
Sodium chloride	Duchefa Biochemie, Haarlem (NL)
Sodium hypochlorite	Roth, Karlsruhe (D)
Sorbitol	Duchefa Biochemie, Haarlem (NL)
Sucrose	Duchefa Biochemie, Haarlem (NL)
Talcum	Flora Apotheke, Bonn (D)
Technovit 3040	Heraeus Kulzer GmbH, Werheim (D)
Technovit 7100	Heraeus Kulzer GmbH, Werheim (D)
Tetrahydrofuran	Merck, Darmstadt (D)
Thionyl chloride	Fluka, Sigma-Aldrich, Saint-Louis (USA)
Toluene	Prolabo VWR, Darmstadt (D)
Toluidine blue	Sigma-Aldrich, Taufkirchen (D)
Tricine	Sigma-Aldrich, Taufkirchen (D)
Tris-(hydroxymethyl)-aminomethane	Duchefa Biochemie, Haarlem (NL)
Trizol®	Life Technologies (Invitrogen), Darmstadt (D)
Tween-20	Sigma-Aldrich, Taufkirchen (D)
Tryptone	AppliChem, Darmstadt (D)
Wheat germ agglutinin (WGA) alexa fluor	Life Technologies (Invitrogen), Darmstadt (D)
Yeast Extract	Duchefa Biochemie, Haarlem (NL)

2.1.4 Plant Hormones and Antibiotics

Benzylaminopurine (BAP)	Duchefa Biochemie, Haarlem (NL)
2,4-Dichlorophenoxyacetic acid (2,4-D)	Duchefa Biochemie, Haarlem (NL)
Indolbutyric acid	Sigma-Aldrich, Taufkirchen (D)
Kinetine	Duchefa Biochemie, Haarlem (NL)
Cefotaxime	Duchefa Biochemie, Haarlem (NL)
Geneticin-418 (G-418)	Duchefa Biochemie, Haarlem (NL)
Hygromycin B	Duchefa Biochemie, Haarlem (NL)
Spectinomycin	Duchefa Biochemie, Haarlem (NL)
Streptomycin	Duchefa Biochemie, Haarlem (NL)
Rifampicin	Duchefa Biochemie, Haarlem (NL)

2.1.5 Kits and Enzymes

First Strand cDNA Synthesis Kit	Fermentas, St. Leon-Rot (D)
MinElute Gel Extraction Kit	Qiagen, Hilden (D)
Plant Total RNA Mini Kit	DNA Cloning Service, Hamburg (D)
Omniscript RT Kit	Qiagen, Hilden (D)
SuperScript ™ III First Strand Synthesis System	Life Technologies (Invitrogen), Darmstadt (D)
T4 DNA Ligase (10 U/µL)	Fermentas, St. Leon-Rot (D)
DCS DNA Polymerase (10 U/µL)	DNA Cloning Service, Hamburg (D)
Taq DNA Polymerase (10 U/µL)	Fermentas, St. Leon-Rot (D)
Paq 5000 hotstart PCR Master Mix	Agilent, Böblingen (D)
*Hind*III (10 U/µL)	Fermentas, St. Leon-Rot (D)
*Hinf*I (10 U/µL)	Fermentas, St. Leon-Rot (D)
*Hph*I (10 U/µL)	Fermentas, St. Leon-Rot (D)
*Avr*II (10 U/µL)	Fermentas, St. Leon-Rot (D)
*Xho*I (10 U/µL)	Fermentas, St. Leon-Rot (D)
*Spe*I (10 U/µL)	Fermentas, St. Leon-Rot (D)

2.1.6 Internal Standards for Lipid Quantification

Pentadecanoic acid (15:0)	Sigma-Aldrich, Taufkirchen (D)
Cholesterol	Sigma-Aldrich, Taufkirchen (D)
Cholestanol	Sigma-Aldrich, Taufkirchen (D)
Stigmasterol	Sigma-Aldrich, Taufkirchen (D)
Stigmastanol	Sigma-Aldrich, Taufkirchen (D)
16:0-Cholesterol	Sigma-Aldrich, Taufkirchen (D)
16:1-Cholesterol	Sigma-Aldrich, Taufkirchen (D)
18:0-Cholesterol	Sigma-Aldrich, Taufkirchen (D)
18:1-Cholesterol	Sigma-Aldrich, Taufkirchen (D)
Cholestanol glucoside	synthesized during this work
Stigmastanol glucoside	synthesized during this work
Esterified (acylated) sterol glucoside mix, from soybean	Matreya LLC, Pleasant Gap (USA)
Gal-d18:1-c12:0	Avanti Polar Lipids, Alabaster AL (USA)
Gal-d18:1-c24:1	Avanti Polar Lipids, Alabaster AL (USA)
d18:1-12:0-Sphingomyelin	Avanti Polar Lipids, Alabaster AL (USA)
d18:1-17:0-Sphingomyelin	Avanti Polar Lipids, Alabaster AL (USA)
14:0 Lyso-PC	Avanti Polar Lipids, Alabaster AL (USA)
18:0 Lyso-PC	Avanti Polar Lipids, Alabaster AL (USA)
di14:0-PC	Avanti Polar Lipids, Alabaster AL (USA)
di20:0-PC	Avanti Polar Lipids, Alabaster AL (USA)
di14:0-PE	Avanti Polar Lipids, Alabaster AL (USA)
di20:0-PE	Avanti Polar Lipids, Alabaster AL (USA)
di14:0-PG	Avanti Polar Lipids, Alabaster AL (USA)
di20:0-PG	Avanti Polar Lipids, Alabaster AL (USA)
di14:0-PA	Avanti Polar Lipids, Alabaster AL (USA)
di20:0-PA	Avanti Polar Lipids, Alabaster AL (USA)
di14:0-PS	Avanti Polar Lipids, Alabaster AL (USA)
di20:0-PS	Avanti Polar Lipids, Alabaster AL (USA)

PI Mix, from soybean	Larodan, Malmö (S)
MGDG mix	Larodan, Malmö (S)
DGDG mix	Larodan, Malmö (S)
SQDG mix	Larodan, Malmö (S)
di-14:0-DAG	Larodan, Malmö (S)
di-14:1$^{\Delta 9cis}$-DAG	Larodan, Malmö (S)
di-20:0-DAG	Larodan, Malmö (S)
di-20:1$^{\Delta 14cis}$-DAG	Larodan, Malmö (S)
tri-10:0-TAG	Larodan, Malmö (S)
tri-11:1$^{\Delta 10cis}$-TAG	synthesized during this work
tri-20:0-TAG	Larodan, Malmö (S)
tri-22:1$^{\Delta 13cis}$-TAG	Larodan, Malmö (S)

2.1.7 Synthetic Oligonucleotides

Oligonucleotides were synthesized by AGOWA, Berlin (D).

bn 213	gaaggactcttgcggattac	Lj *Ubiquitin* forward RT-PCR
bn 214	gaggccacaacaaacgatac	Lj *Ubiquitin* reverse RT-PCR
bn 219	catgttgcggcagcattaag	Lj *GCS* forward RT-PCR
bn 220	ctttggctgatgccattgtg	Lj *GCS* reverse RT-PCR
bn 305	tggtagcctgcctgtacaag	Lj *SGT1* forward RT-PCR
bn 306	acagctccagtcactccatc	Lj *SGT1* reverse RT-PCR
bn 1208	ttgggcctcttgaagatcccac	Lj *SGT2* forward RT-PCR
bn 1209	atcaactgcggcagcaacac	Lj *SGT2* reverse RT-PCR
bn 889	agaccaggaacagctgcattttcaa	Lj *SGT2* forward CAPS
bn 890	tccaagtcaacaggtactgtgc	Lj *SGT2* reverse CAPS
bn 1367	ggaaagggctcttcttcctgac	Lj *SGT1* forward CAPS
bn 1368	taagcgctaggccttggcatac	Lj *SGT1* reverse CAPS

2.1.8 Plants

Arabidopsis thaliana wild type, ecotype Columbia-0	
Arabidopsis thaliana pho1 mutant	(Poirier *et al.*, 1991)
Lotus japonicus wild type, ecotype Gifu	Jens Stougaard, University of Aarhus (DK)

2.1.9 Bacteria and Fungi

Agrobacterium tumefaciens LBA4404	(Stiller *et al.*, 1997)
Escherichia coli XL1Blue	Stratagene (Agilent, Böblingen, (D))
Glomus intraradices	Agrauxine (F)
Glomus intraradices (in axenic root culture with *Agrobacterium rhizogenes* transformed chicory roots)	Department of Genetics, LMU München (D)
Mesorhizobium loti R7a	Department of Microbiology, University Dunedin (NZ)
Pichia pastoris sgt/gcs deletion mutant	Dirk Warnecke, University of Hamburg (D)
Saccharomyces cerevisiae INVScI	Life Technologies (Invitrogen), Darmsatdt (D)

Table 1: Cloning Vectors

Vector	Description	Reference
pLH6000	Binary vector for the expression of RNAi constructs in plants, Sm/Sp^R in bacteria G-418 resistance in plants	Hermann Schmidt, Cloning Service, Hamburg (D)
pLH9000	Binary vector for the expression of RNAi constructs in plants, Sm/Sp^R in bacteria Hygromycin B resistance in plants	Hermann Schmidt, Cloning Service, Hamburg (D)
pDR196	vector for heterologous expression in *Saccharomyces cerevisiae*, Amp^R, URA3	Rentsch *et al.*, 1995
pSC-B	cloning vector, Amp^R	Stratagene (Agilent, Böblingen, (D))
pPic3.5	vector for heterologous expression in *Pichia pastoris,* Amp^R, HIS4	Life Technologies (Invitrogen), Darmsatdt (D)

Table 2: Recombinant Plasmids

Construct	Insert	Expression Vector	Organism of Destination
pLH- RNAi-*SGT1*	*LjSGT1*RNAi	pLH9000	*Lotus japonicus*
pLH- RNAi-*SGT2*	*LjSGT2*RNAi	pLH6000	*Lotus japonicus*
pLH- RNAi-*GCS*	*LjGCS*RNAi	pLH9000	*Lotus japonicus*
pD-oe-*SGT1*	*LjSGT1*	pDR196	*Saccharomyces cerevisiae*
pD-oe-*SGT2*	*LjSGT2*	pDR196	*Saccharomyces cerevisiae*
pD-oe-*GCS*	*LjGCS*	pDR196	*Saccharomyces cerevisiae*
pP-oe-*SGT1*	*LjSGT1*	pPic3.5	*Pichia pastoris*
pP-oe-*SGT2*	*LjSGT2*	pPic3.5	*Pichia pastoris*
pP-oe-*GCS*	*LjGCS*	pPic3.5	*Pichia pastoris*

2.2 Methods

2.2.1 Cultivation of *Arabidopsis thaliana*

Arabidopsis thaliana, wild type and *pho1* mutant plants, grown for four weeks on a mixture of soil and vermiculite (2:1) at 20 °C, 55 % relative humidity and 8 hrs of light (150 µmol m^{-2} s^{-1}) before sampling of leaf and root material. For phosphate deprivation experiments, plants were grown in sterile culture in growth cabinets with 20 °C, 55 % relative humidity and 8 hrs of light (150 µmol m^{-2} s^{-1}). Seeds were germinated on 2 X Murashige and Skoog medium (2 MS) and grown for 2 weeks. Subsequently, seedlings were transferred to synthetic nutrient medium with or without phosphate and grown for at least 2 weeks, until the phosphate deprived plants showed clear signs of phosphate starvation (red leaf color due to anthocyanin accumulation).

Synthetic *Arabidopsis* Nutrient (2 X)

0.8 % (w/v) agarose
1 % (w/v) sucrose
2.5 mM KNO_3
1 mM $MgSO_4$
1 mM $Ca(NO_3)_2$
1 mM KH_2PO_4
25 µM Fe-EDTA
35 µM H_3BO_3
7 µM $MnCl_2$
0.25 µM $CuSO_4$
0.5 µM $ZnSO_4$
0.1 µM Na_2MoO_4
5 µM NaCl
5 nM $CoCl_2$

Murashige and Skoog Medium (2 MS)

4.8 g/L MS salts including vitamins
10 g/L sucrose
9 g/L plant agar

2.2.2 Cultivation of *Lotus japonicus*

Lotus japonicus plants were grown on soil at 22 °C to 24 °C, 55 % relative humidity and 16 hrs of light (150 µmol m^{-2} s^{-1}) for propagation and seed production. For phosphate deprivation experiments, wild type and mutant plants were propagated by cuttings, which were allowed to form roots for 3-4 weeks on a mixture of sand and vermiculite (2:1) with full nutrient supply. The plants were then transferred to pots with silica sand and watered with nutrient solution containing 2.5 mM or 0 mM phosphate for 4 to 8 weeks, until the leaves of phosphate deprived plants showed significantly increased levels of the galactolipid DGDG (for quantification of lipids by Q-TOF MS see 2.2.7.8). For nodulation experiments all equipment, substrates and solutions used for plant cultivation were sterilized prior to use, in order to avoid uncontrolled nodulation. In addition, plants for nodulation experiments were grown in sterile growth cabinets in the absence of soil or nonsterile plants.

***Lotus* Nutrient Solution (1L)**

1.25 mM K_2HPO_4
1.25 mM KH_2PO_4
0.5 mM KNO_3
0.5 mM $MgSO_4$
0.25 mM KCl
0.25 mM $CaCl_2$
0.025 mM Fe-EDTA
0.25 mL trace Elements

Trace Elements Stock Solution

9.2 mM $MnCl_2$
46.3 mM H_3BO_3
0.81 mM $ZnCl_2$
0.11 mM $NaMoO_4$
0.29 mM $CuCl_2$

$CaCl_2$ was added as the final ingredient, in order to avoid salt precipitation. For phosphate or nitrogen deprivation experiments, KNO_3 or K_2HPO_4 and KH_2PO_4 were omitted and substituted with KCl. KNO_3 was increased to 5 mM in nodulation experiments (see 2.2.4)

2.2.3 Stable Transformation of *Lotus japonicus*

Stable transgenic *Lotus japonicus* plants, carrying RNAi constructs for the downregulation of gene expression of the glucosyltranferase genes *SGT1*, *SGT2* or *GCS* were generated by *Agrobacterium tumefaciens* mediated transformation. To this end, wild type seeds of *Lotus japonicus* were shock frozen for 10 sec in liquid nitrogen and submerged in 96 % (v/v) ethanol for another 10 sec. The seeds were then dried thoroughly and sterilized for 20 min with sterilization solution (2 % (v/v) sodium hypochlorite and 0.0001 % (v/v) Tween 20). The sterilization solution was discarded and the seeds rinsed at least five times with sterile water. The surface-sterilized seeds were subsequently germinated on water-agar medium (tap water solidified with 0.6 % (w/v) agar) in the dark, at 21 °C for 5 days, where they formed etiolated hypocotyls. Prior to transformation, the plants were exposed to light for 24 hrs.

Agrobacterium tumefaciens LBA 4404 cells, carrying the RNAi constructs pLH9000-RNAi-*SGT1*, pLH6000-RNAi-*SGT2* or pLH9000-RNAi-*GCS* as well as the empty vector control were grown at 28 °C and 200 rpm in YEB medium containing rifampicin (80 µg/mL), streptomycin (300 µg/mL) and spectinomycin (100 µg/mL), for antibiotic selection as described in 2.2.6.6.1.

For the transformation of *Lotus* hypocotyls, the seedlings were placed in petri dishes containing co-cultivation medium. Roots and cotyledons were removed and the hypocotyls were cut into pieces of 3-5 mm length, in the presence of *Agrobacterium*. At least 100 plants were used for transformation with each construct. The hypocotyls were placed on petri dishes containing several layers of sterile filter paper, moistened with co-cultivation medium. The petri dishes were kept in the dark for the duration of the infection process (7 days), before the hypocotyls were transferred to selective callus medium (SCM), containing antibiotics (G-418 or hygromycin B). In order to monitor selection efficiency and tissue regeneration, 20 hypocotyls each were cut in the absence of *Agrobacterium* and later placed on SCM with or without antibiotics. The hypocotyls were kept on SCM for up to 20 weeks until callus tissue was formed from transformed cells. Calli with a size of 5 mm in diameter were separated from the hypocotyls and placed on shoot induction medium (SIM). They were kept on SIM for a maximum of 6 – 10 weeks, before they were transferred to shoot growth medium (SGM). Calli with shoots were kept on this medium for 2 weeks, before being transferred to shoot elongation medium (SEM). Calli without shoots remained on SGM until shoots were formed. During the whole process, the hypocotyls were placed onto fresh medium every 7-10 days.

For regeneration of mature plants, long shoots with several internodes were cut from the callus. The stem was powdered with 1 % (w/w) indolebutyric acid (in Talcum), placed on soil (Pikiererde) and kept in glass jars until roots were formed. The transformation procedure was repeated until 10 to 20 independent lines could be obtained for each construct.

Co-Cultivation Medium
1/10 Gamborg B5 medium LO
3 µg/mL kinetin
3 µg/mL 2,4-D
40 µL 1000 x B5 vitamins
5 mM MES
pH 5.2 (adjust pH with NaOH)

Gamborg B5 Medium LO
3.052 g Gamborg B5 basal salt mixture
ad 900 mL ddH_2O
pH 5.5 (adjust pH with NaOH)
0.25 % (w/v) gelrite

Selective Callus Medium (SCM)
Gamborg B5 medium LO
3 µg/mL kinetin
3 µg/mL 2,4-D
300 µg/mL cefotaxime
1 x B5 vitamins
2 % (w/v) sucrose
25 µg/mL G-418
or 15 µg/mL hygromycin B

Shoot Induction Medium (SIM)
Gamborg B5 medium LO
5 mM $(NH_4)_2SO_4$
0.2 µg/mL BAP
1 x B5 vitamins
2 % (w/v) sucrose
25 µg/mL G-418
or 15 µg/mL hygromycin B

Shoot Growth Medium (SGM)
Gamborg B5 medium LO
0.2 µg/mL BAP
1 x B5 vitamins
2 % (w/v) sucrose
25 µg/mL G-418
or 15 µg/mL hygromycin B

Shoot Elongation Medium (SEM)
Gamborg B5 medium LO
1 x B5 vitamins
2 % (w/v) sucrose

All antibiotics, vitamins and plant hormones were prepared as 1000 x concentrated stock solutions, sterile filtrated and stored as aliquots at -20 °C. G-418 was used as selective antibiotic for pLH9000 constructs, hygromycin B was used for the selection of pLH6000.

2.2.4 Nodulation of *Lotus japonicus*

Controlled nodulation of *Lotus japonicus* with the soil bacterium *Mesorhizobium loti* was achieved by semi-sterile cultivation of *Lotus* prior to the inoculation procedure. Wild type, transgenic empty vector control or transgenic RNAi plants were grown from seeds or propagated via cuttings and kept on autoclaved sand-vermiculite (2:1) in surface-sterilized pots and trays, in order to avoid premature nodulation. To exclude contamination by rhizobia, plants grown for nodulation experiments were kept separate from plants grown on soil, in semi-sterile growth cabinets. The plants were grown on sand-vermiculite (2:1) under full nutrient supply for 3-4 weeks, until they formed roots. They were subsequently placed on autoclaved sand and watered with nutrient solutions (see 2.2.2) containing 5 mM nitrogen and 2.5 mM or 0 mM phosphate. The plants were deprived of phosphate for 4 to 8 weeks until a significant increase in the amounts of the galactolipid DGDG could be detected in the leaves (see 2.2.2). Leaves of plants grown under full phosphate supply generally contained around 30 mol% DGDG. Plants were

designated as sufficiently deprived of phosphate, when the DGDG content was increased to around 35 mol%.

2.2.4.1.1 Cultivation of *Mesorhizobium loti*

Mesorhizobium loti was cultivated at 28°C and 300 rpm in TY medium for 3-5 days. The cells were harvested by centrifugation (10 min, 4000 g) and resuspended in nutrient solution without phosphate to an OD_{600} of 0.01 to 0.05. For the inoculation of *Lotus* plants, 5 to 20 mL were applied to each pot and the plants were removed from the sterile cabinets and placed into plant growth chambers. For an optimal infection process, the inoculation procedure was repeated once, within one week. After 2 to 4 weeks, the number of nodules per plant was determined and tissue samples were taken for microscopy, RT-PCR or lipid quantification.

TY medium
0.5 % (w/v) tryptone
0.3 % (w/v) yeast extract
0.45 mM $CaCl_2$

1.5 % (w/v) bacto agar was added for solidified medium.

2.2.5 Mycorrhization of *Lotus japonicus*

Granular inoculum, containing spores of *Glomus intraradices* was purchased from Agrauxine, France. For the analysis of mycorrhiza formation in transgenic *Lotus japonicus* plants, seedlings or cuttings were grown as described before (see 2.2.2), but under non-sterile conditions. No phosphate source was contained in the nutrient solution. However, residual phosphate derived from the purchased inoculum and from the vermiculite could not be excluded. For the inoculation, plants were transferred onto a mixture of sand-vermiculite (2:1) and inoculum (1:10). After 3 weeks, the degree of fungal colonization in the roots was determined.

Staining of Mycorrhized Roots with Ink and Vinegar

The degree of fungal colonization in mycorrhized *Lotus* roots was determined by light microscopy, after the staining of fungal structures with ink and vinegar. *Lotus* plants were mycorrhized for 3 weeks and then stained according to the protocol described by (Vierheilig *et al.*, 1998). Root systems were incubated in 1 mL 10 % (w/v) KOH at 95 °C for 7 min and then rinsed with water. The roots were washed with 10 % (v/v) acetic acid and then incubated in staining solution (5 % (v/v) ink and 5 % (v/v) acetic acid) for 7 min at 95 °C. Subsequently, the roots were washed with water 3 times and then incubated in 5 % (v/v) acetic acid for 30 min at

RT and then overnight at 4 °C. The next day, the samples were washed with water three times and then stored at 4°C.

Staining of Mycorrhized Roots with WGA Alexa Fluor ®

The staining of the fungal polysaccharide chitin with wheat germ agglutinin (WGA) coupled to Alexa Fluor was used to qualitatively analyze fungal structures via fluorescence microscopy. *Lotus* roots were incubated in 1 mL 10 % (w/v) KOH at 95 °C for 7 min and then rinsed with water, before they were placed into WGA staining solution. The Eppendorf tubes were wrapped in aluminum foil to protect the samples from light. In order to improve the infiltration of the root tissue with the staining solution, the lids of the tubes were perforated and the samples were placed into a desiccator for at least 1 h. The vacuum was renewed every 15 minutes. Subsequently the roots were rinsed with 1x PBS and stored at 4 °C for up to 2 months. WGA Alexa Fluor has an excitation wavelength of 495 nm and an emission wavelength of 519 nm.

WGA Alexa Fluor ® Solution	**1x PBS**
2 mM sodium azide	137 mM NaCl
1 mg /mL WGA Alexa Fluor	2.7 mM KCl
in 1x PBS pH 7.4	12 mM phosphate (Na_2HPO_4, KH_2PO_4)
	pH 7.4

Quantification of the Degree of Fungal Colonization

The degree of fungal colonization was determined as described by McGonigle *et al.*, (1990). *Lotus japonicus* roots with endomycorrhizal structures were stained with ink and vinegar and analyzed by light microscopy. Root fragments were placed onto microscope slides in five parallel rows of approx. 6 cm. The roots were screened for hyphae, arbuscules and vesicles at 10 randomly chosen positions in regular intervals. This method allowed the evaluation of 50 representative positions within the root system. For each position, the presence or absence of hyphae, arbuscules and vesicles was recorded. For a statistical evaluation of a mycorrhiza phenotype, at least ten plants should be analyzed.

2.2.6 Molecular Biology Techniques

2.2.6.1 Isolation of TILLING mutants for *SGT1*, *SGT2*, *GCS*

Lotus RNAi lines, which show a downregulated gene expression of the glycosyltransferase genes *SGT1*, *SGT2* and *GCS* can be generated by *Agrobacterium* mediated transformation, as described in 2.2.3. However, using this method no null mutations of the target

genes which are totally devoid of expression can be obtained. Alternatively, *Lotus* mutants affected in a gene of interest can be obtained by the generation of *Lotus* EMS (ethyl methanesulfonate) mutants. The genomes of these plants carry point mutations (or insertions/deletions) induced by EMS treatment, which can cause an amino acid exchange or lead to a truncated protein due to a premature stop codon in the gene. In a reverse genetic approach, mutants affected in a specific gene of interest can be isolated by a process termed TILLING (Targeting Induced Local Lesions in Genomes). The TILLING approach for the genes *SGT1*, *SGT2* and *GCS* was done by a company (RevGen, UK). This company offers the identification of mutants from an EMS mutant population by TILLING and finally provides seeds of heterozygous mutants with the corresponding sequence information flanking the mutation.

For the identification of these mutants, the information on the complete nucleic acid sequence of the gene of interest has to be provided by the customer.

The sequence information for the genomic loci of *SGT1*, *SGT2* and *GCS* was obtained from Kazusa genomic database (http://www.kazusa.or.jp/lotus/). While the sequence information on *SGT2* and *GCS* was complete, large fragments of the *SGT1* gene were not available.

2.2.6.2 Sequencing of *Lotus japonicus SGT1*

In order to obtain a complete gene sequence for *SGT1*, gene specific primers were designed for the stepwise amplification of the missing fragments of genomic DNA by PCR. PCR products were purified from agarose gels (see 2.2.6.8.2) and sequenced (LGC Genomics, Berlin). The sequences were assembled using the Laser Gene software (DNAStar). Both strands of the SGT1 sequence were sequenced. The sequencing of the *SGT1* gene from *Lotus japonicus* was carried out with the help of Dr. Bettina Kriegs (IMBIO Institute, University of Bonn). The sequence information was submitted to the Genebank database and is available with the accession number JF912509.

2.2.6.3 CAPS Marker Analysis for the Genotyping of *Lotus* TILLING Mutants

Lotus japonicus TILLING (Targeted Induced Local Lesions in Genome) mutants carry point mutations (in some cases also insertions/deletions) in the gene of interest, leading to premature stop codons or amino acid exchanges in the protein sequence. Mutant lines affected in the genes encoding the glycosyltransferases SGT1, SGT2 and GCS were ordered from RevGen, UK. Homozygous plants were identified by CAPS (Cleaved Amplified Polymorphic Sequences) marker analysis, a technique designed to detect polymorphisms at a specific gene locus. Gene specific primers were designed to amplify gene fragments spanning the mutation site and restriction enzymes were chosen which exclusively cleave either the mutated sequence or the wild type sequence.

2.2.6.4 Isolation of Genomic DNA from Plant Tissue

For the extraction of genomic DNA from *Lotus japonicus*, 10-100 mg of leaf tissue were frozen in liquid nitrogen and ground to a fine powder using a ball mill (Precellys). 1 mL of CTAB (cetyltrimethylammonium bromide) buffer was added and the mixture was incubated at 65 °C for 10 min with occasional shaking. Subsequently, 0.4 mL of chloroform was added, mixed with the sample and phase separation was achieved by centrifugation for 5 min at 1800 g. The aqueous phase was transferred to a fresh tube, mixed with 0.7 mL of isopropanol and incubated on ice for 10 min. Precipitated DNA was harvested by centrifugation (10000 g, 5 min) and the pellet was washed with cold 70 % (v/v) ethanol by an additional centrifugation step (10000 g, 5 min). The pellet was dried and the DNA was dissolved in 50 µL ddH_2O. DNA concentration was determined with the Nanodrop 1000 photometer by measuring the absorption at a wavelength of 260 nm.

CTAB Buffer
0.1 M Tris, pH 8.0
20 mM EDTA, pH 8.0,
280 mM NaCl
20 % (w/v) CTAB

The pH for Tris was adjusted with HCl, the pH for EDTA was adjusted with NaOH.

2.2.6.4.1 Polymerase Chain Reaction

DNA fragments from *Lotus* DNA were amplified by polymerase chain reaction with DNA-polymerases from *Pyrococcus* (*Paq*) or *Thermus aquaticus* (*Taq*) with 100 ng of DNA as a template. Gene specific primers were designed for *SGT1* and *SGT2* to amplify a fragment of the DNA including the mutation site (see Table 3). DNA was amplified by 35 cycles of denaturation, primer annealing and elongation and used for CAPS marker analysis. Annealing temperature was 58 °C for *SGT1* and 64 °C for *SGT2*.

PCR Reaction-Mix (*Taq*)
0.5 µL *Taq*-polymerase (1 U/µL)
1 µL DNA
1 µL primer forward (10 pmol/µL)
1 µL primer reverse (10 pmol/µL)
2.5 µL 10 X buffer
2 µL dNTPs (2.5 mM per nucleotide)
1.5 µL $MgCl_2$ (25 mM)
add ddH_2O to a final volume of 25 µL

PCR-Program
94 °C denaturation 3 min
94 °C denaturation 30 sec
58 °C or 64 °C annealing 30 sec
72 °C elongation 60 sec
72 °C elongation 10 min

2.2.6.4.2 Restriction Analysis of DNA with Endonucleases

CAPS (Cleaved Amplified Polymorphic Sequences) marker analysis is a tool for the genotyping of mutants carrying point mutations. This technique takes advantage of the fact that endonucleases recognize specific nucleic acid sequences of 4-6 base pairs. Exchanges of single nucleotides in the recognition site of endonucleases may prevent the cleavage of the DNA at this position or lead to the formation of additional restriction sites. Therefore, the restriction pattern of a mutant carrying such a point mutation differs from that of a wild type plant. Table 3 shows the numbers and lengths of the DNA fragments obtained after restriction of PCR products for the TILLING mutants *sgt1-5305* and *sgt2-2656*. PCR products were obtained with gene specific primers as described in 2.2.6.4.1 and subsequently cleaved by restriction enzymes for 2 -3 hrs at 37 °C (see Table 3). The cleaved products could be stored at -20 °C or separated immediately by gel electrophoresis on agarose gels as described in 2.2.6.5.5.

Restriction Assay
5 µL PCR product
0.5 µL restriction enzyme (10 U/µL)
2 µL 10 x buffer
add ddH_2O to a final volume of 20 µL

Table 3: CAPS Marker Analysis of the TILLING Mutants *sgt1-5305* and *sgt2-2656*.

TILLING Line	Mutation	Primer	PCR Product	Restriction Enzyme	Wt Fragments	Mutant Fragments
sgt1-5305	10637G>A 338W>X	bn 1367 bn 1368	1150 bp	*Hinf*I	596 bp 423 bp 131 bp	596 bp 554 bp
sgt2-2656	4680G>A 297W>X	bn 889 bn 890	491 bp	*Hph*I	491 bp	160 bp 331 bp

2.2.6.5 Analysis of Gene Expression by Semi-Quantitative RT-PCR

2.2.6.5.1 Isolation of RNA from Plants with TRIzol

For the isolation of RNA from *Lotus japonicus,* RNAse-free plastic ware were used. All solutions were treated with DEPC (diethylpyrocarbonate) to a final concentration of 0.1 % (v/v), incubated overnight at 37 °C with stirring and autoclaved twice, prior to use.

50 -100 mg of plant material were shock frozen in liquid nitrogen and ground to a fine powder in a mixer mill (Retsch). The tissue was incubated in 1 mL of TRIzol at RT for 5 min. Cell debris was sedimented by centrifugation (12000 g, 10 min, 4 °C) and 200 µL of chloroform were

added to the supernatant. RNA was extracted with vigorous shaking and subsequent incubation at RT for several minutes. Phase separation was achieved by an additional centrifugation step at 12000 g and 4 °C for 15 min. The supernatant was harvested and added to 500 µL of isopropanol. The mixture was inverted and RNA was precipitated at RT for 10 min. RNA was sedimented by centrifugation (12000 g, 10 min,4 °C) and the pellet was washed twice with 75 % (v/v) ethanol p. A. (7500 g, 5 min, 4 °C). The ethanol was removed and the pellet was dried at RT for several minutes. Subsequently the dried pellet was dissolved in 30-50 µL of DEPC treated water and stored at –80 °C. The RNA concentration was determined with the NanoDrop 1000 photometer at a wavelength of 260 nm. At this wavelength, a signal of 1.0 corresponds to a concentration of 40 µg/mL RNA. For quality control, the absorption at 230 nm and 280 nm was also determined. The ratio of A_{260}/A_{280} is indicative for contaminations, e.g. from DNA. An A_{260}/A_{280} ratio of 1.8 to 2.0 is considered an indicator for good quality RNA, free of contaminations. In addition, contaminants like chaotropic salts, proteins and phenol show a high absorption at approximately 230 nm. Therefore, the ratio of A_{260}/A_{230} is another indicator for sample purity, which should ideally also be close to 2.0.

2.2.6.5.2 Isolation of RNA from Plants with RNA Extraction Kits

Extraction of RNA from *Lotus japonicus* roots and from phosphate deprived plants was performed with an RNA extraction kit (DNA Cloning Service) according to the supplier's instructions.

2.2.6.5.3 RNA Gel Electrophoresis

RNA gel electrophoresis was employed for quality control and exact adjustment of RNA amounts required for semi-quantitative RT-PCR. For the preparation of a formaldehyde gel, agarose was mixed with ddH_2O and melted in the microwave oven. MOPS buffer (pH 8) was added and the mixture was cooled down at RT for several minutes before formaldehyde was added. After the addition of formaldehyde, the gel was immediately poured and was allowed to polymerize for at least 30 min. RNA running buffer, containing formaldehyde, could be reused several times when stored in a closed glass bottle. 10 x stock solutions of MOPS buffer were autoclaved prior to use and stored in the dark.

1-3 µg of RNA were mixed with DEPC treated water to a final volume of 10 µL and added to the same volume of RNA sample buffer. RNA samples were incubated at 65 °C for 10 min, placed on ice and separated on a formaldehyde gel for 30 min at 90 V. The RNA was detectable under UV light (λ=302 nm) due to fluorescence caused by intercalation of the RNA with ethidium bromide. High quality samples displayed distinct bands of ribosomal RNAs with no sign of degradation. For samples displaying bands with deviating intensity, sample volumes were

corrected and gel electrophoresis was repeated until all samples showed ribosomal bands of comparable intensity. The RNA concentrations applied for these gels were subsequently used for cDNA synthesis.

RNA Sample Buffer
65 % (v/v) formamide
8 % (v/v) formaldehyde
1.3 % (w/v) 1x MOPS, pH 8
54 µg/ml ethidium bromide

10 x MOPS Buffer
0.2 M MOPS
50 mM sodium acetate
10 mM Na-EDTA
adjusted to pH 7 or pH 8 with NaOH

1.5 % (w/v) Agarose Gel
1.5 % (w/v) agarose
6 % (v/v) formaldehyde
in 1x MOPS, pH 8

RNA Running Buffer
10 % (v/v) formaldehyde
in 1x MOPS, pH 7

2.2.6.5.4 First Strand cDNA Synthesis and Reverse Transcription PCR (RT-PCR)

Semi-quantitative RT-PCR was employed to analyze the gene expression of *SGT1*, *SGT2* and *GCS* in the transgenic RNAi lines and during plant-microbe interactions. To this end, mRNA from *Lotus japonicus* was transcribed into cDNA using a first strand cDNA synthesis kit (from Fermentas, Qiagen or Invitrogen). The cDNA was subsequently amplified by a semi-quantitative PCR reaction with gene specific primers.

RNA samples of high quality and equal concentrations as verified by RNA gel electrophoresis were used for cDNA synthesis with reverse transcriptase. cDNA was synthesized with a cDNA synthesis kit, using oligo dT primers according to the instructions supplied by the manufacturer. Generally 1 µg of RNA was diluted with DEPC treated water to a final volume of 8 µL and added to 1 µL of dNTPs and 1µL of oligo dT_{20} primers. The mixture was incubated at 65 °C for 5 min and then cooled down on ice. A master mix of 2 µL RT buffer, 4 µL 25 mM $MgCl_2$, 2 µL 0.1 M DTT, 1 µL RNAse Out and 1 µL reverse transcriptase for each sample was prepared and 10 µL added to each sample. The reaction took place at 50 °C for 50 min and was stopped by an incubation step at 85 °C for 5 min. For removal of RNA after cDNA synthesis, 1 µL of RNAse H was added and the samples were incubated at 37 °C for 20 min. cDNA was stored at -20 °C and used as a template for subsequent PCR reactions.

Polymerase chain reaction was carried out with a DNA polymerase from *Pyrococcus* (*Paq*) for amplification of *SGT1* and *GCS*. For the amplification of *SGT2* and *Ubiquitin*, DNA polymerase from *Thermus aquaticus* (*Taq*) was used. Gene specific primers were designed for *GCS*, *SGT1* and *SGT2* and for the housekeeping gene *Ubiquitin*, which was used as a control. Where possible, primers were designed to amplify DNA fragments spanning intron-exon borders in order to be able to distinguish fragments amplified from cDNA from those amplified from residual genomic DNA. DNA was amplified by 25 to 27 cycles of denaturation, primer annealing

and elongation and later loaded onto agarose gels and stained with ethidium bromide. The signal intensities of the PCR products from different samples were compared for an estimation of gene expression.

PCR Reaction-Mix (*Taq*)
0.5 µL *Taq*-polymerase (1 U/µL)
2 µL cDNA
1 µL primer forward (10 pmol/µL)
1 µL primer reverse (10 pmol/µL)
2.5 µL 10 X buffer
2 µL dNTPs (2.5 mM per nucleotide)
1.5 µL $MgCl_2$ (25 mM)
add ddH_2O to a final volume of 25 µL

PCR-Program
95 °C denaturation 5 min
94 °C denaturation 30 sec
58 °C annealing 45 sec
72 °C elongation 120 sec
72 °C final elongation 10 min

PCR Reaction-Mix (*Paq*)
5 µL *Paq*-polymerase mix (2 x)
2 µL cDNA
1.5 µL primer forward (10 pmol/µL)
1.5 µL primer reverse (10 pmol/µL)

2.2.6.5.5 DNA Gel Electrophoresis

10 µL of PCR samples were mixed with 2 µL 6 x DNA loading dye and then loaded onto 1 % (w/v) agarose gels. The DNA was separated at 90 V for 20-30 min in 1 x TBE running buffer and then made visible under UV light (λ=302 nm) by fluorescence caused by intercalation of the DNA with ethidium bromide. The identity of the PCR products was confirmed by comparing the visible bands with a DNA standard of known size (Gene Ruler 1 kb DNA ladder, Fermentas).

10 x TBE Buffer
890 mM Tris-base
890 mM boric acid
20 mM Na_2-EDTA (pH 8.0)
pH 8.3

TBE Gel
1 % (w/v) agarose
0.01% (v/v) ethidium bromide
(ethidium bromide stock solution: 1 mg/mL ethidium bromide in ddH_2O)
in 1 x TBE buffer

6 x DNA Loading Dye
10 mM Tris-HCl (pH 7.6)
0.03 % (w/v) bromophenol blue
0.03 % (w/v) xylene cyanol FF
60 % /v/v) glycerol

2.2.6.6 Introduction of RNAi Constructs into *A. tumefaciens* for Transformation of *L. japonicus*

RNAi constructs for the downregulation of *SGT1*, *SGT2* and *GCS* in *Lotus japonicus* were available at the beginning of this work. They were produced by Helder Henrique Paiva (from Brazil) at the Max-Planck-Institute of Molecular Plant Physiology (group of Peter Dörmann) in

2008. Constructs comprised several hundred base pairs of the coding region of the respective gene, cloned into a binary vector (pLH6000 or pLH9000) in sense and antisense orientation, separated by the FAD2 intron from *Arabidopsis,* under the control of the 35S promoter from Cauliflower Mosaic Virus (CaMV). The RNAi construct pLH9000-RNAi-*SGT1*, for the downregulation of *SGT1*, contained 560 bp of exons 4-8 (614-1174 bp of *SGT1* cDNA). For the downregulation of *SGT2*, pLH6000-RNAi-*SGT2* contained 598 bp of exons 5-10 of the *SGT2* gene (580-1178 bp of *SGT2* cDNA). pLH9000-RNAi-*GCS*, was designed for the downregulation of *GCS* with 565 bp of exons 4-11 of the *GCS* gene (375-940 bp of *GCS* cDNA). Vector maps and the detailed cloning strategy can be found in the appendix (chapter 7.1).

Agrobacterium tumefaciens LBA4404, carrying RNAi constructs for the downregulation of *Lotus SGT1*, *SGT2* and *GCS*, was generated for subsequent transformation of *Lotus japonicus* hypocotyls (see 2.2.3). To this end, agrobacteria were transformed with pLH6000-RNAi-*SGT2*, pLH9000-RNAi-*SGT1* and pLH9000-RNAi-*GCS*.

2.2.6.6.1 Generation of Electrocompetent Agrobacteria

Agrobacterium tumefaciens LBA 4404 was grown at 28 °C and 200 rpm in YEB medium containing rifampicin (80 µg/mL). For the generation of electrocompetent agrobacteria, 100 mL cultures were grown overnight until the culture reached an OD_{600} of 0.5-0.7. The bacteria were cooled on ice for 15 min and subsequently sedimented by centrifugation at 2500 g for 20 min. The cell pellet was resuspended in 200 mL of sterile ddH_2O and incubated on ice for another 15 min. The centrifugation and the following wash step were repeated twice and the cells were eventually suspended in 1 mL of sterile 10 % (v/v) glycerol. 40 µL aliquots were shock frozen in liquid nitrogen and then stored at -80 °C.

YEB Medium
0.5 % (w/v) beef extract
0.1 % (w/v) yeast extract
0.5 % (w/v) peptone
0.5 % (w/v) sucrose
2 mM $MgSO_4$

2.2.6.6.2 Transformation of *Agrobacterium tumefaciens* by Electroporation

Aliquots of competent cells of the *A. tumefaciens* strain LBA 4404 were thawed on ice, 1-2 µL of plasmid DNA were added and the mixture was incubated on ice for 30 min. The incubated cells were transferred to pre-cooled electroporation cuvettes and electroporated by application of an electric pulse of 12.5 kV/cm. The transformed cells were quickly diluted in 1 mL YEB medium and kept on ice for 2 min. The cells were incubated at 28 °C for 4 hrs and subsequently

plated on agar-solidified selective YEB medium with rifampicin (80 µg/mL), streptomycin (300 µg/mL) and spectinomycin (100 µg/mL) and grown at 28 °C and 200 rpm for 2 days.

2.2.6.7 Confirmation of Successful Transformation of *Agrobacterium tumefaciens*

Standard methods for the verification of successful transformation of bacteria such as *E. coli* include colony PCR or plasmid preparation followed by PCR and restriction analysis. The two methods are not well suited for the analysis of plasmids from *Agrobacterium,* due to a low yield of plasmid DNA obtained by plasmid preparation from these bacteria. Therefore, plasmids prepared from transformed *Agrobacterium* colonies were used for the re-transformation of *Escherichia coli.* Plasmid DNA was subsequently prepared from *E. coli* and analyzed by restriction analysis.

2.2.6.7.1 Plasmid Preparation from *Agrobacterium tumefaciens*

A. tumefaciens transformed with RNAi constructs was grown as described in 2.2.6.6.2 in 30 mL of selective YEB medium. The cells were harvested by centrifugation at 2500 g for 20 min at 4 °C and resuspended in GTE buffer. The suspension was transferred to a 2 mL Eppendorf tube and incubated at RT for 5 min. 400 µL of lysis buffer were added and the mixture was incubated on ice for 5 – 20 min, until a white precipitate was visible. After the addition of 300 µL of 5 M sodium acetate, the samples were incubated on ice for 5 min and subsequently centrifuged for 10 min at 20000 g. The supernatant was transferred to a fresh tube and 1 volume isopropanol was added for DNA precipitation. The sample was again centrifuged for 15 min at 20000 g and 4 °C and the pellet was washed twice with 70 % (v/v) ethanol. The wet pellet was resuspended in 400 µL TE buffer (10:1). For RNA degradation, 2 µL of RNAse A (20 mg/mL) were added and the samples were incubated at 37 °C for 10 min. Subsequently, 400 µL of phenol-chloroform-isoamylalcohol (25:24:1) was added and the mixture was vortexed for 30 sec before centrifugation at 20000 g for 5 min at 4 °C. The upper aqueous phase was transferred to a fresh tube and the DNA was washed. To this end, 40 µL 5 M sodium acetate and 400 µL isopropanol were added and the samples were incubated on ice for 10 min. DNA was harvested by centrifugation (15 min, 20000 g, 4 °C) and the pellet was washed twice with 70 % (v/v) ethanol. The dried pellet was dissolved in 50 µL TE buffer (10:1).

GTE Buffer
50 mM glucose
10 mM EDTA
25 mM Tris, pH 8.0
adjust pH with HCl

Lysis Buffer
0.2 M NaOH
1 % (w/v) SDS

TE Buffer
10 mM Tris-HCl, pH 8.0
1 mM EDTA, pH 8.0
adjust pH of EDTA with NaOH.

2.2.6.7.2 Generation of Electrocompetent *Escherichia coli* Cells

A 3 mL culture of *E. coli* was grown from a single colony overnight at 37 °C and 200 rpm in LB medium. This culture was used for the inoculation of 250 mL LB medium. The bacteria were grown to an OD_{600} of 0.4 and were subsequently harvested by centrifugation (4000 g, 5 min, 4 °C). The cells were resuspended in 125 mL of ice cold 50 mM $CaCl_2$ and incubated at 4 °C for 20 min. The bacteria were centrifuged a second time (4000 g, 5 min, 4 °C), resuspended in 20 ml of 50 mM $CaCl_2$ and kept on ice for 4 hrs. Finally the suspension was mixed with 7 mL of ice cold 50 % (v/v) glycerol and 50 µL aliquots were frozen in liquid nitrogen stored at -80°C until use.

LB Medium
1 % (w/v) tryptone
0.5 % (w/v) yeast extract
0.5 % (w/v) NaCl

For agar-solidified medium bacto agar was added to a concentration of 1.5 % (w/v).

2.2.6.7.3 Transformation of *Escherichia coli*

1 µL of plasmid was added to a 50 µL aliquot of frozen, chemically competent cells of *E. coli* and the cells were thawed on ice for 30 min. The bacteria were transformed by a 3 fold application of a 30 sec heat pulse at 42 °C. Between the pulses, the cells were cooled down on ice for 15 sec. After the last pulse, 1 mL of ice cold LB medium was added and the bacteria were allowed to regenerate at 37 °C for 40 min. Eventually the bacteria were plated on agar-solidified LB medium containing the selective antibiotics streptomycin (20 µg/ml) or spectinomycin (50 µg/ml) and incubated overnight at 37 °C.

2.2.6.7.4 Preparation of Plasmid DNA from *Escherichia coli*

E. coli carrying RNAi constructs for transformation of *Lotus japonicus* was grown on agar-solidified LB-medium or in liquid cultures at 37 °C and 180 rpm. For antibiotic selection of plasmid containing cells, the medium contained 20 µg/mL streptomycin and 50 µg/mL spectinomycin.

For plasmid preparation cells were harvested from 2 mL of an overnight culture by centrifugation (1 min, 18000 g). The supernatant was discarded and the pellet was resuspended in 200 µL of BF buffer with 10 µL 20 mg /mL lysozyme and incubated at room temperature for

several minutes. Subsequently the samples were incubated at 95 °C for 1 min and cooled down on ice. Cell debris and genomic DNA were sedimented by a centrifugation step at 18000 g for 25 min. The supernatant was transferred to a fresh tube, mixed with 480 µL of IS mix and incubated at room temperature for 1 – 2 min, in order to precipitate the plasmids. Plasmid DNA was sedimented by centrifugation at 18000 g for 20 min. The supernatant was discarded and the pellet was rinsed with 500 µL 75 % (v/v) ethanol. After another centrifugation step at 18000 g for 10 min the ethanol was discarded and the plasmid DNA was dried at room temperature for a few minutes. The plasmids were dissolved in 100 µL ddH_2O and stored at -20 °C.

BF Buffer
8 % (w/v) sucrose
0.5 % (v/v) Triton-x 100
50 mM EDTA, pH 8
10 mM Tris-HCl, pH 8

IS Mix
400 µL isopropanol
80 µL 5M ammonium acetate

2.2.6.8 Heterologous Expression of *Lotus SGT1*, *SGT2* and *GCS* in Yeast

Lotus cDNAs bearing high homologies to the glycosyltransferases *SGT1*, *SGT2* and *GCS* from *Arabidopsis* were heterologously expressed in *S. cerevisiae* and *P. pastoris* in order to confirm the catalytic function of the expressed enzymes.

2.2.6.8.1 Cloning of Constructs for the Heterologous Expression of *SGT1*, *SGT2* and *GCS* in *S. cerevisiae*

E. coli carrying cloning vectors (pPIC 3.5) with the full length cDNAs of *SGT1*, *SGT2* and *GCS* was stored at -80 °C. For the heterologous expression of *SGT1*, *SGT2* and *GCS* in *S. cerevisiae*, the cDNAs were cloned into the overexpression vector pDR196. To this end, the cDNAs were cut from the vector pPIC3.5 with the restriction endonucleases *Avr*II and *Xho*I in buffer red. The vector pDR196, carrying a different insert, was cleaved with the endonucleases *Spe*I and *Xho*I in buffer green. The restriction took place for 8 hrs.

Restriction Assay
10 µL plasmid DNA
5 µL 10 x buffer
2 µL endonuclease A
2 µL endonuclease B
add ddH_2O to a final volume of 50 µL

2.2.6.8.2 Elution of DNA Fragments from Agarose Gels

Plasmid DNA, which had previously been cleaved by restriction enzymes, was separated by gel electrophoresis on an agarose gel, as described in 2.2.6.5.5. The vector pDR196 and the

cDNA inserts of *SGT1*, *SGT2* and *GCS* were identified by comparison with a size marker and the gel pieces cut from the gel with scalpels. To avoid cross-contamination, the scalpel was cleaned with ethanol between samples. In order to avoid DNA degradation, extended exposure to UV light was avoided. The elution of DNA from the agarose gel was performed with a gel elution kit (MinElute Gel Extraction Kit, Qiagen). All experimental procedures were performed according to the supplier's instructions.

2.2.6.8.3 Ligation

For optimal ligation efficiency, the ratio of vector and insert in a ligation assay should be about 1:3 (based on band intensity in the agarose gel). In order to obtain such a ratio, 1 µL of the purified DNA fragments acquired by elution from agarose gels was loaded on a new agarose gel, stained with ethidium bromide and separated by gel electrophoresis for 5 min (see 2.2.6.5.5). The signal intensities of vector and inserts were compared and the amounts required for ligation were estimated. Vector and insert were mixed with 1 µL 10 x ligation buffer and 0.5 µL T4 DNA ligase (10 U/µL) and ddH_2O was added to a final volume of 10 µL. The mixture was incubated 4 °C overnight for ligation. The constructs obtained by ligation were used for the transformation of *E. coli* as described in 2.2.6.7.3. Plasmids were subsequently prepared from *E. coli* as described in 2.2.6.7.4 and submitted to restriction by endonucleases to confirm successful transformation with the construct of interest. pD-oe-*SGT1* and pD-oe-*SGT2* were cleaved with *Hind*III, pD-oe-*GCS* was cleaved with *BamH*I.

Restriction Assay
1 µL plasmid DNA
1 µL 10 x buffer
0.3 µL endonuclease
add ddH_2O to a final volume of 10 µL

2.2.6.8.4 Generation of Electrocompetent Cells of *Saccharomyces cerevisiae*

Single colonies of *S. cerevisiae* INVScI were used for starting 3 mL cultures in YPD medium. The yeasts were grown overnight at 30 °C and 200 rpm. One overnight culture was used for the inoculation of 500 mL YPD medium. This culture was grown to an OD_{600} of 1.3-1.5 and centrifuged for 10 min at 4000 g and 4 °C. The cell pellet was then resupended in 500 mL of ice cold ddH_2O and washed by centrifugation (10 min, 4000 g, 4 °C). Subsequently, the cells were washed again in 250 mL ddH_2O and centrifuged as before. The cell pellet was resuspended in 20 mL ice cold 1 M sorbitol and the samples were submitted to a final centrifugation step (10 min, 4000 g, 4 °C). Eventually, the cells were resuspended in 1 mL 1 M sorbitol with 10 % (v/v) glycerol and 65 µL aliquots were slowly frozen at -80 °C.

YPD Medium
1 % (w/v) yeast extract
2 % (w/v) bacto-peptone
2 % (w/v) glucose

Solidified medium contained 2 % (w/v) bacto agar.

2.2.6.8.5 Transformation and Cultivation of *Saccharomyces cerevisiae*

For the electroshock transformation of *S. cerevisiae* INVScI, 1-5 µL plasmid (pD-oe-*SGT1*, pD-oe-*SGT2*, pD-oe-*GCS* or empty vector pDR196) were added to 80 µL of competent yeast cells. The cells were electroporated with 750 V in a 1 mm cuvette before 1 mL of cold 1M sorbitol was added and the suspension was cooled on ice for a several minutes. The cells were harvested by centrifugation (1 min, 1000 g) and resuspended in 100 µL 1 M sorbitol with 10 % (v/v) glycerol.

Transgenic yeasts containing constructs for the heterologous expression of *Lotus* glucosyltransferases were cultivated at 30 °C for 2-3 days on agar-solidified selective medium depleted in uracil. Colonies were transferred to a second plate with the same medium and cultivated for another 24 hrs before liquid cultures were started. For lipid isolation, 100 mL cultures were grown for 2 -3 days at 30 °C and 200 rpm in selective yeast medium without uracil.

Selective Yeast Medium (-Uracil)
1.16 g/L dropout powder
2 % (w/v) glucose
0.67 % (w/v)YNB
(yeast nitrogen base with ammonium sulfate, without amino acids)
20 mg/L histidine
60 mg /L leucine
40 mg/L tryptophane

Dropout Powder
2.5 g adenine (hemisulfate)
1.2 g L-arginine
6 g L-aspartate
6 g L-glutamate (sodium-salt)
1.8 g L-lysine (HCl)
1.2 g L-methionine
3 g L-phenylalanine
22.5 g L-serine
12 g L-threonine
1.8 g L-tyrosine
9 g L-valine
(mixture ground to a fine powder)

Solidified medium contained 2 % (w/v) bacto agar

2.2.6.8.6 Heterologous Expression of *SGT1*, *SGT2* and *GCS* in *Pichia pastoris*

Constructs for the overexpression of *SGT1*, *SGT2* and *GCS* in *Pichia pastoris* were available at the beginning of this work (Helder Henrique Paiva, Max-Planck-Institute of Molecular Plant Physiology, Golm). Full length cDNAs, cloned into the overexpression vector pPIC3.5 were sent

to Dr. Dirk Warnecke (University of Hamburg) for transformation of a *Pichia pastoris sgt/gcs* deletion mutant (see appendix, chapter 7.2 for detailed cloning strategy). This strain lacks the ability to synthesize both sterol glucosides and glucosylceramides and was therefore chosen for heterologous expression of the respective glycosyltransferases from *Lotus japonicus*. Cultivation of transgenic *P. pastoris* and lipid extraction for thin layer chromatography were carried out by Dr. Dirk Warnecke following protocols similar to those described for *Saccharomyces* in 2.2.6.8.5, 2.2.7.4 and 2.2.7.6.

2.2.7 Analytical Tools for Lipid Quantification

2.2.7.1 Internal Standards for Lipid Analysis

Lipids were quantified by Q-TOF MS analysis in relation to internal standards of known concentrations. For each lipid class at least two different internal standards were selected, which are absent from plant tissue. For the quantification of sterol esters (SE), diacylglycerol (DAG) and triacylglycerol (TAG), standards with saturated and mono-unsaturated fatty acids were used, to account for differences in signal responses due to possible ion suppression effects or differences in fragmentation. Commercially available standards were purchased from Sigma, Avanti Polar Lipids, Matreya LLC and Larodan (see 2.1.6).

Hydrogenation of Internal Standards

For some lipid classes no suitable lipid standards were commercially available. However, purified mixtures containing acylated sterol glucosides (ASG), monogalactosyldiacylglycerol (MGDG), digalactosyldiacylglycerol (DGDG), sulfoquinovosyldiacylglycerol (SQDG) or phosphatidylinositol (PI) from biological sources could be purchased. Hydrogenation resulting in the saturation of double bonds, yielded saturated lipid molecules which are not present in plant tissues. The lipids were dissolved in chloroform, a small amount of platinum(IV)oxide was added and the mixture was hydrogenated with H_2 gas for several hours at room temperature (Buseman *et al.*, 2006). Purification of the hydrogenated lipids was achieved by solid phase extraction (see 2.2.7.5). Q-TOF MS analysis was applied to confirm the complete saturation of both, the sterol and the fatty acid moieties.

Synthesis of Internal Standards for Sterol Glucoside Quantification

Internal standards for sterol glucoside quantification were not commercially available. Therefore, cholestanol-Glc and stigmastanol-Glc were synthesized from cholestanol and stigmastanol according to the protocol described by Iga *et al.* (2005). 1.25 g of glucopyranosyl-bromide-tetrabenzoate were dissolved in 10 mL of toluene and added to a suspension of 0.61 g sterol, 2 g drierite, and 2 g cadmium carbonate ($CdCO_3$) in 12 mL of toluene. This mixture was

incubated for 7 hrs at 130 °C and then cooled down to room temperature. The suspension was diluted with 24 mL of chloroform and a small amount of celite was added. The mixture was filtered, dried under a stream of air and resuspended in 40 mL of 0.15 M sodium methylate. After incubation overnight with shaking at room temperature, the solution was neutralized with 1 N methanolic HCl. SGs were extracted after the addition of 2 Vol chloroform/methanol (2:1) and 1 Vol water. After phase separation by centrifugation, the lower chloroform phase, containing the SGs, was harvested. Purification of the SGs was achieved by solid phase extraction (see 2.2.7.5). The free sterols used as substrates were eluted from the silica material with chloroform and discarded. SGs were then eluted from the column with acetone/isopropanol (1:1) and quantified by GC as described (see 2.2.7.11)

Synthesis of Internal Standards for TAG Quantification

One of the four internal standards employed for TAG quantification was not commercially available. Therefore, tri-11:1$^{\Delta 10cis}$ was synthesized from 11:1$^{\Delta 10cis}$ (Larodan) and glycerol, adapting a protocol from Gellerman *et al.* (1975), which originally describes the synthesis of fatty acid phytyl esters. The synthesis of tri-11:1$^{\Delta 10cis}$ was carried out by Helga Peisker (Institute of Molecular Physiology and Biotechnology of Plants, University of Bonn). 0..2 mmol of undecenoic acid (11:1$^{\Delta 10cis}$) and 0.28 mmol of oxalyl chloride were incubated in 1 mL toluene at 60-65 °C for 1.5–2 h in a water bath. The mixture was dried under airflow to remove the solvent, HCl and oxalyl chloride. The thus obtained acid chloride of undecenoic acid (11:1$^{\Delta 10cis}$) was added to 0.17 mmol glycerol, 1 mL of dry diethyl ether and 0.25 mL pyridine. The mixture was incubated at 80 °C for 2-3 h. After cooling, TAGs were extracted twice from the mixture with hexane and the combined hexane phases were washed with water. High purity TAGs were obtained by subsequent separation of the extracts by TLC with hexane/diethyl ether/acetic acid (70:30:1). TAGs were identified by comparison with co-migrating standards, and subsequently eluted from the silica material with hexane.

Quantification of Internal Standards

For the quantification of internal standards for phospho- and galactolipids, DAGs and TAGs the lipids were transmethylated for 20 min at 80 °C in 1 mL of 1 N methanolic HCl with 5 µg pentadecanoic acid (15:0) as internal standard. The resulting fatty acid methyl esters (FAMEs) were subsequently quantified by GC-FID (see 2.2.7.12). For the quantification of sphingolipids, the transmethylation was carried out overnight.

FAMEs derived from SEs and ASGs were quantified by GC-FID as described in 2.2.7.12. The sterol moieties of FSs, SGs and ASGs were quantified by GC-MS with cholesterol and stigmasterol as internal standards (see 2.2.7.11).

The quantified standards were combined to yield final standard mixtures of defined concentrations, dissolved in chloroform-methanol (2:1) and stored in aliquots at -20°C.

Sterol Lipid Standard Mix

50 µL of sterol standard mix in chloroform-methanol (2:1) contained 5 nmol each of cholestanol, stigmastanol, cholestanol-Glc and stigmastanol-Glc and 2.5 nmol each of the sterol esters 16:0-cholesterol, 16:1-cholesterol, 18:0-cholesterol and 18:1-cholesterol. In addition, the mixture contained 0.2 nmol 16:0-Glc-campestanol, 0.5 nmol 16:-Glc-stigmastanol, 0.3 nmol 18:0-Glc-campestanol, 1 nmol 18:0-Glc-stigmastanol.

Phospho- and Galactolipid Standard Mix

10 µL of phospho- and galactolipid standard mix in chloroform-methanol (2:1) contained 0.1 nmol each of di14:0-PC and di20:0-PC, 0.1 nmol each of di14:0-PE and di20:0-PE PE, 0.1 nmol each of di14:0-PG and di20:0-PG, 0.07 nmol each of di14:0-PA and di20:0-PA, 1.4 nmol di14:0-PS, 0.15 nmol 34:0-PI, 0.07 nmol 34:0-MGDG and 0.05 nmol 36:0 MGDG, 0.1 nmol 34:0-DGDG and 0.2 nmol 36:0-DGDG and 0.2 nmol 34:0-SQDG.

Sphingolipid Standard Mix

10 µL of sphingolipid standard mix in chloroform-methanol (2:1) contained 1 nmol each of Gal-d18:1-c12:0 and Gal-d18:1-c24:1.

DAG and TAG Standard Mix

10 µL of DAG and TAG standard mix in chloroform-methanol (2:1) contained 1 nmol each of di14:0, di14:1, di20:0 and di21:0 or tri10:0, tri11:1, tri20:0 and tri22:1, respectively.

2.2.7.2 Synthesis of *N*-Chlorobetainyl chloride

N–Chlorobetainyl chloride, used for the derivatization of free sterols for quantification by Q-TOF MS/MS analysis, was synthesized following the protocol by Vassel and Skelly (1963). A mixture of 1g of betaine hydrochloride and 0.93 g of thionyl chloride was slowly heated to 70°C and incubated overnight in a glass tube. 1 mL of warm toluene was added and the mixture was continuously stirred with a glass rod, while cooling down to room temperature. Then, more toluene was added and the mixture was heated until all crystals were dissolved. The solution was cooled down again while stirring and crystals formed, which were washed repeatedly with methylene chloride. The crystals were then dried, and stored in air-tight glass tubes at 4°C.

2.2.7.3 Extraction of Lipids from Plant Material

The extraction of sterol lipids and glycerolipids and glucosylceramide from plant tissue for Q-TOF MS analysis was performed using a modification of the protocol described by Bligh and Dyer (1959). In order to minimize contamination during Q-TOF MS analysis, plastic ware was avoided in favor of glass ware wherever possible and all solvents were tested for highest purity, prior to use. To avoid oxidation of fatty acid residues, all solvents contained 0.01 % (w/v) BHT (Welti *et al.*, 2002). Lipid degradation by lipases was prevented by the presence of formic acid in the solvent mixture during lipid isolation (Browse *et al.*, 1986). For the extraction of GIPCs from plant tissues see 2.2.7.13.

25-100 mg of plant tissue were harvested and the exact fresh weight was determined quickly to minimize the risk of lipid degradation by lipases. The material was then quickly frozen in liquid nitrogen and immediately processed or stored at -80°C. The samples were ground to a fine powder in 2 mL reaction tubes using a ball mill (Precellys) at 5000 Hz for 10 seconds. To ensure complete extraction of lipids, the samples were ground a second time in the presence of chloroform/methanol/formic acid (1:1:0.1). Lipids were extracted with 2 volumes of chloroform/methanol/formic acid (1:1:0.1) and 1 volume of 1 M KCl/0.2 M H_3PO_4. At this point, the internal standard was added for all lipid classes except for phospho- and galactolipids. The mixture was vortexed and phase separation was achieved by centrifugation at 5000 g for 3-5 min. The lower organic phase was harvested and the upper phase re-extracted twice with chloroform. The organic phases were combined in a fresh glass tube and dried under an air stream.

The dried lipids were dissolved in 1 mL of chloroform. For the analysis of sterols, lyso-phospholipids, DAGs and TAGs the lipids were applied to a silica column and purified by solid phase extraction (see 2.2.7.5). For the quantification of phospho- and galactolipids, 10 µL of the chloroform extract was added to 10 µL of the internal standard mix and diluted with 80 µL of Q-TOF running buffer (chloroform/methanol/300 mM ammonium acetate (300:665:35)). The samples were measured immediately or stored at -20°C.

2.2.7.4 Extraction of Lipids from Yeast

For lipid isolation, 100 mL cultures of *S. cerevisiae* were grown for 2 - 3 days at 30 °C and 200 rpm in selective yeast medium without uracil (see 2.2.6.8.5). Cells were harvested by centrifugation at 3200 g for 15 min and the pellet was resuspended in 20 mL water. The samples were transferred to a glass tube and centrifuged again at 800 g for 15 min. The pellet was resuspended in chloroform/methanol (1:2) and incubated with shaking for at least 30 min or overnight. The samples were centrifuged again and the supernatant (extract I) was transferred to a fresh glass tube. The pellet was re-extracted with chloroform/methanol (2:1) for 30 min,

centrifuged and the supernatant (extract II) was combined with extract I. The solvent was evaporated under a stream of air and the dried lipids were dissolved in 3 mL chloroform/methanol (2:1) and 0.75 mL 0.9 % (w/v) NaCl. The lipids were extracted into the lower organic phase by shaking and subsequent centrifugation at 800 g for 3 min. Finally the chloroform phase was evaporated under airflow and the lipids were dissolved in 20 – 50 µL chloroform/methanol (2:1) for TLC separation (see 2.2.7.6).

2.2.7.5 Solid Phase Extraction of Lipid Extracts

The Q-TOF MS analysis of conjugated sterols and nonpolar lipids like TAGs and DAGs required an additional purification step of the crude lipid extracts. Solid phase extraction on silica columns was employed for the fractionation of the crude lipid extract. The fractions obtained by this procedure were enriched in the desired lipid classes and the samples showed reduced ion suppression during Q-TOF MS analysis.

Chloroform lipid extracts were applied to a 100 mg Strata silica column equilibrated in chloroform. In order to avoid the loss of polar lipids by adhesion to the glass tube, the tube was rinsed with acetone/isopropanol (1:1), methanol and methanol/water (1:1), respectively, and the solvents were applied to the column in the subsequent elution steps. In a second step, glycolipids, including SG, ASG, GlcCer, MGDG, DGDG and SQDG were eluted with 2 bed volumes of acetone/isopropanol (1:1). An additional elution step with methanol yielded the more polar lipids, PC, PE, PG, PA, Lyso-PE, Lyso-PG. For the elution of Lyso-PC, an additional wash-step with methanol/water (1:1) was required.

The nonpolar fraction (chloroform) containing FS and SE could be further separated by using an additional SPE step with a different solvent system. To this end, the lipids were applied to a silica column in hexane, and eluted with hexane/diethylether (99:1) (for SE) and hexane/diethylether (85:15) (for FS) (see http://www.cyberlipid.org). This additional purification step was applied for subsequent analysis of FSs and SEs by GC-MS (see 2.2.7.11).

For further analysis, all lipid extracts were dried under a stream of air, dissolved in Q-TOF solvent (see 2.2.7.8) and stored at -20°C. For the analysis of free sterols and sterol esters, the neutral lipid fraction was divided into two aliquots. One aliquot was used for the analysis of sterol esters and other nonpolar lipids, while the other one was used for the quantification of free sterols after derivatization with *N*-chlorobetainyl chloride (see 2.2.7.7).

2.2.7.6 Separation of Lipids by Thin Layer Chromatography

Thin layer chromatography (TLC) plates were submerged in 0.15 M ammonium sulfate and dried at RT for several days before activation at 120 °C for 2.5 hrs prior to use. The lipids were loaded onto the plate in 20-50 µL chloroform/methanol (2:1) and separated for 45 to 60 min in acetone/toluene/water (91:30:8). Lipids were identified with the help of co-migrating standards.

For the detection of glycolipids in lipid extracts from transgenic yeast carrying overexpression constructs for *Lotus* glucosyltransferases, the plates were sprayed with α-naphthol reagent and heated to 137 °C. After a few seconds, sugar containing lipids were specifically stained red with α-naphthol.

For the detection of glycosterols, separated by TLC prior to quantification by GC analysis, a different staining method was applied. Iodine is a non-specific coloring agent, which binds reversibly to the double bonds of all unsaturated lipids. Co-migrating standards were applied to lanes at the edge of the plate and stained with iodine vapor. This was achieved by placing iodine crystals into a pasteur pipette, which was connected to the airflow. Only the part of the plate containing the co-migrating standards was exposed to the iodine vapor, which resulted in a yellow staining of all lipids. Lipids from plant extracts were identified by comparison with the stained standards, the silica material was scraped off the glass plate and lipids were extracted with 2 Vol chloroform/methanol (2:1) and 1 Vol water for further analysis.

2.2.7.7 Derivatization of Free Sterols for Q-TOF MS/MS

Free sterols were quantified by Q-TOF MS/MS after derivatization with *N*-chlorobetainyl chloride, as has been described before for diacylglycerol derivatization (Li *et al.*, 2007). Sterols were dissolved in 0.5 mL of anhydrous methylene chloride and 50 µL of anhydrous pyridine, before 5 mg of *N*-chlorobetainyl chloride were added. The mixture was incubated overnight at room temperature or for 4 hrs at 42 °C. Derivatized sterols were extracted from this mixture with 2 volumes of chloroform-methanol (1:1) and 1 volume of water. The betainylated sterols were measured immediately, to exclude partial degradation of the derivatized product.

2.2.7.8 Analysis of Lipids by Q-TOF MS/MS

Lipids were analyzed with a 6530 Accurate-Mass Quadrupole Time-of-Flight (Q-TOF) LC/MS (Agilent) mass spectrometer using nanoflow direct infusion Chip Cube technology. Samples were purified and diluted as described before (see 2.2.7.3 and 2.2.7.5) and applied to the Q-TOF MS in chloroform/methanol/300 mM ammonium acetate (300:665:35) at a flow rate of 1 µL/min. Depending on the number of analyzed molecular species, 5 to 15 µL of the sample

were injected. Lipids were detected in the positive mode and fragmented in the collision cell with nitrogen gas. Optimal collision energies were determined for each lipid class. Lipids were quantified relative to internal standards (see 2.2.7.1). Mass spectra were recorded at a rate of 0.731 spectra per second. The Vcap voltage was 1700 V, the fragmentor voltage was set to 200 V. Tables in the appendix (chaper 7.6) show the targeted lists for all lipid classes with their respective collision energies and product ions after fragmentation.

2.2.7.9 Data Analysis for Quantification of Lipids by Q-TOF MS/MS

Data were analyzed using the Agilent Mass Hunter Qualitative Analysis Software (Version B.02.00) and further processed with Microsoft Excel 2007. For statistical analyses, mean and standard deviation were determined for at least three biological replicates. Trend calculation was carried out, when two internal standards of different molecular masses were used, in order to account for deviating signal responses dependent on the size of the molecular species analyzed. Calculation of exact molecular masses and isotope distribution was carried out using the Agilent Mass Hunter Calculator and the Isotope Distribution Calculator tools. Isotopic correction was applied for all substances containing a varying number of double bonds, in order to take into account the presence of ^{13}C isotopes as described by (Ejsing *et al.*, 2006) (see 2.2.7.10)

2.2.7.10 Calculation of Isotopic Overlap

Correction for isotopic overlap, taking into account the presence of ^{13}C containing molecules, was calculated for molecules which show different degrees of unsaturation, therefore differing in mass to charge ratio (m/z) by two hydrogen atoms (m/z = 2) (Ejsing *et al.*, 2006). This phenomenon is found for all fatty acid containing lipids and for sterols. Taking into consideration the fragmentation patterns of these molecules, a statistical probability of a molecular fragment containing two ^{13}C atoms was calculated. For example, the presence of two ^{13}C atoms in a monounsaturated molecule results in a m/z of (M+2), almost identical to the m/z of a saturated molecule of the same lipid class. The signal response of the saturated molecule was subsequently corrected by subtracting the calculated value of the contribution of the $^{13}C_2$ containing, monounsaturated molecule. This calculation was slightly more complex for SE and ASG, as these lipids show different numbers of double bonds not only in the fatty acid residue, but additionally in the sterol moiety. For these lipids, a stepwise calculation was performed, taking into consideration both scenarios, i.e. the contribution by a $^{13}C_2$ containing acyl residue and a $^{13}C_2$ containing sterol residue.

2.2.7.11 Quantification of Sterols by Gas Chromatography

For the analysis of free sterols, 100 mg of plant tissue were harvested and lipids were extracted as described before (see 2.2.7.3).

For the quantification of free sterols and conjugated sterols, 2 g of leaf material were ground under liquid nitrogen and lipids were extracted in the presence of internal standards as described above. Lipid extracts in chloroform were separated by solid phase extraction into a nonpolar and a polar fraction. The nonpolar fraction (chloroform) containing FS and SE was further fractionated by an additional SPE step; thereby separating FSs and SEs (see 2.2.7.5).

The polar fraction (acetone/isopropanol (1:1)) was purified by thin layer chromatography to separate SG from ASG. SG and ASG were identified with the help of co-migrating standards and were extracted from the silica material with chloroform/methanol (2:1) (see 2.2.7.6).

At this point, purified FS, SE, SG and ASG extracts were divided into two aliquots each. These aliquots were used for quantification of sterols by Q-TOF MS and GC-MS, respectively. Sample preparation for Q-TOF MS analysis was carried out as described before (see 2.2.7.8). For GC-MS analysis, conjugated sterols were hydrolyzed in 1 mL of 6 % (w/v) KOH in methanol at 90 °C for 1 h (SE) (Schaller *et al.*, 1995), or in 1mL of 1 N methanolic HCl at 90 °C for 1 h (SG and ASG). The hydrolyzed sterols were then extracted with hexane after the addition of 1 mL of 0.9 % (w/v) NaCl. Free sterols and hydrolyzed conjugated sterols were derivatized with 100 µL of N-methyl-N-(trimethylsilyl)-trifluoroacetamide (MSTFA) at 80°C for 30 min, prior to GC analysis. MSTFA was then evaporation under a stream of air and the samples were dissolved in hexane. Quantitative GC analysis was performed with an Agilent 7890A Plus GC with flame ionization detector (Agilent), while GC-MS was employed for sterol identification and quantification. Silylated sterols were separated on a 30 m HP-5MS column (Agilent) using a temperature gradient of 150 °C increased to 280 °C at 10 °C min, held for 10.5 min, and decreased to 150 °C at 20°C min .

2.2.7.12 Analysis of Fatty Acid Methyl Esters by Gas Chromatography

Quantification of fatty acids was performed by analysis of their respective methyl esters via gas chromatography (GC) using a flame ionization detector (FID). To this end, fatty acids were released from more complex lipids by acidic transmethylation. The formation of fatty acid methyl esters (FAME) was achieved by incubation of the dried lipid extracts in 1 mL 1 N methanolic HCL for 30 min at 80 °C. For the formation of FAMEs from conjugated sterols, the incubation time was 1 h at 90 °C. FAMEs were extracted by addition of 1 mL 0.9 % (w/v) NaCl and 1 mL hexane. Samples were mixed and phase separation was obtained by centrifugation (3

min, 2000 g). The upper hexane phase was harvested and directly applied to the GC or concentrated by evaporation under airflow.

The FAMEs were eluted from the GC column (HP-5MS, 30 m, Agilent) with a temperature gradient starting with 100 °C, increased to 160 °C by 25 °C/min, then to 220 °C by 10 °C/min and finally decreased to 100 °C by 25 °C/min. The fatty acids were identified according to their retention time by comparison with the retention times of FAMEs from a rapeseed standard mixture (Supelco).

2.2.7.13 Extraction of Sphingolipids from Plant Tissue for Q-TOF MS Analysis

Sphingolipids were extracted from plant tissue following a modified protocol by Markham *et al.* (2006) suited for the extraction of polar substances including GIPCs. 250-500 mg of plant material was ground to a fine powder in liquid nitrogen. Sphingolipids were extracted with 1 mL sphingolipid extraction solvent for 15 minutes at 60 °C. Cell debris was sedimented by centrifugation (1 min, 1000 g) and the extract was transferred to a fresh glass tube. The extraction was repeated 5 to 8 times with fresh solvent to ensure complete extraction of lipids. The combined lipid extracts were dried under a stream of air.

The presence of high amounts of glycerolipids in total lipid extracts from plants can lead to ion suppression of less abundant lipid classes including sphingolipids during direct infusion Q-TOF MS analysis. In order to obtain satisfactory signal responses of sphingolipids such as GIPCs it is therefore advisable to remove glycerolipids prior to Q-TOF analysis. To this end, the lipid extracts were submitted to alkaline cleavage. Fatty acid residues were cleaved from glycerolipids by incubation of the dried lipids at 53 °C in 2 mL methylamine solution for 30-60 minutes. Alternatively, the cleavage was performed according to a protocol modified after (Imgrund *et al.*, 2009). In this protocol, dried lipid extracts were dissolved in 2 mL of chloroform-methanol (1:1) and mixed thoroughly before 150 µL of 1 M KOH (in methanol) was added. The mixture was incubated at 40 °C for 2 hours and subsequently neutralized with 6 µL of concentrated acetic acid and dried under a stream of air.

Fatty acids were removed from the hydrolyzed extracts by an extraction step with methanol and hexane. Alkaline cleavage in methanolic KOH resulted in the formation of FAMEs, which could easily be extracted with hexane (Ichihara *et al.*, 1996). During methylamine cleavage, fatty acids were converted into their respective methylamides, which were more difficult to remove from the extract. Lipids after methylamine treatment were dissolved in 1 mL methanol/acetic acid (99:1), and free fatty acids were extracted after addition of 1 mL hexane and vigorous shaking and subsequent centrifugation (1 min, 1000 g). The extraction was repeated a second time with fresh hexane. Because hexane extraction of fatty acid methyl esters

was found to be superior to the extraction of fatty acid methylamides, glycerolipids were usually removed by KOH treatment rather than by methylamine treatment.

Subsequently, the dried extracts were desalted by liquid/liquid extraction with 1 mL of a mixture of butanol (saturated with water)/acetic acid (99:1) and 1 mL of water. The samples were vortexed vigorously and phase separation was achieved by centrifugation at 1000 g for 1 min. Salts were extracted into the lower aqueous phase and sphingolipids were retained in the upper butanol phase. The butanol phase was harvested and transferred into a fresh glass tube. The aqueous phase was re-extracted twice with butanol (saturated with water)/acetic acid (99:1) and the organic phases were combined and dried under a stream of air. The dried extracts were dissolved in 200-500 µL Q-TOF solvent (see 2.2.7.8.) and analyzed by Q-TOF MS.

Sphingolipid Extraction Solvent
lower phase of:
55 % (v/v) isopropanol
20 % (v/v) hexane
25 % (v/v) ddH_2O

Methylamine Solution
70 % (v/v) methylamine stock solution
(33 % (w/v) methylamine in ethanol)
30 % (v/v) ddH_2O

2.2.7.14 Quantification of Sphingolipid Long Chain Bases from Plants by HPLC

Long chain base (LCB) quantification of sphingolipids from *Lotus japonicus* was performed by HPLC analysis in order to validate data obtained by Q-TOF MS. Methods are based on protocols by Morrison and Hay (1970), Merill *et al.* (1988) and Markham *et al.* (2006), with modifications as described by vom Dorp (2010).

Alkaline Hydrolysis of Sphingolipids for LCB Analysis

Total sphingolipids were extracted from plant tissues as described in 2.2.7.13. In addition, sphingolipid extracts devoid of GIPCs were obtained by silica column separation of total sphingolipid extracts and elution of glucosylceramides and ceramides with acetone/isopropanol (1:1) as described in 2.2.7.5. The polar GIPCs are not eluted from the silica material and are thereby removed from the extracts.

Free LCBs were obtained from lipid extracts by alkaline hydrolysis following a protocol by Morrison and Hay (1970). The dried lipid extracts were dissolved 1 mL of 1,4-dioxane and 1 mL of 10 % (w/v) $Ba(OH)_2$ (in water), mixed thoroughly and incubated overnight at 110 °C. After cooling, 2 mL of 2 % (w/v) ammonium sulfate and 2 mL diethylether were added. The samples were mixed and phase separation was achieved by centrifugation at 800 g for 10 minutes. LCBs were extracted into the upper diethylether phase, while barium ions were precipitated and remained in the interphase. The diethylether phase was transferred to a fresh

glass tube and the aqueous phase was re-extracted once with diethylether. The diethylether phases were combined and dried under air flow.

Derivatization of Long Chain Bases with *ortho*-Phthaldialdehyde

Long chain bases (LCB) were derivatized with *ortho*-phthaldialdehyde (OPA) and *β*-mercaptoethanol as described by Merill *et al.* (1988). LCBs were dissolved in 100 µL methanol and derivatized with 50 µL of OPA derivatization mixture (OPA reagent in 9.9 mL borate buffer, pH 10.5), which was freshly prepared and stored in the dark at 4 °C for no longer than 5 days. The samples were derivatized for at least 35 min at room temperature. Subsequently, 350 µL methanol were added and the samples were centrifuged for 20 minutes at 800 g. Thereby, free OPA was sedimented and the derivatized LCBs were retained in the methanol for quantification by HPLC analysis.

OPA Reagent
5 mg *ortho*-phthaldialdehyde
5 µL *β*-mercaptoethanol
100 µL ethanol
sonicated for 10 min

Borate Buffer
3 % (w/v) boric acid
adjust to pH 10.5 with KOH

HPLC Analysis of Sphingolipid Long Chain Bases

Reverse phase high pressure liquid chromatography (HPLC) analysis of sphingolipid long chain bases from *Lotus japonicus* was performed according to a protocol by Markham *et al.* (2006). Analysis was carried out using an Agilent 1100 series HPLC system, equipped with a Fluorescent Light Detector (FLD).

20 µL of the samples in methanol were injected to the HPLC in 20 µL methanol. OPA derivatives of LCBs were eluted from the column (Agilent Zorbax RP, C-18, 150 x 4.6 mm inner diameter) at a column temperature of 30 °C and a flow rate of 1 mL/min of a gradient of 5 mM potassium phosphate (K_2HPO_4/KH_2PO_4 at pH 7.0) (solvent A) and methanol (solvent B).

The gradient was started with 80 % solvent B, which was linearly increased to 90 % within 3.5 min. This was maintained for 4 minutes and was subsequently increased to 100 % solvent B in 5 minutes. The concentration of 100 % solvent B was kept for 2.5 min and then decreased to 80 % solvent B in 1.5 min and held at 80 % for 1 min before the run was stopped. For the detection of OPA-derivatives of LCBs, the parameters of the FLD were set to an excitation wavelength of 345 nm and an emission wavelength of 440 nm. LCB-OPA peaks were identified based on retention times of LCB standards and by comparison with published chromatograms (Markham *et al.*, 2006).

3 Results

3.1 Quantification of Sterol Lipids in Plants by Q-TOF MS/MS

In the past, the quantification of sterol lipids in plants has mostly been based on the measurement of sterol residues by gas chromatography (GC). While this method is very accurate and well-suited for the analysis of free sterols (FSs), there are numerous disadvantages concerning the quantification of conjugated sterols. Sterol glucosides (SGs) and acylated sterol glucosides (ASGs) in particular cannot be measured by GC as intact molecules, because they are not volatile. Therefore, GC analysis of conjugated sterols requires the separation of the different sterol classes and subsequent cleavage of the molecules prior to quantification, to release the sterol residues. This approach is highly laborious and requires large amounts of plant material, which represents a severe disadvantage, especially for the quantification of those sterols which are less abundant in most plant tissues i.e. SGs and ASGs. In the last years LC-MS and ESI-MS based methods have been established for the quantification of different lipid classes, i.e. phospho- and galactoglycerolipids (Welti *et al.*, 2002), sphingolipids (Markham and Jaworski, 2007) and nonpolar lipids such as di- and triacylglycerol (Ejsing *et al.*, 2009; vom Dorp *et al.*, 2012). However, the comprehensive analysis of conjugated sterol lipids from plants via LC-MS has not yet been described.

One of the aims of this thesis, and a prerequisite for subsequent analysis of plant lipid metabolism during plant-microbe interactions, was the establishment of a mass spectrometry based method for the accurate quantification of FSs, SGs, ASGs and SEs in plants. The strategy included the quantification of all four sterol lipid classes by Q-TOF MS/MS analysis. In this approach, sterols were applied to the mass spectrometer via direct infusion through an HPLC nanoflow infusion chip and ionized in the positive mode. Lipids were analyzed after fragmentation of the molecule ions in the collision cell and quantified relative to internal standards.

3.1.1 Q-TOF MS Parameters and Selection of Internal Standards

To develop the method for measuring sterol lipids in plants, the MS/MS parameters were optimized with synthetic standards for each lipid class. 200 V was found to be the optimum fragmentor voltage for sterol lipid analysis, as higher voltages induced a premature fragmentation of lipids in the ion source in MS only mode. The capillary voltage (V_{cap}) was set to 1700 V. The samples were infused into the mass spectrometer at a flow of 1 µl/min. All sterol lipids were ionized in the positive mode. Based on the literature, GC-MS measurements and

preliminary Q-TOF MS experiments with plant extracts, targeted lists with the exact molecular masses for all expected molecular species were generated. Accurate masses and isotopic distribution correction were calculated as described in 2.2.7.10. Molecular formulas and exact masses of intact molecules and fragment ions are listed in the appendix. Stigmasterol and the sterol precursor isofucosterol have the same molecular mass, therefore the two lipids could not be distinguished by Q-TOF MS/MS analysis. In *Arabidopsis*, isofucosterol represents a minor sterol, nevertheless all data obtained for stigmasterol in the following experiments represent a mixture of stigmasterol and isofucosterol.

The choice of adequate internal standards is crucial for reliable quantification of lipids by mass spectrometry. Wherever possible, at least two different internal standards should be employed to account for deviating signal response depending on the size of the molecule (Brügger *et al.*, 1997). Ideally, internal standards should be very similar in size and molecular structure to the naturally occurring plant lipids. However, the internal standards should not be identical to the authentic plant lipids, because this would interfere with the measurement of plant sterol lipids. In plants, only unsaturated sterols were detectable in considerable amounts. Therefore, saturated sterols were considered to be suitable internal standards for sterol lipid quantification.

For the quantification of FSs, the saturated sterols cholestanol and stigmastanol were commercially available.

Plant derived SEs predominantly contain campesterol, stigmasterol and sitosterol, esterified to 18:2 and 18:3 fatty acid residues. Therefore, 16:1-cholesterol and 18:1-cholesterol were selected as internal standards for SE quantification. Analysis of equimolar mixtures of SEs in plant lipid extracts showed a reduction in signal response of SEs with saturated fatty acids. This effect inversely correlated with sample purity, which was indicative of ion suppression. As SEs with saturated fatty acids are less polar than SEs with unsaturated fatty acid residues, they are more prone to suppression. The set of internal standards was therefore expanded to include also a pair of saturated SEs. In subsequent analyses, unsaturated plant derived SEs were quantified in relation to 16:1-cholesterol and 18:1-cholesterol, while saturated SEs were quantified in the presence of 16:0-cholesterol and 18:0-cholesterol.

SG standards with saturated sterol moieties were not commercially available. Therefore, saturated standards for SG quantification were synthesized by glucosylation of cholestanol and stigmastanol, yielding cholestanol-Glc and stigmastanol-Glc (see 2.2.7.1).

ASGs from soybean were commercially available, which contained a mixture of unsaturated molecular species. However, unsaturated plants ASGs were not suitable for use as internal standards for lipid quantification. Saturated ASGs could be obtained by hydrogenation of both, the sterol and the fatty acid moiety, in the presence of hydrogen gas and platinum(IV)oxide (as described in method chapter 2.2.7.1).

Figure 8 shows the mass spectra of unfragmented sterol lipid extracts and internal standards measured after direct infusion to the Q-TOF mass spectrometer by nanospray ionization.

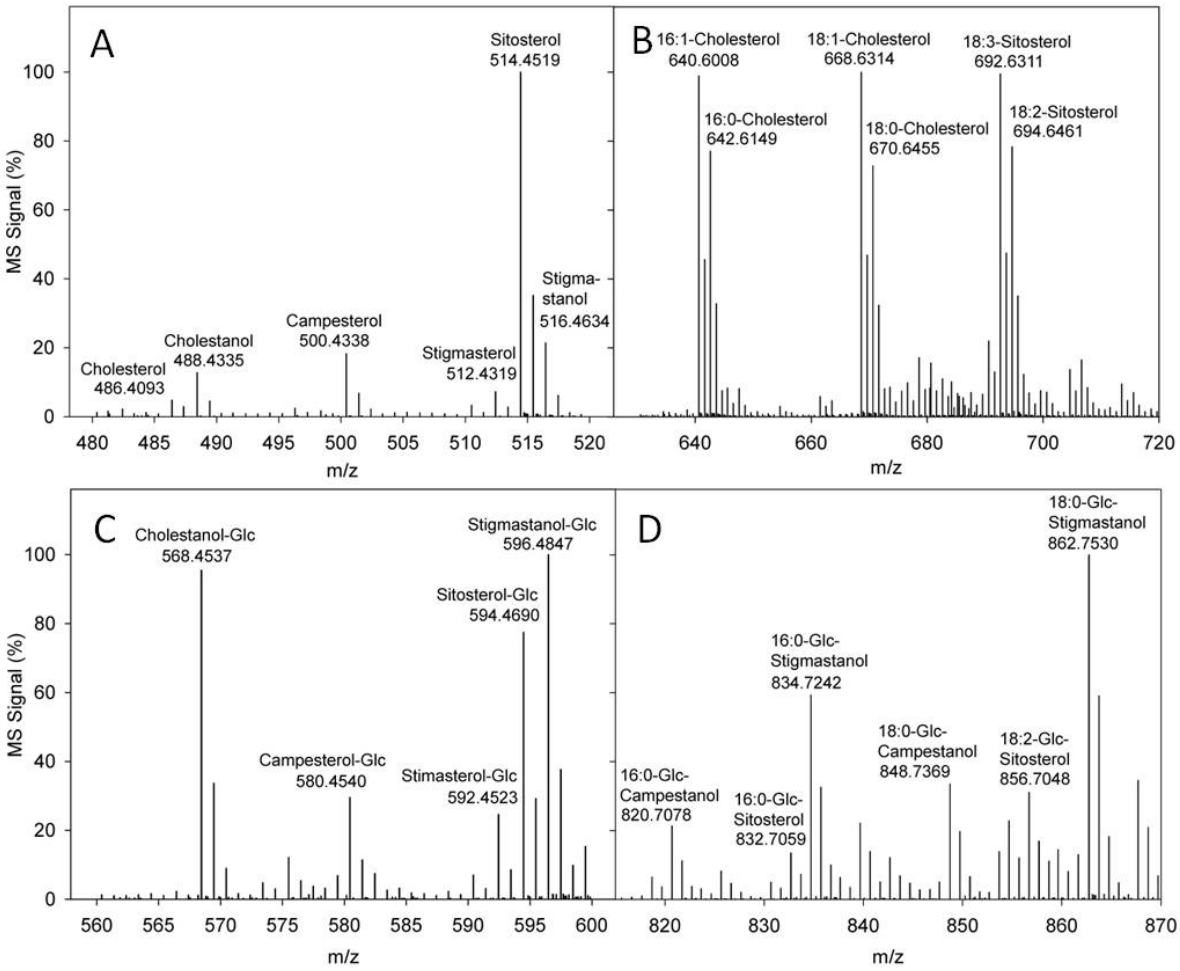

Figure 8: Spectra of Unfragmented Sterol Lipids as Detected by Q-TOF MS. Sterol lipids were applied to the Q-TOF mass spectrometer via nanospray infusion. Plant extracts from *Arabidopsis* were purified by SPE on silica columns prior to analysis. Masses are displayed as detected by Q-TOF MS. **A**: FSs from *Arabidopsis* leaves after derivatization with *N*-chlorobetainyl chloride. Cholestanol and stigmastanol were used as internal standards. **B**: SEs from *Arabidopsis* leaves containing the internal standards 16:0-cholesterol, 16:1-cholesterol, 18:0-cholesterol, and 18:1-cholesterol. **C**: SG mix from soybean; cholestanol-Glc and stigmastanol-Glc were used as internal standards. **D**: ASG mix from soybean; internal standards were 16:0-Glc-stigmastanol, 18:0-Glc-stigmastanol, 16:0-Glc-campestanol, and 18:0-Glc-campestanol.

3.1.2 Fragmentation Patterns and Correction Factors

Fragmentation patterns were analyzed in plant sterols and in internal standards and the most prominent characteristic fragments were chosen for quantification. While conjugated sterols were readily ionized as ammonium adducts and showed clear fragmentation patterns upon collision induced dissociation, ionization of FSs was not satisfactory. In addition, fragmentation of FSs did not yield a fragment suitable for quantification for lack of a strong leaving group. In order to overcome these difficulties, FSs were derivatized with *N*-

chlorobetainyl chloride. Betainylation of sterols yielded a positively charged molecule which displayed a clear fragmentation pattern, resulting in the neutral loss of the sterol moiety. The fragmentation patterns of derivatized FSs and SEs are in depicted in Figure 9. Comparative measurement of betainylated FSs by Q-TOF MS/MS analysis and of silylated FSs by GC-MS analysis, in the presence of saturated internal standards, was conducted to validate the derivatization procedure. Relative signal intensities were lower for unsaturated sterols in Q-TOF MS/MS analysis than in GC-MS analysis. This was indicative of a lower degree of derivatization in unsaturated sterols compared with saturated sterols. The quotient of the values obtained for unsaturated FSs by GC-MS and by Q-TOF MS/MS, when saturated FSs were used as internal standards, was used as a correction factor of 1.61 ± 0.06 (n=7) for the subsequent quantification of betainylated FSs by Q-TOF MS/MS analysis.

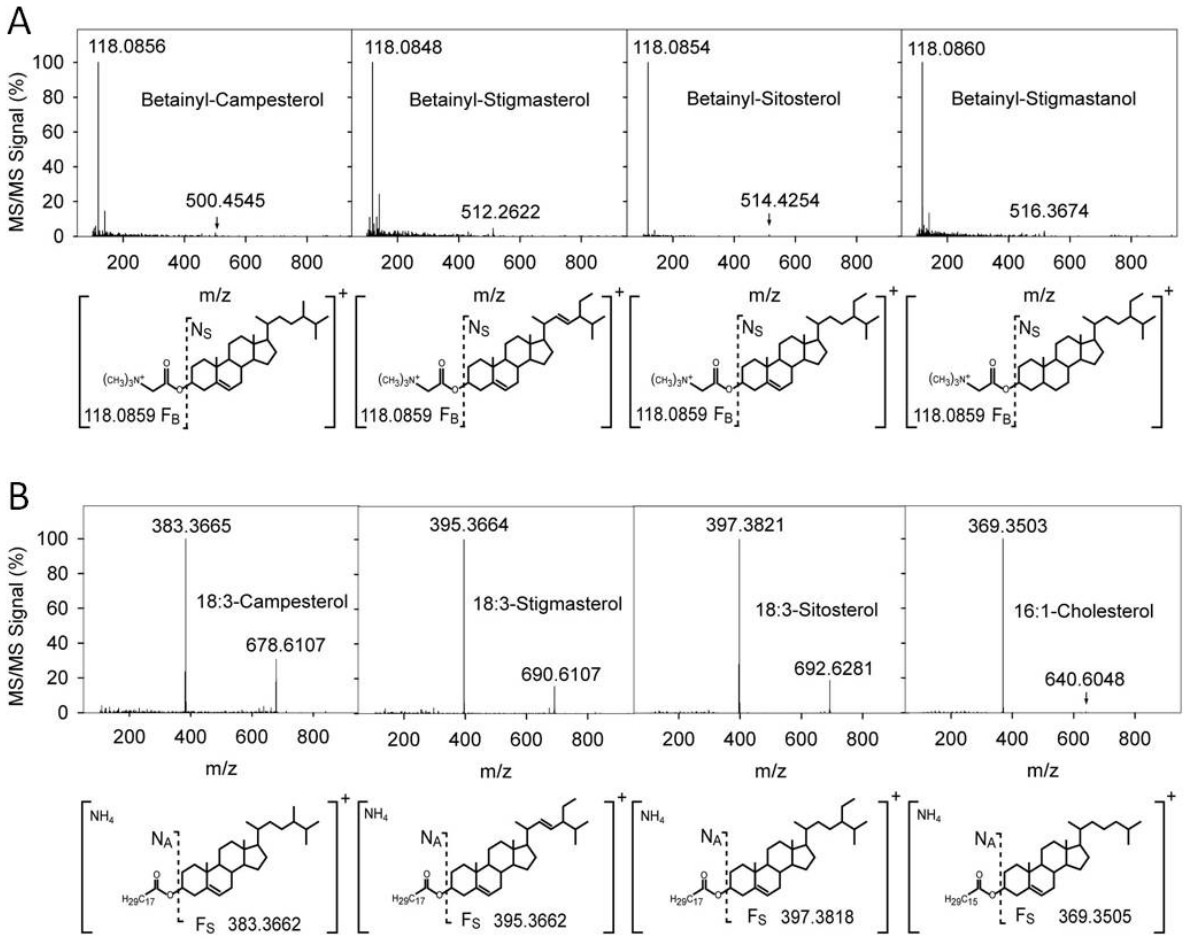

Figure 9: Q-TOF MS/MS Spectra of Free Sterols and Sterol Esters. Fragmentation patterns and molecular structures are shown for the most abundant plant molecular species containing campesterol, stigmasterol and sitosterol and for the internal standards stigmastanol (FS) and 16:1-cholesterol (SE). Calculated masses are given with the molecular structures, fragmentation patterns show the masses as detected by Q-TOF MS/MS **A**: Fragmentation patterns of FSs derivatized with *N*-chlorobetainyl chloride. Collision induced dissociation of betainylated sterols results in the neutral loss of the sterol backbone and the formation of the positively charged betainyl fragment F_B at m/z of 118.0859. **B**: Q-TOF MS/MS spectra of SEs. Fragmentation of the ammonium adducts of SEs leads to the neutral loss of the fatty acid residue and results in the formation of the sterol moiety F_S.

SGs and ASGs were adequately ionized as ammonium adducts and collision induced dissociation produced distinct signal peaks corresponding to the sterol residues. However, when comparing the fragmentation patterns of the saturated internal standards with those of the unsaturated plant sterols, a deviating fragmentation pattern was observed. Figure 10 shows the fragmentation patterns of SGs and ASGs.

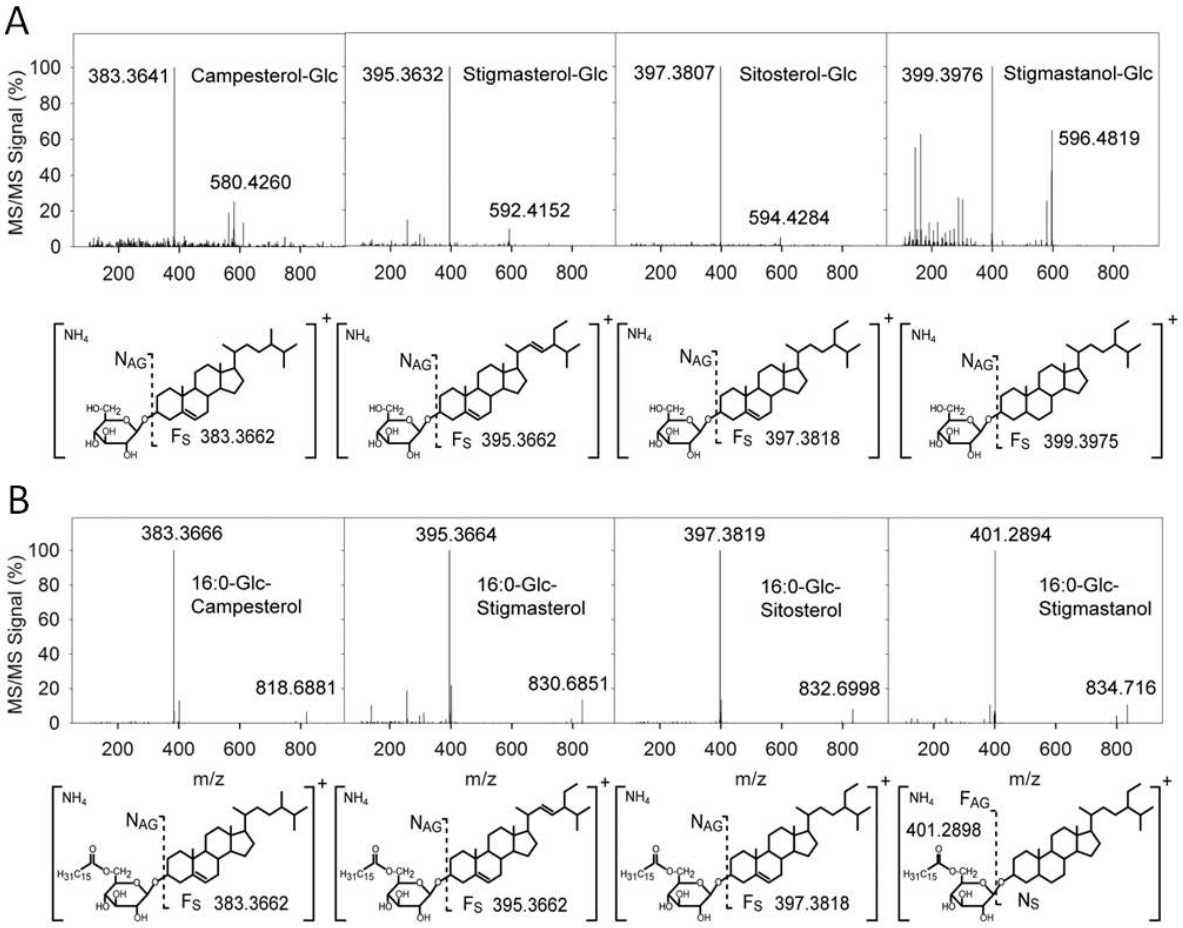

Figure 10: Q-TOF MS/MS Spectra of Sterol Glucosides and Acylated Sterol Glucosides. Fragmentation patterns and molecular structures of ammonium adducts of the respective glycosterols are shown for the most abundant plant molecular species campesterol, stigmasterol and sitosterol and for the internal standard stigmastanol. Calculated masses are given with the molecular structures, fragmentation patterns show the masses as detected by Q-TOF MS/MS **A**: Fragmentation patterns of SGs. Collision induced dissociation results in the neutral loss of the glucose residue and the formation of the sterol moiety F_S. Fragmentation of the internal standard stigmastanol-Glc produces a number of additional fragments and a fragment F_S of a lower intensity. **B**: Q-TOF MS/MS spectra of ASGs. Fragmentation of ASGs containing campesterol, stigmasterol and sitosterol leads to the neutral loss of the fatty acid and glucose residues N_{AG} and results in the formation of the sterol moiety F_S. Fragmentation of the saturated internal standard stigmastanol leads to the neutral loss of the sterol moiety N_S and produces the 16:0-Glc fragment F_{AG} at m/z 401.2898.

Analyses of the fragmentation patterns of saturated and unsaturated SGs showed that all molecular species produced the sterol moiety as the major detectable fragment F_S after collision induced dissociation. However, while unsaturated SGs produced only a single fragment, the fragmentation pattern of saturated SGs as depicted in Figure 10 revealed several additional signal peaks. Due to this deviating fragmentation, the signal intensity corresponding to equal

numbers of molecules was much lower for saturated SGs than for unsaturated SGs. In this case, the use of saturated SGs as internal standards led to an overestimation of SG amounts in the quantified samples.

Mixtures of saturated SGs and unsaturated SGs from soybean were measured by Q-TOF MS/MS and by GC-MS after cleavage of the glycosidic bonds in methanolic HCl. As expected, the results obtained by Q-TOF MS/MS were not consistent with those obtained by GC-MS. A correction factor of 0.169 ± 0.017 (n=3) was determined for unsaturated SGs by forming the quotient of the values obtained for unsaturated SGs by GC-MS and by Q-TOF MS/MS. This correction factor was employed for future quantification based on the presence of saturated SGs as internal standards.

The fragmentation of the saturated ASG 16:0-Glc-stigmastanol resulted in the neutral loss of the sterol residue N_S. At the same time, the fragmentation of plant-derived ASG species, such as 16:0-Glc-sitosterol, led to the neutral loss of the acylated sugar N_{AG} and produced a positively charged sterol fragment F_S, which could be used for quantification. Simultaneous analysis of samples by Q-TOF MS and by GC-MS after cleavage revealed that saturated ASGs were suitable internal standards, when the acylated sugar residue was used for quantification. In this case, no correction factor was needed, because both saturated and unsaturated ASGs produced only one fragment upon collision induced dissociation.

3.1.3 Limit of Detection and Signal Linearity

For every analytical method there are limits of detection and linear quantification of compounds. Q-TOF MS/MS analysis operating in the nanoflow mode is a very sensitive method for lipid analysis. However, with regard to the very low abundances of some molecular species of certain lipid classes in plants, the minimum amounts of each sterol lipid class for reliable quantification needed to be determined. On the other hand, some lipids classes, which are very abundant in plants, might exceed the linear range for exact quantification. In order to define the range of accurate quantification for sterol lipids by Q-TOF MS/MS, signal linearity was determined for all four sterol lipid classes. To this end, a sterol lipid standard was measured at various concentrations in the presence of a second internal standard, which was kept at a constant concentration. Figure 11 shows the signal linearity of FSs, SEs, SGs and ASGs. Signal responses for FSs, SEs and SGs were linear in a range of 0.01 nmol to 1000 nmol in 200 µL of sample volume. Linear signal responses for ASG could be confirmed for a range of 0.1 nmol to 100 nmol in 200 µL of sample volume.

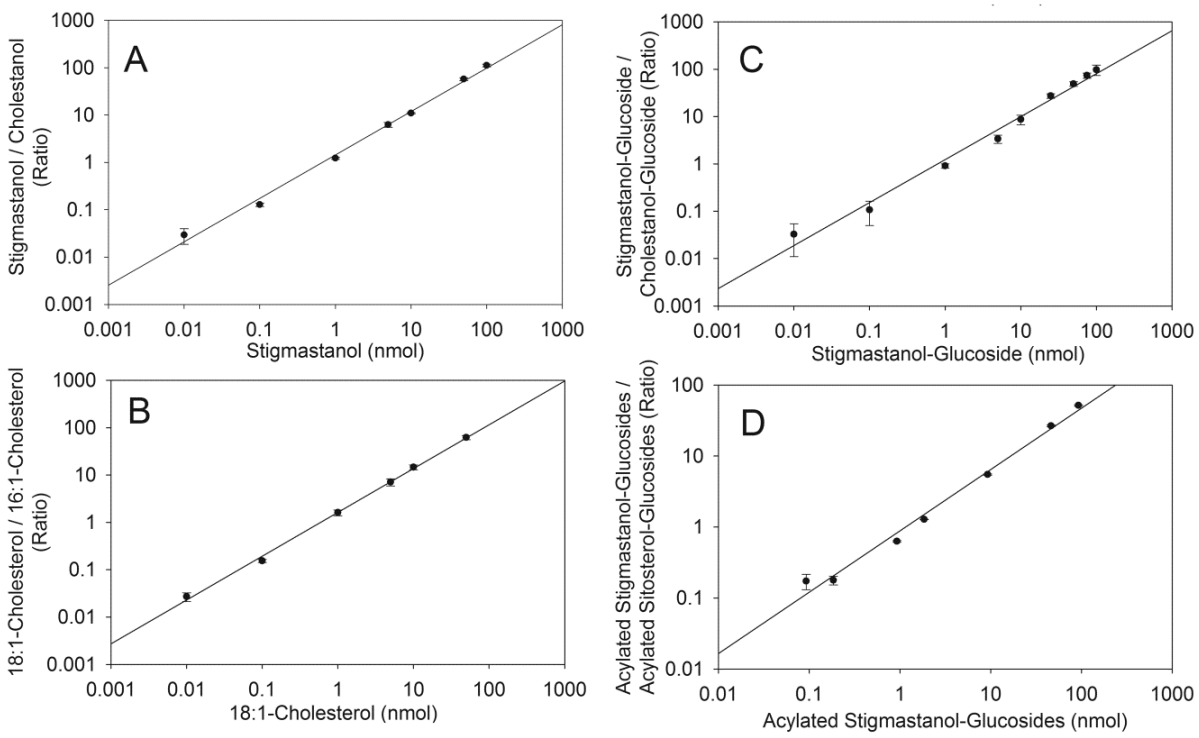

Figure 11: Signal Linearity of Sterol Lipids in Q-TOF MS/MS Analysis. Sterol standards were measured by Q-TOF MS/MS analysis at different concentrations in the presence of a constant amount of a second internal standard. 1000 nmol to 0.01 nmol were dissolved in 200 µL running buffer and 2µL were injected via direct infusion. The data show means and SD of at least three experiments. The graphs show regression lines with logarithmic scaling of the axes. **A** Standard curve of betainylated stigmastanol normalized to betainylated cholestanol. **B** Standard curve of 18:1 cholesterol normalized to 16:1 cholesterol. **C** Standard curve of stigmastanol-Glc normalized to cholestanol-Glc. **D** Standard curve of acylated stigmastanol-Glc normalized to acylated sitosterol-Glc.

.

3.1.4 Comparison of Q-TOF MS/MS Analysis with TLC/GC-MS Analysis

The establishment of novel quantification methods requires the validation by comparison with established methods, which are acknowledged in their field of application. Sterol lipid analysis has previously been conducted mainly by GC based quantification of sterol residues after separation of sterol classes by TLC and subsequent cleavage of conjugated sterols. Figure 12 displays the workflow required for the quantitative analysis of FSs, SEs, SGs and ASGs by Q-TOF MS/MS as compared to GC-MS analysis. Lipid extraction from plant tissue with chloroform and methanol is the first step for sterol lipid analysis in both methods. Due to the high sensitivity of the Q-TOF MS/MS analysis, 20 mg of leaf material was sufficient for quantitative analysis of all sterol lipids. However, in order to accurately quantify the less abundant sterol lipid classes, i.e. ASG and SG, 2 g of leaf tissue were required for TLC/GC analysis. Lipid extracts were then separated by solid phase extraction (SPE) on silica columns into a nonpolar (FS, SE) and a polar (SG, ASG) lipid fraction. SGs, ASGs and SEs could be directly

measured by Q-TOF MS/MS analysis, while FSs were derivatized with *N*-chlorobetainyl chloride. For GC-MS analysis, the polar and nonpolar lipid fractions had to be further purified. FS and SE could be separated by an additional SPE step, while the glycosylated sterols had to be purified by TLC. For GC-MS analysis, all conjugated sterols were subjected to acidic or alkaline cleavage in order to obtain the free sterol residues. These were silylated by derivatization with MSTFA and analyzed by GC-MS.

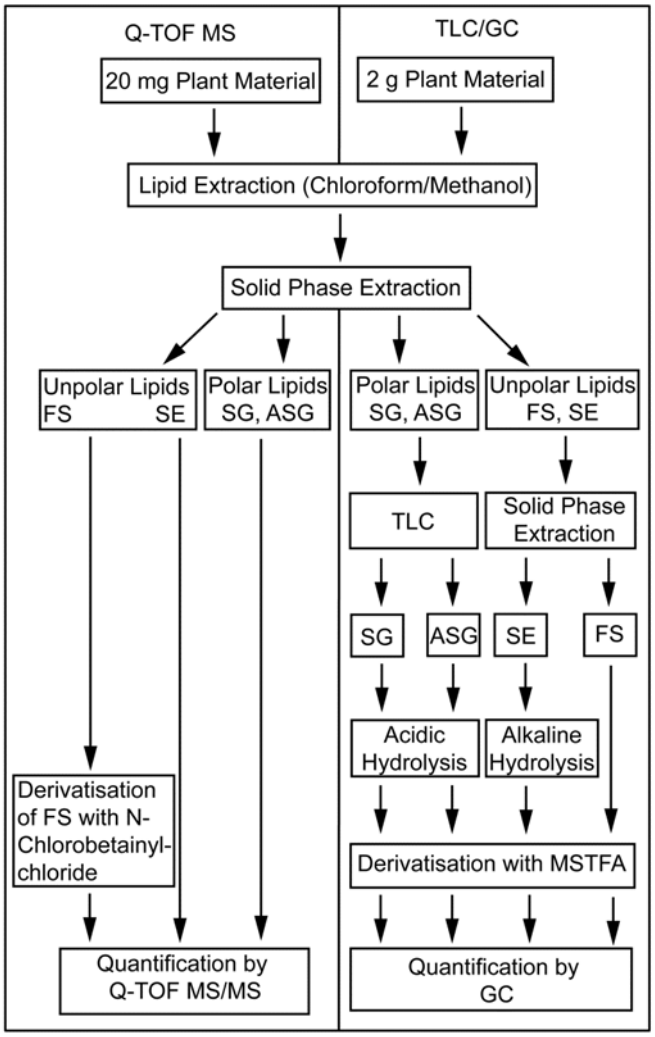

Figure 12: Sterol Lipid Quantification in Plants by Q-TOF MS/MS and TLC/GC. Quantification of all sterol lipid classes from plants via GC analysis required lipid extraction from approx. 2 g of leaf tissue. This was followed by separation of the sterol classes by SPE and TLC and cleavage of conjugated sterols, prior to GC based quantification of the sterol residues. Quantification of sterol lipids by direct infusion Q-TOF MS/MS was possible after lipid extraction from approx. 20 mg of leaf tissue and one purification step by SPE on silica columns.

For validation of the Q-TOF MS/MS based quantification method, sterols were extracted from *Arabidopsis* leaves according to the protocols described above and employing the correction factors described in 3.1.2. Figure 13 shows the amounts of FSs, SEs, SGs and ASGs in *Arabidopsis* leaves quantified by Q-TOF MS/MS and TLC/GC. The two methods yielded comparable results; thereby validating the novel Q-TOF MS/MS based quantification method.

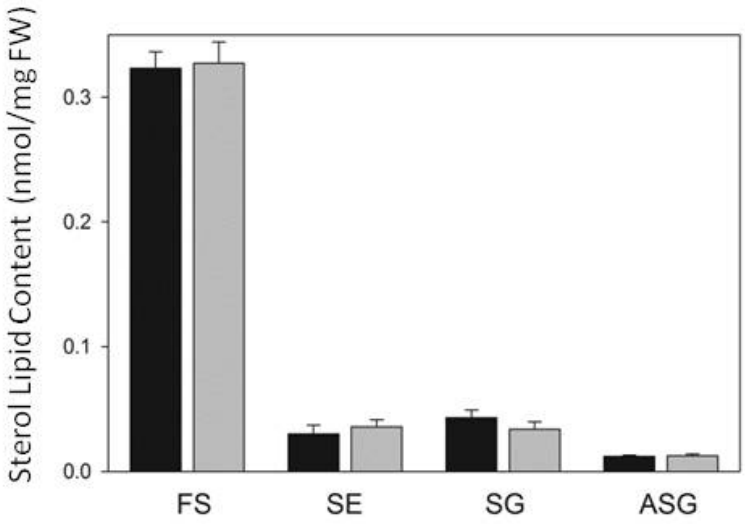

Figure 13: Quantification of Sterol Lipids in *Arabidopsis* by Q-TOF MS/MS analysis compared to analysis by TLC/GC. Lipids were extracted from approx. 2 g of *Arabidopsis* leaves in the presence of internal standards. Fractionation of the crude lipid extract into nonpolar lipids (FS, SE) and polar lipids (SG, ASG) was achieved by SPE on silica columns. Sterols were subsequently analyzed by TLC/GC (black bars) or Q-TOF MS/MS (grey bars). The data present means and standard deviation of four measurements.

3.1.5 Quantification of *Arabidopsis* Sterol Lipids during Phosphate Deprivation

Phosphate deprivation is known to have a large impact on membrane lipid composition. In order to save phosphate for other important cellular processes, phospholipids are degraded and replaced by glycolipids. The galactolipid DGDG is known to strongly increase in plasma membranes of phosphate deprived *Arabidopsis* plants (Härtel *et al.*, 2000; Härtel *et al.*, 2001). However, while there are reports on the increase of other glycolipids such as ASG in phosphate limited oat (Tjellström *et al.*, 2010), the regulation of sterol lipid composition during phosphate deprivation in *Arabidopsis* has not been investigated so far. Taking advantage of the newly established quantification method of sterol lipids in plants by Q-TOF MS/MS, the sterol lipid composition in *Arabidopsis* during phosphate deprivation was analyzed. To this end, wild type plants were grown for two weeks on synthetic medium with or without phosphate and leaves and roots of these plants were harvested. In addition, wild type plants and the *pho1* mutant were grown on soil and leaves were harvested for lipid extraction. The *pho1* mutant is affected in the transport of phosphate to the xylem which results in a constant phosphate starvation of the shoot (Delhaize and Randall, 1995; Poirier *et al.*, 1991). Results of sterol lipid quantification by Q-TOF MS/MS analysis are displayed in Figure 14.

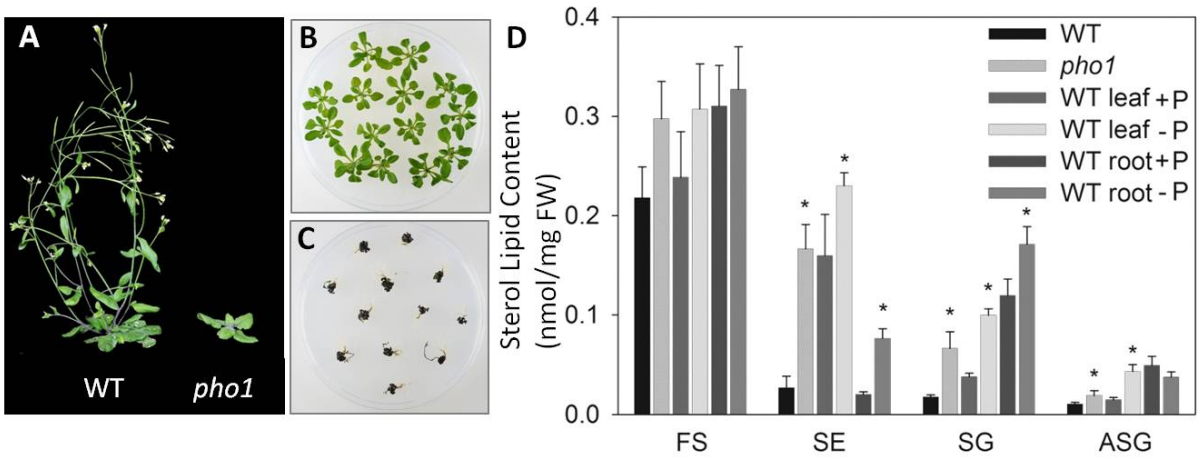

Figure 14: Sterol Lipid Content in *Arabidopsis* during Phosphate Deprivation as Measured by Q-TOF MS/MS. The wild type and the *pho1* mutant, which exhibits a constant phosphate deprivation phenotype in the leaves, were grown on soil (**A**). In addition, wild type plants were grown on synthetic medium with (**B**) or without (**C**) phosphate. Sterols were extracted from leaves of the wild type and the *pho1* mutant and from leaves and roots of wild type plants grown on synthetic medium. Sterol Lipid quantification was performed by Q-TOF MS/MS (**D**). The bars represent means and standard deviations of five replicas and were confirmed by a second independent biological experiment. Asterisks indicate values that are significantly different from those of the wild type or the controls grown with phosphate (according to Student's *t* test; $P<0.02$)

FSs represented by far the most abundant sterol lipid class in leaves of wild type plants grown on soil, and only minor amounts of conjugated sterols were measured. Although the FS content varied between the samples, no significant changes could be detected in either of the conditions analyzed. In contrast, SEs were five-fold increased in the *pho1* mutant. In leaves of wild type plants grown on synthetic medium the SE content was consistently very high, regardless of phosphate availability. However, when grown on phosphate deprived medium, the SE content was even further increased in both leaves and roots. The content of SG and ASG was significantly increased in leaves of phosphate deprived wild type plants and the *pho1* mutant. In roots of wild type plants grown under phosphate deprivation the amount of SGs was significantly increased. At the same time, the amount of ASGs was slightly decreased.

The sterol composition in FS, SEs, SGs and ASGs was analyzed by Q-TOF MS/MS analysis (Figure 15). Campesterol was found to be significantly increased in leaves of phosphate deprived plants grown on synthetic medium when compared to the phosphate supplemented control. This increase was detected in all four sterol lipid classes, but particularly in SEs where a concomitant decrease of stigmasterol/isofucosterol was measured. At the same time, campesterol content was slightly but significantly reduced in FSs, SGs and ASGs of phosphate deprived roots.

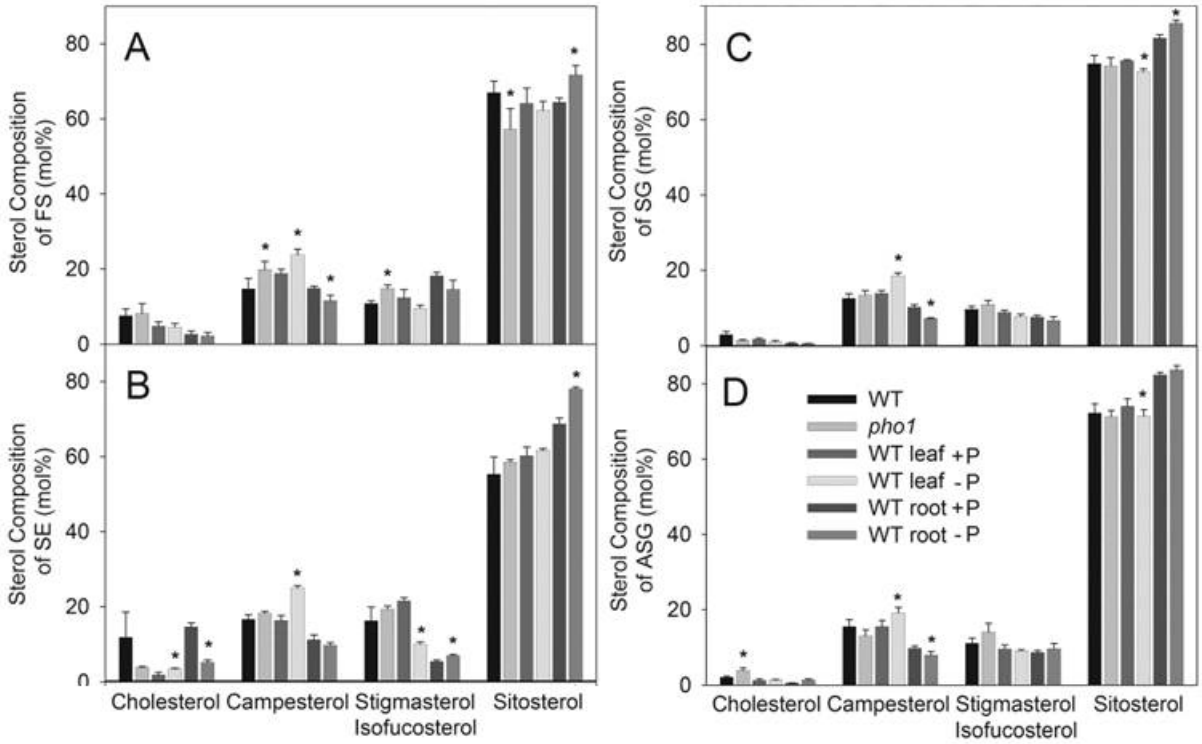

Figure 15: Sterol Composition in *Arabidopsis* during Phosphate Deprivation as Measured by Q-TOF MS/MS. The wild type and the *pho1* mutant were grown on soil. In addition, wild type plants were grown on synthetic medium with or without phosphate. Sterols were extracted from leaves of the wild type and the *pho1* mutant and from leaves and roots of wild type plants grown on synthetic medium. **A**: sterol composition of FSs, **B**: sterol composition of SEs, **C**: sterol composition of SGs, **D**: sterol composition of ASGs. The data present means and standard deviations of five replicas and were confirmed by a second independent biological experiment. Note that stigmasterol and isofucosterol were not distinguished by Q-TOF MS/MS. Asterisks indicate values that are higher than 2 mol% and significantly different from those of the wild type or the controls grown with phosphate (according to Student's *t* test; $P<0.02$)

In addition to sterol composition, the fatty acid composition of SEs and ASGs was measured by Q-TOF MS/MS analysis. Figure 16 shows the fatty acid distribution in ASGs of *Arabidopsis* during phosphate deprivation. Phosphate deprivation results in a significant decrease of 18:2 containing ASGs and a concomitant increase of 18:3 containing ASGs in leaves of the *pho1* mutant and the wild type. In leaves of phosphate deprived wild type plants, 16:0 containing ASGs were also decreased, though not significantly. Fatty acid distribution of SEs in leaves of the *pho1* mutant and the wild type grown without phosphate revealed similar reductions of 18:2 containing ASGs and concomitant accumulation of 18:3 containing fatty acids (data not shown). In roots of phosphate limited wild type plants, 18:2 containing ASGs were not reduced. Instead a significant increase of 18:3 containing ASGs was accompanied by a reduction of 16:0 containing ASGs.

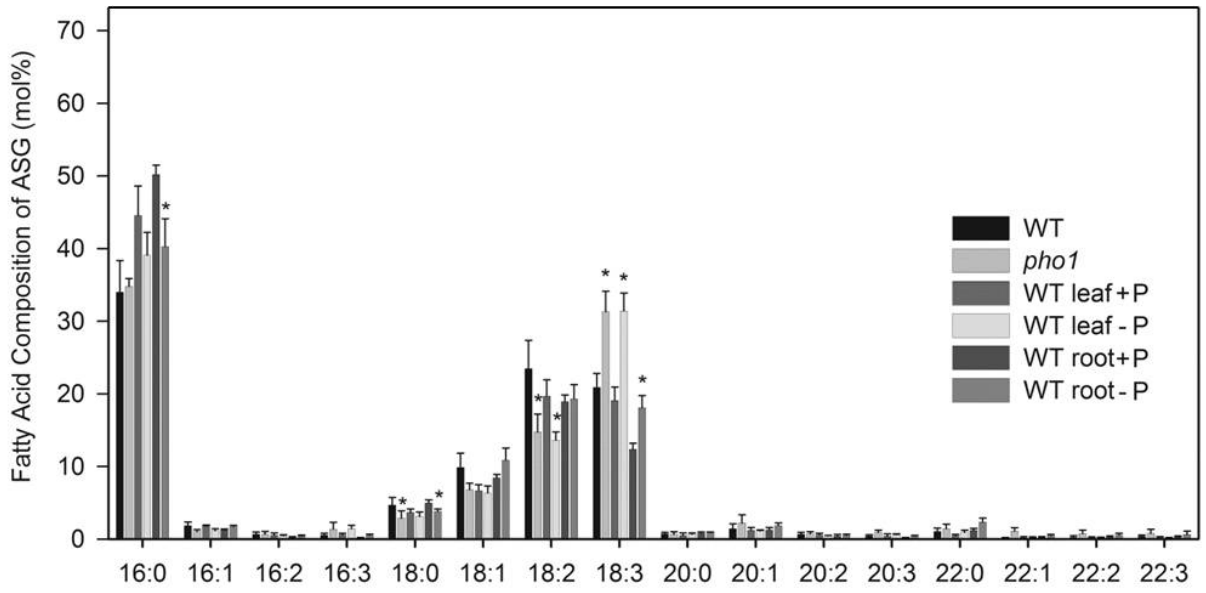

Figure 16: Fatty Acid Composition of Acylated Sterol Glucosides in *Arabidopsis* during Phosphate Deprivation. Sterols were extracted from leaves of the wild type and the *pho1* mutant grown on soil and from leaves and roots of wild type plants grown on synthetic medium with or without phosphate. The data present means and standard deviations of five replicas and were confirmed by a second independent biological experiment. Asterisks indicate values that are higher than 2 mol% and differ significantly from those of the wild type or the controls grown with phosphate (according to Student's *t* test; $P<0.02$)

3.2 Membrane Lipid Profiling of *Lotus japonicus*

A novel method for sterol lipid quantification in plants by Q-TOF MS/MS analysis was established in this work, as described in chapter 3.1. Similar approaches were used to establish the quantification of sphingolipids, on the basis of a method described by Markham and Jaworski (2007) for the measurement of sphingolipids by tandem mass spectrometry (vom Dorp, 2010). A mass spectrometry based method for the analysis of phospho- and galactoglycerolipids, which had previously been described by Welti *et al.* (2002), was adapted by Dr. Isabel Dombrink and Helga Peisker. In addition, the quantitative analysis of nonpolar lipids such as DAG and TAG by Q-TOF MS/MS was shown to be a sensitive and suitable method (vom Dorp *et al.*, 2012 *in press*).

These methods provide the means for a thorough characterization of the lipid composition in plants. *Lotus japonicus* was chosen as a model plant to investigate the role of glycolipids in symbiotic plant microbe interactions. *Lotus* can establish root nodule symbiosis with the nitrogen fixing soil bacterium *Mesorhizobium loti* and arbuscular mycorrhiza formation with the mycorrhizal fungus *Glomus intraradices*. These two symbioses are tightly regulated by the availability of phosphate in the soil. In *Arabidopsis,* the role of glycolipids for the upkeep of membrane stability during low phosphate conditions is well documented (see 1.1.1). In this work, the characterization of membrane lipids during phosphate deprivation should provide further insight into membrane remodeling in different tissues of *Lotus japonicus*.

During the interaction of *Lotus japonicus* with *Mesorhizobium*, the development of nodules requires large amounts of lipids for the synthesis of symbiotic membranes. In order to investigate the putative functions of glycolipids in these membranes, nodules were harvested and lipids were quantified for comparison with roots lipids.

In arbuscular mycorrhiza formation the symbiotic fungus *Glomus intraradices* colonizes the roots and forms mycorrhiza specific structures, which enable the exchange of nutrients between the plant and the fungus. Mycorrhiza formation leads to an improved phosphate supply to the plant and is induced by phosphate starvation. Lipids were analyzed in mycorrhized roots and compared with non-mycorrhized roots to monitor putative changes in lipid composition.

3.2.1 Lipid Quantification in Different Tissues of *Lotus japonicus* during Phosphate Deprivation

Lotus japonicus wild type plants were grown from seeds on a mixture of sand and vermiculite under non-sterile conditions and watered with 2.5 mM phosphate and 0.5 mM nitrogen for several weeks. The plants were transferred to silica sand and watered with deionized water for two weeks, prior to fertilization with an artificial nutrient solution containing a full mineral mixture with either 2.5 mM or 0 mM phosphate (see 2.2.4). After nine weeks, plant growth was retarded in the phosphate deprived plants, which contained a lower number of young leaves compared to the plants grown under full phosphate supply, as can be seen in Figure 17. Figure 17 E and F show the upper and lower side of individual *Lotus* leaves. The leaves of phosphate deprived plants showed a tinge of red, which was more distinct on the lower surface of the leaves, indicative of anthocyanin accumulation. Regardless of their phosphate status, all plants were well nodulated. Nodulation was presumably due to infection by *Mesorhizobium loti* cells that were present in the pots and trays of the plant growth chamber. Figure 17 C and D show photographs of exemplary roots containing nodules of different size and color. The plants grown under full phosphate supply, contained a large number of young nodules, characterized by a small size and a light-red color, in addition to more mature nodules of a larger size and a dark-red appearance. On the contrary, most nodules found on roots of phosphate deprived plants appeared to have reached a mature stage.

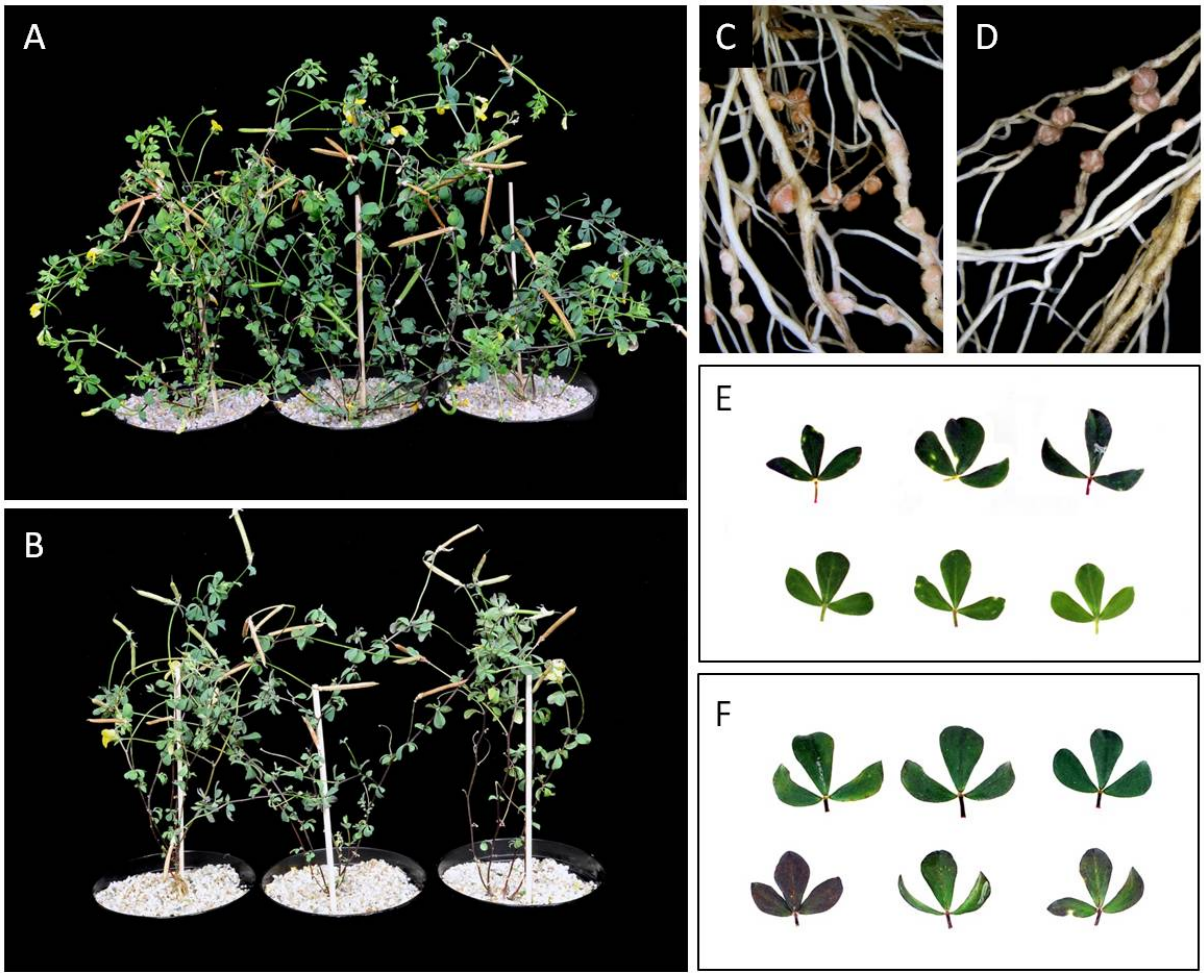

Figure 17: *Lotus japonicus* Wild Type Plants Grown under Phosphate Deprivation. *Lotus* wild type plants were grown from seeds on a mixture of sand and vermiculite and watered with full mineral solution for several months before being transferred to silica sand. Plants were watered with deionized water for two weeks prior to fertilization with mineral mixture containing 0.5 mM nitrogen and 2.5 mM (**A**) or 0 mM (**B**) phosphate for nine weeks. Roots of wild type plants grown under 2.5 mM (**C**) and 0 mM (**D**) phosphate contained nodules of different size and color. **E** and **F**: Leaves of plants grown under full phosphate supply (**E**) and under phosphate deprivation (**F**); showing the upper side (upper row) and the lower side (lower row) of the leaves.

Lipids were extracted from leaves, roots and nodules of *Lotus japonicus* grown with or without phosphate, for subsequent analysis by Q-TOF MS/MS. Figure 18 shows the distribution of phospho- and galactolipids in leaves, roots and nodules. Evaluation of the absolute amounts of phospho- and galactolipids revealed that all phospholipids, PS, PI, PG, PE and PC were decreased in leaves, roots and nodules during phosphate deprivation.

PA represents a minor lipid in plant tissues, but it is released from PC in large amounts by catalytic activity of phospholipase D after wounding (Wang *et al.*, 2000). Delays during tissue harvest and extraction procedures can lead to PC degradation and subsequent accumulation of PA. Therefore, PA can be considered a marker lipid for PC integrity and thus for sample quality. The low amounts of PA detected in all tissues are indicative of a high sample quality.

The decrease of phospholipids during phosphate deprivation was accompanied by an increase of DGDG in all tissues. In phosphate deprived leaves, the absolute amount of DGDG was

only slightly increased. At the same time, the absolute amount of MGDG was significantly reduced, which is indicative of chloroplast degradation. However, due to the strong reduction of all other lipid classes, the proportion of DGDG was increased from 31.5 mol% to 44.9 mol% in phosphate deprived leaves.

In roots, the absolute amounts of MGDG and SQDG were marginally increased. The strong reduction of phospholipid content resulted in an increase of the percentages of MGDG and SQDG in roots and nodules under low phosphate conditions. MGDG and SQDG constituted 5.4 mol% and 2.5 mol% in roots and 5.0 mol% and 3.0 mol% in nodules, when plants were grown under full phosphate supply. During phosphate deprivation, these lipids were increased to 9 mol% and 5.1 mol% in roots and to 6.8 mol% and 5.2 mol% in nodules. In comparison, DGDG was much more strongly accumulated in both roots and nodules during phosphate starvation. The absolute amount of DGDG was about doubled, from 0.25 nmol/mg FW to 0.53 nmol/mg FW in roots and from 0.29 nmol/mg FW to 0.55 nmol/mg FW in nodules. The proportion of DGDG in roots and nodules was even more strikingly increased from 12.2 mol% to 37.1 mol% in roots and from 10.0 mol% to 35.9 mol% in nodules, rendering DGDG three-fold more abundant than during full phosphate supply. While the absolute amounts give a more detailed overview of the lipid metabolism during phosphate deprivation, the proportions of phospho- and galactolipids are very stable between experiments and can therefore serve as references to determine the degree of phosphate deprivation in a plant.

In addition to the analysis of phospho- and galactolipids, a comprehensive study of sterol lipids during phosphate deprivation in *Lotus japonicus* was conducted. Changes in sterol lipid content during phosphate starvation were previously detected in *Arabidopsis thaliana* as described in chapter 3.1.5. Figure 19 panels A-C display the sterol lipid distribution in leaves, roots and nodules during phosphate deprivation in *Lotus japonicus*. Absolute amounts of total sterol lipid content were unaltered in all tissues; however there were some changes in sterol lipid distribution. The proportion of FSs was slightly but significantly reduced during phosphate starvation. In leaves and nodules this decrease was accompanied by an increase of SEs and SGs. SEs were increased from 30.7 mol% to 37.8 mol% in leaves and from 21.3 mol% to 24.9 mol% in roots. SGs were increased from 9.0 mol% to 12.8 mol% in leaves and from 8.7 mol% to 10.8 mol% in roots. In nodules, the SE amount remained unchanged, and SGs were the only sterol lipids to be elevated under low phosphate conditions. This tissue showed the strongest increase of SGs from 15.7 mol% to 22.5 mol%. The ASG content remained constant in all tissues during phosphate deprivation.

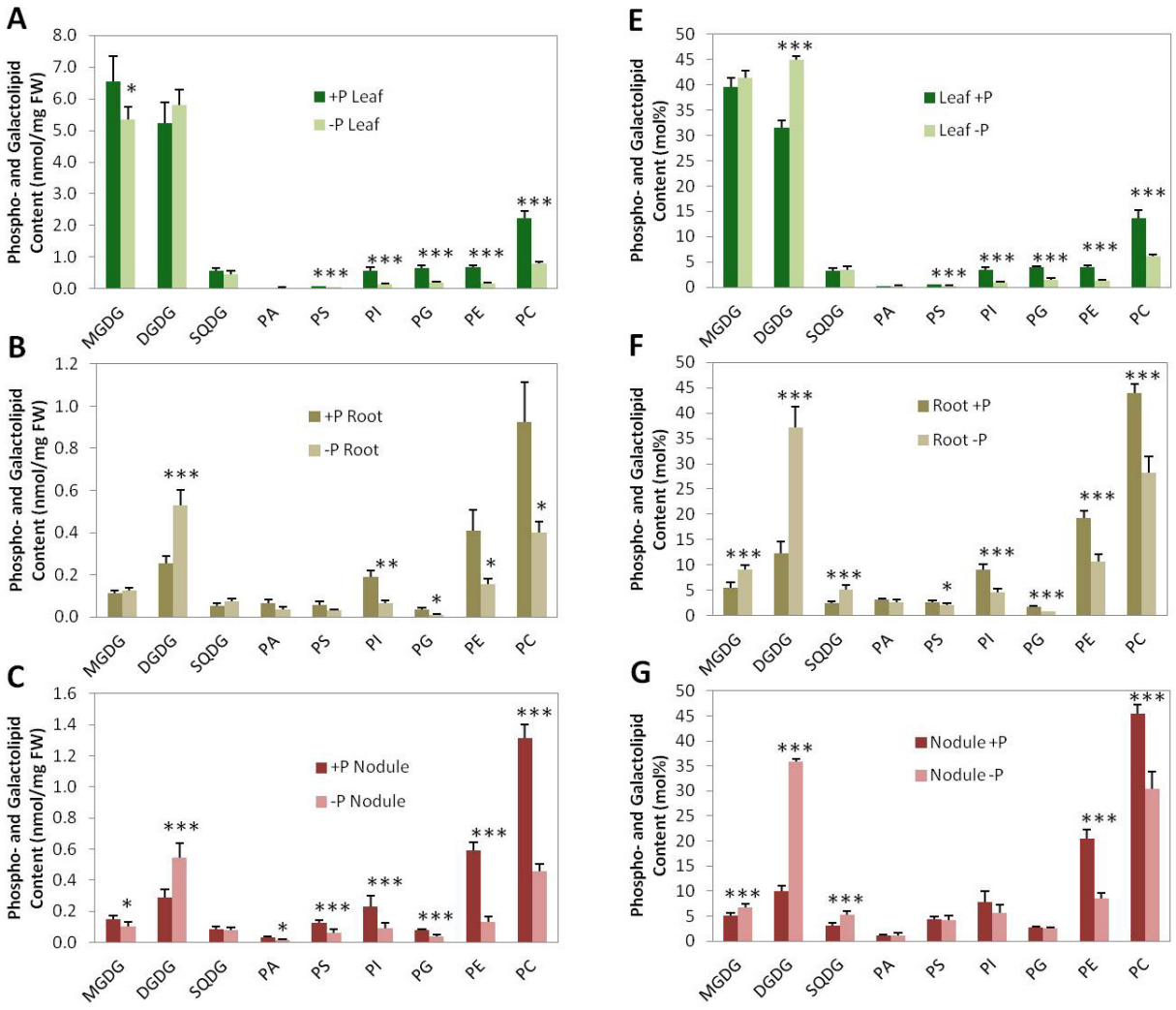

Figure 18: Phospho- and Galactolipid Distribution in *Lotus japonicus* during Phosphate Deprivation. *Lotus japonicus* wild type plants were watered with deionized water for two weeks and subsequently fertilized with mineral mixture containing 0.5 mM nitrogen and 2.5 mM or 0 mM phosphate for nine weeks. Lipids were extracted from leaves (**A; E**), roots (**B; F**), nodules (**C, D**) and analyzed by Q-TOF MS/MS analysis in the presence of internal standards. Absolute (**A-C**) and relative amounts (**E-G**) of phospho- and galactolipids are displayed. Data are mean and standard deviation of five measurements. Asterisks indicate values that are significantly different from the control (according to Student's *t* test, Welch correction, $P<0.05$ (*); $P<0.02$ (**); $P<0.01$ (***)).

In Figure 19 panels D-F, the amounts of the nonpolar glycerolipids DAG and TAG during phosphate starvation in leaves, roots and nodules of *Lotus japonicus* are depicted. While DAGs were not changed during phosphate starvation in leaves and roots, the TAG content was considerably increased from 0.6 nmol/mg FW to 2.0 nmol/mg FW in leaves and from 1.3 nmol/mg FW to 2.9 nmol/mg FW in roots. In phosphate deprived nodules, the TAG content remained unaltered and the amount of DAG was slightly decreased from 0.50 nmol/mg FW to 0.35 nmol/mg FW.

GlcCers were quantified by Q-TOF MS/MS analysis in leaves and roots of *Lotus* transgenic empty vector control plants (see 3.5.2) grown under phosphate deprivation and under

phosphate replete conditions. While a slight increase of GlcCer was detected in leaves of phosphate deprived plants, this lipid class was moderately reduced in roots.

In conclusion, phosphate deprivation resulted in a strong decrease of phospholipid content in leaves, roots and nodules of *Lotus japonicus*. This was compensated by a drastic accumulation of DGDG in all tissues, especially in roots and nodules. Furthermore, there was a considerable increase of TAG in leaves and roots during phosphate starvation. Likewise, the contents of the nonpolar SEs were elevated in phosphate deprived leaves and roots but not in nodules. SGs were moderately increased in leaves and roots at the expense of FSs. This effect was more pronounced in nodules.

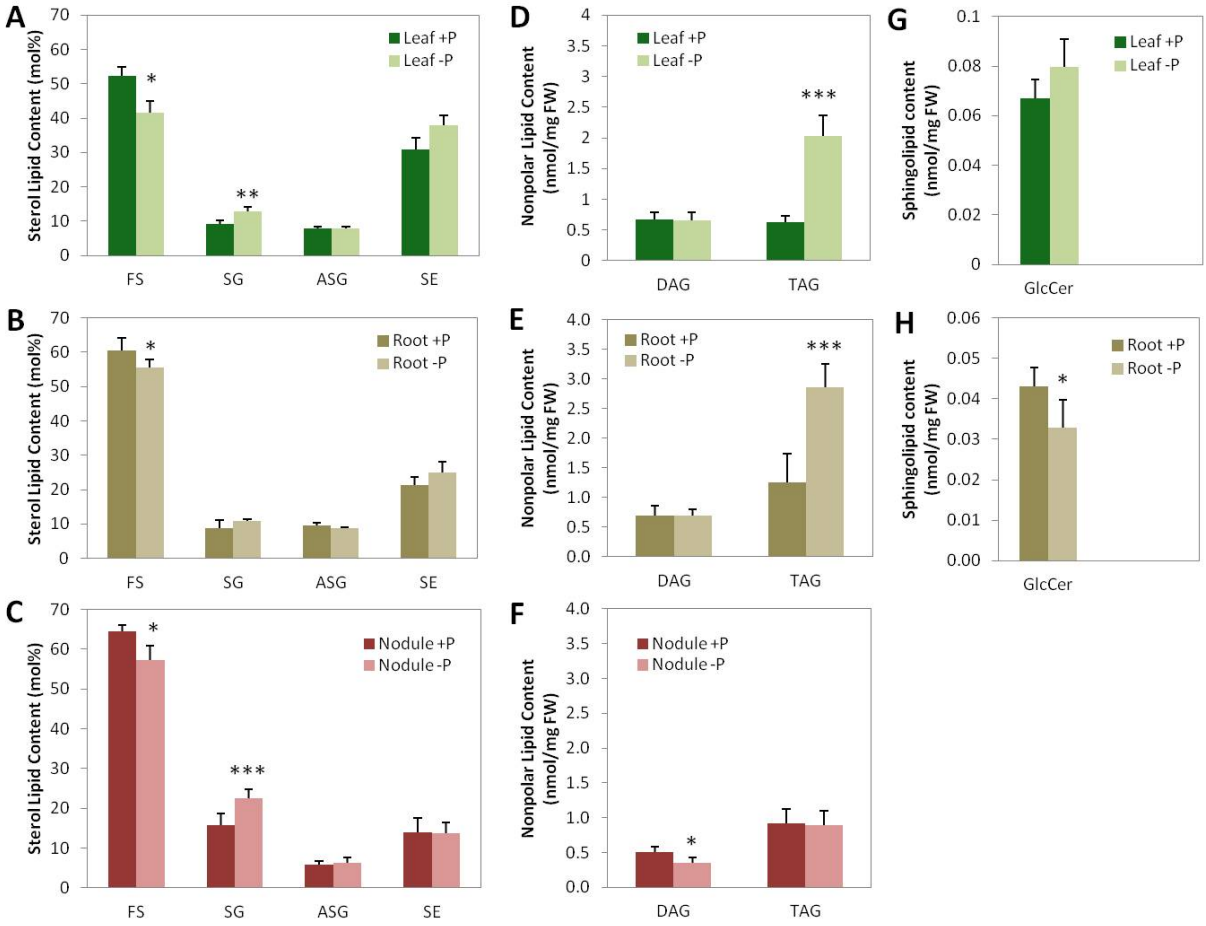

Figure 19: Distribution of Sterols, Nonpolar Glycerolipids and Sphingolipids in *Lotus japonicus* during Phosphate Starvation. A-C: sterol lipid distribution in leaves, roots and nodules in mol% of total sterol lipids; **D-F**: distribution of nonpolar glycerolipids in leaves, roots and nodules; **G-H**: glucosylceramide content in leaves and roots and nodules. *Lotus japonicus* wild type plants were watered with deionized water for two weeks and subsequently fertilized with mineral mixture containing 0.5 mM nitrogen and 2.5 mM or 0 mM phosphate for nine weeks. Lipids were extracted from the tissue and analyzed by Q-TOF MS/MS in the presence of internal standards. Data are mean and standard deviation of five measurements. Asterisks indicate values that are significantly different from the control (according to Student's *t* test, Welch correction, $P<0.05$ (*); $P<0.02$ (**); $P<0.01$ (***)).

3.2.2 Changes in Lipid Composition during Nodulation in *Lotus japonicus*

The formation of a new plant organ, the nodule, requires large amounts of lipids for membrane establishment. Approximately one half of the total lipid content in nodules is associated with the symbiosomes (Gaude *et al.*, 2004). These are surrounded by the peribacteroid membrane, which is of plant origin and is therefore constituted of plant derived membrane lipids. While the phospho- and galactolipid composition of the peribacteroid membrane has been previously studied in soybean (Gaude *et al.*, 2004), the sterol lipid and sphingolipid content in nodules is yet to be determined. The galactolipid DGDG is a constituent of the peribacteroid membrane, and *Lotus* RNAi mutants affected in DGDG content display severe reduction of nodulation efficiency during phosphate deprivation (Gaude, 2008). Similar to DGDG, SGs were shown to accumulate in leaves and roots of *Arabidopsis* (see 3.1.5) and in *Lotus* (see 3.2.1) under phosphate limitation. Elevated levels of GlcCers could also be detected in *Arabidopsis* grown under phosphate deprivation (vom Dorp, 2010). The accumulation of SGs and GlcCers during phosphate starvation indicates a regulation of these lipids similar to DGDG. In this work, a putative function of SGs and GlcCers during nodulation was analyzed. To this end, sterol lipid and GlcCer content was quantified in nodules and compared with the lipid content in roots. Changes in other lipid classes were monitored to obtain a more comprehensive lipid profile of *Lotus japonicus*.

3.2.2.1 Phospho- and Galactolipid Composition in Leaves, Roots and Nodules

Phospho- and galactolipid distribution in *Lotus japonicus* wild type leaves, roots and nodules was measured by Q-TOF MS/MS and the results are displayed in Figure 20. MGDG and DGDG are abundant constituents of the thylakoid membranes and make up the major proportion of total phospho- and galactolipids in leaves. In this experiment, MGDG and DGDG were found to represent 39.5 mol% and 31.5 mol%, respectively of total membrane glycerolipids. In contrast, the predominant membrane glycerolipids in roots were PC (44.0 mol%) and PE (19.3 mol%), followed by DGDG (12.2 mol%) and PI (9.1 mol%). MGDG is restricted to plastids and therefore represents only a minor lipid in roots and nodules with about 5 mol% of the total phospho- and galactolipid content. The only differences in phospho- and galactolipid distribution between roots and nodules were a slight increase of PS and PG. A higher amount of PA in roots was most probably due to phospholipase D activity induced by the slightly delayed harvest of roots compared to nodules.

Comparison of the absolute amounts of phospho- and galactolipids in roots and nodules revealed an increase of PE from 0.41 to 0.59 nmol/mg FW and an increase of PC from 0.92 to 1.31 nmol/mg FW. Absolute amounts of MGDG, DGDG, SQDG and PI were only marginally elevated, while PS and PG were twice as high in nodules as in roots.

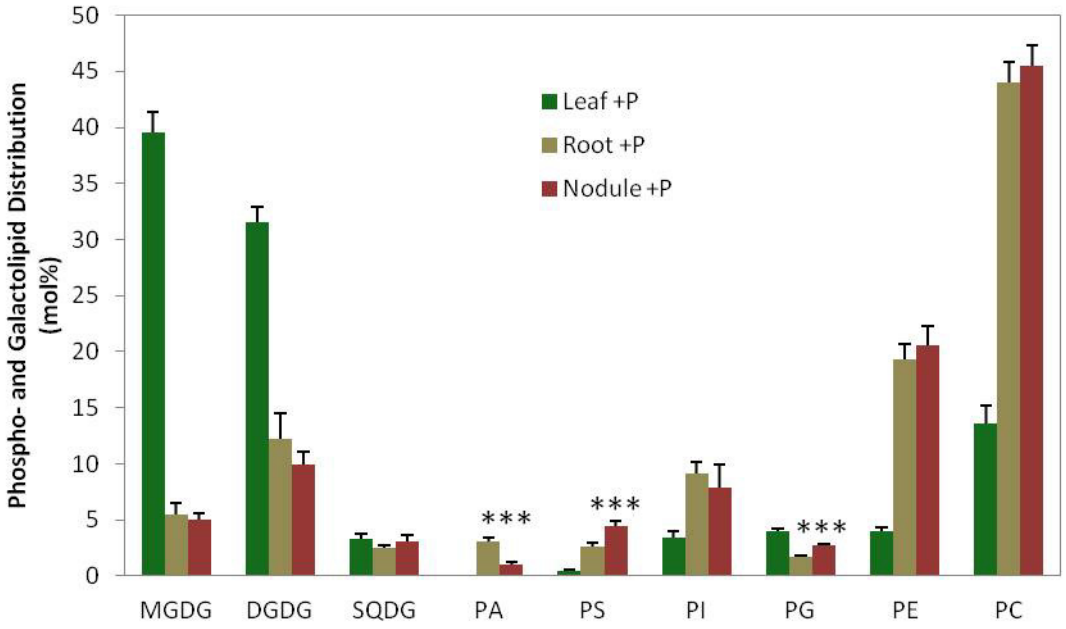

Figure 20: Distribution of Phospho- and Galactolipids in *Lotus japonicus* Leaves, Roots and Nodules. *Lotus japonicus* wild type plants were grown on sand and fertilized with mineral mixture containing 0.5 mM nitrogen and 2.5 mM phosphate for nine weeks. Lipids were extracted and quantified by Q-TOF MS/MS analysis in the presence of internal standards. Data are mean and standard deviation of five measurements. Asterisks indicate values obtained for nodules that are significantly different from those obtained for roots (according to Student's *t* test, Welch correction, $P<0.01$ (***)).

Due to the nature of nodules as symbiotic plant organs, the impact of bacterial lipids on the lipid profile obtained by Q-TOF MS/MS analysis has to be taken into consideration. *Mesorhizobium* contains appreciable amounts of PG and PC (Devers *et al.*, 2011), therefore the fatty acid profiles of these lipids in roots and nodules were compared (see appendix for fatty acid profiles). Putative bacterial lipids were identified by comparison with the literature and their presence discussed in 4.4.

3.2.2.2 Sterol Lipid Composition in Leaves, Roots and Nodules

Comprehensive analysis of sterol lipids by Q-TOF MS/MS was performed in leaves, roots and nodules of *Lotus japonicus* wild type. Prior to quantification by Q-TOF MS/MS analysis, the molecular species composition of sterols was determined by GC-MS analysis in leaves, roots and nodules, as well as in flowers and siliques. The major sterols in *Lotus japonicus* were identified as campesterol, stigmasterol and sitosterol. Figure 21 shows the distribution of these sterols in the different tissues. Cholesterol was also present in lower amounts but could not be reliably quantified by GC-MS analysis.

The measurements revealed striking differences in the distribution of the different sterols within the plant. Campesterol was found to constitute around 10 mol% of total sterol lipids in leaves, roots and flowers and was slightly elevated in siliques and nodules. In addition, there were major changes in the ratio of stigmasterol and sitosterol in the different tissues.

Stigmasterol was barely detectable in flowers and made up around 5 mol% in siliques and nodules and 10 mol% in leaves. Strikingly, the stigmasterol content was increased to almost 50 mol% in roots, at the expense of the otherwise predominant sitosterol. Further analyses showed that the stigmasterol content was always very high in roots compared to leaves and nodules, but the exact proportions varied between experiments.

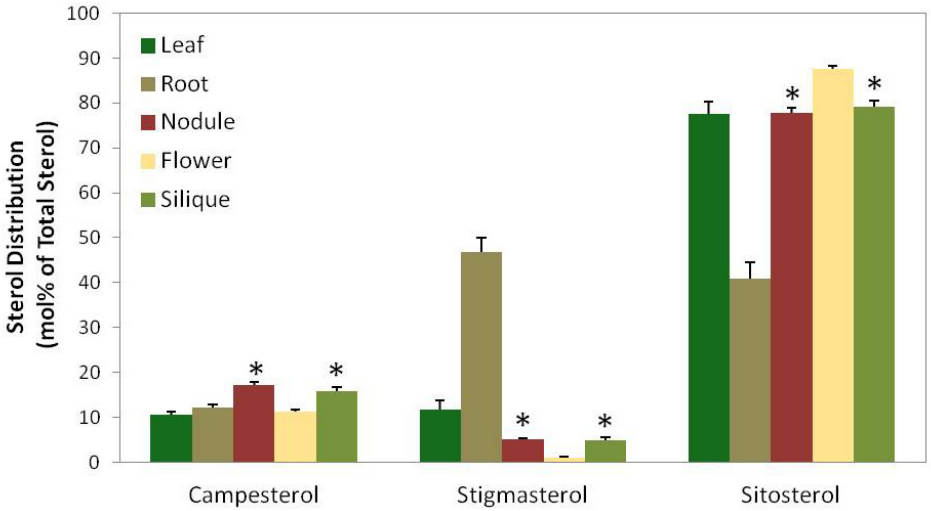

Figure 21: Sterol Composition of Total Sterols from *Lotus japonicus*. Sterols were extracted from leaves, roots, nodules, flowers and siliques of *Lotus japonicus* grown on silica sand under full nutrient supply. Conjugated sterols were cleaved by alkaline hydrolysis and the released sterol moieties were silylated for subsequent identification and quantification by GC-MS analysis. Data are mean and standard deviation of at least three measurements. Asterisks indicate values obtained for nodules that are significantly different from roots; or for siliques that are significantly different from flowers (according to Student's *t* test, Welch correction, $P<0.01$ (*)).

Q-TOF MS/MS analysis yielded further information on the distribution of stigmasterol and sitosterol in free and conjugated sterols in leaves, roots and nodules as depicted in Figure 22. Stigmasterol was reproducibly very high in *Lotus* roots and significantly lower in the root derived nodules. The most severe accumulation of stigmasterol in roots was detected in FSs, were it made up 33.8 mol%. Stigmasterol was also elevated, to a lower degree, in SGs and ASGs. The nonpolar storage lipid SE, however, displayed a stigmasterol content of 12.7 mol% in roots, which was similar to that of leaves and nodules. These findings indicate that the accumulation of stigmasterol in *Lotus* roots was restricted to membrane forming sterol lipids.

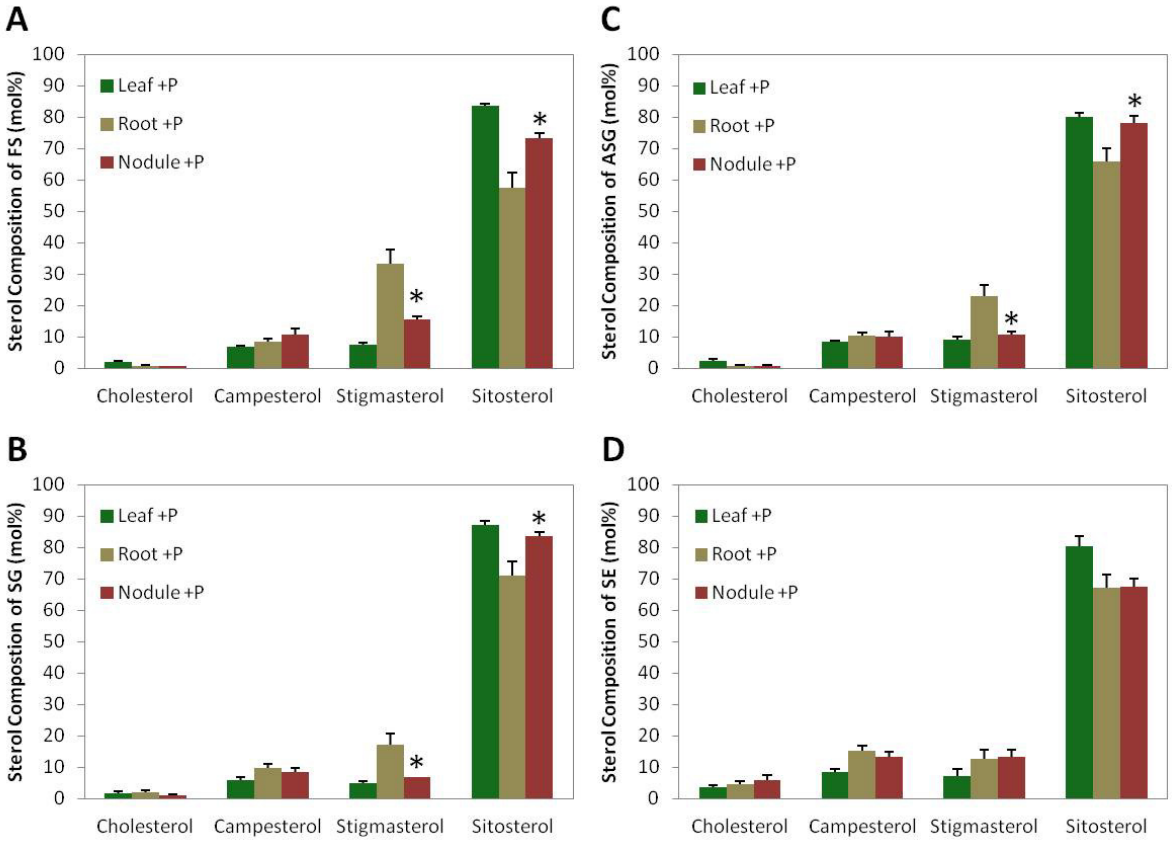

Figure 22: Distribution of Sterol Molecular Species in Sterol Lipid Classes of *Lotus japonicus* Leaves, Roots and Nodules. A: sterol composition of free sterols (FS); **B**: sterol glucosides (SG); **C**: acylated sterol glucosides (ASG); **D**: sterol esters (SE). *Lotus japonicus* wild type plants were grown on silica sand and fertilized with mineral mixture containing 0.5 mM nitrogen and 2.5 mM phosphate for nine weeks. Lipids were extracted and quantified by Q-TOF MS/MS analysis in the presence of internal standards. Data are mean and standard deviation of five measurements. Asterisks indicate values obtained for nodules that are significantly different from those obtained for roots (according to Student's *t* test, Welch correction, $P<0.01$ (*)).

In addition to the sterol composition of sterol lipids, the distribution of sterol lipid classes was compared in *Lotus* leaves, roots and nodules (see Figure 23). Quantification of FSs, SGs, ASGs and SEs by Q-TOF MS/MS analysis revealed a significant increase of SGs from 8.7 mol% to 15.7 mol% during nodulation, accompanied by a decrease of ASG from 9.5 mol% to 5.7 mol%. At the same time, the amount of FSs was slightly increased in nodules, from 60.6 mol% in roots to 64.5 mol% and SEs were decreased from 21.3 mol% to 14.0 mol%.

Additional experiments indicated that, while the low amounts of ASGs can already be observed in very young nodules, the increase of SG was more prominent in mature tissue (data not shown). Comparison of the absolute amounts of sterol lipids during nodulation revealed an increase of FSs from 0.32 to 0.47 nmol/mg FW. SG content was increased from 0.05 nmol/mg FW in roots to 0.11 nmol/mg FW in nodules. At the same time, ASGs and SEs were marginally decreased.

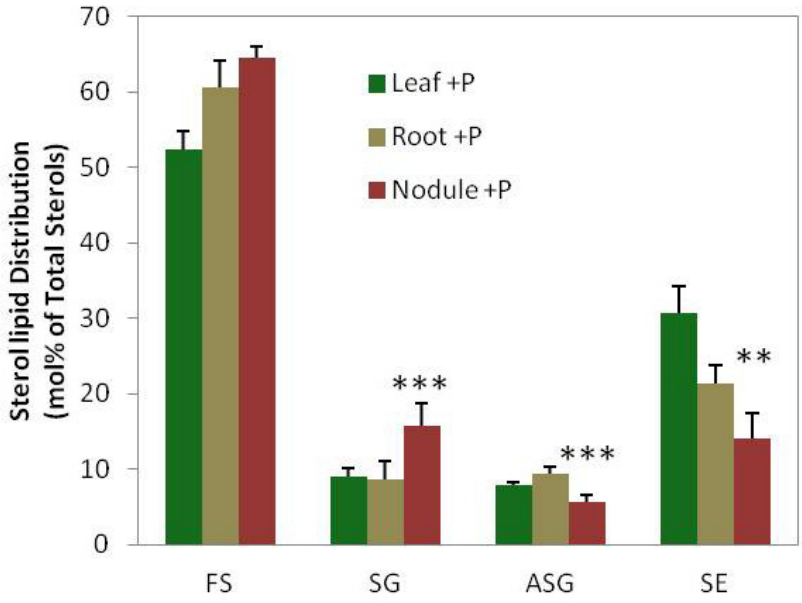

Figure 23: Distribution of Sterol Lipids Classes in *Lotus japonicus* Leaves, Roots and Nodules. FS: free sterols, SG: sterol glucosides; ASG: acylated sterol glucosides; SE: sterol esters. *Lotus japonicus* wild type plants were grown on sand and fertilized with mineral mixture containing 0.5 mM nitrogen and 2.5 mM phosphate for nine weeks. Lipids were extracted in the presence of internal standards and quantified by Q-TOF MS analysis. Data are mean and standard deviation of five measurements. Data are mean and standard deviation of five measurements. Asterisks indicate values obtained for nodules that are significantly different from those obtained for roots (according to Student's *t* test, Welch correction, $P<0.02$ (**); $P<0.01$ (***)).

3.2.2.3 Analysis of Glucosylceramides during Nodulation

For the quantification of GlcCer in leaves, roots and nodules of *Lotus japonicus,* transgenic empty vector control plants (see 3.5.2) were grown on sand with full nutrient supply for 10 weeks. Samples were harvested 6 weeks after infection with *Mesorhizobium loti*.

It has been previously shown that *Lotus japonicus* GlcCer contains large amounts of d18:2 LCBs in addition to t18:1, which is the most abundant LCB in *Arabidopsis* (vom Dorp, 2010). These LCBs are linked via an amide bond to hydroxylated fatty acids, ranging in chain length from h16:0 to h26:0. In leaves and roots, the predominant molecular species of GlcCers was d18:2-h16:0, followed by GlcCers containing t18:1 LCBs attached to h16:0, h22:0 and h24:0 fatty acids. During nodulation, the amount of GlcCer species containing t18:1 LCBs strongly increased, while d18:2-h16:0 was only slightly elevated, as can be seen in Figure 24. Notably, the only detectable d18:1 GlcCer species, d18:1-h16:0, which represents only a minor compound in leaves and roots, was very strongly increased in nodules. In addition, GlcCer species containing odd chained fatty acids, like h21:0, h23:0 and h25:0 accumulated during nodulation.

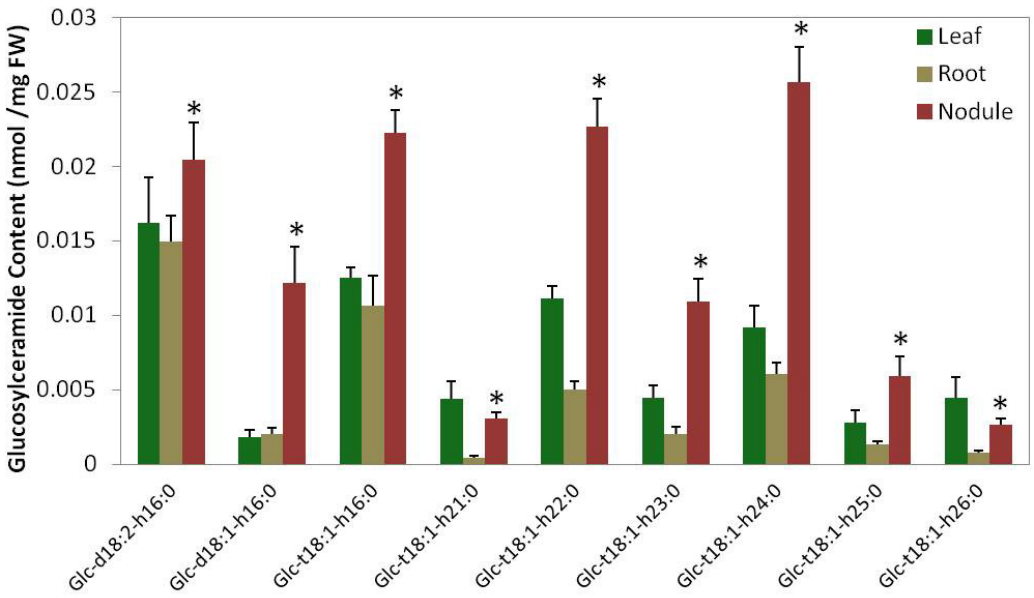

Figure 24: Glucosylceramides in *Lotus japonicus* Leaves, Roots and Nodules. *Lotus japonicus* empty vector control plants were grown on sand and fertilized with mineral mixture containing 0.5 mM nitrogen and 2.5 mM phosphate for 10 weeks. Lipids were extracted in the presence of internal standards and quantified by Q-TOF MS analysis. All major glucosylceramide species found in *Lotus japonicus* are depicted. Data are mean and standard deviation of five measurements. Asterisks indicate values obtained for nodules that are significantly different from those obtained for roots (according to Student's *t* test, Welch correction, $P<0.01$).

3.2.2.4 Regulation of Gene Expression of *SGT1*, *SGT2* and *GCS* during Nodulation

Previous analysis of the gene expression of the galactolipid synthases *DGD1* and *DGD2* in soybean revealed a strong induction, not only during phosphate starvation but also during nodulation, more specifically in mature nodules (Gaude *et al.*, 2008). The authors of this study performed a time course experiment to monitor the gene expression during all stages of the infection process in soybean. A similar approach was used in the present work to examine the regulation of gene expression for *SGT1*, *SGT2* and *GCS* in comparison to *DGD1* and *DGD2* during the nodulation process in *Lotus japonicus*. *Lotus* wild type plants were grown from seeds in sterile culture on a mixture of sand and vermiculite. Three-week-old plants were inoculated with *Mesorhizobium loti* at an OD_{600} of 0.05 in 0.5 mM nitrogen and 2.5 mM phosphate and cultivated for another 45 days while nodule formation took place. As a control group, *Lotus* plants were mock-inoculated with 0.5 mM nitrogen and 2.5 mM phosphate without *Mesorhizobium* and co-cultivated. At 32 days post infection (dpi), the mock-inoculated plants displayed a severe nitrogen deficiency, resulting from the lack of nodules, which are essential for nitrogen fixation, as can be seen in Figure 25.

RNA was isolated from control roots at 1 dpi and 3 dpi, and from infected roots at 1 dpi, 3 dpi and 18 dpi. At 18 dpi, the samples contained a mixture of roots and developing nodules. Nodules were harvested at 32 dpi and 45 dpi and RNA was extracted. cDNA was synthesized from the isolated RNA and PCR was performed with gene specific primers for *SGT1*, *SGT2*, *GCS,*

DGD1 and *DGD2*, and for the housekeeping gene Ubiquitin. Figure 25 shows the PCR products after separation on an agarose gel and staining with ethidium bromide. None of the analyzed glycosyltransferases displayed an induction of gene expression during early infection. *DGD1,* which is upregulated in mature nodules of soybean, showed an induced gene expression in nodules at 32 dpi, which was further enhanced at 45 dpi. *SGT1* and *SGT2* were also upregulated in nodules after 45 dpi, an effect which appeared to be stronger for *SGT2*. Gene expression of *GCS* and *DGD2* showed no clear induction during nodulation.

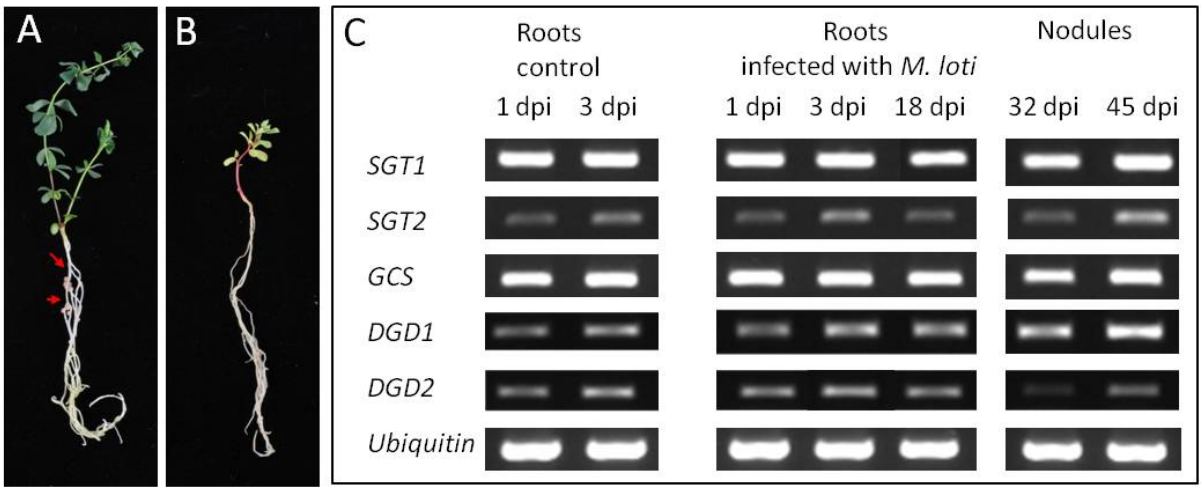

Figure 25: Gene expression of Lipid Glycosyltransferases in *Lotus japonicus* during Nodulation. *Lotus* plants were grown from seeds under sterile condition on a mixture of sand and vermiculite and watered with 2.5 mM phosphate and 0.5 mM nitrogen. At 0 dpi the plants were infected with *Mesorhizobium loti* in mineral solution at an OD of 0.05. The control plants were mock-inoculated with mineral solution without *Mesorhizobium*. At 18 dpi the roots of the inoculated plants displayed visible nodules (**A**), while the mock-inoculated plants showed a diminished growth and chlorosis (**B**), presumably due to nitrogen deficiency. Nodulation sites are indicated with red arrows. Semi-quantitative RT-PCR was performed with gene specific primers for *SGT1*, *SGT2*, *GCS*, *DGD1* and *DGD2* and for the housekeeping gene ubiquitin. The PCR products were separated on an agarose gel and stained with ethidium bromide (**C**). dpi: days post infection

3.2.3 Analysis of Lipid Changes during Mycorrhiza Formation

During arbuscular mycorrhiza formation in *Lotus japonicus*, *Glomus intraradices* spores germinate and produce hyphae which grow towards the plant roots, following a gradient of signal molecules exuded by the plant (Akiyama *et al.*, 2005). The hyphae invade the roots and expand inside the intercellular space until they enter root cortical cells and form arbuscules. These are tree-like structures of branched hyphae within the cell, which are surrounded by the periarbuscular membrane. This membrane is derived from the plant plasma membrane and separates the fungal and plant cellular structures. The periarbuscular membrane plays an important role in the regulation of nutrient and signal exchange. *Lotus* benefits from the symbiosis mainly by the improved uptake of phosphate and water, while the fungus receives carbon and energy from the plant in the form of hexoses (Solaiman and Saito, 1997; Bago *et al.*, 2003; Finlay, 2008). It has previously been postulated, that TAG is synthesized by the fungus as a

means of carbon and energy storage, and that it is transported within the hyphal network in differentiated fungal structures, the so-called vesicles (Jabaji-Hare *et al.*, 1984; Olsson and Johansen, 2000).

In the present work, the lipid composition of *Lotus japonicus* roots colonized with the arbuscular mycorrhiza fungus *Glomus intraradices* was analyzed. Arbuscular mycorrhiza formation is induced by phosphate deprivation and inhibited by high concentrations of inorganic phosphate in the soil. Thus, it was of special interest to monitor the distribution of phospholipids and glycolipids as a response to a presumed improved phosphate supply provided by the fungus. Therefore, the experiments were performed under low phosphate conditions. The inoculum, containing spores of *Glomus intraradices,* was from a commercial source. It was generated by harvesting soil of leek plants infected with *Glomus intraradices*. This inoculum was suspected to be a source of residual inorganic phosphate. A beneficial effect of residual inorganic phosphate on phospholipid biosynthesis cannot be excluded; therefore control plants were mock-inoculated with inoculum which had been autoclaved prior to the experiment. The inoculated (+myc) and mock-inoculated (-myc) plants were grown on a mixture of sand and inoculum (10:1) and deprived of phosphate for 8 weeks, before samples were taken for lipid analysis.

3.2.3.1 The Role of Mycorrhiza Formation for Phospholipid Homeostasis during Phosphate Deprivation

Figure 26 shows the distribution of phospho- and galactolipids in mycorrhized and non-mycorrhized plants during phosphate deprivation, as measured by Q-TOF MS/MS analysis.

PC was increased from 29.0 mol% in non-mycorrhized roots to 31.6 mol% in mycorrhized roots. Furthermore, the DGDG content was reduced from 26.4 mol% in roots of non-mycorrhized plants to 21.6 mol% in mycorrhized plants. The distribution of the other phospho- and galactolipids remained unchanged.

Comparative analysis of the absolute amounts of phospho- and galactolipid during mycorrhization revealed a slight decrease of DGDG from 0.45 nmol/mg FW to 0.43 nmol/mg FW. PE and PC were significantly increased from 0.31 nmol/mg FW to 0.37 nmol/mg FW and from 0.49 nmol/mg FW to 0.65 nmol/mg FW. In addition, there was a minor increase of all other phospho- and galactolipids. When monitoring the proportions of phospho- and galactolipids during mycorrhization, a significant increase of PC and a concomitant decrease of DGDG can be observed, while the percentages of all other lipid classes are unaltered.

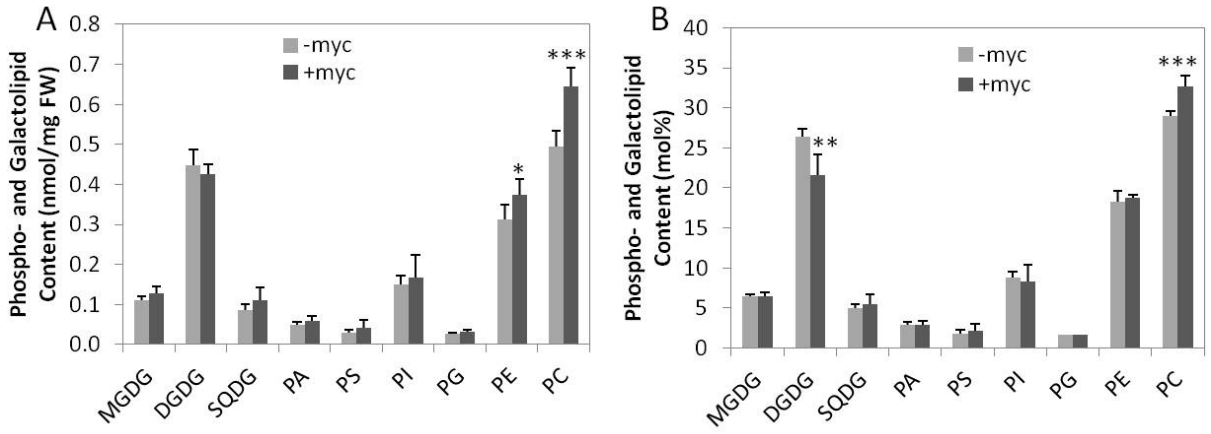

Figure 26: Phospho- and Galactolipid Content of Mycorrhized Roots of *Lotus japonicus*. Plants were grown on a mixture of sand and granular inoculum containing spores of *Glomus intraradices* (10:1) for 8 weeks (+myc) before sampling. Control plants were mock-inoculated (-myc) with autoclaved inoculum and cultivated in parallel. Lipids were quantified by Q-TOF MS/MS analysis in the presence of internal standards. Absolute (**A**) and relative amounts (**B**) of phospho- and galactolipids are displayed. Data are mean and standard deviation of five measurements. Asterisks indicate values that are significantly different from the control (according to Student's *t* test, Welch correction, $P<0.05$ (*); $P<0.02$ (**); $P<0.01$ (***)).

Sterol lipid analysis was performed in mycorrhized and non-mycorrhized roots of *Lotus japonicus* as displayed in Figure 27. FSs and SEs were slightly increased in mycorrhized plants from 0.345 nmol/mg FW to 0.379 nmol/mg FW and from 0.086 nmol/mg FW to 0.103 nmol/mg FW. In contrast, the SG content was significantly reduced from 0.053nmol/mg FW to 0.037 nmol/mg FW during mycorrhiza formation. No changes were observed in the amounts of ASGs during mycorrhization. Analysis of molecular species composition of FSs showed no changes of cholesterol and campesterol content in mycorrhized roots. However, there was a slight increase of stigmasterol and a concomitant decrease of sitosterol during mycorrhiza formation.

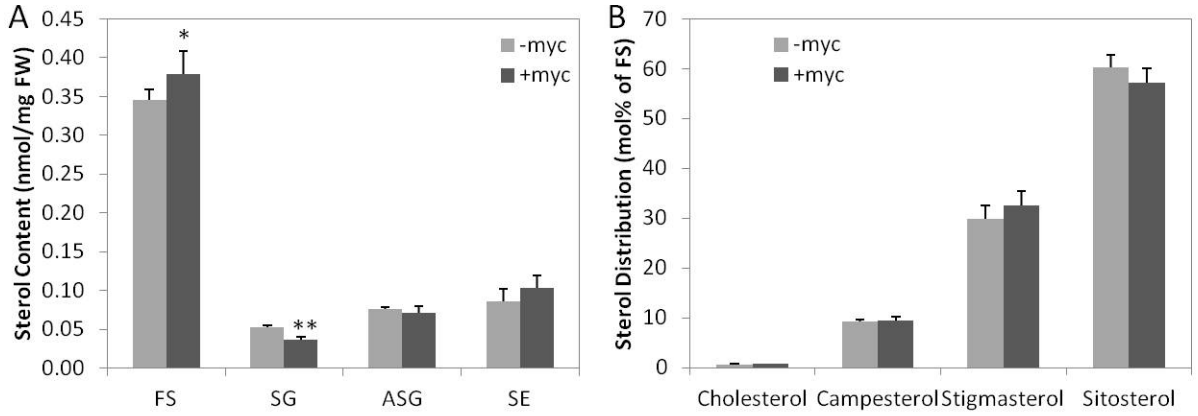

Figure 27: Sterol Lipid Classes and Molecular Species Distribution during Mycorrhiza Formation in *Lotus japonicus*. The bars show sterol lipid content (**A**) and sterol distribution of FSs (**B**) in mycorrhized and non-mycorrhized roots. *Lotus* was grown on a mixture of sand and granular inoculum containing spores of *Glomus intraradices* (10:1) for 8 weeks (+myc) before sampling. Control plants were mock-inoculated (-myc) with autoclaved inoculum. All plants were grown without additional phosphate fertilization. Lipids were quantified by Q-TOF MS/MS analysis in the presence of internal standards. Data are mean and standard deviation of five measurements. Asterisks indicate values that are significantly different from the control (according to Student's *t* test, Welch correction, $P<0.05$ (*); $P<0.02$ (**)).

Figure 28 shows the amounts of the major GlcCer molecular species in roots of mycorrhized and non-mycorrhized plants as measured by Q-TOF MS/MS analysis. A minor decrease upon mycorrhization was observed for Glc-d18:2-h16:0 and Glc-t18:1-h24:0. The total GlcCer content was not significantly changed in mycorrhized roots.

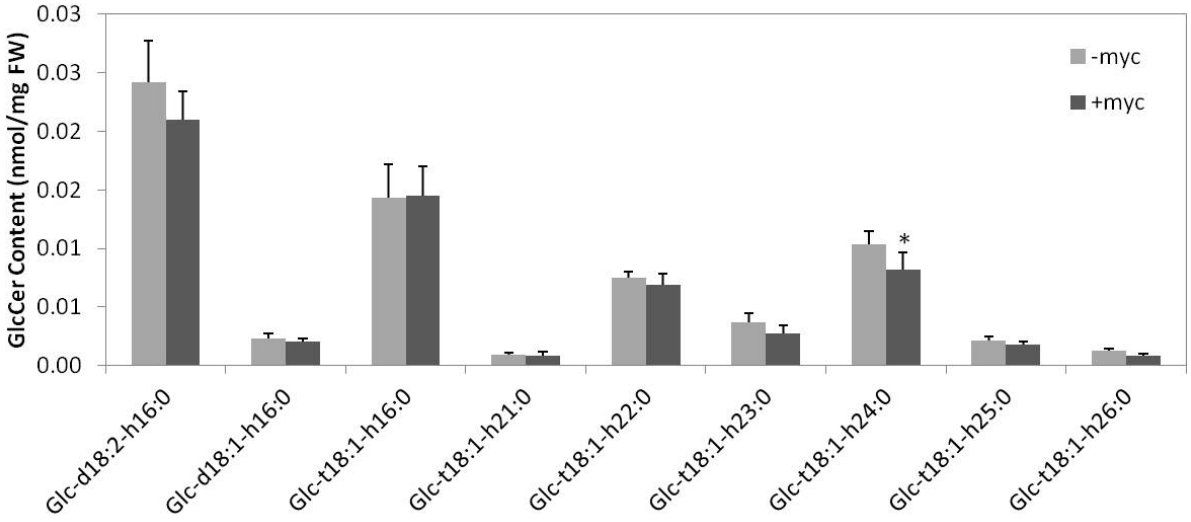

Figure 28: Glucosylceramide Content during Mycorrhiza Formation in *Lotus japonicus.* Plants were grown on a mixture of sand and granular inoculum containing spores of *Glomus intraradices* (10:1) for 8 weeks (+myc). Control plants were mock-inoculated (-myc) with autoclaved inoculum. All plants were grown under low phosphate conditions. Lipids were quantified by Q-TOF MS/MS analysis in the presence of internal standards. Data represent mean and standard deviation of five measurements. Asterisks indicate values that are significantly different from the control (according to Student's *t* test, Welch correction, $P<0.05$).

3.2.3.2 Lyso-Phosphatidylcholine as a Putative Signaling Molecule during Arbuscular Mycorrhiza Formation

Lyso-phosphatidycholine (LPC) has previously been reported to be of major importance during arbuscular mycorrhiza formation in plants. It has been suggested that LPC plays a role as a signaling molecule, which accumulates upon mycorrhization. In order to analyze the amounts of LPCs during mycorrhiza formation, a quantification method using Q-TOF MS/MS was established, following a protocol described by Welti *et al.*, (2002) for mass spectrometry based analysis of phospholipids. Lyso-phospholipids are minor components in plant tissues and cannot be detected by Q-TOF analysis of crude lipid extracts due to ion suppression. Therefore, an additional purification step of LPC via solid phase extraction on silica columns was performed, prior to measurements by Q-TOF MS/MS analysis. This method was employed for the quantification of LPC in mycorrhized and non-mycorrhized roots. The results of these measurements are displayed in Figure 29. Fatty acid composition of LPC showed large amounts of 16:0, 18:0, 18:1, 18:2 and 18:3 fatty acids. 16:1 and 20:1 fatty acids and saturated very long chain fatty acids such as 22:0, 24:0 and 26:0 were also detectable, though in minor amounts. No

notable differences were detected in the amounts of LPC in mycorrhized and non-mycorrhized roots of *Lotus japonicus*.

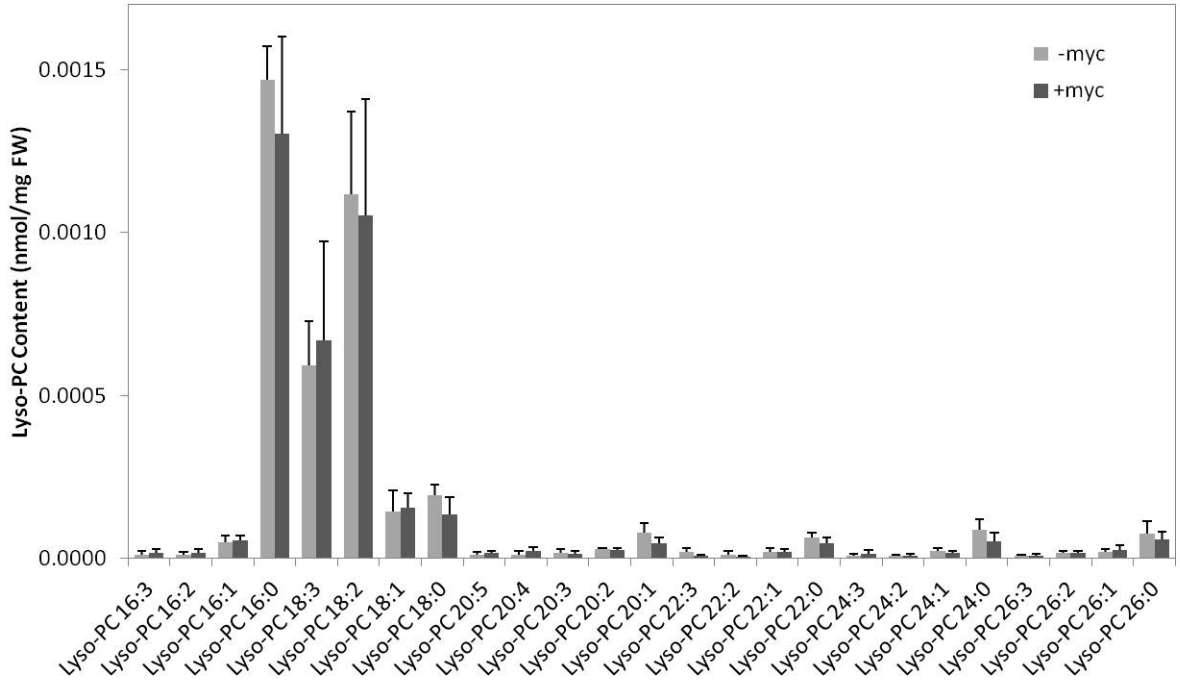

Figure 29: Lyso-Phosphatidylcholine Content in *Lotus* Roots during Mycorrhiza Formation. Plants were grown on a mixture of sand and granular inoculum containing spores of *Glomus intraradices* (10:1) for 8 weeks (+myc) before sampling of root material. Control plants were mock-inoculated (-myc) with autoclaved inoculum and cultivated in parallel under low phosphate conditions. Lipids were quantified by Q-TOF MS/MS analysis in the presence of internal standards. Data represent mean and standard deviation of five measurements.

3.2.3.3 Synthesis of Triacylglycerol as a Major Storage Lipid of *Glomus intraradices*

Glomus intraradices profits from arbuscular mycorrhiza formation by obtaining energy and carbon from the host plant in the form of hexoses. These are subsequently used for TAG biosynthesis in the arbuscules. TAGs serve as storage lipids, which are transported within the hyphal network in characteristic fungal structures, the so-called vesicles. (Jabaji-Hare *et al.*, 1984; Johansen *et al.*, 1996).

In the present work, the accumulation of TAG during mycorrhiza formation under phosphate deprivation could be confirmed. Figure 30 shows a slight increase in total TAG content in mycorrhized roots, accompanied by a specific accumulation of some molecular species during mycorrhization. It has been previously discussed, whether biochemical markers e.g. fatty acids or sterols would be suitable for the quantification of fungal colonization in plant roots (Hart and Reader, 2002). TAG measurements by Q-TOF MS/MS analysis revealed the accumulation of 48:3, 48:2 and 48:1 TAGs in mycorrhized roots. These molecular species, containing combinations of 16:0 and 16:1 fatty acids, were almost absent from plants but abundant in *Glomus intraradices* grown in axenic root culture (Brands, 2010).

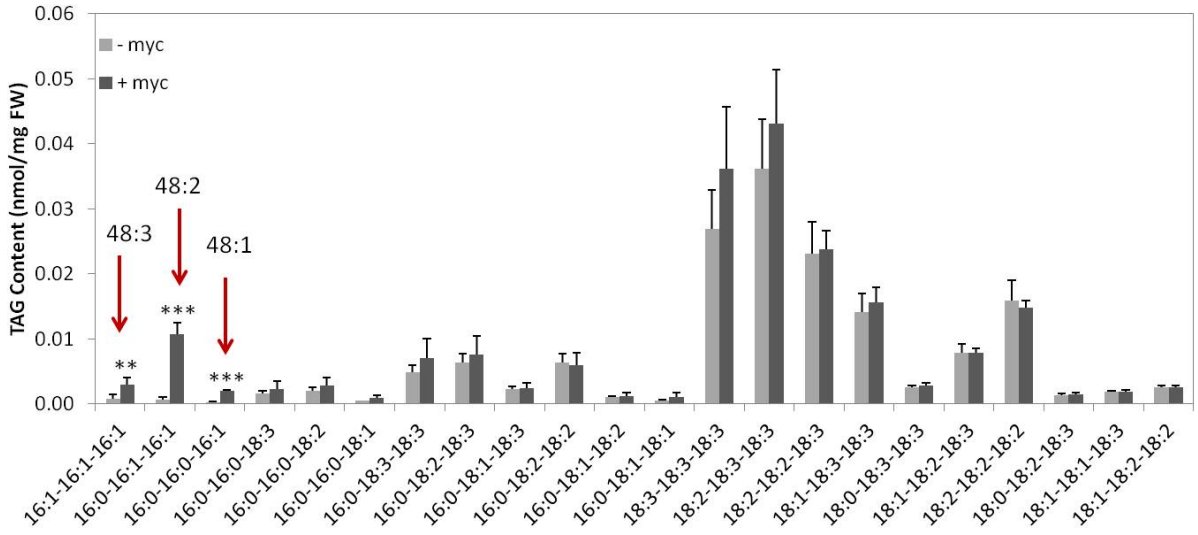

Figure 30: Triacylglycerol Content of *Lotus japonicus* Roots Colonized with *Glomus intraradices*. Plants were grown on a mixture of sand and granular inoculum containing spores of *Glomus intraradices* (10:1) for 8 weeks (+myc) before sampling of root material. Control plants were mock-inoculated (-myc) with autoclaved inoculum. All plants were cultivated without phosphate supplementation. Lipids were quantified by Q-TOF MS/MS analysis in the presence of internal standards. Only the most abundant TAG molecular species are depicted. The *Glomus* specific molecular species of 16:0-16:1-16:1 TAG accumulates during mycorrhization. Data are mean and standard deviation of five measurements. Asterisks indicate values that are significantly different from the control (according to Student's *t* test, Welch correction, $P<0.02$ (**); $P<0.01$ (***))

The accumulation of these *Glomus* specific TAGs was decreased in plants grown under phosphate replete conditions (data not shown). This is in accordance with the well-documented suppression of mycorrhiza formation by high phosphate availability. These findings indicate that 48:3, 48:2 and 48:1 TAG molecular species might be suitable biochemical markers for the degree of fungal colonization of plant roots.

3.2.4 Measurement of GIPCs by Q-TOF MS/MS in *Lotus japonicus*

Next to GlcCer, GIPCs represent the second abundant class of sphingolipids in plants. Therefore, the analysis of this lipid class would provide an important insight into sphingolipid metabolism in *Lotus*. Due to their very polar nature, caused by a very large, sugar containing head group, these lipids are only poorly extracted from plant tissues by chloroform-based extraction methods. Alternative extraction protocols, optimized for the quantification of sphingolipids, have been described previously (Markham *et al.*, 2006). Until now, no data on the amount and composition of GIPC lipids in *Lotus japonicus* are available. Therefore, in the present work, first steps were taken towards the identification and quantification of GIPCs in *Lotus japonicus*. GIPCs were extracted from 500 mg of *Lotus* leaves and roots and purified by cleavage of glycerolipids and subsequent removal of fatty acid methyl esters and residual salts (see 2.2.7.13). In addition, *Arabidopsis* leaves were analyzed for method validation.

Figure 31 shows the total ion chromatograms (TICs) of the analyzed samples in a mass range from 1140 to 1320. In *Arabidopsis* leaves, the most prominent signals correspond to GIPCs containing t18:1 LCBs and even chained, hydroxylated, saturated or monounsaturated fatty acid residues; e.g. t18:1-h24:0 and t18:1-h24:1. In *Lotus* leaves, GIPCs were detected which contained t18:1 or t18:0 LCBs. Monounsaturated fatty acid residues such as h24:1 were not detectable (see Figure 31). However, similar to the fatty acid distribution in GlcCer, distinct signals could be detected for GIPCs with hydroxylated fatty acid residues with uneven chain lengths, such as h21:0, h23:0 and h25:0.

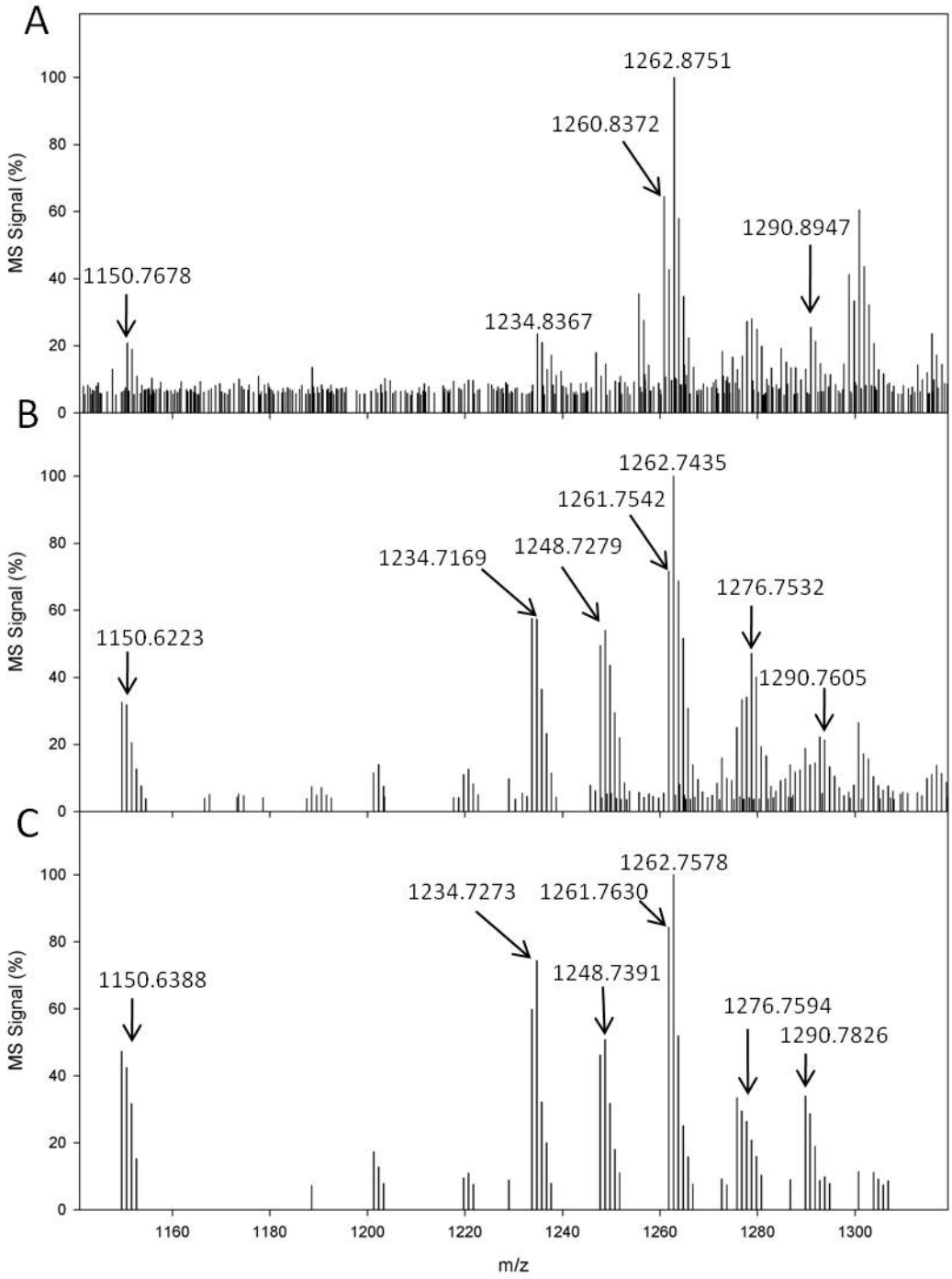

Figure 31: GIPCs in *Arabidopsis thaliana* and *Lotus japonicus*. Mass spectra of GIPCs extracted from *Arabidopsis* leaf (**A**), *Lotus* leaf (**B**) and *Lotus* root (**C**), without fragmentation (total ion chromatograms). Given are the mass to charge ratios (m/z) as detected by Q-TOF MS.

Furthermore, Figure 31 reveals the presence of additional GIPC species, which differ from the above described molecules by (m/z = -1); e.g. 1261.7542 in addition to 1262.7435. These GIPCs were absent from the *Arabidopsis* samples. Fragmentation of these molecular species in Q-TOF MS/MS analysis yielded the phosphorylated ceramide backbone, which was identical for both ions (see Figure 32). The observed neutral losses of 598.1146 and 597.1306 were found to correspond to the polar head groups, containing inositolphosphate, hexuronic acid and a hexose, which was substituted with an amino group in the *Lotus* specific GIPCs.

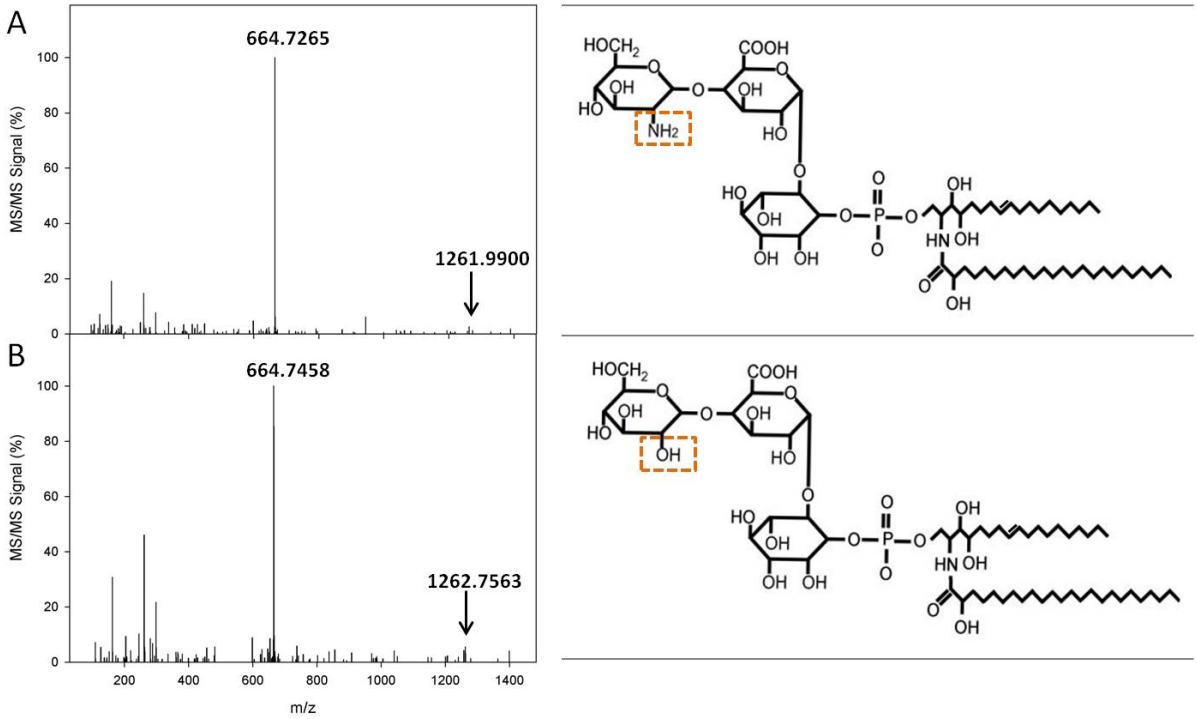

Figure 32: Fragmentation Patterns of Selected GIPCs from *Lotus japonicus*. Q-TOF MS/MS spectra of GIPC molecular species with the calculated molecular masses of 1261.7550 (**A**) and 1262.7390 (**B**). Fragmentation at 55 V yields the phosphorylated ceramide backbone, while the uncharged headgroup is lost (neutral loss = 597.1306 (**A**) and 598.1146 (**B**)). The fragmentation patterns correspond to t18:1-h24:0 GIPCs with headgroups containing inositolphosphate, hexuronic acid and hexose (**B**), which can be substituted with an amino group (**A**).

Table 4 compiles all GIPC species in *Arabidopsis* leaves and *Lotus* leaves and roots that were detected by Q-TOF MS analysis and confirmed by MS/MS analysis after fragmentation with 55 V.

Table 4: GIPC Molecular Species in *Arabidopsis* and *Lotus*

Exact Molecular Mass	Sum Formula (head group InsP, GlcA, Glc; R1=OH) [a]	GIPC Molecular Species	*Arabidopsis* Leaf	*Lotus* Leaf	*Lotus* Root
1150.6138	$C_{52}H_{96}O_{24}NP$	t18:1-h16:0	yes	yes	yes
1220.6921	$C_{57}H_{106}O_{24}NP$	t18:1-h21:0	n.d.[b]	yes	yes
1234.7077	$C_{58}H_{108}O_{24}NP$	t18:1-h22:0	yes	yes	yes
1248.7234	$C_{59}H_{110}O_{24}NP$	t18:1-h23:0	n.d.	yes	yes
1250.7390	$C_{60}H_{110}O_{24}NP$	t18:0-h23:0	n.d.	yes	yes
1260.7234	$C_{60}H_{110}O_{24}NP$	t18:1-h24:1	yes	n.d.	n.d.
1262.7390	$C_{60}H_{112}O_{24}NP$	t18:1-h24:0	yes	yes	yes
1264.7547	$C_{60}H_{114}O_{24}NP$	t18:0-h24:0	n.d.	yes	yes
1276.7547	$C_{61}H_{114}O_{24}NP$	t18:1-h25:0	n.d.	yes	yes
1278.7703	$C_{61}H_{116}O_{24}NP$	t18:0-h25:0	n.d.	yes	yes
1290.7703	$C_{62}H_{116}O_{24}NP$	t18:1-h26:0	yes	yes	yes
1316.7860	$C_{64}H_{118}O_{24}NP$	t18:1-h28:1	n.d.	yes	yes

Exact Molecular Mass	Sum Formula (head group InsP, GlcA, Glc; R1=NH_2) [a]	GIPC Molecular Species	*Arabidopsis* Leaf	*Lotus* Leaf	*Lotus* Root
1149.6298	$C_{52}H_{97}O_{23}N_2P$	t18:1-h16:0	n.d.	yes	yes
1219.7081	$C_{57}H_{107}O_{23}N_2P$	t18:1-h21:0	n.d.	yes	yes
1233.7237	$C_{58}H_{109}O_{23}N_2P$	t18:1-h22:0	n.d.	yes	yes
1247.7394	$C_{59}H_{111}O_{23}N_2P$	t18:1-h23:0	n.d.	yes	yes
1261.7550	$C_{60}H_{113}O_{23}N_2P$	t18:1-h24:0	n.d.	yes	yes
1275.7707	$C_{61}H_{115}O_{23}N_2P$	t18:1-h25:0	n.d.	yes	yes
1289.7863	$C_{62}H_{117}O_{23}N_2P$	t18:1-h26:0	n.d.	yes	yes

[a] The head group contains inositolphosphate (INsP), hexuronic acid which is likely glucuronic acid (GlcA) and a hexose (Glc). R1 represents the substitution of the hexose at C2 with either a hydroxy group or an amino group.
[b] n.d. = not detected

The quantification of lipids by Q-TOF MS/MS analysis is dependent on the availability of suitable internal standards for each lipid class. For the very complex GIPCs, no synthetic standards are available. Therefore, the use of alternative lipids such as gangliosides has been proposed (Markham and Jaworski, 2007). However, quantification based on such standards requires careful measurement and calculation of putative correction factors, as the response factor for the analyte (GIPC) and the internal standard might be different. For future quantification of *Lotus* GIPCs by Q-TOF MS/MS analysis, a correction factor for GIPCs needs to be determined by HPLC analysis of LCBs. To this end, sphingolipids were extracted from *Lotus* leaves and analyzed as described (see 2.2.7.14). For the quantification of total sphingolipids, comprising mainly GIPCs, GlcCers and minor amounts of Cers, the lipids were hydrolyzed and LCBs were measured by HPLC analysis after derivatization with *ortho*-phthaldialdehyde. In

addition, samples were prepared that were devoid of GIPCs due to a purification step by solid phase extraction on silica columns. Cers and GlcCers are readily eluted from the silica columns with acetone/isopropanol (1:1). The very polar GIPCSs are not eluted with organic solvents. Both samples were analyzed by HPLC analysis and the LCB patterns were compared. The amount of total GIPCs was estimated by comparison of total sphingolipid extracts with sphingolipid extracts devoid of GIPCs. Q-TOF MS analysis had revealed t18:1 and t18:0 to be the prevalent LCBs in *Lotus* GIPCs. On the other hand, *Lotus* GlcCers were shown to contain considerable amounts of d18:2 LCBs. Therefore, d18:2 LCBs were selected as GlcCer specific LCBs and the corresponding signals were set to 100%. The amounts of t18:0 and t18:1 LCBs were calculated accordingly. Figure 33 shows the LCB distribution of t18:0 and t18:1 in *Lotus* sphingolipid extracts with and without GIPCs, relative to the amounts of d18:2 LCBs. As expected, the LCB content of t18:0 and t18:1 is strongly increased in the total sphingolipid fractions. The LCB content in total sphingolipid extracts is about twice as high as in the sphingolipid fraction containing only Cer and GlcCer. As Cers represent only a minor proportion of sphingolipids in plants, these data indicate the presence of GIPCs at a concentration similar to GlcCer.

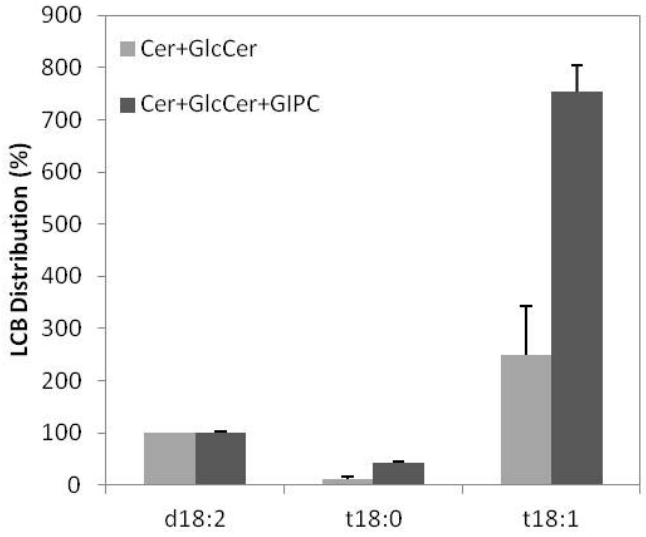

Figure 33: Analysis of *Lotus* Sphingolipid LCB Composition by HPLC. Sphingolipids were extracted from *Lotus japonicus* leaf tissue as described (2.2.7.13). Long chain bases (LCB) were measured by HPLC analysis as described in 2.2.7.14. The data are expressed as LCB content relative to d18:2 content, which was set to 100%. Data are mean and standard deviation of at least 3 measurements.

3.3 Identification of Two Sterol Glucosyltransferase Genes and a Glucosylceramide Synthase Gene in *Lotus japonicus*

The galactolipid DGDG accumulates in extraplastidial membranes during phosphate deprivation to compensate for the lack of phospholipids which are degraded to release phosphate for other cellular processes (Härtel *et al.*, 2000). Previous studies showed that DGDG

is an authentic constituent of the peribacteroid membrane (Gaude *et al.*, 2004), which is crucial for nodulation under phosphate limiting conditions (Gaude, 2005). Similar to DGDG, SG and GlcCer contents in *Arabidopsis* were significantly increased under phosphate deprivation (see 3.1.5 and vom Dorp, 2010). Furthermore, SG and GlcCer accumulated in mature nodules (see 3.2.2). Semi-quantitative RT-PCR also showed an induced of gene expression of *SGT1* and *SGT2*, similar to *DGD1,* during nodulation. These findings suggest a putative role of SG and GlcCer in nodulation during phosphate deprivation.

In *Arabidopsis thaliana*, two UDP-glucose dependent sterol glucosyltransferases have been described, which catalyze the synthesis of SG from FS (At3g07020 and At1g43620) (Warnecke *et al.*, 1997; DeBolt *et al.*, 2009). Furthermore, a glycosyltransferase with sequence homologies to *SGT1* and *SGT2* has been identified in *Arabidopsis* and termed *SGT-like* (At5g24750). In sphingolipid biosynthesis, the UDP-glucose dependent reaction which leads to the formation of glucosyceramide is catalyzed by the glucosylceramide synthase (At2g19880) (Leipelt *et al.*, 2001). The genes encoding the respective glucosyltransferases have not been annotated in *Lotus japonicus* so far.

3.4 Identification of Glucosyltransferase Candidate Genes by Sequence Homology Comparison

Two genes which showed high homologies to the sterol glucosyltransferases from *Arabidopsis* (*SGT1* and *SGT2*) and one gene which was homologous to the glucosylceramide synthase from *Arabidopsis* (*GCS*) were identified in *Lotus japonicus* prior to this work. The full length cDNA for *SGT2* was obtained by PCR amplification from wild type *Lotus* DNA extracted from roots after infection with *Mesorhizobium loti*. Full length cDNAs for *Lotus japonicus SGT1* (MF087a11) and *GCS* (MPDL058e06) were obtained from Kazusa (the Legume Base, The National BioResource Project, University of Miyazaki)(see appendix, chapter 7.1). Figure 34 shows a comparison of the amino acid sequence identities of *SGT1*, *SGT2*, *DGD1*, *DGD2* and *GCS* from *Arabidopsis thaliana* and *Lotus japonicus*. The analysis of evolutionary relationships revealed high homologies between the respective glycosyltransferases. There were higher similarities between the different species than between the different glucosyltransferases of one species. In *Arabidopsis,* an additional gene, termed *SGT-like,* exists which shows homologies to *SGT1* and *SGT2*. No equivalent to this gene could be found in *Lotus japonicus*. However, given that the *Lotus japonicus* genome sequence still contains considerable gaps, it is likely that *Lotus* also contains an ortholog to the *Arabidopsis SGT*-like gene.

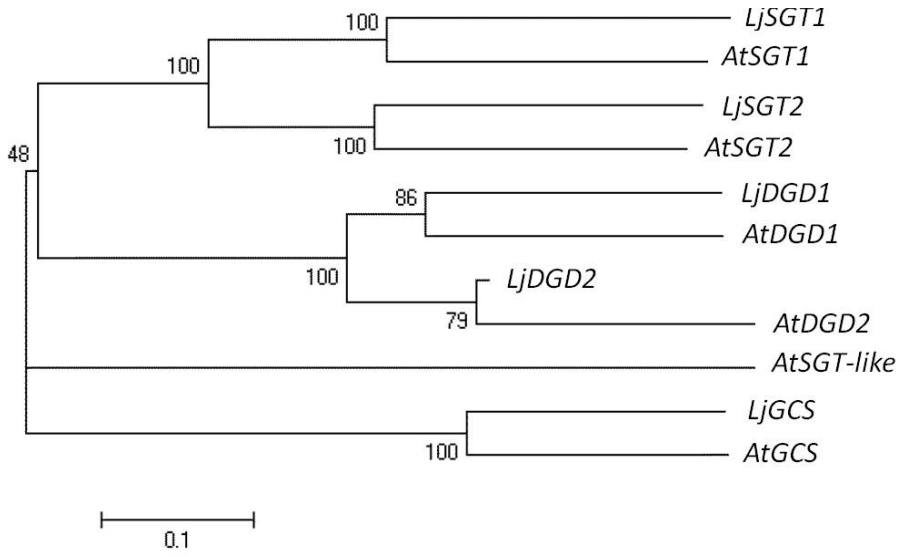

Figure 34: Evolutionary Relationships of Glycosyltransferases from *Arabidopsis thaliana* and *Lotus japonicus*. The unrooted phylogenetic tree shows the amino acid sequence identity between lipid glycosyltransferases. The values next to the branches signifiy the percentages in which the taxa clustered together in the bootstrap test when 1000 replicate trees were used (Felsenstein, 1985). The evolutionary history was deduced using the Neighbor-Joining method (Saitou and Nei, 1987). The evolutionary distances displayed in the x-dimension show the number of amino acid differences per site and were calculated with the *p*-distance method (Nei and Kumar, 2000). Evolutionary analyses were conducted with the MEGA 5.0 software (Tamura *et al.*, 2011).

3.4.1 Sequencing of *Lotus SGT1*

During this work, the full length genomic sequences for *SGT2* and *GCS* were assembled from fragments of sequence information provided by Kazusa (the Legume Base, The National BioResource Project, University of Miyazaki). However, the sequence coverage for *Lotus japonicus SGT1* was incomplete. While the complete information for the coding sequence could be extracted from EST sequences obtained from the database, a large number of exons and introns were missing from the genomic sequence. The missing fragments were amplified by PCR with the help of Dr. Bettina Kriegs (Institute of Molecular Physiology and Biotechnology of Plants, University of Bonn) and sequenced on both strands. The resulting sequence information revealed *SGT1* to be a large gene of 18651 bp, with a coding sequence of only 1875 bp, containing 13 introns. The sequence information was submitted to the Genebank database and is available with the accession number JF912509.

3.4.2 Heterologous Gene Expression of *SGT1*, *SGT2* and *GCS* in *Pichia pastoris* and *Saccharomyces cerevisiae*

Lotus japonicus SGT1, *SGT2* and *GCS* were heterologously expressed in yeast cells, in order to confirm the catalytic activity of these putative glucosyltransferases. To this end, constructs for the heterologous expression in *Saccharomyces cerevisiae* were generated. Constructs for the heterologous expression in *Pichia pastoris* were generated prior to this work

by Helder Paiva (Max-Planck Institute for Molecular Plant Physiology, Golm, group of Peter Dörmann).

Saccharomyces is capable of sterol and ceramide biosynthesis, and thus contains the substrates required for SG and GlcCer synthesis. However, it lacks the glucosyltransferase genes required for biosynthesis of SG and GlcCer and therefore, these lipids cannot be detected in *Saccharomyces* wild type. Expression of the respective glucosyltransferases from *Lotus japonicus* would be expected to result in the synthesis of SG or GlcCer in *Saccharomyces*. *Pichia pastoris,* on the other hand, possesses the biosynthetic pathways for SG and GlcCer biosynthesis. In order to prove the catalytic activity of the glucosyltransferases in this recombinant background, a *Pichia pastoris* double mutant was used as expression host. This experiment was conducted in collaboration with Dr. Dirk Warnecke from the University of Hamburg. In his laboratory, a *Pichia* double mutant was generated, which lacks the ability to synthesize SG and GlcCer, but has retained the biosynthetic pathways for the precursor molecules.

For the heterologous expression of *SGT1*, *SGT2* and *GCS*, the respective cDNAs were cloned into the pDR196 expression vector and *Saccharomyces cerevisiae* INVScI was transformed via electroshock transformation. Transformed cells were grown on selective media as described and cultivated for lipid extraction. Total lipid extracts were separated on a TLC plate and stained with α-naphthol. Figure 35 A shows a TLC plate of the lipid extracts from the *Saccharomyces* overexpression mutant *SGT1-oe* and the empty vector control.

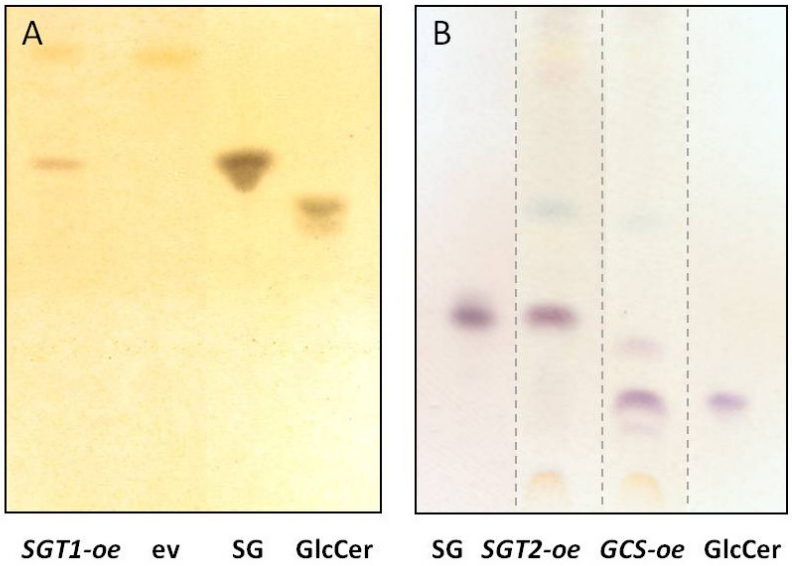

Figure 35: Heterologous Expression of *SGT1*, *SGT2* and *GCS* from *Lotus japonicus* in *Saccharomyces cerevisiae* and *Pichia pastoris*. A: Thin layer chromatography (TLC) of lipid extracts from *SGT1* overexpression line (*SGT1-oe*) and empty vector control (ev) in *Saccharomyces* stained with α-naphthol. **B**: TLC of lipid extracts from *SGT2* (*SGT-2oe*) and *GCS* (*GCS-oe*) overexpression line and empty vector control in *Pichia* stained with α naphthol. SG: synthetic sterol glucoside standard, GlcCer: synthetic glucosylceramide standard

A lipid band is visible for *SGT1-oe*, which is absent from the empty vector control and co-migrated with the synthetic standard steryl glycoside. The lipid was stained with α-naphthol, indicating the presence of a sugar containing head group.

Lipids extracted from the *Pichia pastoris sgt/gcs* deletion mutant, transformed with an *SGT2* (*SGT2-oe)* and a *GCS* (*GCS-oe)* overexpression construct, were separated by TLC and stained with α-naphthol (Figure 35). Distinct lipid bands are visible in lanes 2 and 3, which co-migrated with SG and GlcCer, respectively. The lipid band co-migrating with GlcCer is absent from *SGT2-oe* and the band co-migrating with SG is absent from *GCS-oe.* The two lipids were stained with α-naphthol, which is indicative of glycolipids.

SGT1 could be successfully expressed in *Saccharomyces cerevisiae* while *SGT2* and *GCS* were expressed in *Pichia pastoris*. The expression of the putative glucosyltransferases resulted in the formation of glycolipids that co-migrated with SG and GlcCer, respectively. Thus, the catalytic activities of the respective enzymes as sterol glucosyltransferases and a glucosylceramide synthase were confirmed.

3.5 Generation of *Lotus japonicus* Plants Affected in SG and GlcCer Biosynthesis

Analysis of glycolipid changes, as well as glycosyltransferase gene expression during nodulation in *Lotus japonicus* suggested a putative role of these lipids in plant-microbe symbiosis. In addition, the galactolipid DGDG was shown to be important for nodulation during phosphate limitation in previous studies (Gaude, 2005). In order to determine, whether the glycolipids GlcCer and SG are important for symbiotic plant-microbe interactions, *Lotus* plants affected in glycolipid biosynthesis were generated. To this end, EMS mutants affected in *SGT1* and *SGT2* were identified by TILLING (Targeted Induced Local Lesions in Genome). In addition, transgenic *Lotus* RNAi lines were generated for *SGT1*, *SGT2* and *GCS*. The SG and GlcCer content were measured in the mutants and in transgenic plants with a downregulated gene expression of *SGT1*, *SGT2* and *GCS*. Furthermore, nodulation and mycorrhiza formation were analyzed in plants with a decreased SG or GlcCer content.

3.5.1 Sterol Glucoside Content in *SGT1* and *SGT2* TILLING Lines

Lotus japonicus TILLING mutant lines affected in the genes encoding the glycosyltransferases SGT1, SGT2 and GCS were ordered from RevGen, UK. The genomic sequence information obtained for *SGT1* and *SGT2* (3.4.1) was required to identify *Lotus* EMS mutants affected in sterol glucosyltransferase genes. Mutants for *SGT1* and *SGT2* carried point mutations in the gene of interest, leading to premature stop codons in the coding sequence. The amino acid sequence of SGT1 in the mutant *sgt1-5305* was truncated at position 388 (of 624).

The amino acid sequence of SGT2 in *sgt2-5656* was truncated at position 297 (of 580). For *GCS*, only mutants with point mutations leading to amino acid exchanges were obtained. These mutations did not affect GlcCer content in the plants (data not shown). Figure 36 shows the SG and ASG content in leaves of the TILLING mutants *sgt1-5305* and *sgt2-2656*. No differences in the SG content could be observed between the wild type and *sgt2-2656.* In contrast, the SG content in *sgt1-5305* was significantly reduced to 0.05 nmol/mg FW in comparison to 0.09 nmol/mg FW in the wild type. At the same time, the ASG content was only slightly reduced in the mutant.

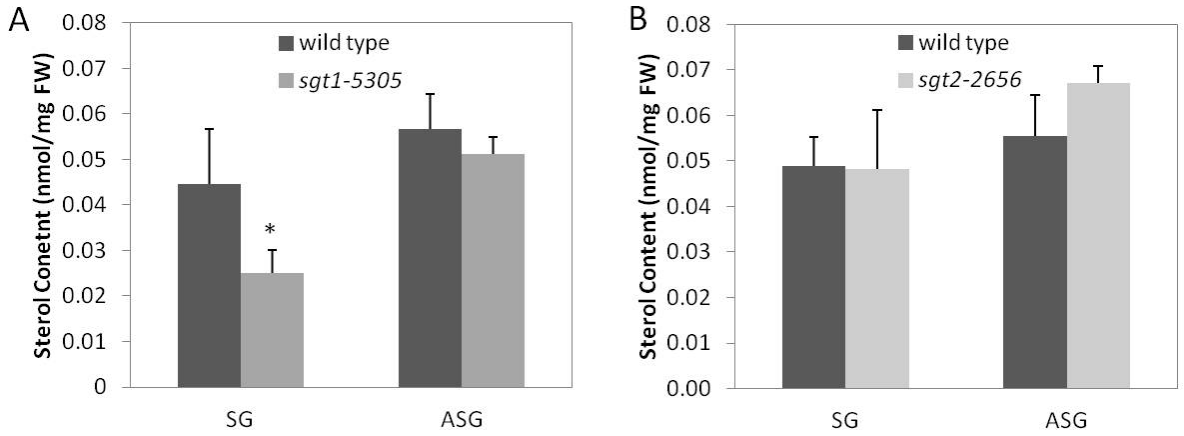

Figure 36: Sterol Content in *Lotus* TILLING Mutants Affected in *SGT1* and *SGT2*. The amino acid sequence of SGT1 in the mutant *sgt1-5305* was truncated at position 388 (of 624), due a premature stop codon in the coding sequence. The amino acid sequence of SGT2 in *sgt2-5656* was truncated at position 297 (of 580). Sterol lipids were extracted from leaves of the wild type and the mutant plants grown on soil and quantified in the presence of internal standards by Q-TOF MS/MS analysis. Data are mean and standard deviation of at least 3 measurements. Asterisks indicate values that are significantly different from the wild type (according to Student's *t* test, Welch correction, $P<0.05$).

3.5.2 Generation of Transgenic RNAi Lines for *SGT1*, *SGT2* and *GCS*

Analysis of TILLING mutants affected in *SGT1* and *SGT2* revealed a moderate reduction of SG content in leaves of the *sgt1-5305* mutant. In a parallel approach transgenic *Lotus* RNAi lines were generated for *SGT1*, *SGT2* and *GCS*. The goal of this experiment was to obtain transgenic *Lotus* plants with a reduced SG and GlcCer content due to a downregulated gene expression of *SGT1*, *SGT2* and *GCS*. In these plants, nodulation and mycorrhiza formation were to be analyzed.

3.5.2.1 Cloning of RNAi Constructs

RNAi constructs containing fragments of *SGT1*, *SGT2* and *GCS* cDNA were generated by Helder Paiva at the Max-Planck-Institute of Molecular Plant Physiology (group of Peter Dörmann) in 2008. The constructs were cloned into the binary vectors pLH6000 or pLH9000. Both vectors carried an antibiotic resistance against spectinomycin and streptomycin in bacteria. Selection in plants was enabled by kanamycin (*SGT1*, *GCS*) or hygromycin B (*SGT2*) resistance conferred by transformation with pLH9000 or pLH6000, respectively. RNAi

constructs for *SGT1* and *SGT2* were targeting highly conserved regions of the coding sequence, to improve the chances of simultaneously downregulating expression of both genes.

3.5.2.2 Transformation of *Lotus japonicus* with *Agrobacterium tumefaciens*

Lotus japonicus transgenic RNAi lines were generated via *Agrobacterium tumefaciens* mediated hypocotyl transformation. The *SGT1* and *SGT2* RNAi constructs were co-transferred into *Lotus* in one transformation experiment with a mixture of *Agrobacterium* cells containing either of the constructs. In separate experiments, the empty vector pLH9000 (control) and the *GCS* RNAi construct were transferred into *Lotus*. Transgenic explants were cultivated on selective media inducing callus formation as described in 2.2.3. *GCS* RNAi lines were grown on kanamycin medium, and *SGT1*/*SGT2* RNAi lines on hygromycin B. The *SGT* RNAi lines carry the *SGT2* RNAi construct based on the resistance to hygromycin B, and in addition, most likely the *SGT1* RNAi construct. Eventually, shoot growth was induced and fully developed plants could be regenerated for all constructs.

3.5.2.3 Selection of Plants with a Downregulated Gene Expression for *SGT1, SGT2* and *GCS*

Semi-quantitative RT-PCR was employed for the selection of plants with a downregulated gene expression of *SGT1*, *SGT2* and *GCS*. From 10 (*SGT*) and 13 (*GCS*) independent transgenic lines, two plants were selected which showed a reduced gene expression for *SGT1* and *SGT2* or *GCS*.

Figure 37 shows the gene expression of the respective glucosyltransferase genes in selected RNAi lines. The gene expression of the housekeeping gene *ubiquitin* was monitored as a control for the amount of cDNA employed for PCR reaction.

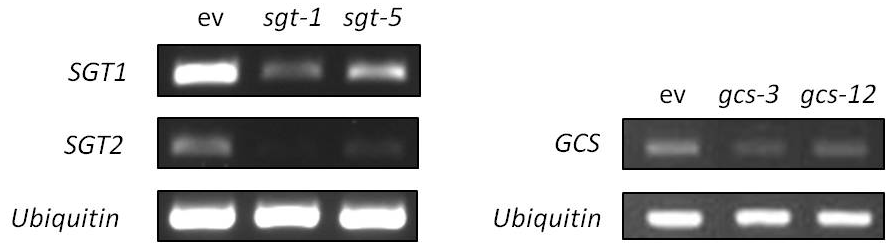

Figure 37: Gene Expression of *SGT1, SGT2* and *GCS* in *Lotus* RNAi lines. RNA was extracted from leaves of *Lotus* plants grown on soil. Semi-quantitative RT-PCR was performed with gene specific primers for *SGT1*, *SGT2*, *GCS* and for the housekeeping gene *ubiquitin*. The PCR products were separated on an agarose gel and stained with ethidium bromide.

The selected *SGT* RNAi lines carry the RNAi construct for the downregulation of *SGT2* and most likely additionally that for the downregulation of *SGT1*. These plants showed a strongly decreased gene expression of both *SGT1* and *SGT2,* when compared to the empty vector control.

The downregulation appeared to more severe in line 1 than in line 5. As these lines showed a reduced expression of both *SGT* genes, they were henceforth termed *sgt-1* and *sgt-5.*

Two independent *Lotus* RNAi plants could be obtained, which showed a reduced gene expression for *GCS*. The lines *gcs-3* and *gcs-12* were selected for further experiments.

3.5.2.4 Characterization of Sterol Lipid Composition in *SGT* RNAi Plants

The sterol lipid content was measured in the *Lotus japonicus* RNAi plants *sgt-1* and *sgt-5*, in order to determine whether a reduced gene expression of the two *SGT* genes resulted in a decrease of SG content. Sterols were extracted from leaves, roots and nodules of the RNAi lines and the empty vector control line, grown on sand under full nutrient supply. Lipid quantification was performed by Q-TOF MS/MS analysis as described in 2.2.7. Figure 38 shows the lipid content of FSs, SGs, ASGs and SEs. The amount of FSs detected by Q-TOF MS/MS analysis was comparable in the RNAi lines and the empty vector control in all tissues. In leaves, the SG content was severely decreased from 0.71 nmol/mg FW in the empty vector control to 0.005 and 0.006 nmol/mg FW in *sgt-1* and *sgt-5*. In addition, the amounts of ASG were slightly decreased from 0.071 nmol/mg FW in the control to 0.058 and 0.056 nmol/mg FW in *sgt-1* and *sgt-5.* Furthermore, there was a slight increase of SEs in the *sgt-5* RNAi line.

In roots, a similar reduction of SGs from 0.045 nmol/mg FW in the control to 0.006 nmol/mg FW was detected in *sgt-1* and *sgt-5,* while ASGs were not reduced. The SE content was more than twofold increased from 0.07 nmol/mg FW to 0.15 nmol/mg FW in the two RNAi lines.

The SG content in nodules of *sgt-1* and *sgt-5* was decreased by around 50 % from 0.108 nmol/mg FW in the control to 0.044 and 0.047 nmol/mg in *sgt-1* and *sgt-5.* In nodules, the ASG content was decreased from 0.046 nmol/mg FW in the control to 0.026 and 0.030 nmol/mg FW in the mutants. Thus, ASGs were more severely reduced in nodules than in leaves and roots. In addition, SEs accumulated in nodules of the *sgt*-lines to a similar degree as in roots.

Analysis of the sterol molecular species composition in leaves and roots revealed no changes in the distribution of campesterol, stigmasterol and sitosterol in any of the sterol classes in the RNAi lines. Furthermore, the fatty acid distribution of ASGs and SEs remained unaltered (data not shown). However, there were minor changes in the molecular species distribution of FSs and SEs in nodules. In both nonpolar sterol lipid classes the amount of sitosterol was slightly but significantly increased at the expense of stigmasterol (P<0.01), while campesterol content remained unchanged. Stigmasterol was significantly decreased from 16.3 ± 1.2 mol% in FSs of the empty vector control to 13.1 ± 0.6 and 13.3 ± 0.4 mol% in *sgt-1* and *sgt-5* (P<0.01). In SEs, the stigmasterol content was reduced from 14.4 ± 1.4 mol% in the empty vector control to 11.9 ± 1.1 and 11.3 ± 1.0 mol% in *sgt-1* and *sgt-5* (P<0.01).

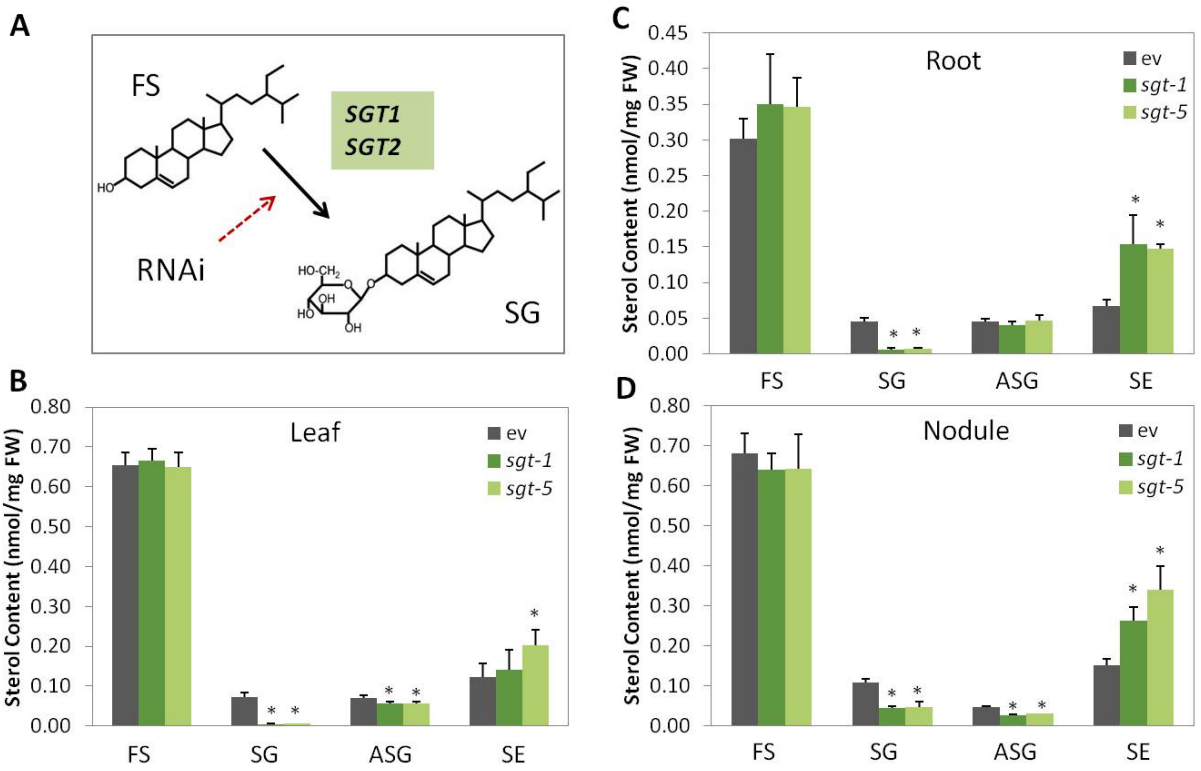

Figure 38: Sterol Content in *SGT* RNAi lines. The sterol glucoside transferase (SGT) catalyzes the synthesis of sterol glucoside (SG) from free sterols (FS) (**A**)**.** Two *Lotus* RNAi lines (*sgt-1* and *sgt-5*), showing a downregulated gene expression for *SGT1* and *SGT2*, and the empty vector control (ev) were grown on sand under full nutrient supply with 0.5 mM nitrogen and 2.5 mM phosphate. 8 weeks after infection with *Mesorhizobium loti* lipids were analyzed in leaves (**B**), roots (**C**) and nodules (**D**) by Q-TOF MS/MS analysis in the presence of internal standards. Data are mean and standard deviation of five measurements. Asterisks indicate values that are significantly different from the control (according to Student's *t* test, Welch correction, $P<0.01$).

3.5.2.5 Quantification of Sphingolipids in *GCS* RNAi Plants

Quantification of GlcCer content in the *GCS* RNAi lines *gcs-3* and *gcs-12* was performed by Q-TOF MS/MS analysis as described in 2.2.7.8. GlcCers were extracted from leaves, roots and nodules of the RNAi lines and the empty vector control, grown on sand under full nutrient supply. Figure 39 shows the amount of total GlcCer in the empty vector control and both RNAi lines. Q-TOF MS/MS analysis revealed a decrease of around 50 % of the total GlcCer content in leaves, roots and nodules of *gcs-3* and *gcs-12,* compared to the empty vector control. Furthermore, analysis of the molecular species composition revealed changes in the LCB distribution of in the RNAi lines, as is depicted in Figure 40.

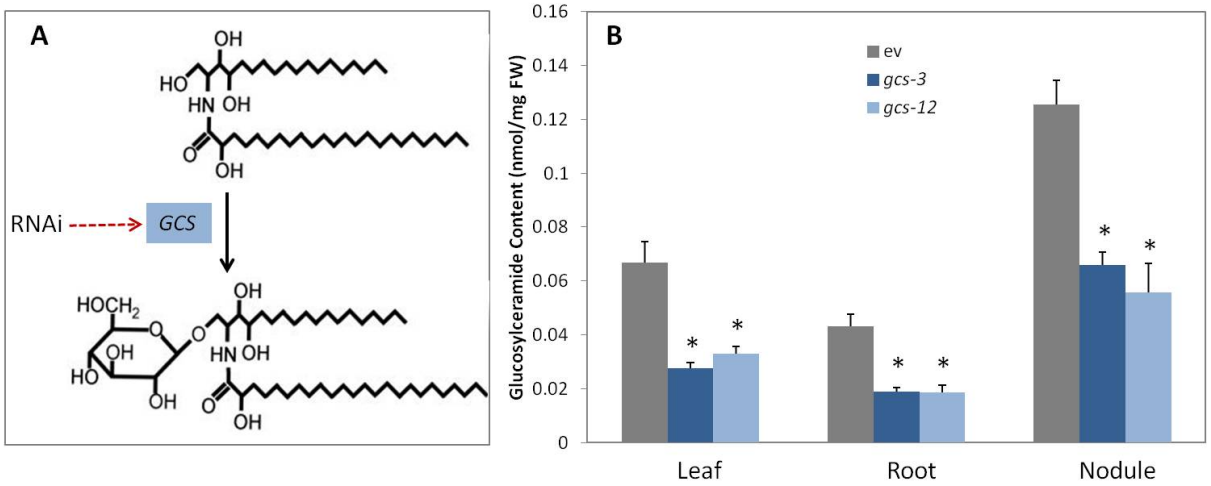

Figure 39: Total Glucosylceramide Content in *Lotus japonicus GCS* RNAi Lines. Two *Lotus* RNAi lines (*gcs-3* and *gcs-12*), showing a downregulated gene expression for *GCS*, and the empty vector control (ev) were grown on sand under full nutrient supply with 0.5 mM nitrogen and 2.5 mM phosphate. Leaves, roots and nodules were harvested 8 weeks after infection with *Mesorhizobium loti.* Lipids were analyzed by Q-TOF MS/MS analysis in the presence of internal standards. Data are mean and standard deviation of five measurements. Asterisks indicate values that are significantly different from the control (according to Student's *t* test, Welch correction, $P<0.01$).

The d18:2 containing GlcCer species d18:2-h16:0 was only marginally decreased in the RNAi lines. In contrast, the amounts of GlcCer species containing t18:1 LCBs were strongly decreased in all tissues. In the leaves of *gcs-3* and *gcs-12,* the abundant GlcCer t18:1-h16:0 was reduced to around 20 % of the amount detected in the empty vector control. Similar reductions were observed for t18:1-h22:0, t18:1-h24:0 and t18:1-h26:0 in leaves and roots of *gcs-3* and *gcs-12.* The only d18:1 containing GlcCer species; d18:1-h16:0 was depleted in leaves and roots of the mutant lines. In nodules of *gcs-3* and *gcs-12*, the t18:1 containing GlcCer species such as t18:1-h16:0 were reduced to about 40 % of the empty vector control. This reduction appeared to be less severe than in leaves and roots. However, as t18:1 species were more abundant in nodules than in leaves and roots, the rather moderate decrease of these GlcCers in nodules of the RNAi lines resulted in a 50 % reduction of total GlcCer, similar to leaves and roots.

In order to gain a more detailed insight into the regulation of the LCB distribution in sphingolipids of *Lotus*, attempts were made to analyze GIPCs, which constitute the second abundant class of sphingolipids in plants. For GIPC analysis in *Lotus* see 3.2.4.

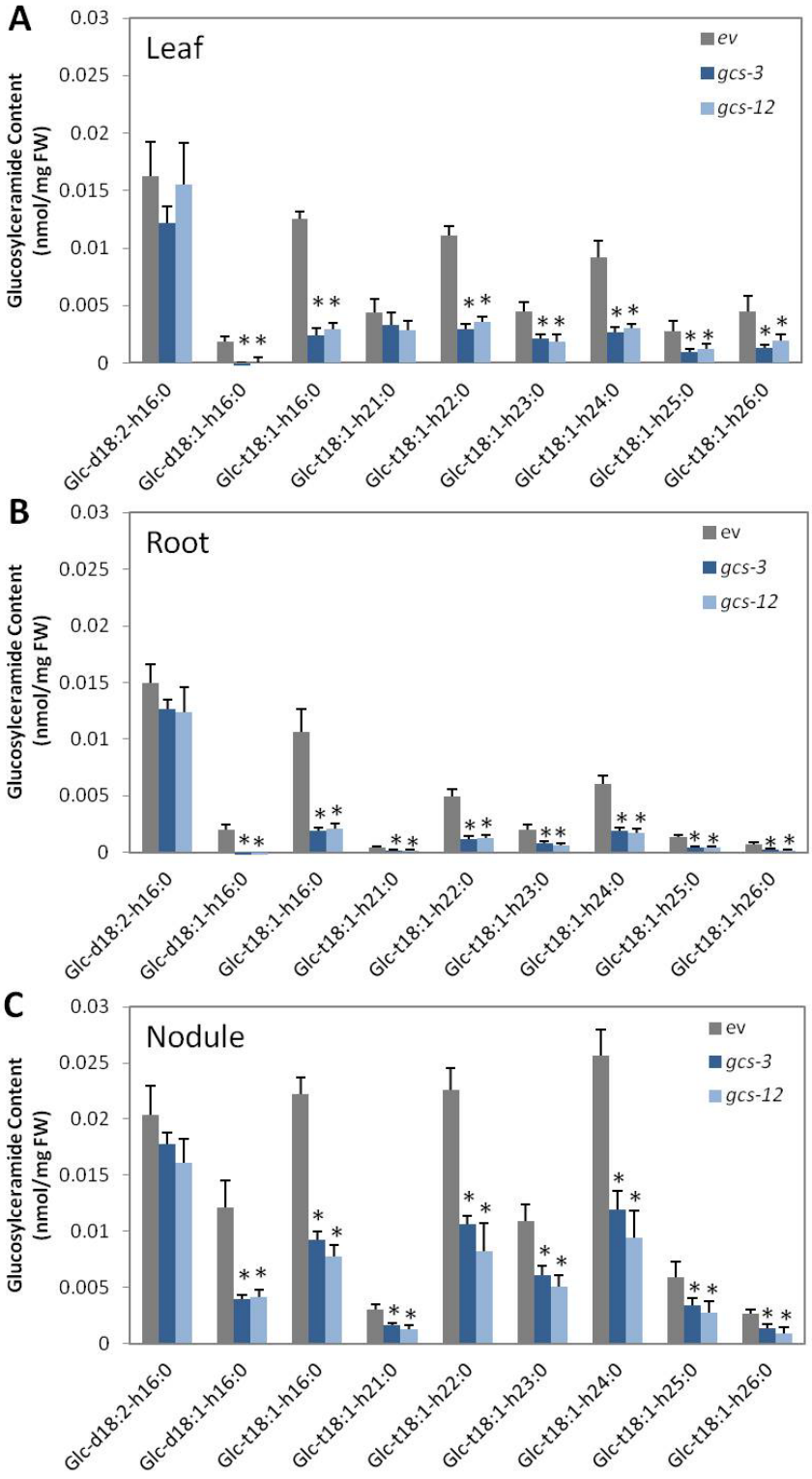

Figure 40: Distribution of Glucosylceramide Molecular Species in *Lotus japonicus GCS* RNAi Lines. Two *Lotus* RNAi lines (*gcs-3* and *gcs-12*), showing a downregulated gene expression for *GCS*, and the empty vector control (eV) were grown on sand with full nutrient supply (0.5 mM nitrogen and 2.5 mM phosphate). Leaves (**A**), roots (**B**) and nodules (**C**) were harvested 8 weeks after infection with *Mesorhizobium loti.* Lipids were analyzed by Q-TOF MS/MS analysis in the presence of internal standards. Data are mean and standard deviation of five measurements. Asterisks indicate values that are significantly different from the control (according to Student's *t* test, Welch correction, $P<0.01$).

3.6 Characterization of Nodulation in *SGT* and *GCS* RNAi Plants

Previous analysis of transgenic *Lotus japonicus* plants with a decreased DGDG content showed a severe phosphate dependent nodulation phenotype (Gaude 2005). In these plants, nodule formation was largely abolished during phosphate starvation, but the plants did not display any nodulation defects when grown under phosphate replete conditions. The goal of the present work was to investigate the putative functions of SG and GlcCer during root-nodule symbiosis. To this end, *Lotus* RNAi plants were generated, which showed a reduced gene expression for *SGT1* and *SGT2* or *GCS*, respectively (see 3.5.2.3). The *SGT* RNAi lines displayed a severe reduction of SG content in leaves, roots and nodules, and a moderate decrease of ASG in nodules (see 3.5.2.4). The *GCS* RNAi lines showed a significant decrease of GlcCer content, along with a change in LCB pattern in GlcCer (see 3.5.2.5). The effects of the reduced glycolipid contents in the RNAi lines on root-nodule symbiosis were to be examined by the evaluation of controlled nodulation in the RNAi lines. All experiments were conducted under phosphate starvation and under full phosphate supply to unravel the impact of the phosphate status and glycolipid deficiency on nodulation.

3.6.1 Evaluation of Nodulation Efficiency

Lotus RNAi plants and empty vector control were propagated vegetatively by cuttings and grown under semi-sterile conditions on a mixture of sand and vermiculite for several weeks until roots were formed. The plants were then transferred to silica sand and watered with nutrient solution containing 5 mM nitrogen to suppress premature nodulation. They were grown on 2.5 mM or 0 mM phosphate for several weeks until phosphate starvation set in. The plant's phosphate status was monitored by measuring the phospho- and galactolipid content in the leaves. Plants grown under full phosphate supply showed a DGDG lipid profile with 30 mol% DGDG and 10 mol% PC. An increase of DGDG and a concomitant decrease of PC were indicative of phosphate starvation. At this point, nitrogen was omitted from the watering solution and the plants were transferred to fresh silica sand. The roots were visually inspected to confirm the absence of nodules derived from uncontrolled infection events. Five days later, the plants were inoculated with *Mesorhizobium loti* at an OD of 0.05. Inoculation was repeated once, within one week. Nodule formation was monitored three weeks after infection and the number of nodules formed on each plant was recorded. The plants were further cultivated for an additional two weeks to monitor nodule maturation.

Figure 41 shows the RNAi lines *sgt-1* and *sgt-5* grown under full nutrient supply and under phosphate deprivation, before and after infection with *Mesorhizobium loti*. All plants exhibited reduced growth and decreased nodulation when grown under phosphate limitation. *sgt-1* and *sgt-5* showed no differences to the empty vector control in growth and appearance.

Size and color of nodules were monitored and no differences could be detected between the control and the *SGT* RNAi lines (data not shown).

Figure 41: Nodulation of *SGT* RNAi Plants during Phosphate Replete and Phosphate Limited Conditions. *Lotus* plants were propagated vegetatively by cuttings and grown on silica sand under full phosphate supply (**A**) and under phosphate deprivation (**B**) for 5 weeks before inoculation with *Mesorhizobium loti*. Nodule formation was evaluated 3 weeks after infection (**C** and **D**). Phosphate deprivation led to a diminished growth (**B**) and decreased nodule formation (**D**) in all lines including the empty vector (ev) control.

In Figure 42 photographs of the RNAi plants *gcs-3* and *gcs-12* and the empty vector control, grown under full nutrient supply and under phosphate limiting conditions, before and after infection with *Mesorhizobium loti* are displayed. Phosphate deprivation resulted in a

reduced growth and decreased number of nodules in all plants. Growth and appearance of *gcs-3* and *gcs-12* were comparable to the empty vector control. No differences in size and color of nodules could be detected among the empty vector control and the RNAi lines (data not shown).

Figure 42: Nodulation of *GCS* RNAi Plants during Phosphate Replete and Phosphate Limited Conditions. *Lotus* plants were propagated vegetatively by cuttings and grown on silica sand under full phosphate supply (**A**) and under phosphate deprivation (**B**) for 5 weeks before inoculation with *Mesorhizobium loti*. Nodule formation was evaluated 3 weeks after infection (**C** and **D**). Phosphate deprivation led to a reduced growth (**B**) and decreased nodule formation (**D**) in all lines including the empty vector (ev) control. Red arrows indicate nodulation sites.

Nodulation efficiency was evaluated in the *SGT* and *GCS* RNAi lines, by assessment of nodule numbers 26 days post infection. Figure 43 shows the numbers of nodules detected on roots of the RNAi plants and the empty vector controls grown under full phosphate supply and under phosphate deprivation. Phosphate deprivation resulted in a strong reduction of nodule formation to about 10 % of the numbers found under phosphate replete conditions. The *sgt-1* and *sgt-5* lines showed no differences in nodule formation when compared to the empty vector control. In a second experiment, a less stringent phosphate limitation experiment resulted in the formation of more than 10 nodules per plant during phosphate starvation. Again, no alterations

were detected in nodulation efficiency among the empty vector control and the RNAi lines (Figure 43 A).

In the *GCS* RNAi lines, no reduction in nodulation efficiency could be detected. *gcs-3* exhibited nodule formation similar to the empty vector control under phosphate deficient and phosphate sufficient conditions. During phosphate deprivation, there was no difference in nodule numbers between *gcs-12* and the empty vector control. The nodule number was increased in *gcs-12* when grown under phosphate replete conditions.

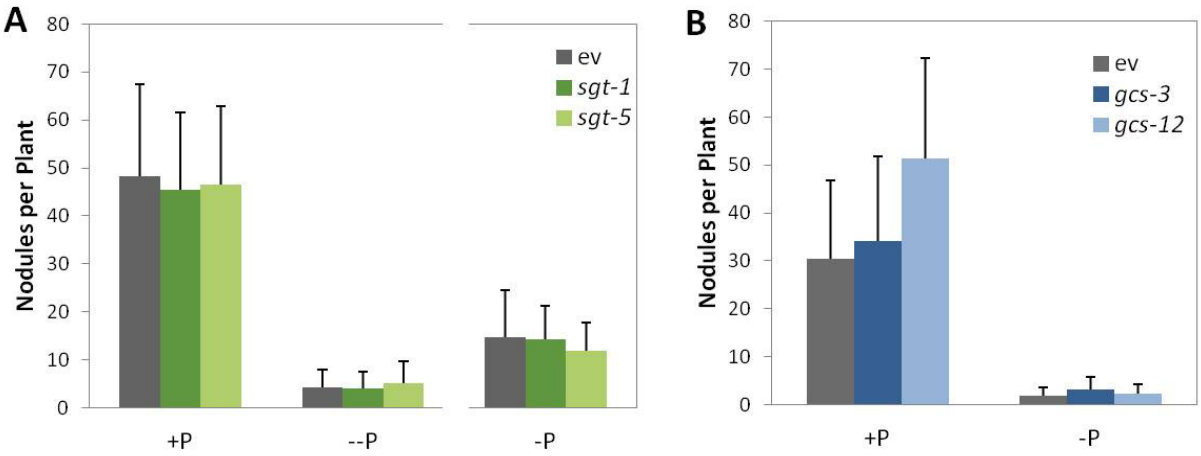

Figure 43: Nodulation Efficiency in *Lotus japonicus SGT* and *GCS* RNAi Plants. *Lotus sgt-1* and *sgt-5* (**A**) or *gcs-3* and *gcs-12* (**B**) and empty vector controls (ev) were grown from cuttings under semi-sterile conditions on a mixture of sand and vermiculite (2:1) and watered with 2.5 mM phosphate and 0.5 mM nitrogen. Rooted plants were further cultivated on sand and watered with nutrient solution containing 5 mM nitrogen and 2.5 mM or 0 mM phosphate. Phosphate deprivation was verified by galactolipid quantification before plants were infected with *Mesorhizobium loti* in mineral solution without nitrogen and phosphate at an OD of 0.05. The plants were further cultivated without nitrogen to induce nodule formation. The number of nodules was determined at 26 days post infection. Data show mean and SD. **A** +P: n=19 (ev), n=15 (*sgt-1*), n=6 (*sgt-5*); -P: n=16 (ev), n=26 (*sgt-1*), n=12 (*sgt-5*); **B** +P: n=10 (ev), n=19 (*gcs-3*), n=14 (*gcs-12*); -P: n=18 (ev), n=22 (*gcs-3*), n=18 (*gcs-12*).

3.7 Analysis of Mycorrhiza Formation in *SGT* and *GCS* RNAi Plants

In addition to root-nodule symbiosis, *Lotus* can undergo a symbiotic interaction with the arbuscular mycorrhizal fungus *Glomus intraradices*. To determine whether SG and GlcCer are important for this symbiosis, mycorrhiza formation was investigated in *Lotus SGT* and *GCS* RNAi plants, which show a reduced SG and GlcCer content. To this end, plants were inoculated with granular inoculum containing *Glomus intraradices* spores, after being deprived of phosphate for two weeks.

3.7.1 Investigation of Fungal Colonization by Light Microscopy

Fungal structures were studied by light microscopy after staining with ink and vinegar, to compare hyphae, arbuscules and vesicles in the RNAi lines with those in the empty vector

control line. In Figure 44, microscopic photographs of mycorrhized roots, containing hyphae, arbuscules and vesicles are shown. No differences were observed in the fungal structures found in *sgt-1* and *sgt-5* when compared with the control.

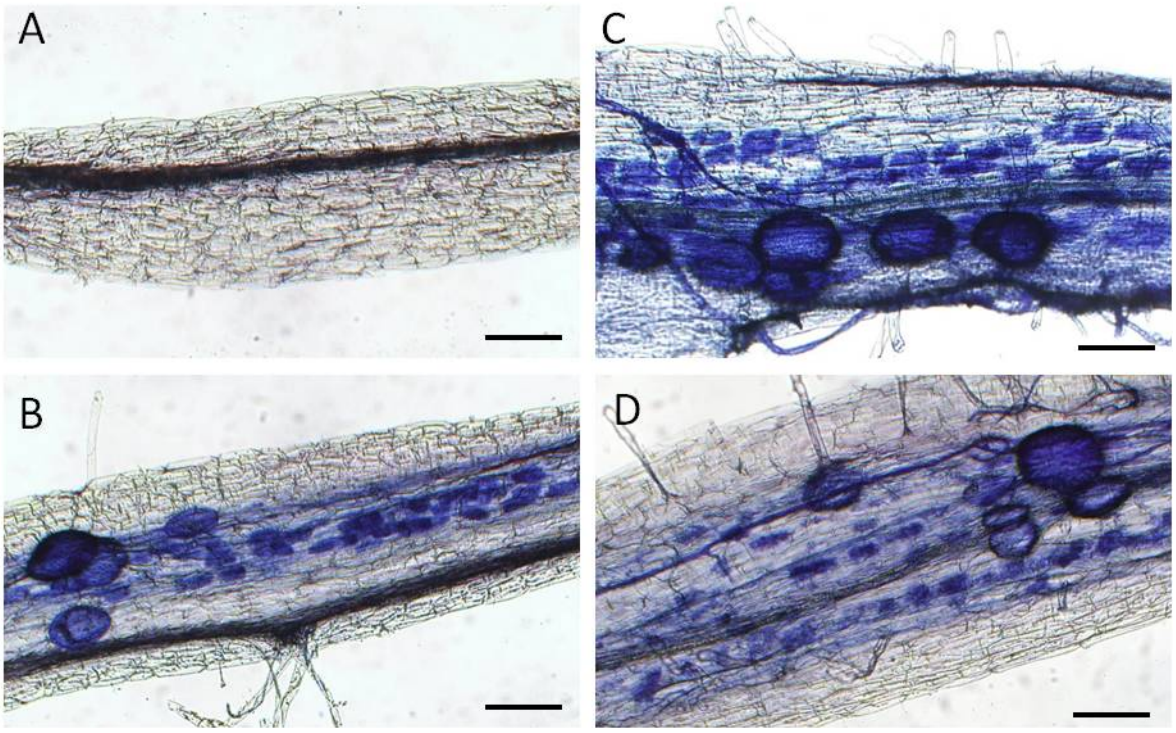

Figure 44: Fungal Structures of Arbuscular Mycorrhiza Formation in *Lotus SGT* RNAi Lines. RNAi plants and the empty vector control were grown for two weeks under phosphate deprivation before inoculation with *Glomus intraradices* spores. After eight weeks, the roots were stained with ink and vinegar and fungal structures were analyzed by light microscopy. Scale bars are 100 µm. **A**: non-colonized root of the empty vector control **B**: colonized root of the empty vector control **C**: colonized root of *sgt-1* **D**: colonized root of *sgt-5*

Figure 45 shows microscopic photographs of mycorrhized roots of *gcs-3* and *gcs-12* and the empty vector control. Hyphae, arbuscules and vesicles found in *gcs-3* and *gcs-12* are indistinguishable from those of the control plants. Arbuscular mycorrhiza formation was evaluated by determination of the degree of fungal colonization in the plant roots. This was achieved by statistical analysis of the fungal structures (McGonigle *et al.*, 1990). The mycorrhized roots were examined by light microscopy after staining of the roots with ink and vinegar. The number of colonization events, i.e. hyphae, arbuscules and vesicles was determined in the roots of inoculated plants. To this end, 50 randomly chosen locations in the root system were analyzed with regard to the presence of these mycorrhiza specific structures. Figure 46 shows the number of fungal structures detected in the roots of the RNAi lines compared to the empty vector control. Although there was a minor reduction of fungal structures in *sgt-1* and *sgt-5*, these differences were not significant (at $P<0.05$). Also, the number of arbuscules found in the *GCS* RNAi lines was slightly lower than in the control, but the difference to the control was not significant (at $P<0.05$). Both *gcs-3* and *gcs-12* also showed a slight reduction of hyphae and

vesicles. This reduction was calculated to be significant for *gcs-3* (at $P<0.05$ for hyphae and $P<0.02$ for vesicles) but not for *gcs-12*.

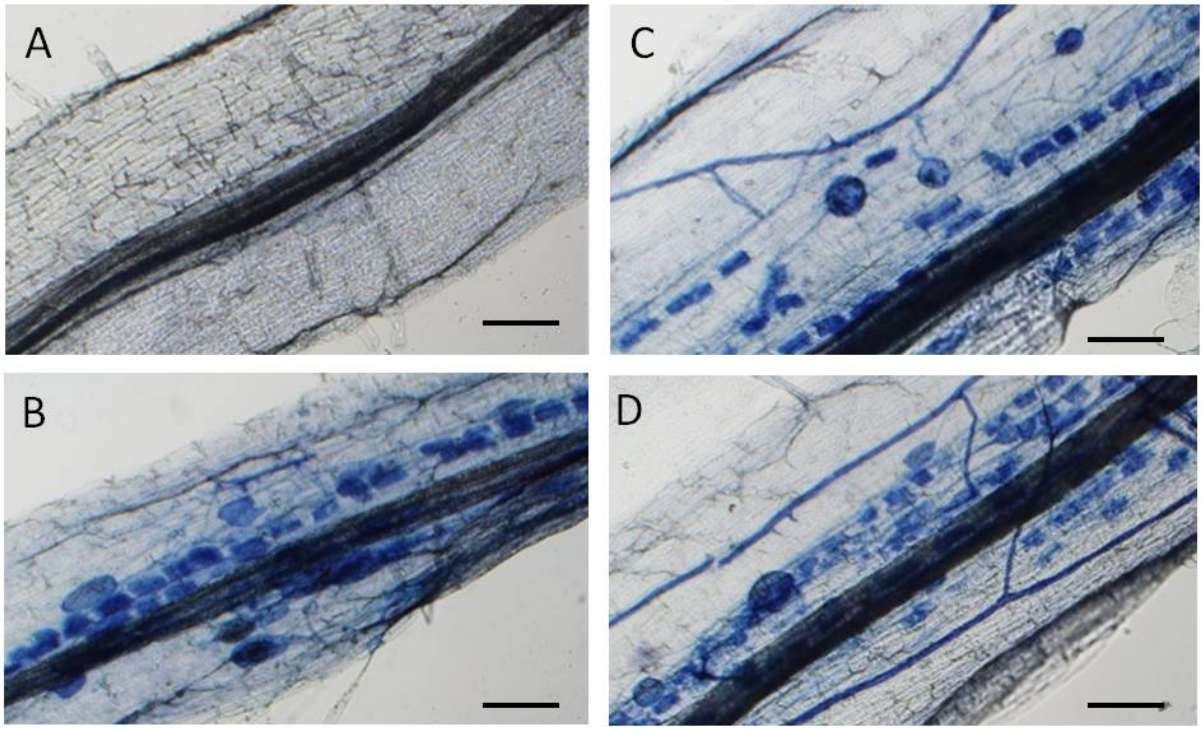

Figure 45: Fungal Structures of Arbuscular Mycorrhiza Formation in *Lotus GCS* RNAi Lines. RNAi plants and the empty vector control were grown for two weeks under phosphate deprivation before inoculation with *Glomus intraradices* spores. After three weeks, the roots were stained with ink and vinegar and fungal structures were analyzed by light microscopy. Scale bars are 100 µm. **A**: non-colonized root of the empty vector control **B**: colonized root of the empty vector control **C**: colonized root of *gcs-3* **D**: colonized root of *gcs-12*

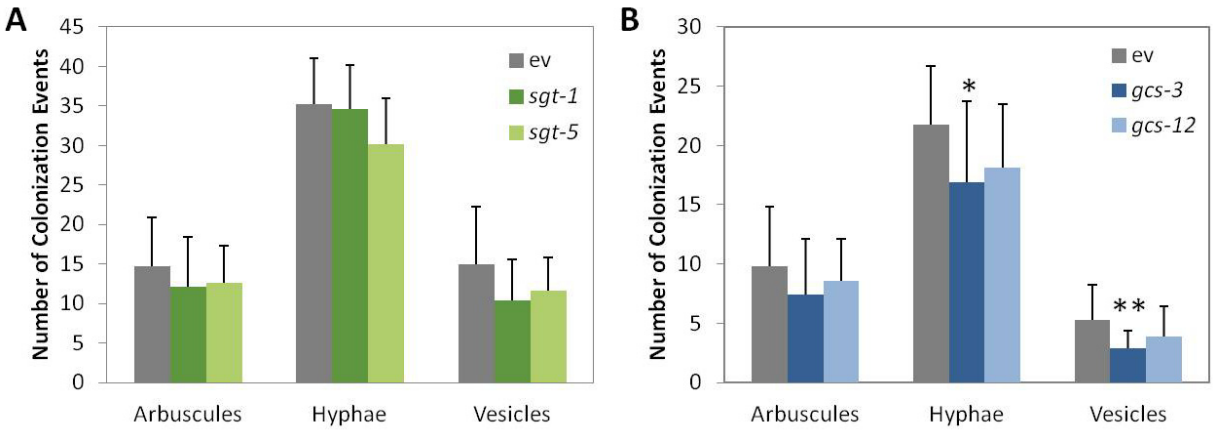

Figure 46: Arbuscular Mycorrhiza Formation in *Lotus SGT* and *GCS* RNAi Lines. RNAi plants and the empty vector control (ev) were grown for two weeks under phosphate deprivation before inoculation with *Glomus intraradices* spores. After 8 weeks, the roots of *sgt-1* and *sgt-5* and the empty vector control were stained with ink and vinegar and the degree of colonization was determined following the protocol by McGonigle *et al.*, (1990) (**A**). Colonization of *gcs-3*, *gcs-12* and the control was assessed 3 weeks after inoculation (**B**). The graphs show the number of colonization events per 50 evaluated positions in the root system. The bars show mean and standard deviations. Asterisks indicate values that are significantly different from the control (according to Student's *t* test, Welch correction, $P<0.05$ (*), $P<0.02$ (**)). **A** n=6 (ev), n=8 (*sgt-1*), n=8 (*sgt-5*); **B** n=13 (ev), n=16 (gcs-*3*), n=14 (*gcs-12*)

3.7.2 Quantification of *Glomus* Lipids as Biochemical Marker for Fungal Colonization

As described above (chapter 3.2.3.3), mycorrhiza specific lipids, like 16:0-16:1-16:1 TAG, are potential biochemical markers for the estimation of the degree of fungal colonization. To monitor the mycorrhization efficiency in *SGT* or *GCS* RNAi lines in an independent way, root samples from these plants were harvested three weeks after inoculation and the TAG content was determined by Q-TOF MS/MS analysis.

The amounts of TAG detected in roots of the empty vector control and *sgt-1* and *sgt-5* are shown in Figure 47. The total TAG content was increased in both RNAi lines, and *sgt-1* showed a stronger accumulation of 16:0-16:1-16:1 TAG than the control. However, this *Glomus* specific TAG was very low in the second independent RNAi line *sgt-5*. Therefore, no conclusive evidence for a role of SG on mycorrhization efficiency could be obtained.

Figure 48 shows the TAG content in *gcs-3*, *gcs-12* and the empty vector control. 16:0-16:1-16:1 TAG was slightly lower in *gcs-3* when compared with the control; however, the same TAG molecular species was moderately increased in *gcs-12*. In all plants, the *Glomus* specific TAG content was very low, as the evaluation was performed early after infection.

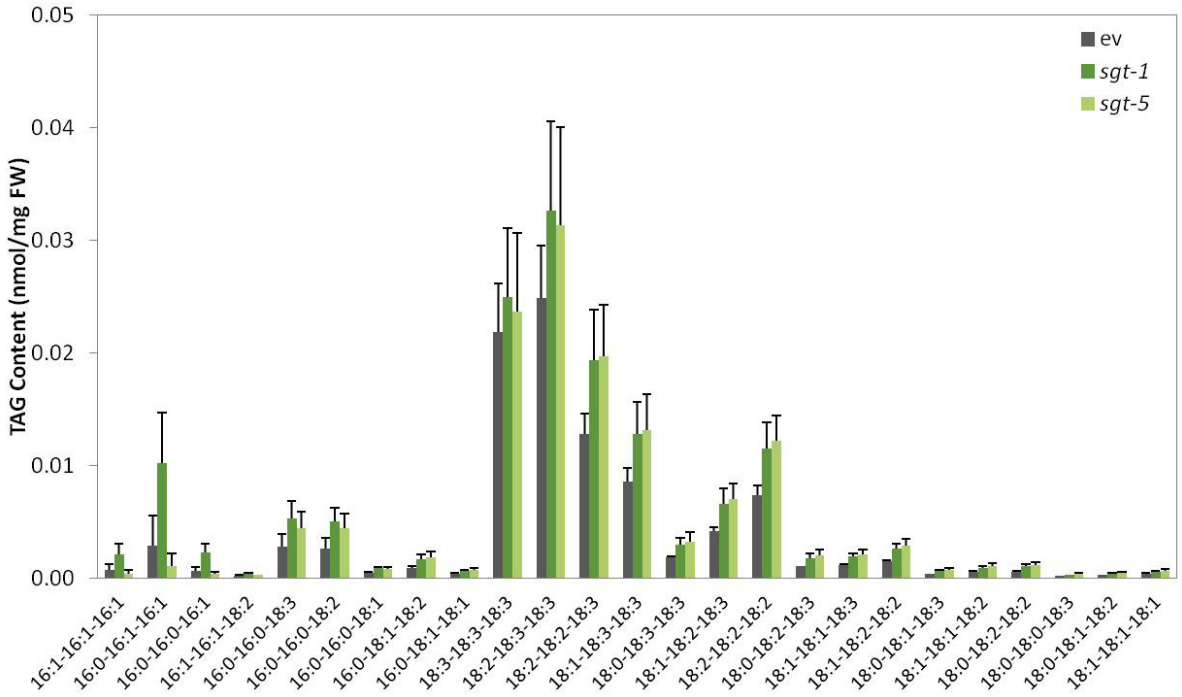

Figure 47: TAG Content in Roots of Mycorrhized *GCS* RNAi Lines. RNAi plants and the empty vector control were grown for two weeks under phosphate deprivation before inoculation with *Glomus intraradices* spores. After three weeks, lipids were isolated from roots for quantification by Q-TOF MS/MS analysis. Data represent mean and standard deviation of 5 measurements.

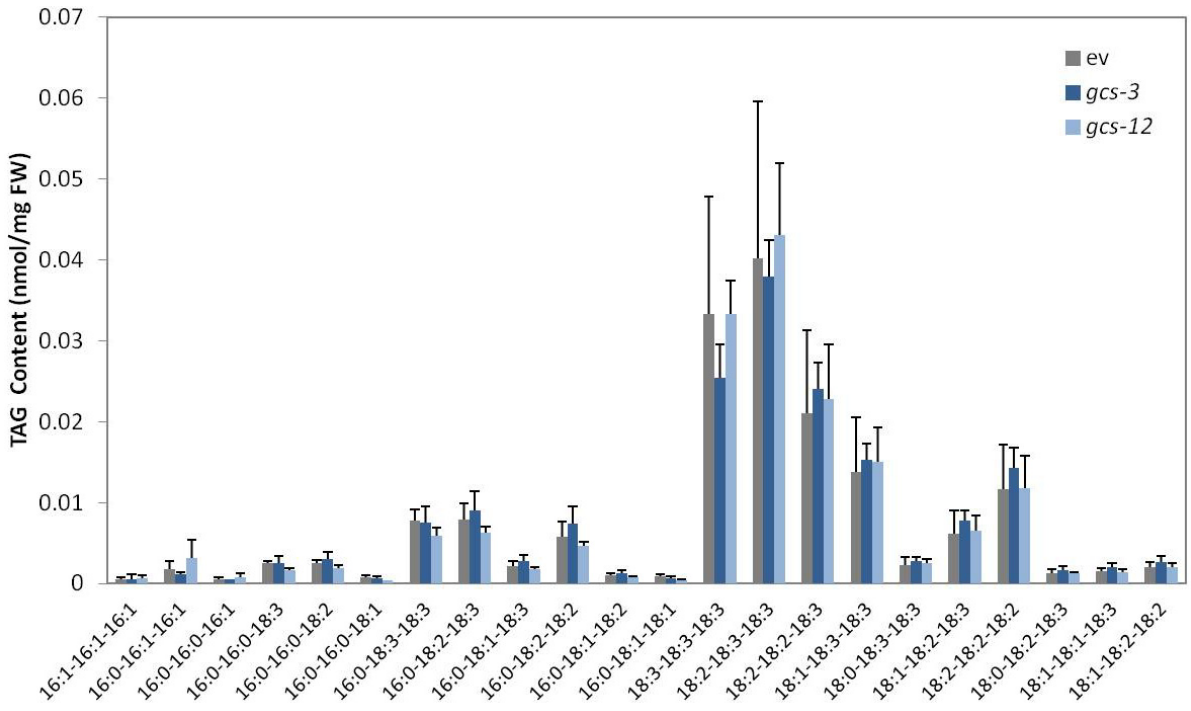

Figure 48: TAG Content in Roots of Mycorrhized *GCS* RNAi Lines. RNAi plants and the empty vector control were grown for two weeks under phosphate deprivation prior to inoculation with *Glomus intraradices* spores. After three weeks, lipids were isolated from roots for quantification by Q-TOF MS/MS analysis. Data represent mean and standard deviation of 5 measurements.

4 Discussion

Plant and microbial membranes represent the interface of plant-microbe interactions. Membrane properties are largely dependent on lipid and protein composition, which can show a great variety between different cellular compartments and plant organs. Plants are capable of changing their membrane composition as a reaction to abiotic or biotic stress. In the present work, membrane lipid remodeling of *Arabidopsis thaliana* and *Lotus japonicus* as a response to phosphate deprivation was investigated. To this end, Q-TOF MS/MS analysis was employed and a novel method for the comprehensive quantification of plant sterols was established. Furthermore, the changes in lipid composition of *Lotus japonicus* during symbiotic interactions with the nitrogen fixing soil bacterium *Mesorhizobium loti* and the arbuscular mycorrhizal fungus *Glomus intraradices* was studied. The role of the glycolipids sterol glucoside and glucosylceramide was studied in greater detail, by generation of transgenic *Lotus* plants with reduced glycolipid content, and by subsequent investigation of nodulation and mycorrhiza formation.

4.1 Q-TOF MS/MS Provides a Robust and Sensitive Method for Sterol Lipid Quantification in Plants

The development of suitable methods for lipid quantification is of great importance to address biological questions involving lipid metabolism. In the last years, technical advances, in particular the availability of high resolution mass spectrometers, have provided the means for the development of novel methods for lipid analysis. In the past, the quantification of complex lipids was performed by separation of plant extracts and subsequent quantification of fatty acid methyl esters or sterols by GC analysis or quantification of long chain bases by HPLC analysis (Browse *et al.*, 1986; Morrison and Hay, 1970; Merrill *et al.*, 1988; Sperling *et al.*, 1998; Bouvier-Navé *et al.*, 2010). These approaches were characterized by a comparatively low sensitivity and allowed only limited insight into the structure of individual molecular species. Technical advances in tandem mass spectrometry allowed the development of nondestructive measuring techniques. Direct infusion of crude lipid extracts from low amounts of plant tissue and subsequent quantification of intact phospho- and galactolipid ions was established on a triple quadrupole mass spectrometer equipped with an electrospray ionization (ESI) source (Welti *et al.*, 2002). Another method, using liquid chromatography coupled with triple quadrupole MS/MS analysis was established a few years later for the quantification of sphingolipids from plants (Markham and Jaworski, 2007). In contrast to the direct infusion approach applied for the quantification of phospho- and galactolipids, sphingolipids were measured after separation on

an HPLC column (Markham and Jaworski, 2007). Attempts at comprehensive "lipidomics" approaches were made in *Saccharomyces cerevisiae,* measuring phospholipids, sphingolipids, free sterols, and the nonpolar lipids DAG and TAG (Ejsing *et al.*, 2009). Furthermore, tandem mass spectrometry based quantification of FSs and SEs from animals was established recently (Liebisch *et al.*, 2006; Honda *et al.*, 2008). However, these methods were restricted to the quantification of cholesterol and cholesterol esters. Plants contain a much greater diversity of conjugated sterols, and the nondestructive measurement of the plant sterol lipids sterol glucosides (SG) and acylated sterol glucosides (ASG) has not been described to date.

In the present work, a novel method for the comprehensive quantification of free and conjugated sterols in plants by Q-TOF MS/MS was developed (Wewer *et al.*, 2011). In this method, lipids are extracted from plant tissue with chloroform in the presence of internal standards. After fractionation of the crude lipid extracts by solid phase extraction on silica columns, the sterols are infused into the mass spectrometer by nanospray direct infusion and ionized. Identification and quantification is based on characteristic fragment ions after fragmentation of selected ions and of internal standards in the collision cell.

Measuring parameters were optimized with the help of internal standards for each lipid class. As plants only contain sterols that carry at least one double bond, saturated sterols were chosen as internal standards for quantification of FSs, SGs, and ASGs. Cholestanol and stigmastanol were applied for the quantification of FSs. Plant SEs contain mainly 18:2 and 18:3 fatty acids, esterified to campesterol, stigmasterol and sitosterol. Cholesterol esters with saturated or mono-unsaturated fatty acids were only detected in trace amounts. Therefore, 16:1- and 18:1-cholesterol were used as internal standards for SE quantification. Saturated SGs were synthesized in this work by glucosylation of cholestanol and stigmastanol following a published protocol (Iga *et al.*, 2005). Saturated ASGs were obtained by hydrogenation of natural, commercially available ASGs from soybean (Buseman *et al.*, 2006). Suitable extraction procedures, ionization and optimum fragmentation energies were determined with these standards. Conjugated sterols were ionized in the positive mode as ammonium adducts and displayed characteristic fragmentation patterns. However, FSs were poorly ionized and their fragmentation resulted in the formation of many small fragment ions. Previous analyses had suggested an improvement of signal intensities of sterols or other nonpolar lipids such as DAGs by derivatization (Liebisch *et al.*, 2006; Li *et al.*, 2007; Honda *et al.*, 2008). In the present work, the derivatization of FSs with *N*-chlorobetainyl chloride was considered to be the best suitable method. Betainylated sterols gave strong signals after fragmentation, which resulted in the neutral loss of the sterol backbone and produced the betaine fragment ion.

While phospho- and galactolipids could be measured in crude lipid extracts from plant tissues in previous studies (Welti *et al.*, 2002), this was not possible for sterol lipids in the present work. Signal intensities of SGs, ASGs and especially of SEs were reduced by ion

suppression. In leaves, where conjugated sterols represent only minor components and chloroplast lipids such as MGDG, DGDG or chlorophyll are abundant, reliable quantification of conjugated sterols was not possible. A purification step by solid phase extraction considerably improved signal intensities for these lipids. However, SEs with saturated fatty acid residues were very prone to ion suppression, even in purified extracts. SEs with unsaturated fatty acids suffered less from ion suppression, regardless of the number of double bonds in the fatty acid residue. A similar behavior was also observed for saturated molecular species of other nonpolar lipids such as TAG (Han and Gross, 2001; Lippold *et al.*, 2012). Ionization is facilitated by the presence of polar head groups such as sugar moieties or phosphate groups. For lack of such polar head groups, nonpolar lipids are less frequently ionized in the presence of polar lipids. Apparently, the presence of at least one double bond in the acyl chains of glycerolipids improves ionization considerably. In order to account for deviating signal responses due to partial ion suppression of SEs with a saturated acyl group, cholesterol esters with saturated and unsaturated fatty acids were used for SE quantification.

Liquid chromatography on HPLC columns can improve sample purity and reduce the risk of contaminations. However, direct infusion of lipid extracts provides numerous advantages, allowing a very fast and universal analysis method for the quantification of many different lipid classes. Sterol lipids were quantified relative to the internal standards after collision induced dissociation. Characteristic fragments were chosen for lipid quantification. Quantification after collision induced dissociation provides several advantages, the most important one being the elimination of contaminations with compounds of similar molecular masses. Comparison of the fragmentation patterns obtained for SGs and ASGs revealed changes in fragmentation between internal standards with saturated sterols and unsaturated sterols from plant extracts. The use of correction factors has been described previously for the quantification of sphingolipids, which also display different fragmentation patterns depending on the presence of double bonds in the long chain base (Markham and Jaworski, 2007). In order to exclude overestimation of SGs in plant lipid extracts, a correction factor was determined by the quantification of mixtures containing saturated and unsaturated SGs by GC-MS and Q-TOF MS/MS. Collision induced dissociation of ASGs with unsaturated sterol moieties resulted in the formation of the sterol backbone, similar to SGs. However, a deviating fragmentation pattern of saturated ASGs produced a different fragment ion, containing the fatty acid and the sugar residue, while the sterol moiety was cleaved as a neutral loss. As the acylated sugar constituted the dominant fragment and no additional peaks were detected, this fragment was chosen for quantification. Side by side analyses of samples by Q-TOF MS/MS and by GC-MS confirmed the suitability of saturated ASGs as internal standards, when the acylated sugar residue was used for quantification. While the presence of a double bond at C5 of the sterol residue had a severe

impact on fragmentation, the presence of an additional double bond at C22 in stigmasterol compared to sitosterol did not result in an altered fragmentation pattern. Also, the saturation of the fatty acid residue in ASGs had no effect on fragmentation.

Signal response linearity was determined for all four sterol lipid classes using internal standards. Signal responses were linear in a range of 0.01 nmol to 1000 nmol in 200 µL of sample volume for FSs, SEs and SGs, and in a range of 0.1 nmol to 100 nmol for AGSs. The linear signal response even in low concentrations of sterol lipids allows the reliable quantification of sterol lipids in lipid extracts from small amounts of plant tissue.

Sterol lipid quantification in plants by Q-TOF MS/MS analysis was validated by simultaneous TLC/GC based quantification of sterol lipids in *Arabidopsis* leaves. The sterol lipid contents determined by Q-TOF MS/MS analysis in wild type *Arabidopsis* plants grown on soil were compared with previous reports on sterol lipids in *Arabidopsis*. Absolute amounts of FSs and SEs, as well as the sterol composition were comparable with these data (Gachotte *et al.*, 1995; Bouvier-Navé *et al.*, 2010). No data on the absolute amounts of SGs and ASGs in *Arabidopsis* were available. However, the ratio of SGs and ASGs to FSs and the ratio of ASGs to SEs were calculated and compared with data from previous studies (DeBolt *et al.*, 2009). Again, the results were very similar. The above described method for the quantification of sterol lipids in plants by Q-TOF MS/MS was therefore considered a valid tool for lipid analysis.

Comparison of Q-TOF MS/MS based quantification of sterol lipids in plants with TLC/GC based quantification revealed advantages of both methods. In contrast to GC analysis, isomers with the same molecular mass, that yield isobaric fragments upon collision induced dissociation, cannot be distinguished by direct infusion Q-TOF MS/MS analysis. The identification of such isomers would require a separation of compounds on HPLC columns prior to infusion into the mass spectrometer. While this is possible, measuring time would be significantly increased and the advantages are limited, as the only sterol isomers present in considerable amounts in *Arabidopsis* are stigmasterol and isofucosterol. The Q-TOF MS/MS based method allows the quantification of FSs, SEs, SGs and ASGs in a large number of samples. Sample preparation is far less time-consuming for Q-TOF MS/MS analysis than for TLC/GC based quantification. Furthermore, the high sensitivity of the nanospray source coupled to the Q-TOF allows the analysis of sterol lipids in very small tissue samples, while TLC/GC based analysis of low abundant sterols such as ASGs requires up to 100 fold larger sample amounts. This is of particular importance for the analysis of sterol lipids in specialized tissues such as root nodules, where sample material is limited. Furthermore, nondestructive analysis of sterols by Q-TOF MS/MS yields direct information on the fatty acid and sterol composition of conjugated sterols which presents another advantage over TLC/GC based quantification.

Q-TOF MS/MS was employed for the subsequent quantification of sterol lipids to address a number of biological questions in various plant species. In the present work, this method was

used for the measurement of sterol lipids during phosphate deprivation in *Arabidopsis thaliana* and *Lotus japonicus.* Furthermore, the sterol lipid content was analyzed in *Lotus* during plant microbe interactions with the nitrogen-fixing soil bacterium *Mesorhizobium loti* and with the arbuscular mycorrhizal fungus *Glomus intraradices*.

4.2 Conjugated Sterols Accumulate in *Arabidopsis* during Phosphate Deprivation

Q-TOF MS/MS analysis was employed to monitor membrane lipid remodeling in *Arabidopsis* under phosphate limiting conditions. While FSs constituted the major sterol lipid class in *Arabidopsis* leaves and roots, conjugated sterols accumulated in leaves and roots of phosphate deprived wild type plants. In addition, SEs were significantly increased in leaves of the *pho1* mutant, which is affected in the transport of phosphate to the shoot and suffers from a constant phosphate deprivation of the leaves (Poirier *et al.*, 1991). SE contents were also significantly elevated in wild type plants grown in sterile culture compared with plants grown on soil. Therefore, the accumulation of SEs during phosphate deprivation might not be specific for phosphate deprivation, but is likely to represent a more general stress response. This would be in accordance with reports on the accumulation of SEs in different developmental stages and as a response to abiotic stress (Dyas and Goad, 1993). The general consensus on the functions of SEs in plants is that these nonpolar lipids regulate the content of FSs in the membranes (Schaller, 2004; Banas *et al.*, 2005; Bouvier-Navé *et al.*, 2010). SEs are believed to localize to the cytosol where they are associated with TAGs in oil bodies (Kemp and Mercer, 1968; Gondet *et al.*, 1994). While the TAG content in phosphate deprived *Arabidopsis* plants was not determined in this experiment, elevated TAG levels could be detected in *Lotus japonicus* leaves and roots during phosphate deprivation (see chapter 4.3). The accumulation of FSs in membranes would severely alter membrane properties, as sterols are important regulators of membrane integrity (Schuler *et al.*, 1991). Because of their "flat" molecular shape derived from the typical four ring backbone, free sterols disturb the bilayer and increase membrane fluidity. As SEs do not localize to the membrane bilayer, esterification of FSs to SEs is an important mechanism to regulate the membrane sterol content in the cell.

The accumulation of SGs and ASGs during phosphate deprivation in *Arabidopsis* leaves indicates a change of membrane lipid composition with a shift from phospholipids to glycolipids. Such mechanisms have previously been studied, and the accumulation of the galactolipid DGDG in extraplastidial membranes is a prominent example (Härtel and Benning, 2000; Härtel *et al.*, 2001). During phosphate deprivation, phospholipids are degraded to release phosphate, which is used for important cellular processes such as protein phosphorylation or the synthesis of sugar phosphates and nucleic acids (Dörmann and Benning, 2002). Phospholipids are replaced

by DGDG, which is otherwise a minor component of extraplastidial membranes. Recent studies revealed that DGDG is not the only glycolipid to accumulate during phosphate deprivation in extraplastidial membranes, but that the glycosterols SG and ASG are increased in phosphate limited oat (*Avena sativa*) (Andersson *et al.*, 2005). Further studies of phosphate limitation in oat showed that ASG localizes specifically to the apoplastic leaflet of the plasma membrane, while DGDG is restricted to the cytosolic leaflet (Tjellström *et al.*, 2010). In the present study, a role in membrane remodeling in *Arabidopsis* leaves was revealed for SG and ASG during phosphate deprivation. Both SGs and ASGs were strongly increased in leaves of wild type plants grown under phosphate deprivation and in leaves of the *pho1* mutant, indicating that glycosterols can replace phospholipids during phosphate deprivation, similar to DGDG. In roots, SGs were significantly increased during phosphate starvation, although to a lower degree than in leaves. ASGs were not increased in roots of phosphate deprived plants; indeed there was even a slight reduction in ASG content. This finding is in contrast to the data obtained by Tjellström *et al.*, (2010) in roots of phosphate limited oat. The lack of ASG accumulation in phosphate deprived roots might be related to the fact that the ASG levels in roots are high during normal growth conditions, when compared with leaves. The same is true for the SG content, while FS contents are only slightly higher in roots than in leaves and SE contents are low. Differences in membrane remodeling between leaves and roots during phosphate deprivation might also be attributed to the different functions of these plant organs during phosphate deprivation. While leaves show only limited growth during phosphate deprivation, roots proliferate, presumably to improve the uptake of phosphate from the soil. Therefore, the maintenance of root functionality during phosphate deprivation is critical for the plant's survival and efficient uptake of phosphate.

It is unclear, whether the accumulation of SG and ASG during phosphate deprivation affects membrane functions. Tjellström *et al.* (2010) hypothesized that the replacement of phospholipids in the apoplastic leaflet by ASGs and not by DGDG was due to the fact that high amounts of DGDG severely reduce lipid acyl chain order. ASGs confer a higher degree of chain order than DGDG (Tjellström *et al.*, 2010). Due to the additional acyl chain of AGSs, the chain ordering ability of this lipid is also increased in comparison to SG. Possibly, an exceeded enrichment of ASGs in root plasma membranes of *Arabidopsis* would lead to very rigid chain ordering, which might interfere with root functions.

4.3 Membrane Remodeling in *Lotus japonicus* as a Response to Phosphate Limitation

The membrane lipid remodeling during phosphate limiting conditions has previously been described for *Arabidopsis* and oat *(Avena sativa)* (see chapter 4.2). In the present work, the influence of phosphate limitation on the membrane lipid composition in the model legume *Lotus*

japonicus was investigated. *Lotus japonicus* undergoes symbiotic interactions with the nitrogen fixing soil bacterium *Mesorhizobium loti*. The bacteria infect the roots and proliferate within the symbiotic organs, the nodules, which provide a specialized environment for bacterial nitrogen fixation.

Lipid measurements by Q-TOF MS/MS revealed changes of lipid composition in leaves, roots and nodules of *Lotus japonicus* during phosphate deprivation. Phosphate limitation resulted in a severe decrease of the phospholipids PS, PI, PG, PE and PC in all tissues. In leaves, the plastidial membrane lipid MGDG was also reduced, indicating a degradation of chloroplast membranes during phosphate deprivation. Similar to MGDG, DGDG localizes to the thylakoid membrane, where it maintains stability of the photosynthetic complexes (Reinsberg *et al.*, 2000; Dörmann and Benning, 2002). During phosphate deprivation, DGDG is known to accumulate in plastidial and extraplastidial membranes, to replace phospholipids (see chapter 4.2) (Härtel and Benning, 2000; Härtel *et al.*, 2001). In agreement with this, DGDG was strongly increased in roots and nodules of *Lotus japonicus* during phosphate limitation. However, the total phospho- and galactolipid content was reduced in all tissues, indicating that DGDG accumulation alone cannot compensate for phospholipid degradation during phosphate starvation. In *Lotus* leaves, the accumulation of DGDG in extraplastidial membranes was accompanied by a degradation of thylakoid membranes, as indicated by the decrease of MGDG. Therefore, the amount of DGDG in leaves was not elevated to the same extent as in roots and nodules. The molar distribution of phospho- and galactolipids revealed a considerable increase of DGDG in leaves and a three-fold increase in roots and nodules. While molar percentages also showed an increase of MGDG and SQDG, the absolute amounts of these glycolipids were not elevated. This is in contrast to previous studies in *Arabidopsis,* which had described an upregulation of SQDG synthase and an accumulation of SQDG in leaves during phosphate limitation, similar to DGDG (Essigmann *et al.*, 1998). However, in this study only the proportion of SQGD of the total phospho- and galactolipids was determined and no data on the absolute amounts of SQDG were obtained. In addition, SQDG exclusively localizes to the plastids and unlike DGDG it is not exported to extraplastidial membranes during phosphate deprivation (Essigmann *et al.*, 1998). Therefore, any accumulation of SQDG in leaves during phosphate deprivation would probably be insufficient to outweigh the decrease of SQGD due to degradation of the thylakoid membrane, which was indicated by a decrease in MGDG content.

Phospholipid degradation by phospholipase C or D leads to the formation of DAG and phosphatidic acid, respectively, after cleavage of the polar head groups (Moellering and Benning, 2011). In the present study, DAGs do not accumulate during phosphate deprivation, therefore they are likely to be further degraded or recycled for lipid biosynthesis. Quantification of nonpolar lipids during phosphate deprivation showed a strong accumulation of TAGs in leaves and roots. TAG accumulation as a response to various stress conditions or during senescence is

well documented (Lippold *et al.*, 2012). It is likely that the majority of DAG released from phospholipid degradation is recycled for DGDG and TAG biosynthesis, to save the costs for *de novo* synthesis of DAG. The accumulation of TAGs in leaves and roots is accompanied by a slight increase of SEs. These have been implicated to localize to oil bodies in the cytosol together with TAGs (Kemp and Mercer, 1968; Zinser *et al.*, 1993). Interestingly, no increase of TAGs or SEs was detected in nodules of phosphate deprived plants, although phospholipid degradation in nodules was similar to roots. This might indicate a further degradation of DAG or the incorporation of DAG into other lipid classes, possibly for the synthesis of bacterial lipids (for discussion of bacterial lipids see chapter 4.4). The exchange of lipids between plants and microorganisms has previously been described for pathogenic oomycetes of the genus *Phytophthora*, which are incapable of sterol biosynthesis (Gaulin *et al.*, 2010) and actively secerete sterol carrier proteins to release sterols from the membranes of its host plant (Mikes *et al.*, 1998). Also the biosynthesis of PC in symbiotic and pathogenic bacteria has been suggested to depend on the uptake of choline from the host plant (Sohlenkamp *et al.*, 2003). This indicates that symbiotic bacteria rely on plant metabolites for lipid biosynthesis. Therefore, the incorporation of fatty acids or DAG from degraded plant phospholipids into bacterial lipids might represent an explanation for the lack of increase of TAG and SEs during phosphate deprivation in nodules. Alternatively, the fatty acids released by phospholipid degradation during phosphate deprivation might be incorporated by the bacteria as a source of energy and carbon.

Quantification of sphingolipids and sterols during phosphate limitation revealed no significant changes of ASG or GlcCer contents. This is in contrast to findings in *Arabidopsis* where both SG and ASG (see chapter 4.2) and GlcCer (vom Dorp, 2010) contents were significantly increased upon phosphate limitation. This discrepancy might be due to a different degree of phosphate starvation in the different experiments. *Arabidopsis* plants grown for two weeks on synthetic medium without phosphate displayed severe growth retardation and anthocyanin accumulation in the leaves, which are signs of phosphate starvation. In contrast, *Lotus* grown on silica sand was deprived of phosphate for a total of 11 weeks until clear signs of phosphate starvation were visible. Thus, a comparatively long duration of phosphate deprivation is required to induce symptoms of phosphate starvation in *Lotus*. It is likely that a prolonged exposure to phosphate starvation would eventually also lead to an increase of ASG and GlcCers in *Lotus,* although the function of these glycolipids for membrane lipid homeostasis during phosphate deprivation in *Lotus* might be less vital than in *Arabidopsis*. However, similar to the accumulation of SGs in *Arabidopsis*, SGs were increased in *Lotus* during phosphate limitation and this increase was particularly strong in nodules. These measurements suggest a function of SG analogous to the role of DGDG, to maintain structural integrity of plant membranes when phosphate availability is limited.

4.4 Changes in Lipid Composition during Root-Nodule Symbiosis

The lipid quantification in symbiotic tissue should provide evidence for putative functions of glycolipids during plant-microbe interactions. During root-nodule symbiosis, a new plant organ, the nodule, is formed to host bacteroids which are capable of nitrogen fixation. The bacteroids are found in symbiosomes, surrounded by the peribacteroid membrane, which is derived from the plant plasma membrane (Whitehead and Day, 1997).

Nodules are symbiotic structures, which are structurally derived from the plant roots but contain large numbers of bacteroids. About half of the total fatty acid content in soybean nodules has been attributed to the symbiosome fraction, containing the bacteroids and the peribacteroid membrane (Gaude *et al.*, 2004). Therefore, bacterial lipids constitute a considerable proportion of lipids in the symbiotic tissue. In the present work, plant membrane lipids should be analyzed, therefore possible contaminations with *Mesorhizobium* lipids were monitored. The lipid composition of *Mesorhizobium* strongly differs from plants, and therefore, contaminations with bacterial lipids affect only few lipid classes. Galactolipids, sterols and sphingolipids are absent from *Mesorhizobium*. The only polar lipid classes described in both *Mesorhizobium* and *Lotus* are PC and PG (Devers *et al.*, 2011). In addition, *Mesorhizobium* contains considerable amounts of ornithine lipid and monomethyl-PE and lower amounts of cardiolipin and dimethyl-PE (Devers *et al.*, 2011). Moreover, in a different study PE was found to be present in lower amounts (Choma and Komaniecka, 2002). The fatty acid residues of these lipids are constituted to about 50 % of 18:1 and to below 10 % of 16:0 and 18:0. 18:1 fatty acids can also be converted into 19:0 ^{11,12cyclo} and 18:1 ^{methyl} which are absent from plants. Together, 18:1, 19:0 ^{11,12cyclo} and 18:1 ^{methyl} constitute more than 80% of the total fatty acids in *Mesorhizobium* (Devers *et al.*, 2011). Targeted lists for Q-TOF MS/MS analysis of phospholipids in plants were adapted from Welti *et al.*, (2002) and predominantly comprise combinations of 18 or 16 fatty acids with up to 3 double bonds (see appendix for Q-TOF MS/MS targeted lists and fatty acid distribution of phospholipids in roots and nodules). Therefore, phospholipids containing combinations with one molecule of 19:0 ^{11,12cyclo} or 18:1 ^{methyl} were not measured. One exception was a PC species with a molecular mass corresponding to 38:2 PC, which was present in plants in low amounts. This molecular species has the same molecular mass as PC containing two residues of 19:0 ^{11,12cyclo} or 18:1 ^{methyl} fatty acids and therefore cannot be distinguished by Q-TOF MS/MS analysis. As expected, phospholipid analysis revealed a significant increase of this particular PC molecular species in nodules. No such increase was detected in PE, confirming the absence of appreciable amounts of non-methylated PE from *Mesorhizobium*. The most prominently increased PC molecular species contained polyunsaturated fatty acid residues, which are unlikely to originate from *Mesorhizobium*. Therefore, an increase of total PC content in nodules can largely be attributed to accumulation of plant derived lipids. However, the accumulation of PG in nodules may result

from the contribution of bacterial lipids, as predominantly 34:2 and 34:1 molecular species were elevated and other molecular species were not increased.

Previous analysis of the phospho- and galactolipid composition of the peribacteroid membrane in *Lotus* and soybean revealed the presence of DGDG as an authentic membrane constituent (Gaude *et al.*, 2004). In the present work, gene expression of *DGD1* was induced in *Lotus* during nodulation. This is in accordance with previous data obtained with soybean (Gaude *et al.*, 2004). However, unlike *DGD1*, *DGD2* was not upregulated in nodules of *Lotus*. This is in contrast to a strong induction of *DGD2* expression in mature nodules of soybean (Gaude *et al.*, 2004). Comparison of phospho- and galactolipid composition of *Lotus* roots and nodules revealed no significant accumulation of DGDG in nodules. Previously, an increase of DGDG in soybean nodules had been demonstrated (Gaude *et al.*, 2004), although this increase was minor. Soybean DGDG represented only 2.5 mol% of total phospho- and galactolipid content roots and was increased to 3.4 mol% in nodules. In the present study, *Lotus* roots contained higher amounts of DGDG, which constituted about 10 mol% of phospho- and galactolipids and there was no further increase during nodulation. The high DGDG content in *Lotus* roots might be a possible explanation for the lack of further accumulationof this lipid in nodules.

No comprehensive information on sterol lipids in nodules is available until now. Previous analysis of the PBM from pea showed stigmasterol to be the predominant sterol, followed by sitosterol (Hernández and Cooke, 1996; Whitehead and Day, 1997). However, no attempts were made to analyze conjugated sterols. Similar to *DGD1*, gene expression of *SGT1* and especially of *SGT2* was induced during nodulation, suggesting a function of SG in nodule formation. In accordance with this, the SG content was significantly higher in nodules than in roots. This was consistently accompanied by a reduction of ASG content in nodules, suggesting a limited acylation of SG, presumably by regulation of an unidentified acyltransferase catalyzing ASG synthesis. Sterol lipid analysis furthermore revealed intriguing differences in sterol composition among plant tissues. Sterol composition was analyzed in flowers, siliques, leaves, roots and nodules, and a strikingly diverging sterol composition was revealed in roots. Campesterol, stigmasterol and sitosterol were detected in all tissues, although stigmasterol was only present in very low amounts in flowers. In roots, the stigmasterol proportion was almost five-fold higher than in leaves and even more elevated when compared with nodules. This accumulation was accompanied by a concomitant reduction of sitosterol and was restricted to the membrane forming sterol lipid classes FS, SG and ASG. Stigmasterol is synthesized from sitosterol by a C22 desaturase (CYP710A1), which introduces a double bond into the alkyl side chain of the sterol (Morikawa *et al.*, 2006). In *Arabidopsis*, stigmasterol is only present in low amounts, but application of the phytopathogen *Pseudomonas syringae* to the leaves induces a strong accumulation of stigmasterol content in plant membranes (Griebel and Zeier, 2010). This accumulation enhances susceptibility towards the pathogen and a mutant affected in CYP710A1

was more resistant to infection with *Pseudomonas*. Furthermore, external application of stigmasterol to the leaves resulted in a reduced resistance of the mutant (Griebel and Zeier, 2010). These findings might suggest a specific role of stigmasterol in the barrier function of the plasma membrane. In a different study, *Arabidopsis* plants with a strongly increased stigmasterol content due to overexpression of *CYP710A1* showed a stronger resistance to pathogens while the T-DNA insertion mutant of the same gene was affected in host and nonhost resistance (Wang *et al.*, 2012). Accumulation of stigmasterol was speculated to regulate efflux of nutrients to the apoplast, which is a prerequisite for optimal pathogen growth. The authors suggested a less permeable membrane due to high stigmasterol content in the overexpression line of *CYP710A1* to be causative for the enhanced resistance against pathogens, leading to a decreased efflux of nutrients to the apoplast (Wang *et al.*, 2012). Although there were discrepancies in the effects observed in the CYP710A1 mutant during plant pathogen interactions, both studies show an increase of stigmasterol upon infection and indicate an involvement of stigmasterol in plant-microbe interactions. The unusually high stigmasterol content in Lotus japonicus roots, which was observed in the present work, raises the question, whether this sterol is essential for efficient infection with *Mesorhizobium*. This hypothesis is supported by the fact that root derived nodules show no enhanced stigmasterol content compared to other plant organs. This is indicative of a role for stigmasterol in nodulation during early infection, but not beyond. Characterization of symbiotic interactions in a mutant affected in the C22 desaturase CYP 450 would elucidate the role of stigmasterol in *Lotus* roots for symbiotic interactions. Such investigations are beyond the scope of this work and should be subject to future research.

Gene expression of *GCS* was slightly induced during nodulation, although to a lower degree than *SGT1*, *SGT2* and *DGD1.* No data on the sphingolipid content in nodules are available to date. Some studies have reported the presence of sphingolipids in the peribacteroid membrane of pea, but no specifications as to the nature or quantity of these sphingolipids were made (Hernández and Cooke, 1996). Another study gave evidence for the presence of GIPCs in the peribacteroid membrane of pea during early infection events (Perotto *et al.*, 1995). In the present work, analysis of the GlcCer content in leaves, roots and nodules of *Lotus japonicus* revealed a significant increase in nodules compared to roots. Furthermore, the GlcCer composition dramatically changed during nodulation (see Figure 24). The predominant molecular species of GlcCer in leaves and roots, d18:2-h16:0, was only moderately increased, while d18:1 and t18:1 containing molecular species were highly accumulated. Among these were GlcCers with odd-chain hydroxy fatty acids, such as h21:0, h23:0 and h25:0. While the presence of odd-chain fatty acids is rare in other lipid classes of higher plants, they are not unusual in sphingolipids (Kaul and Lester, 1978; Imai *et al.*, 1995). Remarkably, most of the molecular species that were increased during nodulation were reduced in roots when compared to leaves. At the same time, the content of d18:2-h16:0 was rather stable between leaves, roots and

nodules. The differential accumulation of some molecular species during nodulation appears to depend on the LCB composition, as all d18:1 and t18:1 species were highly increased and d18:2 was less affected. On the other hand, the contents of all h16:0 containing molecular species were unchanged between leaves and roots, regardless of the LCB composition. Instead, GlcCers with very long chain fatty acids were lower in roots. These findings suggest that the molecular species distribution of GlcCers is differentially regulated in leaves, roots and nodules, possibly by preferential incorporation of ceramides with specific fatty acids or LCBs into the different sphingolipid classes. A long-term goal for the investigation of sphingolipid functions during nodulation is the establishment of a comprehensive method for the analysis of all sphingolipid classes in plants, similar to the method developed for sterol lipid analysis in this work. GIPC analysis in *Lotus* would greatly contribute to the elucidation of the underlying mechanisms of the differential accumulation of GlcCer molecular species in different tissues. GIPCs represent the second abundant sphingolipid class in plants and therefore, their synthesis likely has an impact on the availability of free ceramide for GlcCer biosynthesis. In the present work, first steps towards the analysis of GIPCs by Q-TOF MS/MS analysis were taken, following a protocol for sphingolipid quantification in plants by Markham and Jaworski (2007). GIPCs cannot be extracted from plant tissues with chloroform, due to their very polar nature. The requirement of relatively large sample volumes, alternative extraction protocols and the lack of suitable internal standards render GIPC analysis far more challenging than the analysis of most plant membrane lipids. Analysis of GIPCs from *Lotus* leaves and roots by Q-TOF MS/MS revealed the presence of t18:1 and t18:0 LCB containing molecular species and the absence of d18:2. Similar to GlcCers, GIPCs contained hydroxylated, saturated fatty acids, mainly h16:0, h22:0, h24:0 and h26:0, as well as the odd chain fatty acids h21:0, h23:0 and h25:0. The polar head group contained inositolphosphate, hexuronic acid and a hexose. The hexuronic acid and the hexose most likely are represented by glucuronic acid and glucose, respectively. However, their exact structure cannot be revealed by mass spectrometry and therefore remains unclear at the moment. The same head group could be detected in *Arabidopsis* leaves in the present study, which is in agreement with previous reports (Markham *et al.*, 2006). Unlike in *Arabidopsis,* the glucose moiety of the head group could also be substituted with an amino group, as has been reported for *Nicotiana tabacum* (Kaul and Lester, 1975, 1978). GIPCs containing N-acetylglucosamine were proposed as the predominant molecular species in tomato and soybean (Markham *et al.*, 2006) and were also found in tobacco (Kaul and Lester, 1975, 1978). However, in the present study only the nonacetylated form was detected in *Lotus*. LCB quantification of total sphingolipids by HPLC analysis revealed that GIPCs are equally abundant in *Lotus* leaves as GlcCers. Therefore, an impact of GIPC synthesis on the availability of ceramides for GlcCer synthesis, and *vice versa*, is probable. The increase of t18:1 LCB containing GlcCers during nodulation might result in a reduction of GIPC content in nodules, due to decreased availability

of t18:1 ceramide for GIPC synthesis. GIPC analysis in nodules could provide evidence to support this hypothesis. However, an accurate quantification of GIPCs in plants by Q-TOF MS/MS analysis requires more detailed method development, in particular the validated quantification relative to a suitable internal standard. This should be subject to future research, as part of the development of a comprehensive sphingolipidomics approach by Q-TOF MS/MS analysis. In the meantime, a function of SG and GlcCer during nodulation can be suggested, possibly as constituents of the peribacteroid membrane, based on the specific accumulation of these lipids in nodules and the induced gene expression of the respective glucosyltransferases during nodulation.

4.5 Lipid Metabolism during Arbuscular Mycorrhiza Formation

Arbuscular mycorrhiza formation is an ancient symbiosis between most land plants and symbiotic fungi of the phylum *Glomeromycota* and has contributed greatly to the evolution of land plants (Parniske, 2008). Phosphorous represents one of the major macro elements required for plant growth and constitutes a growth limiting factor for plants on most soils. Plants profit from mycorrhizal symbiosis by an increased uptake of water and phosphate from the soil via an extensive network of fungal hyphae (Javot *et al.*, 2007). The importance of mycorrhiza formation for phosphate uptake is highlighted by the tight regulation of this symbiosis, depending on phosphate availability in the soil (Olsson *et al.*, 2002; Parniske, 2008). Within the plant root, nutrients are exchanged between the plant and the fungus via the periarbuscular membrane, which surrounds the fungal structures inside the plant cells. Similar to the peribacteroid membrane in root nodule symbiosis, the periarbuscular membrane is derived from the plant plasma membrane. Q-TOF MS/MS analysis of lipids in *Lotus* roots, colonized with the mycorrhizal fungus *Glomus intraradices,* provided insight into plant lipid metabolism during mycorrhiza formation. Colonized roots, grown under phosphate limiting conditions, contained significantly increased amounts of the phospholipids PE and PC. At the same time, DGDG was slightly decreased. The amount of DGDG in *Lotus* roots can range from around 12 mol% of total phospho- and galactolipids, in plants grown under phosphate sufficient conditions, to more than 35 mol% during phosphate starvation (see Figure 18). Thus, the DGDG content of 26 mol% in non-mycorrhized roots indicates a moderate phosphate deprivation with a phosphate status considerably improved as compared to full phosphate starvation. The increase of PC and PE in the mycorrhized plants, and the concomitant decrease of DGDG, might indicate an improvement of phosphate availability caused by mycorrhiza formation. Additional phosphate supplied by the fungus would enable the plants to increase their phospholipid biosynthesis for membrane formation. However, contaminations with phospholipids from fungal origin have to be excluded.

Fatty acid composition of phospholipids has previously been studied in *Glomus intraradices* by Johansen *et al.*, (1996). They showed that the predominant fatty acids in extraradical hyphae were 16:0, 16:1 and 18:1 fatty acids, in addition to the very long chain polyunsaturated fatty acids 20:4 and 20:5. From these data, one can predict *Glomus* specific combinations of 18:1, 18:2 and 20:4 and 20:5 fatty acids, resulting in PC molecular species such as 38:6-PC, 38:5-PC and 38:4-PC. In the data obtained by Johansen *et al.,* 20:4 and 20:5 fatty acids together account for up to 15 % of the total fatty acids of the phospholipid fraction. Therefore, a considerable proportion of the phospholipids synthesized by the fungus should be represented by the molecular species 38:6-PC, 38:5-PC and 38:4-PC. In an experiment with *Medicago truncatula* roots, showing an extremely high degree of mycorrhizal colonization with *Glomus intraradices*, these phospholipids were strongly increased (collaboration with Dr. Nicole Gaude, MPIMP Golm). However, the degree of mycorrhization of the *Lotus* roots in the present study was much lower. The *Glomus* specific molecular species were at or below the limit of detection in mycorrhized roots of *Lotus japonicus.* Therefore, the increased phospholipid content in the mycorrhized roots is indeed derived from plant membranes and not from the fungus (see appendix, Figure 55 for phospholipid molecular species in mycorrhized roots).

The sterol composition of *Glomus intraradices* has previously been studied, and was shown to comprise mainly campesterol and lower amounts of stigmasterol and sitosterol, in the free form or as sterol esters (Fontaine *et al.*, 2001). This sterol composition could be confirmed in the present work (data not shown). No increase in campesterol content was detected in mycorrhized roots. Therefore, a considerable contribution of fungal sterol lipids to the total sterol content measured in mycorrhized roots is unlikely. FSs were slightly but significantly increased in colonized roots. While the content of SEs and ASGs was unaltered during mycorrhization, a significant decrease of SGs was detected. Similar to the decrease of DGDG, this might be attributed to an improved phosphate status of the plant. However, the effect of phosphate deprivation on SG content was not as severe as on DGDG, especially in roots (see Figures 18 and 19). Therefore, a physiological function of SG, beyond phosphate dependent regulation of membrane lipid homeostasis, might exist.

Lyso-phosphatidycholine (LPC) has previously been reported to be of major importance during arbuscular mycorrhiza formation in plants (Drissner *et al.*, 2007). It has been suggested that LPC plays a role as a signaling molecule which accumulates upon mycorrhization. Colonization of *Lotus japonicus* with *Glomus intraradices* resulted in a specific increase of very long chained unsaturated fatty acids, which might be derived from the fungus (Vijayakumar, 2012). However, no indications for an involvement of LPC in signaling during mycorrhiza formation were found in the present work. No changes of LPC content or molecular species composition could be detected in mycorrhized roots (see Figure 29). This might be due to a relatively low degree of mycorrhization of *Lotus* roots in the present study. However, the results

were very similar to those obtained from measurements of *Medicago truncatula* roots which showed a much higher degree of mycorrhization (collaboration with Dr. Nicole Gaude, MPIMP Golm). LPC accumulation during mycorrhiza related signaling might be restricted to local sites, such as arbuscules. Plants can distinguish efficient arbuscules from inefficient ones, which are actively degraded. It has been proposed that a phosphate containing molecules such as LPC might serve as a biochemical marker employed by the plant to monitor the efficiency of phosphate deliverance in arbuscules (Parniske, 2008). Cellular fluctuations of LPC content might therefore be important for regulatory processes in mycorrhization but would not necessarily result in changes of total LPC content.

While fungal membrane lipids apparently constitute only a minor proportion of total lipids in mycorrhized *Lotus* roots, a significant accumulation of *Glomus* lipids was detected in the nonpolar lipid fraction. It has been described in previous reports that nonpolar lipid fractions from *Glomus* extraradical hyphae contain considerable amounts of 16:0 and 16:1 fatty acids, and that the predominant nonpolar lipid class is represented by TAG (Johansen *et al.*, 1996). Moreover, in mycorrhiza formation in soybean with the arbuscular mycorrhizal fungus *Glomus fasciculatus* the amount of 16:1ω5 was found to correlate with the number of vesicles observed in soybean roots (Pacoysky and Fuller, 1988). In the present work, the accumulation of 48:3, 48:2 and 48:1 TAGs, which are only present in traces in noncolonized roots, could be shown after colonization with *Glomus intraradices*. The amount of these TAG molecular species correlated with the degree of fungal colonization (data not shown). In exchange for phosphate and other nutrients, the fungus receives hexoses from the plant, which are converted into TAG inside the arbuscules. TAG, as a means of energy and carbon storage, is transported towards the extraradical hyphae within vesicles, and accumulates inside the hyphal network and in spores (Pfeffer *et al.*, 1999; Bago *et al.*, 2002; Bago *et al.*, 2003). It has previously been proposed that the prevalent mycorrhizal fatty acid 16:1ω5 might be employed as a biochemical marker for mycorrhizal colonization (Olsson *et al.*, 1995). We hypothesize that the quantification of 48:3, 48:2 and 48:1 TAGs by Q-TOF MS/MS analysis is a suitable measure for efficient symbiosis, as the amount of TAG transported to the extraradical hyphae represents the share of carbon obtained from the host plant. In densely colonized roots, the presence of 38:6-PC, 38:5-PC and 38:4-PC phospholipids would also be a suitable measure for the estimation of fungal biomass, as membrane lipids are less prone to fluctuation than storage lipids. However, in the present study, these phospholipids were below the detection limit and were therefore no suitable markers for mycorrhization.

4.6 Transgenic *Lotus japonicus* Plants Affected in *SGT1*, *SGT2* and *GCS* Show Severe Reduction of Glycolipid Content

The downregulated gene expression of *SGT1* and *SGT2* in *Lotus* RNAi plants resulted in a severe decrease of SG content. In leaves and roots, the SG content was reduced by more than 90 %, while in nodules around 50% of residual SG content remained. The less severe reduction of SG content in nodules might be explained by the upregulation of *SGT1* and *SGT2* expression during nodulation (Figure 25). The gene expression of *SGT1* and *SGT2* in nodules of the RNAi lines was not analyzed. While the activity of the 35S-CaMV promoter has not been investigated in *Lotus japonicus* nodules, previous studies showed the 35S-CaMV promoter to be equally active in nodules and in roots of soybean and *Lotus corniculatus* (Hansen *et al.*, 1989; Govindarajulu *et al.*, 2008). Other reports showed this promoter to be inactive in the bacteroid containing cells in alfalfa and *Medicago truncatula* (Samac *et al.*, 2004; Auriac and Timmers, 2007).

An alternative explanation for the minor reduction of SG levels in nodules derives from the fact that SG is the precursor for ASG synthesis by an unidentified acyltransferase. The reduced SG content in leaves and roots of the *SGT* RNAi plants only marginally affected the ASG content, indicating that most SG was converted into ASG. This suggests that the acyltransferase is not regulated by substrate availability. It is noteworthy that the ASG content reduction was strongest in nodules, whereas the SG reduction in this tissue was less severe than in leaves and roots. When comparing the total glycosterol content, comprising SG and ASG, a similar reduction can be detected in all tissues, including nodules. In leaves of the RNAi plants, the total glycosterol content is reduced by 44 %, in roots by 43 % and nodules by 46 %. These findings indicate that the different SG levels in leaves, roots and nodules of the RNAi plants are not caused by diverging downregulation of the *SGT1* and *SGT2* gene expression, but rather by the rate of SG to ASG conversion. Taking into consideration the low ASG content in wild type nodules compared with roots, which is usually accompanied by high SG content, one can conclude that there is a low ASG synthase activity in nodules. In the wild type, this leads to an accumulation of SG in maturing nodules, in the RNAi plants, the conversion of SG into ASG is low, therefore SG levels are higher than in leaves and roots, while ASG levels are decreased. The identification of the acyltransferase which catalyzes the conversion of SG into ASG and the characterization of its role during nodulation should be subject to future research.

The reduction of the glycosterol content in the RNAi plants resulted in an accumulation of SEs, while the FS content was barely altered. This accumulation of SEs is another example for the role of this nonpolar lipid class for maintaining FS homeostasis. The details of this function have been discussed in chapter 4.2.

In *Lotus SGT* RNAi plants, both *SGT1* and *SGT2* are strongly downregulated. RNAi constructs were designed for the simultaneous downregulation of both genes, targeting highly conserved regions of the genes. Furthermore, *Lotus* hypocotyls were simultaneously

transformed with both RNAi constructs and most likely carried both constructs, although selection was only carried out for *SGT1*. Thus, a strong downregulation of both *SGT1* and *SGT2* was achieved, which resulted in a reduction of SG and ASG content that was more severe than in *SGT1* or *SGT2* TILLING single mutants. The two TILLING mutants carried premature stop codon mutations for *SGT1* and *SGT2*, respectively. The SG content in leaves of the *sgt2* mutant was unchanged when compared with the wild type, whereas the *sgt1* mutant showed a reduction of SG by about 50 %. ASG contents were barely affected. These findings indicate that SGT1 can fully compensate for the loss of SGT2 in *Lotus* leaves, and that SGT2 can at least partially compensate for the loss of SGT1. The stronger effect of the loss of *SGT1* on SG levels is in agreement with the gene expression monitored by semi-quantitative RT-PCR, which suggests a stronger expression of *SGT1* than of *SGT2*. In *Arabidopsis* single mutants, carrying T-DNA insertions in *SGT1* (At3g07020) or *SGT2* (At1g43620), the ratio of SG and ASG content to FS content in leaves was reduced to about 50 % of the wild type (DeBolt *et al.*, 2009). In this study, SG and ASG were not quantified separately. Therefore, the contribution of SG to the reduced SG/ASG to FS ratio in the mutants is unclear. Neither of the two single mutants showed a more distinct lipid phenotype than the other, but the SG and ASG content was further reduced in the double mutant (DeBolt *et al.*, 2009). Likewise, the generation of double mutants in *Lotus japonicus* by crossing of the *SGT1* and *SGT2* single mutants would likely lead to a further reduction of SG content. However, this was beyond the time frame of this work and should be subject to future research. Meanwhile, further experiments were conducted with the *Lotus* RNAi plants, which showed a stronger reduction of SG and ASG content than the TILLING mutants.

Lotus RNAi plants, carrying RNAi constructs for the downregulation of the glucosylceramide synthase, showed a strongly reduced gene expression of *GCS.* The plants exhibited a decrease of GlcCer content in the leaves, roots and nodules by about 50 % (see Figure 39). There were striking differences in the degree of reduction between the different molecular species. The only d18:2 containing molecular species was barely decreased in any of the tissues analyzed, whereas all other compounds, containing either d18:1 or t18:1 long chain bases, were dramatically reduced. In leaves and roots, most of the t18:1 containing GlcCers were reduced by 80 %, while the d18:1 containing GlcCer were almost depleted down to the detection limit. In nodules, the t18:1 containing GlcCer species were only reduced by about 60 % when compared with the control (see Figure 40). Although this reduction was less severe than in leaves and roots, the total GlcCer content was reduced by 50 % in nodules, similar to leaves and roots, as t18:1 species were more abundant in nodules.

GIPCs represent the second abundant sphingolipid class in plants. It can be postulated that the specific reduction of some molecular species in the *GCS* RNAi plants is connected to GIPC metabolism. Indeed, analysis of GIPCs in *Lotus* roots and nodules had revealed that d18:2 molecular species are absent, while GIPCs with t18:1 and t18:0 long chain bases dominated (see

Figure 31). Ceramides, which constitute the substrates for both, GIPC and GlcCer synthesis, are synthesized at the ER (Lynch, 2000; Sperling and Heinz, 2003). Likewise GlcCer synthesis is located at the ER, while GIPCs are synthesized in the Golgi (Bromley *et al.*, 2003; Hillig *et al.*, 2003; Wang *et al.*, 2008) (see Figure 4 for an overview of sphingolipid biosynthesis). Presumably, those ceramides that are later incorporated into GIPCs are transported from the ER to the Golgi. One could hypothesize that d18:2 containing ceramides remain at the ER, as they are exclusively used for GlcCer synthesis. In the RNAi plants, the downregulation of *GCS* leads to a decreased incorporation of ceramides into GlcCer. It is likely that d18:2 containing ceramides accumulate at the ER, while ceramides with t18:1 and t18:0 LCBs are used for GIPC synthesis at the Golgi. Therefore, the pool of d18:2 ceramide available for GlcCer synthesis continually grows, resulting in a larger proportion of d18:2-h16:0 GlcCer in the RNAi plants.

4.7 Nodulation and Mycorrhiza Formation in Plants with Reduced Contents of Sterol Glucoside and Glucosylceramide

Previous studies had revealed a role for the galactolipid DGDG during nodulation. DGDG is an authentic constituent of the peribacteroid membrane surrounding the symbiosomes (Gaude, 2004). Under phosphate deprivation DGDG is crucial for nodule formation. RNAi plants with a reduced DGDG content displayed a severe inhibition of nodulation under phosphate starvation (Gaude, 2005). Lipid analysis of *Lotus japonicus* showed an accumulation of SG and an induced gene expression of the glycosyltransferases *SGT1* and *SGT2* during nodulation (see Figure 25). Furthermore, the SG content was increased during phosphate deprivation in *Arabidopsis* and *Lotus*, similar to DGDG (see Figures 14 and 19), and GlcCer was strongly increased during nodulation. Therefore, it was possible that SG, ASG and GlcCer have a function during nodule formation, analogous to DGDG. Analysis of nodule formation in the *SGT* and *GCS* RNAi plants revealed no significant differences in nodulation efficiency compared to the control. Phosphate deprivation led to reduced nodule numbers, as was previously described in soybean (Israel, 1987). However, this effect was very similar in the RNAi plants and the control. No differences could be observed in the shape or color of nodules of the *SGT* and *GCS* RNAi plants. Taken together, the reduction of SG and GlcCer content did not affect nodulation. However, this does not exclude a function of these glycolipids during nodulation. The GlcCer content in the *GCS* RNAi plants and the total glycosterol content in the *SGT* RNAi plants were only reduced by about 50 %. This reduction may not be sufficient to affect nodulation, even if these lipids are involved, e.g. as constituents of the peribacteroid membrane. Although SG as well as GlcCer accumulated in nodules of the wild type, their presence in the peribacteroid membrane has yet to be confirmed. To this end, peribacteroid membrane preparations have to be subjected to comprehensive lipid analysis by Q-TOF MS/MS in future experiments.

In addition to nodulation, the second important symbiosis in *Lotus japonicus*, the arbuscular mycorrhiza formation, was investigated in the *SGT* and *GCS* RNAi plants. There is only limited information on the composition of the periarbuscular membrane, which is derived from the plant plasma membrane, similar to the peribacteroid membrane in nodules. In the present work, no accumulation of glycolipids was detected in mycorrhized roots compared to the non-mycorrhized control. However, a significantly reduced SG content was observed in mycorrhized roots. This might be ascribed to an improved phosphate supply in mycorrhized roots, or might indicate a specific membrane lipid change associated with the symbiosis. The *SGT* RNAi lines showed no alterations in mycorrhiza formation. The numbers and appearance of arbuscules, hyphae and vesicles observed in the RNAi lines were very similar to the control (see Figures 44 and 46). However in this experiment mycorrhization was already advanced. Therefore, potential differences in early colonization might have been missed. Therefore, this analysis will have to be repeated, with a different experimental setup, including a shorter colonization period. In an independent experiment, *Glomus* specific TAGs were quantified as biochemical markers of the degree of mycorrhization and found to be higher in *sgt-1* but lower in *sgt-5* compared to the control. As mentioned above (see chapter 4.5), the *Glomus* derived TAG content is rather prone to fluctuation. Therefore, a larger number of samples will need to be analyzed to obtain more reliable results. Moreover, TAG analysis should be conducted at different time points during mycorrhization and correlated with analysis by light microscopy, to validate the use of *Glomus* TAGs as a biochemical marker.

The degree of fungal colonization was slightly but significantly reduced in one of the two *GCS* RNAi lines. However, no differences could be detected in a second independent RNAi line, or in the content and composition of the *Glomus* specific TAGs synthesized during mycorrhization. Furthermore, no changes in fungal structures could be detected by microscopical analysis of the mycorrhized roots. Further experiments will need to be conducted to unravel wether a reduced GlcCer content in *Lotus* roots indeed affects mycorrhiza formation. These should include the analysis of mycorrhiza formation at different time points after inoculation and simultaneous TAG analysis in the *GCS* RNAi plants.

5 Summary

Lipids are important constituents of plant membranes, which represent the interface of plant-microbe interactions. In the present work, the role of membrane lipids of *Lotus japonicus* during root-nodule symbiosis with the nitrogen-fixing soil bacterium *Mesorhizobium loti* and during arbuscular mycorrhiza formation with the symbiotic fungus *Glomus intraradices* was analyzed. The main focus was the investigation of the glycolipids sterol glucoside (SG) and glucosylceramide (GlcCer).

In contrast to the mass spectrometry based quantification of sphingolipids and phospho- and galactolipids, no method for the nondestructive measurement of plant sterol lipids has been described. Therefore, a novel method for the comprehensive quantification of free sterols (FSs), sterol glucosides (SGs), acylated sterol glucosides (ASGs) and sterol esters (SEs) in plants by quadrupole time-of-flight tandem mass spectrometry (Q-TOF MS/MS) was established and validated by comparison to quantification by thin layer chromatography/gas chromatography (TLC/GC). This method was applied to the quantification of sterol lipids in leaves and roots of *Arabidopsis thaliana* during phosphate deprivation. SGs and ASGs were increased upon phosphate deprivation, suggesting a role in the replacement of phospholipids similar to the galactolipid digalactosyldiacylglycerol (DGDG). Furthermore, SEs accumulated as an unspecific response to abiotic stress. A comprehensive membrane lipid profile of *Lotus japonicus* during phosphate deprivation was obtained by Q-TOF MS/MS analysis. SGs were increased, as was DGDG, while all phospholipids were severely reduced. Leaves and roots, but not nodules showed a strong accumulation of the nonpolar lipid triacylglycerol (TAG) during phosphate starvation.

Lipid analysis during nodulation revealed changes in sterol and sphingolipid metabolism. Stigmasterol was highly increased in roots compared to all other plant organs, including nodules, and this accumulation was restricted to membrane forming sterol lipids. SGs were increased in nodules, while ASGs were decreased. Furthermore, GlcCers were strongly increased in nodules and showed a change of long chain base composition. Analysis of glycosylinositolphosphorylceramides (GIPCs) in *Lotus* revealed t18:1 as the predominant long chain base and a fatty acid pattern comparable to that of GlcCer. Mycorrhiza formation in phosphate deprived *Lotus* plants led to an improved phosphate supply and subsequent increase of phospholipids accompanied by a decrease of DGDG. Furthermore, SGs were decreased upon mycorrhization. Analysis of the nonpolar lipid fraction revealed an accumulation of *Glomus* specific TAG species, which correlated with the degree of mycorrhization.

The accumulation of SG and GlcCer during nodulation suggested that these two lipids are important to establish plant-microbe interactions. Putative sterol glucosyltransferases genes (*SGT1*, *SGT2)* and glucosylceramide synthase *(GCS)* genes from *Lotus* were identified by sequence homologies to the respective genes from *Arabidopsis*. Heterologous expression

confirmed that the cDNAs harbor sterol glucosyltransferase and glucosylceramide synthase activities, respectively. Gene expression of *SGT1*, *SGT2* and of *GCS* was upregulated during nodulation. A *Lotus* TILLING mutant with a premature stop codon in *SGT1* showed a 50 % reduction of the SG content in leaves, while the SG content in the *SGT2* TILLING mutant, which also carries a premature stop codon was not affected. ASG content was not reduced in either of the two mutants. *SGT* RNAi lines with a downregulated gene expression of both *SGT1* and *SGT2* showed a severe reduction of SG content in leaves, roots and nodules and a moderate reduction of ASG content in leaves and nodules, with a concomitant increase of SEs. RNAi lines with a downregulated gene expression of *GCS* showed a 50 % reduction of total GlcCer content in leaves, roots and nodules, with a relatively high residual amount of d18:2 containing GlcCer molecular species and a strong reduction of GlcCers with d18:1 and t18:1 long chain bases. Nodulation and mycorrhiza formation in the *SGT* RNAi plants and nodulation in the *GCS* RNAi plants were not affected by the reduced glycolipid content. The *GCS* RNAi lines exhibited a slightly reduced degree of mycorrhiza formation. Considering the strong accumulation of SG and GlcCer, the induction of *SGT1*, *SGT2* and *GCS* expression during nodulation, and the fact that these two glycolipids localize to the plasma membrane, it is likely that SG and GlcCer play a role during plant-microbe interactions. This function, however, might be subtle, and other glycolipids such as DGDG might compensate for the loss of SG and GlcCer in the RNAi lines. Further experiments, employing plant lines totally deficient in SG or GlcCer, might be required to unravel the contribution of these glycolipids to the establishment of plant-*Rhizobium* and plant-*Glomus* interactions.

6 References

Abel S (2011) Phosphate sensing in root development. Current Opinion in Plant Biology **14:** 303-309

Akiyama K, Matsuzaki K-i, Hayashi H (2005) Plant sesquiterpenes induce hyphal branching in arbuscular mycorrhizal fungi. Nature **435:** 824-827

Andersson MX, Larsson KE, Tjellström H, Liljenberg C, Sandelius AS (2005) Phosphate-limited oat. The plasma membrane and the tonoplast as major targets for phospholipid-to-glycolipid replacement and stimulation of phospholipases in the plasma membrane. Journal of Biological Chemistry **280:** 27578-27586

Andersson MX, Stridh MH, Larsson KE, Liljenberg C, Sandelius AS (2003) Phosphate-deficient oat replaces a major portion of the plasma membrane phospholipids with the galactolipid digalactosyldiacylglycerol. FEBS Letters **537:** 128-132

Appleby CA (1984) Leghemoglobin and *Rhizobium* respiration. Annual Review of Plant Physioly. **35:** 443-478

Auriac M-C, Timmers ACJ (2007) Nodulation studies in the model legume *Medicago truncatula*: advantages of using the constitutive EF1α promoter and limitations in detecting fluorescent reporter proteins in nodule tissues. Molecular Plant-Microbe Interactions **20:** 1040-1047

Awai K, Maréchal E, Block MA, Brun D, Masuda T, Shimada H, Takamiya K, Ohta H, Joyard J (2001) Two types of *MGDG* synthase genes, found widely in both 16:3 and 18:3 plants, differentially mediate galactolipid syntheses in photosynthetic and nonphotosynthetic tissues in *Arabidopsis thaliana*. Proceedings of the National Academy of Sciences of the United States of America **98:** 10960-10965

Bago B, Pfeffer PE, Abubaker J, Jun J, Allen JW, Brouillette J, Douds DD, Lammers PJ, Shachar-Hill Y (2003) Carbon export from arbuscular mycorrhizal roots involves the translocation of carbohydrate as well as lipid. Plant Physiology **131:** 1496-1507

Bago B, Zipfel W, Williams RM, Jun J, Arreola R, Lammers PJ, Pfeffer PE, Shachar-Hill Y (2002) Translocation and utilization of fungal storage lipid in the arbuscular mycorrhizal symbiosis. Plant Physiology **128:** 108-124

Banas A, Carlsson AS, Huang B, Lenman M, Banas W, Lee M, Noiriel A, Benveniste P, Schaller H, Bouvier-Navé P, Stymne S (2005) Cellular sterol ester synthesis in plants is performed by an enzyme (phospholipid:sterol acyltransferase) different from the yeast and mammalian acyl-CoA:sterol acyltransferases. Journal of Biological Chemistry **280:** 34626-34634

Benning C, Ohta H (2005) Three enzyme systems for galactoglycerolipid biosynthesis are coordinately regulated in plants. Journal of Biological Chemistry **280:** 2397-2400

Benveniste P (2004) Biosynthesis and accumulation of sterols. Annual Review of Plant Biology **55:** 429-457

Bhat R, Panstruga R (2005) Lipid rafts in plants. Planta **223:** 5-19

Bligh EG, Dyer WJ (1959) A rapid method of total lipid extraction and purification. Canadian Journal of Biochemistry and Physiology. **37**: 911-917

Bonfante P, Requena N (2011) Dating in the dark: how roots respond to fungal signals to establish arbuscular mycorrhizal symbiosis. Current Opinion in Plant Biology **14:** 451-457

Borner GH, Sherrier DJ, Weimar T, Michaelson LV, Hawkins ND, Macaskill A, Napier JA, Beale MH, Lilley KS, Dupree P (2005) Analysis of detergent-resistant membranes in *Arabidopsis*. Evidence for plasma membrane lipid rafts. Plant Physiology **137:** 104-116

Botté C, Jeanneau C, Snajdrova L, Bastien O, Imberty A, Breton C, Maréchal E (2005) Molecular modeling and site-directed mutagenesis of plant chloroplast monogalactosyldiacylglycerol synthase reveal critical residues for activity. Journal of Biological Chemistry **280:** 34691-34701

Boutté Y, Grebe M (2009) Cellular processes relying on sterol function in plants. Current Opinion in Plant Biology **12:** 705-713

Bouvier-Navé P, Berna A, Noiriel A, Compagnon V, Carlsson AS, Banas A, Stymne S, Schaller H (2010) Involvement of the *phospholipid sterol acyltransferase1* in plant sterol homeostasis and leaf senescence. Plant Physiology **152:** 107-119

Brands M (2012) Lipid biosynthesis during plant-microbe symbiosis in *Lotus japonicus.* Bachelor thesis, Hogeschool Van Hall Larenstein - Institute of Molecular Physiology and Biotechnology of Plants, University of Bonn

Brewin N (2004) Plant cell wall remodelling in the *Rhizobium*-legume symbiosis. Critical Reviews in Plant Sciences **23:** 293-316

Bromley PE, Li YO, Murphy SM, Sumner CM, Lynch DV (2003) Complex sphingolipid synthesis in plants: characterization of inositolphosphorylceramide synthase activity in bean microsomes. Archives of Biochemistry and Biophysics **417:** 219-226

Browse J, McCourt PJ, Somerville CR (1986) Fatty acid composition of leaf lipids determined after combined digestion and fatty acid methyl ester formation from fresh tissue. Analytical Biochemistry **152:** 141-145

Brügger B, Erben G, Sandhoff R, Wieland FT, Lehmann WD (1997) Quantitative analysis of biological membrane lipids at the low picomole level by nano-electrospray ionization tandem mass spectrometry. Proceedings of the National Academy of Sciences of the United States of America **94:** 2339–2344

Buseman CM, Tamura P, Sparks AA, Baughman EJ, Maatta S, Zhao J, Roth MR, Esch SW, Shah J, Williams TD, Welti R (2006) Wounding stimulates the accumulation of glycerolipids containing oxophytodienoic acid and dinor-oxophytodienoic acid in *Arabidopsis* leaves. Plant Physiology **142:** 28-39

Cahoon EB, Lynch DV (1991) Analysis of glucocerebrosides of rye (*Secale cereale* L. *cv* Puma) leaf and plasma membrane. Plant Physiology **95:** 58-68

Chen M, Han G, Dietrich CR, Dunn TM, Cahoon EB (2006) The essential nature of sphingolipids in plants as revealed by the functional identification and characterization of the *Arabidopsis* LCB1 subunit of serine palmitoyltransferase. The Plant Cell **18:** 3576-3593

Chen M, Markham JE, Cahoon EB (2011) Sphingolipid Δ8 unsaturation is important for glucosylceramide biosynthesis and low-temperature performance in *Arabidopsis*. The Plant Journal **69:** 769-781

Chen M, Markham JE, Dietrich CR, Jaworski JG, Cahoon EB (2008) Sphingolipid long-chain base hydroxylation is important for growth and regulation of sphingolipid content and composition in *Arabidopsis*. The Plant Cell **20:** 1862-1878

Chen Q, Steinhauer L, Hammerlindl J, Keller W, Zou J (2007) Biosynthesis of phytosterol esters: Identification of a sterol O-acyltransferase in *Arabidopsis*. Plant Physiology **145:** 974-984

Choma A, Komaniecka I (2002) Analysis of phospholipids and ornithine-containing lipids from *Mesorhizobium* spp. Systematic and Applied Microbiology **25:** 326-331

Clouse SD (2002) *Arabidopsis* mutants reveal multiple roles for sterols in plant development. The Plant Cell **14:** 1995-2000

Conzelmann A, Puoti A, Lester R, Desponds C (1992) Two different types of lipid moieties are present in glycophosphoinositol-anchored membrane proteins of *Saccharomyces cerevisiae*. The EMBO Journal **11:** 457-466

DeBolt S, Scheible WR, Schrick K, Auer M, Beisson F, Bischoff V, Bouvier-Navé P, Carroll A, Hematy K, Li Y, Milne J, Nair M, Schaller H, Zemla M, Somerville C (2009) Mutations in UDP-glucose:sterol glucosyltransferase in *Arabidopsis* cause transparent testa phenotype and suberization defect in seeds. Plant Physiology **151:** 78-87

Delhaize E, Randall PJ (1995) Characterization of a phophate-accumulator mutant of *Arabidopsis thaliana*. **107**: 207-213

Demel R, De Kruyff B (1976) The function of sterols in membranes. Biochimica et Biophysica Acta (BBA) - Reviews of Biomembranes 2

Denarie J, Cullimore J (1993) Lipo-oligosaccharide nodulation factors: a minireview new class of signaling molecules mediating recognition and morphogenesis. Cell **74**: 951-954

Devers E, Wewer V, Dombrink I, Dörmann P, Hölzl G (2011) A processive glycosyltransferaseinvolved in glycolipid synthesis during phosphate deprivation in *Mesorhizobium loti*. Journal of Bacteriology **193:** 1377-1384

Diener AC, Li H, Zhou W-x, Whoriskey WJ, Nes WD, Fink GR (2000) Sterol methyltransferase 1 controls the level of cholesterol in plants. The Plant Cell **12:** 853-870

Dörmann P, Benning C (2002) Galactolipids rule in seed plants. Trends in Plant Science **7:** 112-118

Downie JA, Walker SA (1999) Plant responses to nodulation factors. Current Opinion in Plant Biology **2:** 483-489

Drissner D, Kunze G, Callewaert N, Gehrig P, Tamasloukht MB, Boller T, Felix G, Amrhein N, Bucher M (2007) Lyso-phosphatidylcholine is a signal in the arbuscular mycorrhizal symbiosis. Science **318:** 265-268

Duperon R, Thiersault M, Duperon P (1984) High level of glycosylated sterols in species of *Solanum* and sterol changes during the development of the tomato. Phytochemistry **23:** 743-746

Dyas L, Goad L (1993) Steryl fatty acyl esters in plants. Phytochemistry **34:** 17-29

Ejsing CS, Duchoslav E, Sampaio JL, Simons K, Bonner R, Thiele C, Ekroos K, Klemm RW, Shevchenko A (2006) Automated identification and quantification of glycerophospholipid molecular species by multiple precursor ion scanning. Analytical Chemistry **78**: 6202-6214

Ejsing CS, Sampaio JL, Surendranath V, Duchoslav E, Ekroos K, Klemm RW, Simons K, Shevchenko A (2009) Global analysis of the yeast lipidome by quantitative shotgun mass spectrometry. Proceedings of the National Academy of Sciences of the United States of America **106:** 2136-2141

Essigmann B, Güler S, Narang RA, Linke D, Benning C (1998) Phosphate availability affects the thylakoid lipid composition and the expression of *SQD1*, a gene required for sulfolipid biosynthesis in *Arabidopsis thaliana*. Proceedings of the National Academy of Sciences of the United States of America **95:** 1950-1955

Fahy E, Subramaniam S, Brown HA, Glass CK, Merrill AH, Murphy RC, Raetz CRH, Russell DW, Seyama Y, Shaw W, Shimizu T, Spener F, van Meer G, VanNieuwenhze MS, White SH, Witztum JL, Dennis EA (2005) A comprehensive classification system for lipids. Journal of Lipid Research **46:** 839-862

Felsenstein J (1985). Confidence limits on phylogenies: An approach using the bootstrap. Evolution **39**:783-791.

Finlay RD (2008) Ecological aspects of mycorrhizal symbiosis: with special emphasis on the functional diversity of interactions involving the extraradical mycelium. Journal of Experimental Botany **59:** 1115-1126

Fontaine J, Grandmougin-Ferjani A, Hartmann MA, Sancholle M (2001) Sterol biosynthesis by the arbuscular mycorrhizal fungus *Glomus intraradices*. Lipids **36:** 1357-1363

Frey B, Buser HR, Schüepp H (1992) Identification of ergosterol in vesicular-arbuscular mycorrhizae. Biology and Fertility of Soils **13:** 229-234

Fujioka S, Takatsuto S, Yoshida S (2002) An early C-22 oxidation branch in the brassinosteroid biosynthetic pathway. Plant Physiology **130:** 930-939

Fujioka S, Yokota T (2003) Biosynthesis and metabolism of brassinosteroids. Annual Review of Plant Biology **54:** 137-164

Gachotte D, Meens R, Benveniste P (1995) An *Arabidopsis* mutant deficient in sterol biosynthesis: heterologous complementation by *ERG3* encoding a Δ7-sterol-C-5-desaturase from yeast. The Plant Journal **8:** 407-416

Gaude N (2005) Die Regulation der Galaktolipidbiosynthese unter verschiedenen Umweltbedingungen in *Arabidopsis thaliana*, *Glycine max* und *Lotus japonicus*. PhD thesis, University of Potsdam

Gaude N, Bortfeld S, Duensing N, Lohse M, Krajinski F (2012) Arbuscule-containing and non-colonized cortical cells of mycorrhizal roots undergo extensive and specific

reprogramming during arbuscular mycorrhizal development. The Plant Journal **69:** 510-528

Gaude N, Tippmann H, Flemetakis E, Katinakis P, Udvardi M, Dörmann P (2004) The galactolipid digalactosyldiacylglycerol accumulates in the peribacteroid membrane of nitrogen-fixing nodules of soybean and *Lotus*. Journal of Biological Chemistry **279:** 34624-34630

Gaulin E, Bottin A, Dumas B (2010) Sterol biosynthesis in oomycete pathogens. Plant Signaling & Behavior **5:** 258-260

Gellerman JL, Anderson WH, Schlenk H (1975) Synthesis and analysis of phytyl and phytenoyl wax esters. Lipids **10**: 656-661

Genre A, Chabaud M, Timmers T, Bonfante P, Barker DG (2005) Arbuscular mycorrhizal fungi elicit a novel intracellular apparatus in *Medicago truncatula* root epidermal cells before infection. The Plant Cell **17:** 3489-3499

Gondet L, Bronner R, Benveniste P (1994) Regulation of sterol content in membranes by subcellular compartmentation of steryl-esters accumulating in a sterol-overproducing tobacco mutant. Plant Physiology **105:** 509-518

Gonzalez-Guerrero M, Azcon-Aguilar C, Mooney M, Valderas A, MacDiarmid CW, Eide DJ, Ferrol N (2005) Characterization of a *Glomus intraradices* gene encoding a putative Zn transporter of the cation diffusion facilitator family. Fungal Genetics and Biology **42:** 130-140

Govindarajulu M, Elmore JM, Fester T, Taylor CG (2008) Evaluation of constitutive viral promoters in transgenic soybean roots and nodules. Molecular Plant-Microbe Interactions **21:** 1027-1035

Govindarajulu M, Pfeffer PE, Jin H, Abubaker J, Douds DD, Allen JW, Bucking H, Lammers PJ, Shachar-Hill Y (2005) Nitrogen transfer in the arbuscular mycorrhizal symbiosis. Nature **435:** 819-823

Grebe M, Xu J, Möbius W, Ueda T, Nakano A, Geuze HJ, Rook MB, Scheres B (2003) *Arabidopsis* sterol endocytosis involves actin-mediated trafficking via ARA6-positive early endosomes. Current Biology **13:** 1378-1387

Griebel T, Zeier J (2010) A role for β-sitosterol to stigmasterol conversion in plant-pathogen interactions. The Plant Journal **63:** 254-268

Grunwald D (1971) Effects of free sterols, steryl ester, and steryl glycoside on membrane permeability. Plant Physiology **48:** 653-655

Guan XL, Souza CM, Pichler H, Dewhurst Gl, Schaad O, Kajiwara K, Wakabayashi H, Ivanova T, Castillon GA, Piccolis M, Abe F, Loewith R, Funato K, Wenk MR, Riezman H (2009) Functional interactions between sphingolipids and sterols in biological membranes regulating cell physiology. Molecular Biology of the Cell **20:** 2083-2095

Hamilton JA, Small DM (1982) Solubilization and localization of cholesteryl oleate in egg phosphatidylcholine vesicles. A carbon 13 NMR study. Journal of Biological Chemistry **257:** 7318-7321

Han X, Gross R (2001) Quantitative analysis and molecular species fingerprinting of triacylglyceride molecular species directly from lipid extracts of biological samples by electrospray ionization tandem mass spectrometry. Analytical Biochemistry **295:** 88-100

Handberg K, Stougaard J (1992) *Lotus japonicus*, an autogamous, diploid legume species for classical and molecular genetics. The Plant Journal **2:** 487-496

Hannun YA, Obeid LM (2008) Principles of bioactive lipid signalling: lessons from sphingolipids. Nature Reviews Molecular Cell Biology **9:** 139-150

Hansen J, Jørgensen J-E, Stougaard J, Marcker KA (1989) Hairy roots - a short cut to transgenic root nodules. Plant Cell Reports **8:** 12-15

Harrison MJ, van Buuren ML (1995) A phosphate transporter from the mycorrhizal fungus *Glomus versiforme*. Nature **378:** 626-629

Hart MM, Reader RJ (2002) Taxonomic basis for variation in the colonization strategy of arbuscular mycorrhizal fungi. New Phytologist **153:** 335-344

Härtel H, Benning C (2000) Can digalactosyldiacylglycerol substitute for phosphatidylcholine upon phosphate deprivation in leaves and roots of *Arabidopsis*? Biochemical Society Transactions **28:** 729-732

Härtel H, Dörmann P, Benning C (2000) DGD1-independent biosynthesis of extraplastidic galactolipids after phosphate deprivation in *Arabidopsis*. Proceedings of the National Academy of Sciences of the United States of America **97:** 10649-10654

Härtel H, Dörmann P, Benning C (2001) Galactolipids not associated with the photosynthetic apparatus in phosphate-deprived plants. Journal of Photochemistry and Photobiology B **61:** 46-51

Hartmann M-A, Benveniste P (1987) Plant membrane sterols: isolation, identification, and biosynthesis. *In* Methods in Enzymology, Vol **148**. Academic Press, pp 632-650

Hernández LE, Cooke DT (1996) Lipid composition of symbiosomes from pea root nodules. Phytochemistry **42:** 341-346

Hillig I, Leipelt M, Ott C, Zähringer U, Warnecke D, Heinz E (2003) Formation of glucosylceramide and sterol glucoside by a UDP-glucose-dependent glucosylceramide synthase from cotton expressed in *Pichia pastoris*. FEBS Letters **553:** 365-369

Honda A, Yamashita K, Miyazaki H, Shirai M, Ikegami T, Xu G, Numazawa M, Hara T, Matsuzaki Y (2008) Highly sensitive analysis of sterol profiles in human serum by LC-ESI-MS/MS. Journal of Lipid Research **49:** 2063-2073

Hsieh TC, Lester RL, Laine RA (1981) Glycophosphoceramides from plants. Purification and characterization of a novel tetrasaccharide derived from tobacco leaf glycolipids. Journal of Biological Chemistry **256:** 7747-7755

Ichihara Ki, Shibahara A, Yamamoto K, Nakayama T (1996) An improved method for rapid analysis of the fatty acids of glycerolipids. Lipids **31:** 535-539

Iga DP, Iga S, Schmidt RR, Buzasc M-C (2005) Chemical synthesis of cholesteryl β-D-galactofuranoside and -pyranoside. Carbohydrate Research **340:** 2052–2054

Imai H, Ohnishi M, Kinoshita M, Kojima M, Ito S (1995) Structure and distribution of cerebroside containing unsaturated hydroxy fatty acids in plant leaves. Bioscience, Biotechnology and Biochemistry **59:** 1309-1313

Imgrund S, Hartmann D, Farwanah H, Eckhardt M, Sandhoff R, Degen J, Gieselmann V, Sandhoff K, Willecke K (2009) Adult ceramide synthase 2 (CERS2)-deficient mice exhibit myelin sheath defects, cerebellar degeneration, and hepatocarcinomas. Journal of Biological Chemistry **284**: 33549-33560

Jabaji-Hare S, Deschene A, Kendrick B (1984) Lipid content and composition of vesicles of a vesicular-arbuscular mycorrhizal fungus. Mycologia **76:** 1024-1030

Jang J-C, Fujioka S, Tasaka M, Seto H, Takatsuto S, Ishii A, Aida M, Yoshida S, Sheen J (2000) A critical role of sterols in embryonic patterning and meristem programming revealed by the *fackel* mutants of *Arabidopsis thaliana*. Genes & Development **14:** 1485-1497

Javot H, Pumplin N, Harrison MJ (2007) Phosphate in the arbuscular mycorrhizal symbiosis: transport properties and regulatory roles. Plant, Cell & Environment **30:** 310-322

Johansen A, Finlay RD, Olsson PA (1996) Nitrogen metabolism of external hyphae of the arbuscular mycorrhizal fungus *Glomus intraradices*. New Phytologist **133:** 705-712

Jones KM, Kobayashi H, Davies BW, Taga ME, Walker GC (2007) How rhizobial symbionts invade plants: the *Sinorhizobium-Medicago* model. Nat ure Reviews Microbiology **5:** 619-633

Joyard J, Block MA, Malhèrbe A, Maréchal E, Douce R (1994) Origin and synthesis of galactolipid and sulfolipid head groups. *In* TSJ Moore, ed, Lipid Metabolism in Plants. CRC Press, Boca Raton, pp 231-258

Kaul K, Lester RL (1975) Characterization of inositol-containing phosphosphingolipids from tobacco leaves. Plant Physiology **55:** 120-129

Kaul K, Lester RL (1978) Isolation of six novel phosphoinositol-containing sphingolipids from tobacco leaves. Biochemistry **17:** 3569-3575

Kelly AA, Dörmann P (2002) *DGD2*, an *Arabidopsis* gene encoding a UDP-galactose-dependent digalactosyldiacylglycerol synthase is expressed during growth under phosphate-limiting conditions. Journal of Biological Chemistry **277:** 1166-1173

Kelly AA, Froehlich JE, Dörmann P (2003) Disruption of the two digalactosyldiacylglycerol synthase genes *DGD1* and *DGD2* in *Arabidopsis* reveals the existence of an additional enzyme of galactolipid synthesis. The Plant Cell **15:** 2694-2706

Kemp RJ, Mercer EI (1968) The sterol esters of maize seedlings. Biochemical Journal **110:** 111-118

Laloi M, Perret A-M, Chatre L, Melser S, Cantrel C, Vaultier M-Nl, Zachowski A, Bathany K, Schmitter J-M, Vallet M, Lessire R, Hartmann M-Ae, Moreau P (2007) Insights into the role of specific lipids in the formation and delivery of lipid microdomains to the plasma membrane of plant cells. Plant Physiology **143:** 461-472

Leipelt M, Warnecke D, Zähringer U, Ott C, Müller F, Hube B, Heinz E (2001) Glucosylceramide synthases, a gene family responsible for the biosynthesis of

glucosphingolipids in animals, plants and fungi. Journal of Biological Chemistry **276:** 33621-33629

Lewis TA, Rodriguez RJ, Parks LW (1987) Relationship between intracellular sterol content and sterol esterification and hydrolysis in *Saccharomyces cerevisiae*. Biochimica et Biophysica Acta (BBA) - Lipids and Lipid Metabolism **921:** 205-212

Li YL, Su X, Stahl PD, Gross ML (2007) Quantification of diacylglycerol molecular species in biological samples by electrospray ionization mass spectrometry after one-step derivatization. Analytical Chemistry **79:** 1569-1574

Liang H, Yao N, Song JT, Luo S, Lu H, Greenberg JT (2003) Ceramides modulate programmed cell death in plants. Genes & Development **17:** 2636-2641

Liebisch G, Binder M, Schifferer R, Langmann T, Schulz B, Schmitz G (2006) High throughput quantification of cholesterol and cholesteryl ester by electrospray ionization tandem mass spectrometry (ESI-MS/MS). Biochimica et Biophysica Acta **1761:** 121-128

Lindsey K, Pullen ML, Topping JF (2003) Importance of plant sterols in pattern formation and hormone signalling. Trends in Plant Science **8:** 521-525

Lippold F, vom Dorp K, Abraham M, Hölzl G, Wewer V, Lindberg Yilmaz J, Lager I, Montandon C, Besagni C, Kessler F, Stymne S, Dörmann P (2012) Fatty acid phytyl ester synthesis in chloroplasts of *Arabidopsis*. The Plant Cell **24:** 2001-2014

Lopez-Pedrosa A, Gonzalez-Guerrero M, Valderas A, Azcon-Aguilar C, Ferrol N (2006) *GintAMT1* encodes a functional high-affinity ammonium transporter that is expressed in the extraradical mycelium of *Glomus intraradices*. Fungal Genetics and Biology **43:** 102-110

Lynch DV (2000) Enzymes of sphingolipid metabolism in plants. *In* Methods in Enzymology, Vol **311**. Academic Press, pp 130-149

Lynch DV, Dunn TM (2004) An introduction to plant sphingolipids and a review of recent advances in understanding their metabolism and function. New Phytologist **161:** 677-702

Lynch DV, Fairfield SR (1993) Sphingolipid long-chain base synthesis in plants (characterization of serine palmitoyltransferase activity in squash fruit microsomes). Plant Physiology **103:** 1421-1429

Maillet F, Poinsot V, Andre O, Puech-Pages V, Haouy A, Gueunier M, Cromer L, Giraudet D, Formey D, Niebel A, Martinez EA, Driguez H, Becard G, Denarie J (2011) Fungal lipochitooligosaccharide symbiotic signals in arbuscular mycorrhiza. Nature **469:** 58-63

Markham JE, Jaworski JG (2007) Rapid measurement of sphingolipids from *Arabidopsis thaliana* by reversed-phase high-performance liquid chromatography coupled to electrospray ionization tandem mass spectrometry. Rapid Communications in Mass Spectrometry **21:** 1304-1314

Markham JE, Li J, Cahoon EB, Jaworski JG (2006) Separation and identification of major plant sphingolipid classes from leaves. Journal of Biological Chemistry **281:** 22684-22694

McGonigle TP, Miller MH, Evans DG, Fairchild GL, Swan JA (1990) A new method which gives an objective measure of colonization of roots by vesicular-arbuscular mycorrhizal fungi. New Phytologist **115:** 495-501

Meijer HJ, Munnik T (2003) Phospholipid-based signaling in plants. Annual Review of Plant Biology **54:** 265-306

Men S, Boutte Y, Ikeda Y, Li X, Palme K, Stierhof Y-D, Hartmann M-A, Moritz T, Grebe M (2008) Sterol-dependent endocytosis mediates post-cytokinetic acquisition of PIN2 auxin efflux carrier polarity. Nature Cell Biology **10:** 237-244

Merrill AH, Wang E, Mullins RE, Jamison WCL, Nimkar S, Liotta DC (1988) Quantitation of free sphingosine in liver by high-performance liquid chromatography. Analytical Biochemistry **171:** 373-381

Mikes V, Milat M-L, Ponchet M, Panabières F, Ricci P, Blein J-P (1998) Elicitins, proteinaceous elicitors of plant defense, are a new class of sterol carrier proteins. Biochemical and Biophysical Research Communications **245:** 133-139

Moellering ER, Benning C (2011) RNA interference silencing of a major lipid droplet protein affects lipid droplet size in *Chlamydomonas reinhardtii*. Eukaryotic Cell **9:** 97-106

Mongrand S, Morel J, Laroche J, Claverol S, Carde JP, Hartmann M, Bonneu M, Simon-Plas F, Lessire R, Bessoule JJ (2004) Lipid rafts in higher plant cells. Journal of Biological Chemistry **279:** 36277-36286

Moreau P, Hartmann M-Ae, Perret A-M, Sturbois-Balcerzak Bnd, Cassagne C (1998) Transport of sterols to the plasma membrane of leek seedlings. Plant Physiology **117:** 931-937

Morikawa T, Mizutani M, Aoki N, Watanabe B, Saga H, Saito S, Oikawa A, Suzuki H, Sakurai N, Shibata D, Wadano A, Sakata K, Ohta D (2006) Cytochrome P450 *CYP710A* encodes the sterol C-22 desaturase in *Arabidopsis* and tomato. The Plant Cell **18:** 1008-1022

Morrison WR, Hay JD (1970) Polar lipids in bovine milk II. Long-chain bases, normal and 2-hydroxy fatty acids, and isomeric *cis* and *trans* monoenoic fatty acids in the sphingolipids. Biochimica et Biophysica Acta (BBA) - Lipids and Lipid Metabolism **202:** 460-467

Nei M, Kumar S (2000) Molecular Evolution and Phylogenetics. Oxford University Press, New York

Nieto B, Fores O, Arro M, Ferrer A (2009) *Arabidopsis* 3-hydroxy-3-methylglutaryl-CoA reductase is regulated at the post-translational level in response to alterations of the sphingolipid and the sterol biosynthetic pathways. Phytochemistry **70:** 53-59

Nomura T, Kitasaka Y, Takatsuto S, Reid JB, Fukami M, Yokota T (1999) Brassinosteroid/sterol synthesis and plant growth as affected by *lka* and *lkb* mutations of pea. Plant Physiology **119:** 1517-1526

Ohyama K, Suzuki M, Kikuchi J, Saito K, Muranaka T (2009) Dual biosynthetic pathways to phytosterol via cycloartenol and lanosterol in *Arabidopsis*. Proceedings of the National Academy of Sciences of the United States of America **106:** 725-730

Oldroyd GED, Downie JA (2006) Nuclear calcium changes at the core of symbiosis signalling. Current Opinion in Plant Biology **9:** 351-357

Olsson PA, Bååth E, Jakobsen I, Söderström B (1995) The use of phospholipid and neutral lipid fatty acids to estimate biomass of arbuscular mycorrhizal fungi in soil. Mycological Research **99:** 623-629

Olsson PA, Larsson L, Bago B, Wallander H, Van Aarle IM (2003) Ergosterol and fatty acids for biomass estimation of mycorrhizal fungi. New Phytologist **159:** 7-10

Olsson PlA, Johansen A (2000) Lipid and fatty acid composition of hyphae and spores of arbuscular mycorrhizal fungi at different growth stages. Mycological Research **104:** 429-434

Olsson PlA, van Aarle IM, Allaway WG, Ashford AE, Rouhier H (2002) Phosphorus effects on metabolic processes in monoxenic arbuscular mycorrhiza cultures. Plant Physiology **130:** 1162-1171

Ott T, van Dongen J, Günther C, Krusell L, Desbrosses G, Vigeolas H, Bock V, Czechowski T, Geigenberger P, Udvardi M (2005) Symbiotic leghemoglobins are crucial for nitrogen fixation in legume root nodules but not for general plant growth and development. Current Biology **15:** 531-535

Pacoysky RS, Fuller G (1988) Mineral and lipid composition of *Glycine* - *Glomus* - *Bradyrhizobium* symbioses. Physiologia Plantarum **72:** 733-746

Páli T, Garab G, Horváth LI, Kóta Z (2003) Functional significance of the lipid-protein interface in photosynthetic membranes. Cellular and Molecular Life Sciences **60:** 1591-1606

Palta JP, Whitaker BD, Weiss LS (1993) Plasma membrane lipids associated with genetic variability in freezing tolerance and cold acclimation of *Solanum* species. Plant Physiology **103:** 793-803

Parniske M (2008) Arbuscular mycorrhiza: the mother of plant root endosymbioses. Nature Reviews Microbiology **6:** 763-775

Pata MO, Hannun YA, Ng CK (2010) Plant sphingolipids: decoding the enigma of the sphinx. New Phytologist **185:** 611-630

Paul W (1953) A new mass spectrometer without magnetic field. Zeitschrift für Naturforschung **8A:** 448-450

Peng L, Kawagoe Y, Hogan P, Delmer D (2002) Sitosterol-β-glucoside as primer for cellulose synthesis in plants. Science **295:** 59-60

Perotto S, Donovan N, Drobak B, Brewin N (1995) Differential expression of a glycosyl inositol phospholipid antigen on the peribacteroid membrane during pea nodule development. Molecular Plant-Microbe Interactions **8:** 560-568

Perry JA, Wang TL, Welham TJ, Gardner S, Pike JM, Yoshida S, Parniske M (2003) A TILLING reverse genetics tool and a web-accessible collection of mutants of the legume *Lotus japonicus*. Plant Physiology **131:** 866-871

Pfeffer PE, Douds DD, Becard G, Shachar-Hill Y (1999) Carbon uptake and the metabolism and transport of lipids in an arbuscular mycorrhiza. Plant Physiology **120:** 587-598

Pike LJ (2006) Rafts defined: a report on the Keystone symposium on lipid rafts and cell function. Journal of Lipid Research **47:** 1597-1598

Poirier Y, Thoma S, Somerville C, Schiefelbein J (1991) Mutant of *Arabidopsis* deficient in xylem loading of phosphate. Plant Physiology **97:** 1087-1093

Popp C, Ott T (2011) Regulation of signal transduction and bacterial infection during root nodule symbiosis. Current Opinion in Plant Biology **14:** 458-467

Ramamoorthy V, Cahoon EB, Li J, Thokala M, Minto RE, Shah DM (2007) Glucosylceramide synthase is essential for alfalfa defensin-mediated growth inhibition but not for pathogenicity of *Fusarium graminearum*. Molecular Microbiology **66:** 771-786

Reinsberg D, Booth PJ, Jegerschold C, Khoo BJ, Paulsen H (2000) Folding, assembly, and stability of the major light-harvesting complex of higher plants, LHCII, in the presence of native lipids. Biochemistry **39:** 14305-14313

Rittenour WR, Chen M, Cahoon EB, Harris SD (2011) Control of glucosylceramide production and morphogenesis by the Bar1 ceramide synthase in *Fusarium graminearum*. PLoS ONE **6:** e19385

Saitou N, Nei M (1987) The neighbor-joining method: A new method for reconstructing phylogenetic trees. Molecular Biology and Evolution **4**:406-425

Samac D, Tesfaye M, Dornbusch M, Saruul P, Temple S (2004) A comparison of constitutive promoters for expression of transgenes in alfalfa (*Medicago Sativa*). Transgenic Research **13:** 349-361

Schaarschmidt S, Roitsch T, Hause B (2006) Arbuscular mycorrhiza induces gene expression of the apoplastic invertase LIN6 in tomato (*Lycopersicon esculentum*) roots. Journal of Experimental Botany **57:** 4015-4023

Schaeffer A, Bronner R, Benveniste P, Schaller H (2001) The ratio of campesterol to sitosterol that modulates growth in *Arabidopsis* is controlled by STEROL METHYLTRANSFERASE 2;1. The Plant Journal **25:** 605-615

Schaller H (2004) New aspects of sterol biosynthesis in growth and development of higher plants. Plant-Physiology and Biochemistry **42:** 465-476

Schaller H, Grausem B, Benveniste P, Chye M-L, Tan C-T, Song Y-H, Chua N-H(1995)Expression of the *Hevea brasiliensis* (H.B.K.) Müll. Arg. 3-hydroxy-3-methylglutaryl-coenzyme A reductase 1 -in tobacco results in sterol overproduction. Plant Physiology **109**: 761-770

Schrick K, Fujioka S, Takatsuto S, Stierhof Y-D, Stransky H, Yoshida S, Jürgens G (2004) A link between sterol biosynthesis, the cell wall, and cellulose in *Arabidopsis*. The Plant Journal **38:** 227-243

Schrick K, Mayer U, Horrichs A, Kuhnt C, Bellini C, Dangl J, Schmidt J, Jürgens G (2000) FACKEL is a sterol C-14 reductase required for organized cell division and expansion in *Arabidopsis* embryogenesis. Genes & Development **14:** 1471-1484

Schrick K, Mayer U, Martin G, Bellini C, Kuhnt C, Schmidt J, Jürgens G (2002) Interactions between sterol biosynthesis genes in embryonic development of *Arabidopsis*. The Plant Journal **31:** 61-73

Schrick K, Shiva S, Arpin J, Delimont N, Isaac G, Tamura P, Welti R (2012) Steryl glucoside and acyl steryl glucoside analysis of *Arabidopsis* seeds by electrospray ionization tandem mass spectrometry. Lipids **47:** 185-193

Schuler I, Milon A, Nakatani Y, Ourisson G, Albrecht AM, Benveniste P, Hartman MA (1991) Differential effects of plant sterols on water permeability and on acyl chain ordering of soybean phosphatidylcholine bilayers. Proceedings of the National Academy of Sciences of the United States of America **88:** 6926-6930

Schüßler A, Schwarzott D, Walker C (2001) A new fungal phylum, the *Glomeromycota*: phylogeny and evolution. Mycological Research **105:** 1413-1421

Sohlenkamp C, López-Lara IM, Geiger O (2003) Biosynthesis of phosphatidylcholine in bacteria. Progress in Lipid Research **42:** 115-162

Solaiman M, Saito M (1997) Use of sugars by intraradical hyphae of arbuscular mycorrhizal fungi revealed by radiorespirometry. New Phytologist **136:** 533–538

Souter M, Topping J, Pullen M, Friml J, Palme K, Hackett R, Grierson D, Lindsey K (2002) *hydra* mutants of *Arabidopsis* are defective in sterol profiles and auxin and ethylene signaling. The Plant Cell **14:** 1017-1031

Spassieva SD, Markham JE, Hille J (2002) The plant disease resistance gene *Asc-1* prevents disruption of sphingolipid metabolism during AAL-toxin-induced programmed cell death. The Plant Journal **32:** 561-572

Sperling P, Franke S, Lüthje S, Heinz E (2005) Are glucocerebrosides the predominant sphingolipids in plant plasma membranes? Plant Physiology and Biochemistry **43:** 1031-1038

Sperling P, Heinz E (2003) Plant sphingolipids: structural diversity, biosynthesis, first genes and functions. Biochimica et Biophysica Acta **1632:** 1-15

Sperling P, Zähringer U, Heinz E (1998) A sphingolipid desaturase from higher plants. Journal of Biological Chemistry **273:** 28590-28596

Stiller J, Martirani L, Tuppale S, Chian R-J, Chiurazzi M, Gresshoff PM (1997) High frequency transformation and regeneration of transgenic plants in the model legume *Lotus japonicus*. Journal of Experimental Botany **48:** 1357-1365

Sturley SL (1997) Molecular aspects of intracellular sterol esterification: the acyl coenzyme A: cholesterol acyltransferase reaction. Current Opinion in Lipidology **8:** 167-173

Sullivan JT, Patrick HN, Lowther WL, Scott DB, Ronson CW (1995) Nodulating strains of *Rhizobium loti* arise through chromosomal symbiotic gene transfer in the environment. Proceedings of the National Academy of Sciences of the United States of America **92:** 8985-8989

Suzuki M, Muranaka T (2007) Molecular genetics of plant sterol backbone synthesis. Lipids **42:** 47-54

Svetek J, Yadav MP, Nothnagel EA (1999) Presence of a glycosylphosphatidylinositol lipid anchor on rose arabinogalactan proteins. Journal of Biological Chemistry **274:** 14724-14733

Svoboda J, Weirich G (1995) Sterol metabolism in the tobacco hornworm, *Manduca sexta* - A review. Lipids **30:** 263-267

Takahashi Y, Berberich T, Kanzaki H, Matsumura H, Saitoh H, Kusano T, Terauchi R (2008) Serine palmitoyltransferase, the first step enzyme in sphingolipid biosynthesis, is involved in nonhost resistance. Molecular Plant-Microbe Interactions **22:** 31-38

Tamura K, Peterson D, Peterson N, Stecher G, Nei M, Kumar S (2011) MEGA5: Molecular evolutionary genetics analysis using maximum likelihood, evolutionary distance, and maximum parsimony methods. Molecular Biology and Evolution **28**: 2731-2739

Ternes P, Franke S, Zähringer U, Sperling P, Heinz E (2002) Identification and characterization of a sphingolipid Δ4-desaturase family. Journal of Biological Chemistry **277:** 25512-25518

Tirichine L, Herrera-Cervera JA, Stougaard J (2005) Transformation-regeneration procedure for *Lotus japonicus*. *In* AJ Marquez, ed, *Lotus Japonicus* Handbook. Springer, Dordrecht, Netherlands, pp 279-284

Tjellström H, Hellgren LI, Wieslander A, Sandelius AS (2010) Lipid asymmetry in plant plasma membranes: phosphate deficiency-induced phospholipid replacement is restricted to the cytosolic leaflet. The FASEB Journal **24:** 1128-1138

Udvardi MK, Day DA (1997) Metabolic transport across symbiotic membranes of legume nodules. Annual Review of Plant Physiology and Plant Molecular Biology **48:** 493-523

Vassel B, Skelly WG (1963) N-Chlorobetainlyl chloride. Organic Syntheses **4**:154

Vesper H, Schmelz E-M, Nikolova-Karakashian MN, Dillehay DL, Lynch DV, Merrill AH (1999) Sphingolipids in food and the emerging importance of sphingolipids to nutrition. The Journal of Nutrition **129:** 1239-1250

Vierheilig H, Coughlan AP, Wyss U, Piché Y (1998) Ink and vinegar, a simple staining technique for arbuscular-mycorrhizal fungi. Applied and Environmental Microbiology **64**: 5004-5007

Vijayakumar V (2012) Phospholipids and lysophosphatidylcholine - diversity and metabolism in arbuscular mycorrhizal *Lotus japonicus* (Regel) K. Larsen. PhD thesis, University of Cologne

vom Dorp K (2010) Measurements of sphingolipids via HPLC and Q-TOF mass spectrometry. Master thesis, Institute of Molecular Physiology and Biotechnology of Plants, University of Bonn

Wang H, Li J, Bostock RM, Gilchrist DG (1996) Apoptosis: a functional paradigm for programmed plant cell death induced by a host-selective phytotoxin and invoked during development. The Plant Cell **8:** 375-391

Wang K, Senthil-Kumar M, Ryu C-M, Kang L, Mysore KS (2012) Phytosterols play a key role in plant innate immunity against bacterial pathogens by regulating nutrient efflux into the apoplast. Plant Physiology **158**: 1789-1802

Wang L, Wang T, Fehr WR (2006) HPLC quantification of sphingolipids in soybeans with modified palmitate content. Journal of Agricultural and Food Chemistry **54:** 7422-7428

Wang W, Yang X, Tangchaiburana S, Ndeh R, Markham JE, Tsegaye Y, Dunn TM, Wang G-L, Bellizzi M, Parsons JF, Morrissey D, Bravo JE, Lynch DV, Xiao S (2008) An inositolphosphorylceramide synthase is involved in regulation of plant programmed cell death associated with defense in *Arabidopsis*. The Plant Cell **20:** 3163-3179

Warnecke D, Heinz E (2003) Recently discovered functions of glucosylceramides in plants and fungi. Cellular and Molecular Life Sciences **60:** 919-941

Warnecke DC, Baltrusch M, Buck F, Wolter FP, Heinz E (1997) UDP-glucose:sterol glucosyltransferase: cloning and functional expression in *Escherichia coli*. Plant Molecular Biology **35:** 597-603

Welti R, Li W, Li M, Sang Y, Biesiada H, Zhou H-E, Rajashekar C, Williams T, Wang X (2002) Profiling membrane lipids in plant stress responses. Role of phospholipase Dα in freezing-induced lipid changes in *Arabidopsis*. Journal of Biological Chemistry **277:** 31994-32002

Wewer V, Dombrink I, vom Dorp K, Dörmann P (2011) Quantification of sterol lipids in plants by quadrupole time-of-flight mass spectrometry. Journal of Lipid Research **52:** 1039-1054

Whitehead L, Day D (1997) The peribacteroid membrane. Physiologica Plantarum **100:** 30-44

Wright BS, Snow JW, O'Brien TC, Lynch DV (2003) Synthesis of 4-hydroxysphinganine and characterization of sphinganine hydroxylase activity in corn. Archives of Biochemistry and Biophysics **415:** 184-192

Xu X, Bittman R, Duportail G, Heissler D, Vilcheze C, London E (2001) Effect of the structure of natural sterols and sphingolipids on the formation of ordered sphingolipid/sterol domains (rafts). Journal of Biological Chemistry **276:** 33540-33546

Yokota K, Fukai E, Madsen LH, Jurkiewicz A, Rueda P, Radutoiu S, Held M, Hossain MS, Szczyglowski K, Morieri G, Oldroyd GED, Downie JA, Nielsen MW, Rusek AM, Sato S, Tabata S, James EK, Oyaizu H, Sandal N, Stougaard J (2009) Rearrangement of actin cytoskeleton mediates invasion of *Lotus japonicus* roots by *Mesorhizobium loti*. The Plant Cell **21:** 267-284

Zappel NF, Panstruga R (2008) Heterogeneity and lateral compartmentalization of plant plasma membranes. Current Opinion in Plant Biology **11:** 632-640

Zinser E, Paltauf F, Daum G (1993) Sterol composition of yeast organelle membranes and subcellular distribution of enzymes involved in sterol metabolism. Journal of Bacteriology **175:** 2853-2858

7 Appendix

7.1 Cloning of RNAi Constructs for the Downregulation of *SGT1*, *SGT2* and GCS in *Lotus japonicus*

This procedure was performed by Helder Paiva at the Max-Planck Institute for Molecular Plant Physiology, Golm, in the group of Peter Dörmann in 2008.

SGT1 cDNA (MF087a11) was obtained from Kazusa (Legume Base, The National BioResourse Project, University of Miyazaki)

SGT2 full length cDNA (1754 bp) was obtained by RT-PCR using wild type *Lotus* RNA from nodulated roots as a template.

Primers:
(*Avr*II)atcctaggtATGGGTAGTGATGGGATTGATT
(*Xho*I)ctcgagTTAAACACCACCACAAGGGGC

GCS cDNA (MPDL058e06) was obtained from Kazusa (Legume Base, The National BioResourse Project, University of Miyazaki.

Overhanging primers employed for the cloning of RNAi constructs:

LjSGT1-sense:	(*Pst*I) ctgcagATGGCCATCGTGTTAGATTAG
	(*Mlu*I) acgcgtGATGAGGACTCCATATATACG
LjSGT1-antisense:	(*EcoR*I) gaattcATGGCCATCGTGTTAGATTAG
	(*BamH*I) ggatccGATGAGGACTCCATATATACG
LjSGT2-sense:	(*Pst*I) ctgcagGGTTTAATCCCTTCTGGTCCG
	(*Mlu*I) acgcgtGTGGGATCTTCAAGAGGCATG
LjSGT2-antisense:	(*EcoR*I) gaattcGGTTTAATCCCTTCTGGTCCG
	(*BamH*I) ggatccGTGGGATCTTCAAGAGGCATG
LjGCS-sense:	(*Mlu*I) acgcgtTCCTCAGGTAATTCCAGTATC
	(*Pst*I) ctgcagTGCTTACCATGCTATATCACG
LjGCS-antisense:	(*BamH*I) ggatccTCCTCAGGTAATTCCAGTATC
	(*EcoR*I) gaattcTGCTTACCATGCTATATCACG

Constructs were cloned into the pSC-B vector, using the Strataclone Blunt PCR Cloning Kit (Stratagene).

The constructs were cleaved with the following enzymes to confirm the successful cloning of sense and anti-sense RNAi fragments into the pSC-B vector:

Construct	Restriction endonucleases	Fragments obtained for orientation A	Fragments obtained for orientation B
pS*SGT1*-sense	*Mlu*I/*Xmn*I	3026 bp, 1016 bp	2463 bp, 1579 bp
pS*SGT1*-antisense	*BamH*I/*Xmn*I	3026 bp, 975 bp, 41 bp	2453 bp, 971 bp, 608 bp
pS*SGT2*-sense	*Pst*I/*Pvu*I	2692 bp, 754 bp, 637 bp	3298 bp, 756 bp, 29 bp
pS*SGT2*-sense	*Mlu*I/*Pvu*I	3296 bp, 787 bp	2694 bp, 1389 bp
pS*SGT2*-antisense	*BamH*I/*Pvu*I	3296 bp, 746 bp, 41 bp	2694 bp, 740bp, 649
pS*GCS*-sense	*Mlu*I/*Pvu*I	3255bp, 787 bp	2688 bp, 1354 bp
pS*GCS*-antisense	*BamH*I/*Xmn*I	3026 bp, 975 bp, 11 bp	2459 bp, 975 bp, 608 bp

Restriction of Sense and Anti-Sense Constructs for Cloning into the p35 Vector

pS*SGT1*-sense
Restriction with: *Pst*I/*Mlu*I
Fragments: 4.3 kb (empty pSC-B vector) and 573 bp (*SGT1*-sense)

pS*SGT1*-anti-sense
Restriction with: *Eco*RI/*BamH*I.
Fragments: 4.3 kb (empty pSC-B vector) and 573 bp (*GCS*-anti-sense)

pS*SGT2*-sense
Restriction with: *Pst*I/*Mlu*I.
Fragments: 4.3 kb (empty pSC-B vector) and 614 bp (*SGT2*-sense)

pS*SGT2*-anti-sense
Restriction with: *Eco*RI/*BamH*I.
Fragments: 4.3 kb (empty pSC-B vector) and 614 bp (*SGT2*-anti-sense)

pS*GCS*-sense
Restriction with: *Pst*I/*Mlu*I.
Fragments: 4.3 kb (empty pSC-B vector) and 578 bp (*GCS*-sense)

pS*GCS*-anti-sense
Restriction with: *Eco*RI/*BamH*I.
Fragments: 4.3 kb (empty pSC-B vector) and 578 bp (*GCS*-anti-sense)

The vector p35iF2D1Ex1, containing an RNAi contruct for the downregulation of *DGD1* from a previous study, was cleaved to obtain the empty vector p35 and also the intron *FAD2*, from *Arabidopsis*:

Restriction with: *BamH*I/*Mlu*I
Fragments: 3775 bp (empty vector), 1236 bp, 450 bp
Restriction with: *Pst*I/*Eco*RI
Fragments: 3801 bp, 1138 bp (intron FAD2), 302 bp, 2 bp

The cleaved fragments were separated by DNA gel electrophoresis and the desired fragments were excised from the gel and purified with a gel elution kit (Wizard PCR Preps DNA Purification System, Promega).
Vectors and inserts were ligated in a single step using the T4 DNA ligase kit (Promega) to obtain p35-RNAi-*SGT1*, p35-RNAi-*SGT* and p35-RNAi-*GCS*.

Restriction to Confirm Successful Cloning of the RNAi Constructs into the p35 Vector

p35-RNAi-*SGT1*
Restriction with: *Mlu*I/*BamH*I
Fragments: 3557 bp (empty vector), 2268 bp (sense-*FAD2*-anti-sense)
Restriction with: *Sph*I/*Sfi*I
Fragments: 4736 bp, 2894 bp, 1591 bp, 625 bp, 242 bp

p35-RNAi-*SGT2*
Restriction with: *Mlu*I/*BamH*I
Fragments: 3557 bp (empty vector), 2350 bp (sense-*FAD2*-anti-sense)
Restriction with: *Spe*I/*Hind*III
Fragments: 3798 bp, 1233 bp, 661 bp, 255 bp

p35-RNAi-*GCS*
Restriction with: *Mlu*I/*BamH*I
Fragments: 3557 bp (empty vector), 2278 bp (sense-*FAD2*-anti-sense)
Restriction with: *Sph*I/*Sfi*I
Fragments: 2894 bp, 1428 bp, 641 bp, 462 bp, 410 bp

Restriction of Sense and Anti-Sense Fragments for Cloning into pLH9000 and pLH6000

p35-RNAi-*SGT1*, p35-RNAi-*GCS*
Restriction with: *Sfi*I/*Sca*I/*Bsa*I.
Fragments: 2941bp (*Sfi*I-RNAi), 1786 bp, 669 bp, 439 bp

p35-RNAi-*SGT2*
Restriction with: *Sfi*I/*Sca*I
Fragments: 3013 bp (promoter-RNAi-terminator), 1786 bp, 1108 bp

pLH9000 and pLH6000
Both empty vectors were linearized with *Sfi*I.

Constructs were first cleaved for 3h at 37°C, and subsequently for 3h at 50°C for restriction with *Sfi*I. The cleaved fragments were separated by DNA gel electrophoresis and the desired fragments were excised from the gel and purified with a gel elution kit (Wizard PCR Preps DNA Purification System, Promega)

Ligation of RNAi Fragments with the Binary Vectors pLH9000 and pLH6000

Vectors and inserts were ligated using the T4 DNA Ligase kit (Promega).
pLH9000 confers spectinomycin and streptomycin resistance in bacteria and kanamycin resistance in plants. This vector was used for pLH-RNAi-*SGT1* and pLH-RNAi-*GCS*.
pLH6000 confers spectinomycin and streptomycin resistance in bacteria and hygromycin B resistance in plants. This vector was used for pLH-RNAi-*SGT2*.

The constructs were cleaved with the following enzymes to confirm the successful cloning of sense and anti-sense RNAi fragments into pLH9000 and pLH6000:

Construct	Restriction endonucleases	Fragments
pLH9000	*Dra*I/*Pvu*II	5203 bp, 1802 bp, 1140 p, 931 bp, 78 bp
pLH6000	*Nhe*I/*Eco*RI	4808 bp, 2820 bp, 1078 bp, 695 bp
pLH-RNAi-*SGT1*	*Pvu*II	9003 bp, 1764 bp, 1254 bp
pLH-RNAi-*SGT2*	*Nhe*I/*Pvu*II/*Xmn*I	5551 bp, 3112 bp, 1752 bp, 1236 bp, 699 bp
pLH-RNAi-*GCS*	*Mun*I/*Pvu*II	7906 bp, 1633 bp, 1522 bp, 970 bp

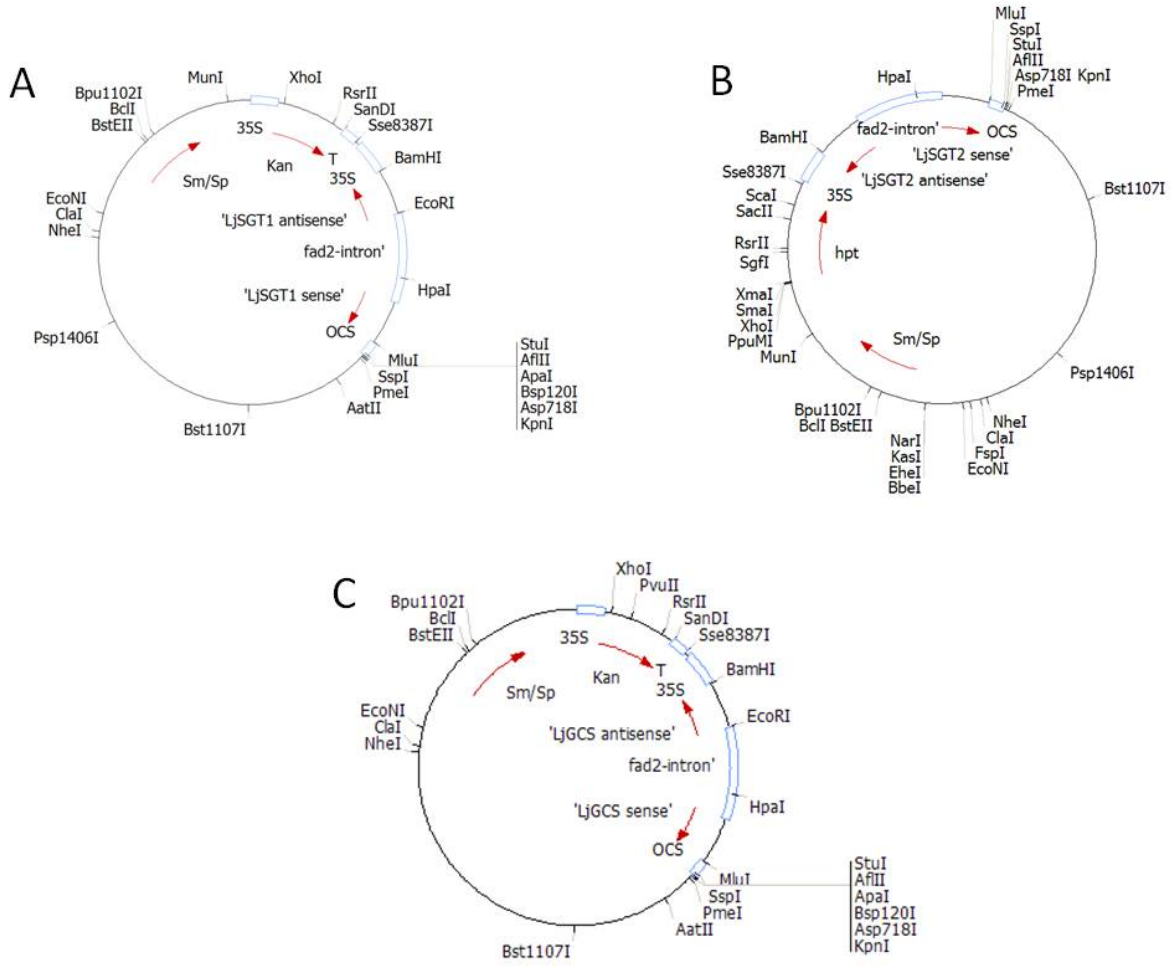

Figure 49: RNAi Constructs for the Downregulation of *SGT1*, *SGT2* and *GCS* in *Lotus japonicus*.
A: RNAi construct for the downregulation of *SGT* in pLH9000; **B**: RNAi construct for the downregulation of *SGT2* in pLH6000; **C**: RNAi construct for the downregulation of *GCS* in pLH9000

7.2 Cloning of *SGT1*, *SGT2* and *GCS* for Heterologous Expression in *Pichia pastoris*

This procedure was performed by Helder Paiva at the Max-Planck Institute for Molecular Plant Physiology, Golm, in the group of Peter Dörmann in 2008.

Cloning of *SGT1*, *SGT2* and *GCS* full cDNAs into the pSC-B Vector

Overhanging primers employed for the cloning of constructs for heterologous expression in *Pichia*.

Lj-SGT1 (1890 bp)
(*Avr*II) atcctaggtATGGCGGACTTGCCGGAAAA
(*Xho*I) ctcgagTCAGGAACAACCAAAACATCTG

Lj-SGT2 (1754 bp)
(*Avr*II) atcctaggtATGGGTAGTGATGGGATTGATT
(*Xho*I) ctcgagTTAAACACCACCACAAGGGGC

Lj-GCS (1578 bp)
(*Avr*II) atcctaggtATGGTGGCTTCATTGGATTCG
(*Xho*I) ctcgagCTAGTTATCAAATTTCTTTGGCTG

The constructs were cleaved with the following enzymes to confirm the successful cloning of sense and anti-sense RNAi fragments into pSC-B:

Construct	Restriction endonucleases	Fragments obtained for orientation A	Fragments obtained for orientation B
pSGT1	*Xho*I/*Sph*I	3423 bp, 1213 bp, 723 bp	4576 bp, 731 bp, 52 bp
pSSGT2	*Xho*I/*Xmn*I	2407 bp, 1804 bp, 1015 bp	2764 bp, 2411 bp, 52 bp
pSGCS	*Avr*II/*Sph*I/*Xmn*I	2461 bp, 1823 bp, 757 bp	3274 bp, 1018 bp, 749 bp
pSGCS	*Xho*I/*Nde*I	3423 bp, 737 bp, 520 bp, 361 bp	4106 bp, 522 bp, 361 bp, 52 bp

Cloning of p*SSGT1*, p*SSGT2* and p*SGCS* cDNAs into the *Pichia pastoris* Expression Vector pPIC 3.5

pPic3.5
Restricted with: *Avr*II/*Not*I
Fragments: 7744 bp

p*SGCS*
Restricted with: *Avr*II/*Not*I
Fragments: 3417 bp (empty pSC-B vector), 1630 bp (*GCS* cDNA)

Cloning of *GCS* cDNA into pPic3.5 resulted in the introduction of an *Xho*I restriction site into the vector, as *GCS* cDNA contained an *Xho*I site at the 3'-end due to amplification with overhanging primers. p*GCS* was cleaved with *Avr*II/*Xho*I for cloning of p*SSGT1* and p*SSGT2*.

p*SSGT1*
Restricted with: *Avr*II/*Xho*I
Fragments: ~3.5kb (empty pSC-B vector), 1890 bp (*SGT1* cDNA)

p*SSGT2*

Restricted with: *Avr*II/*Xho*I
Fragments: ~3.5 kb (empty pSC-B vector), 1754 bp (*SGT1* cDNA)

The restricted fragments were separated by DNA gel electrophoresis and the desired fragments were excised from the gel and purified with a gel elution kit (Wizard PCR Preps DNA Purification System, Promega). Vectors and inserts were ligated using the T4 DNA ligase kit (Promega) to obtain pP*GCS*, pP*SGT2* and pP*GCS*.

The constructs were cleaved with the following enzymes to confirm the successful cloning of sense and anti-sense RNAi fragments into pPic3.5:

Construct	**Restriction endonucleases**	**Fragments**
pP-oe-*SGT1*	*Sph*I/*Cla*I	3195 bp, 3166 bp, 2189 bp, 1136 bp
pP-oe-*SGT2*	*Sph*I/*Cla*I	3195 bp, 3166 bp, 2371 bp, 957 bp
pP-oe-*GCS*	*Sph*I/*Nco*I	4953 bp, 3270 bp, 1151 bp

7.3 Molecular Species Composition of Lipids during Phosphate Deprivation in *Lotus japonicus*

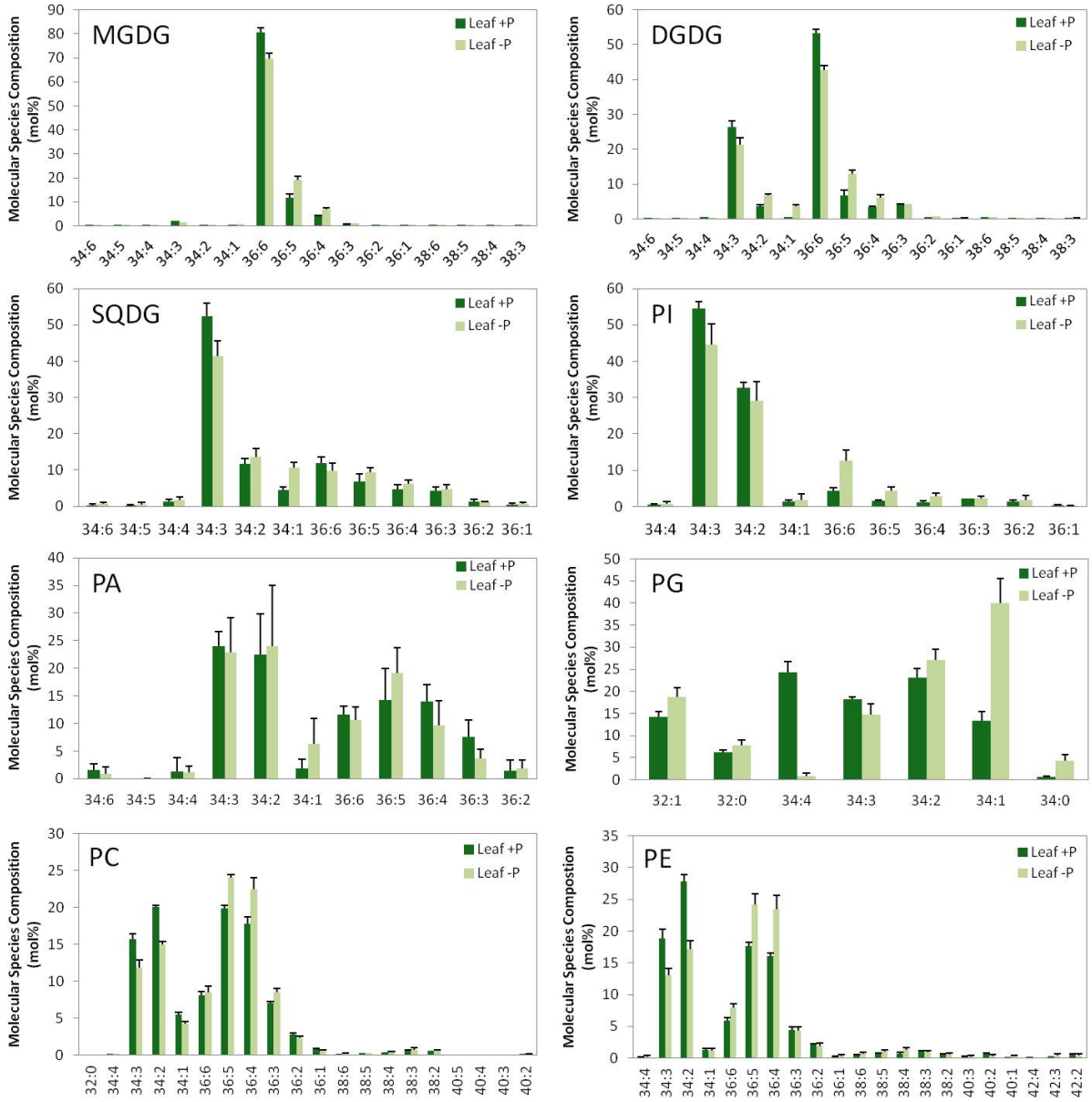

Figure 50: Molecular Species Composition of Phospho- and Galactolipids during Phosphate Deprivation in *Lotus* Leaves. *Lotus japonicus* wild type plants were watered with deionized water for two weeks and subsequently fertilized with mineral mixture containing 0.5 mM nitrogen and 0 mM phosphate for nine weeks. Lipids were extracted from leaves of phosphate deprived plants and analyzed by Q-TOF MS/MS analysis in the presence of internal standards. Data are mean and standard deviation of five measurements.

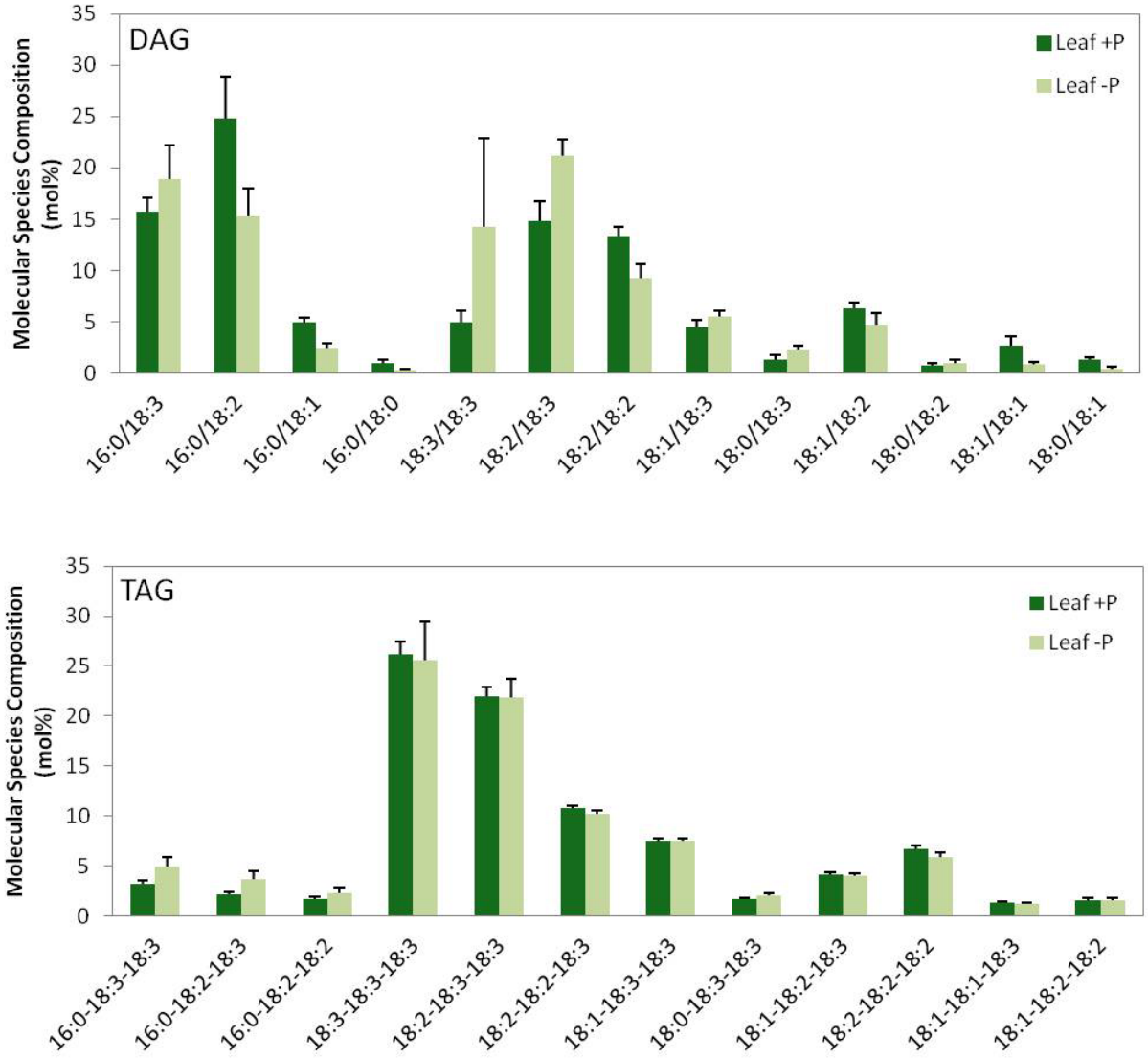

Figure 51: Molecular Species Composition in Nonpolar Glycerolipids during Phosphate Deprivation in *Lotus* Leaves. *Lotus japonicus* wild type plants were watered with deionized water for two weeks and subsequently fertilized with mineral mixture containing 0.5 mM nitrogen and 0 mM phosphate for nine weeks. Lipids were extracted from leaves of phosphate deprived plants and analyzed by Q-TOF MS/MS analysis in the presence of internal standards. Only DAG and TAG molecular species that represent more than 1 mol% of the total DAG or TAG content are depicted. Data are mean and standard deviation of five measurements.

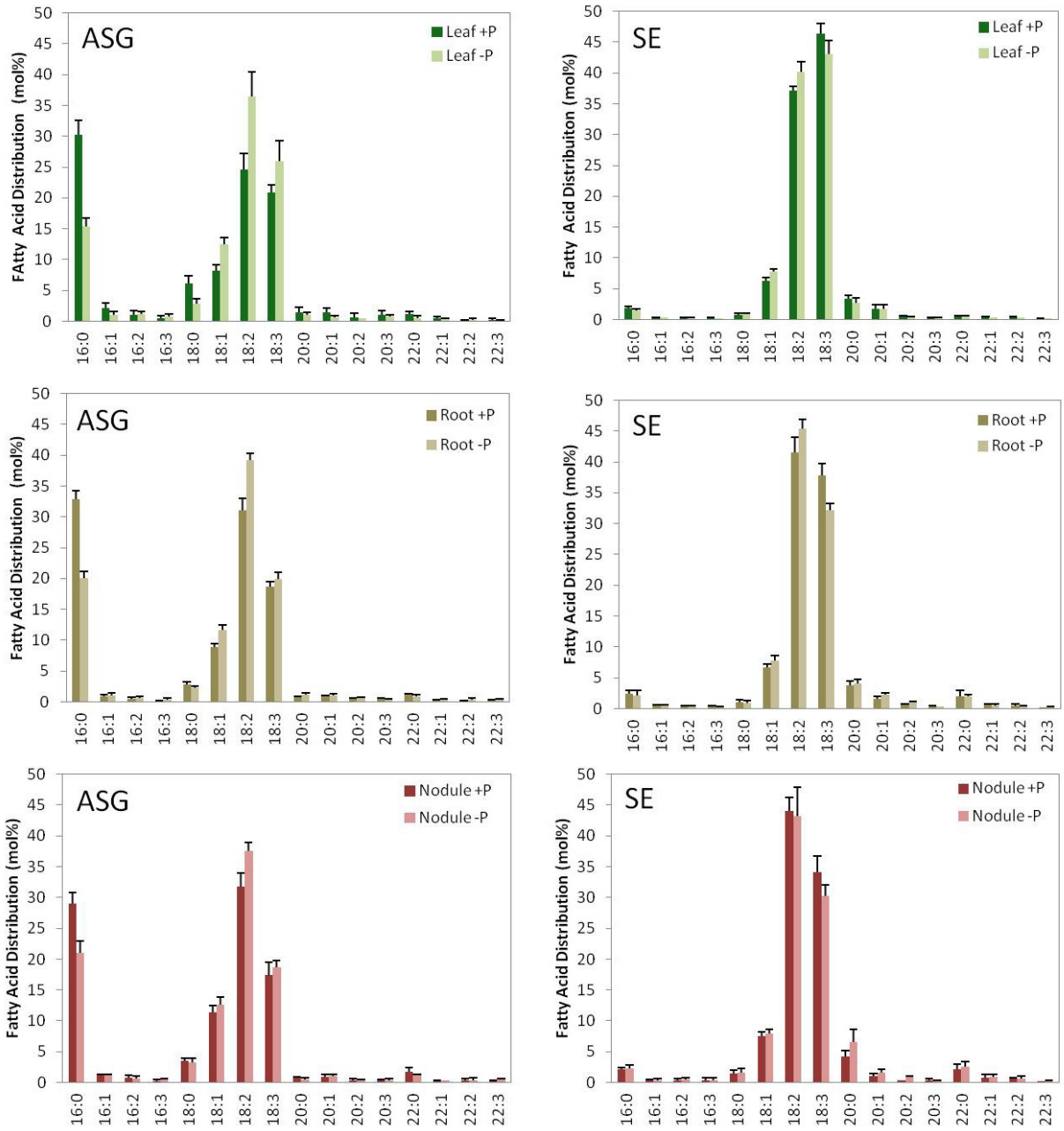

Figure 52: Fatty Acid Composition of Sterol Lipids during Phosphate Deprivation in *Lotus japonicus*. *Lotus japonicus* wild type plants were watered with deionized water for two weeks and subsequently fertilized with mineral mixture containing 0.5 mM nitrogen and 0 mM phosphate for nine weeks. Lipids were extracted from leaves, roots and nodules of phosphate deprived plants and analyzed by Q-TOF MS/MS analysis in the presence of internal standards. Data are mean and standard deviation of five measurements.

7.4 Molecular Species Composition of Lipids during Nodulation in *Lotus japonicus*

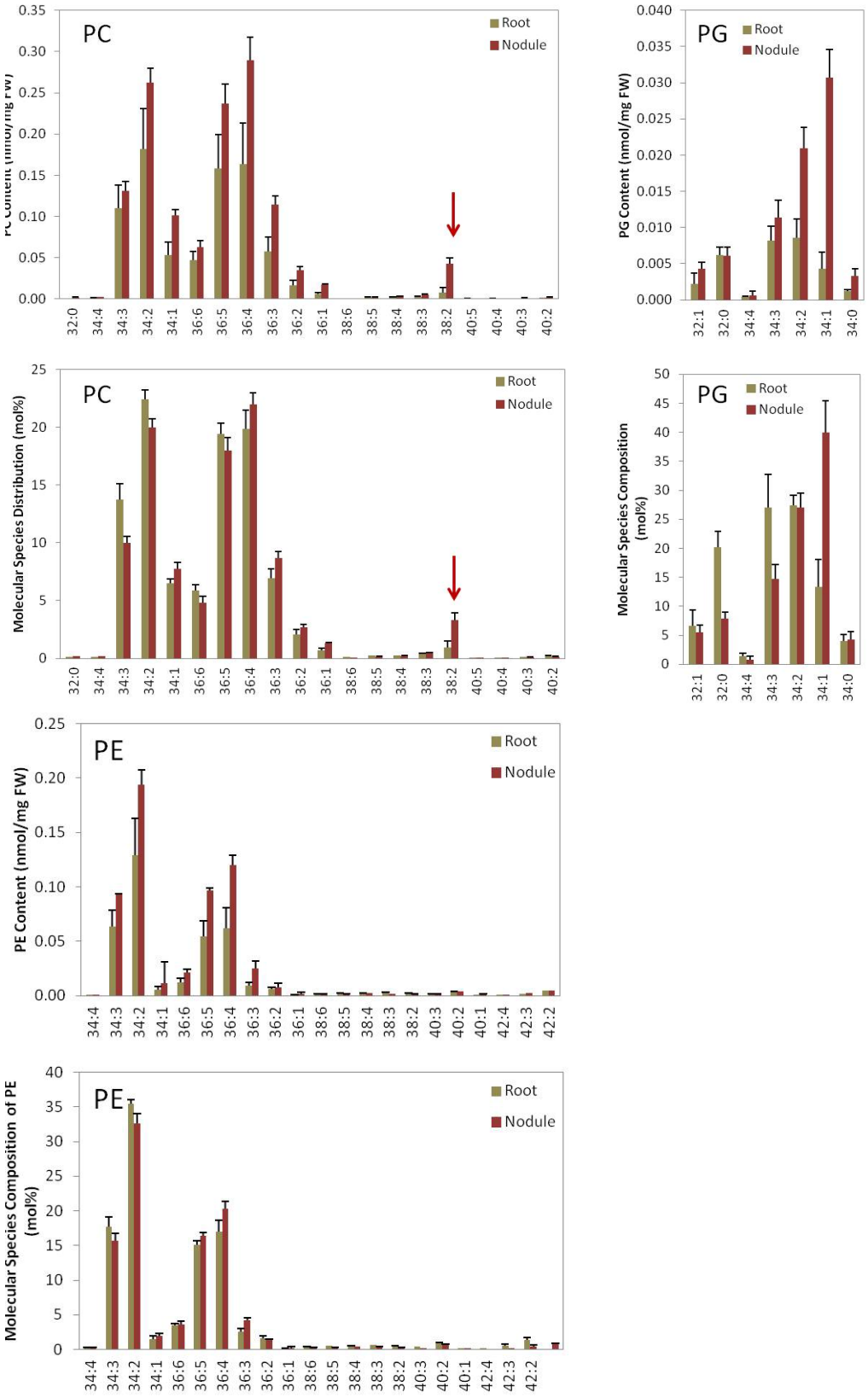

Figure 53: Molecular Species Distribution of PC, PG and PE in *Lotus japonicus* Roots and Nodules. Lipids were extracted from roots and nodules grown on sand with full nutrient supply. Lipid analysis was performed by Q-TOF MS/MS analysis in the presence of internal standards. Data are mean and standard deviation of five measurements.

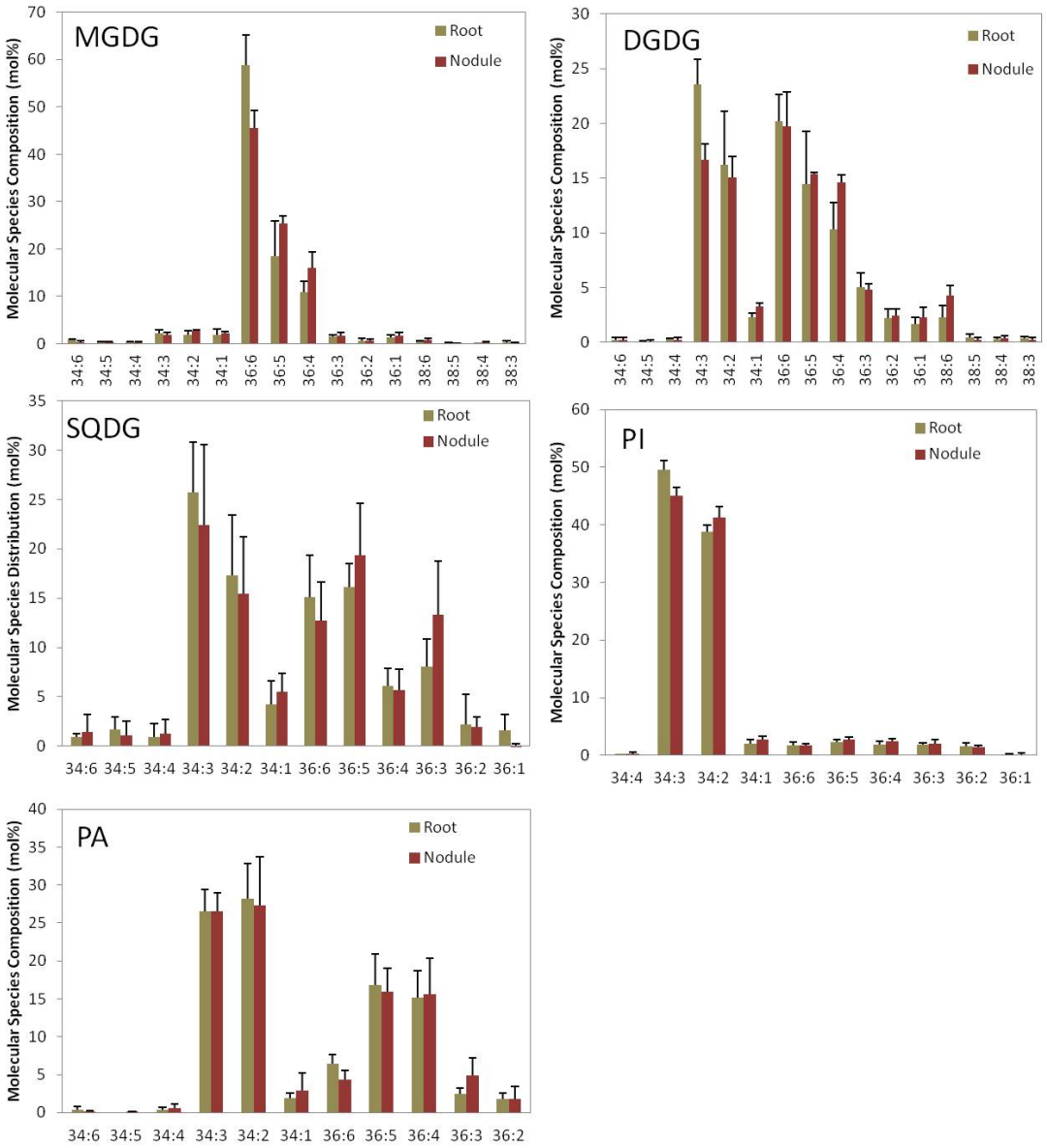

Figure 54: Molecular Species Distribution of Phospho- and Galactolipids in *Lotus japonicus* Roots and Nodules. Lipids were extracted from roots and nodules grown on sand with full nutrient supply. Lipid analysis was performed by Q-TOF MS/MS analysis in the presence of internal standards. Data are mean and standard deviation of five measurements.

7.5 Molecular Species Composition of Lipids during Mycorrhiza Formation in *Lotus japonicus*

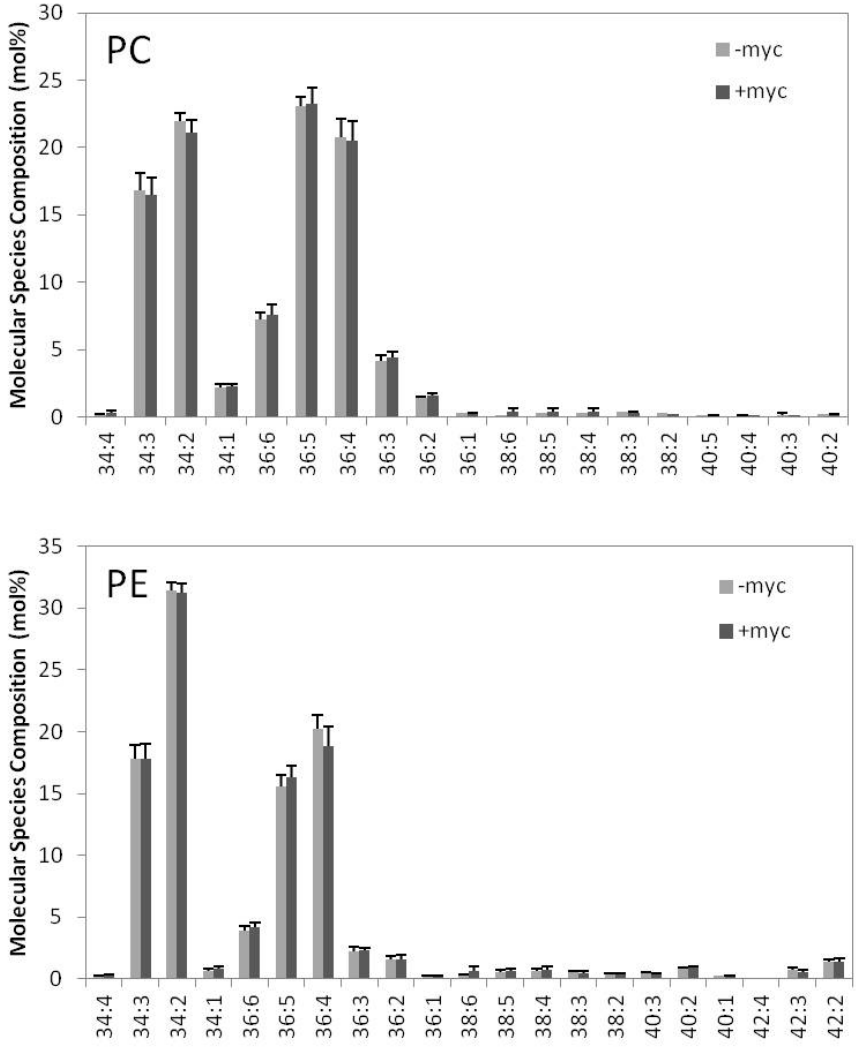

Figure 55: Molecular Species Composition of PC and PE during Mycorrhization of *Lotus* Roots. Plants were inoculated with granular inoculum containing *Glomus intraradices* spores (+myc). Control plants were mock-inoculated with autoclaved inoculum (-myc). Lipids were extracted from mycorrhized and non-mycorrhized roots grown on sand under low phosphate conditions. Lipid analysis was performed by Q-TOF MS/MS analysis in the presence of internal standards. Data are mean and standard deviation of five measurements.

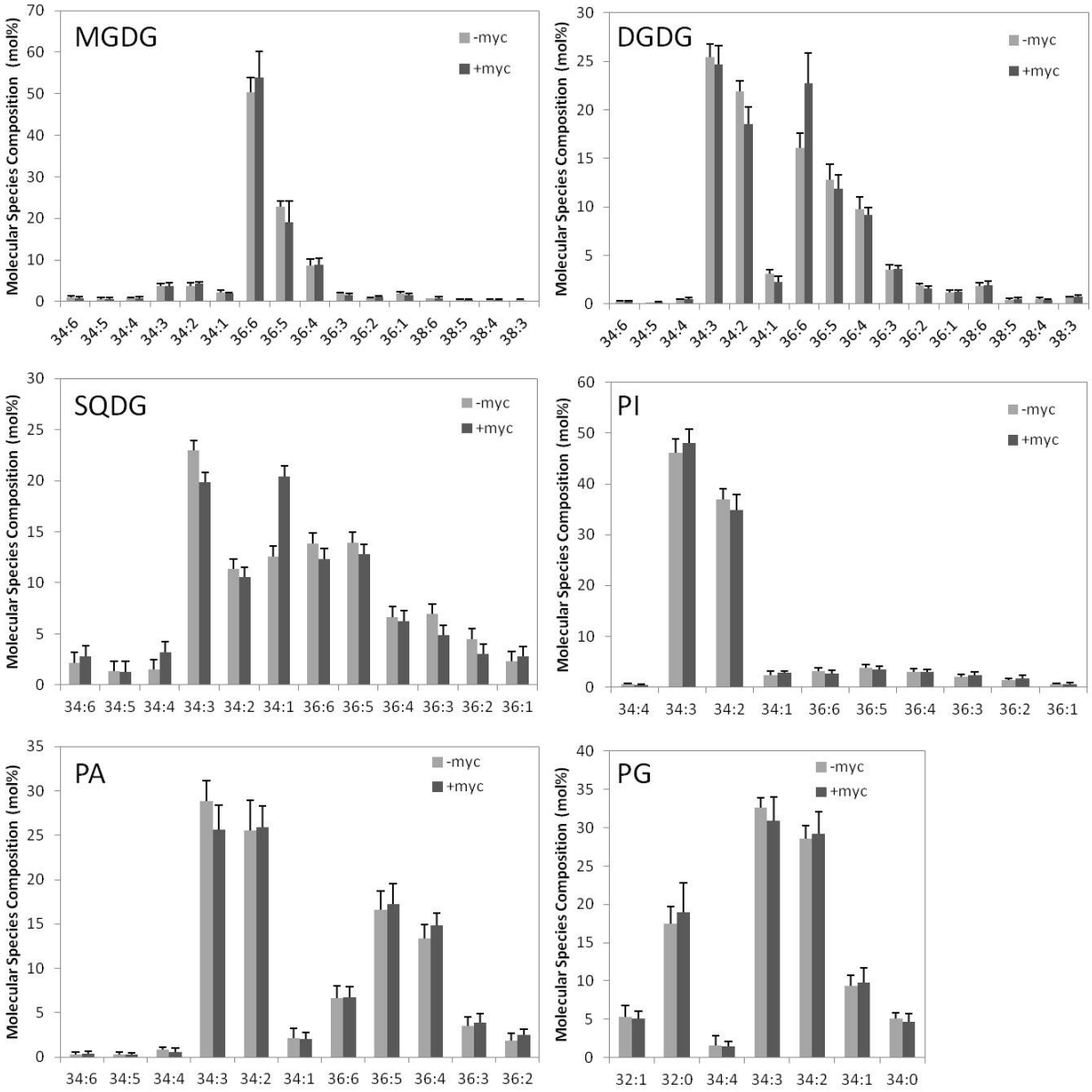

Figure 56: Molecular Species Composition of Phospho- and Galactolipids during Mycorrhization of *Lotus* Roots. Plants were inoculated with granular inoculum containing *Glomus intraradices* spores (+myc). Control plants were mock-inoculated with autoclaved inoculum (-myc). Lipids were extracted from mycorrhized and non-mycorrhized roots grown on sand under low phosphate conditions. Lipid analysis was performed by Q-TOF MS/MS analysis in the presence of internal standards. Data are mean and standard deviation of five measurements.

7.6 Parameters for the Measurement of Different Lipid Classes by Q-TOF MS/MS

Table 5: Q-TOF MS/MS Parameters for Lipid Quantification

Lipid Class	Collision Energy (V)	Neutral loss (m/z)	Product Ion (m/z)
FS	35		118.0859
SE	13		*see Table7*
SG	10	197.0910	
ASG	15	*see Table 9*	
GlcCer	35; 20[a]	180.0634	
GIPC	55	598.1146	
MGDG	12	179.0556	
DGDG	17	341.1084	
SQDG	19	261.0518	
PA	20	115.0034	
PS	22	185.0089	
PI	20	277.0563	
PE	20	141.0190	
PG	20	189.0402	
PC	35		184.0739
LPC	35		184.0739
DAG	20	NL of the FA	
TAG	20	NL of the FA	

[a] Collision energy was set to 20 V for d18:2 containing GlcCer species and to 35 V for all other GlcCers.

7.7 Targeted Lists for the Quantification of Lipids by Q-TOF MS/MS Analysis

Table 6: Profiling of Free Sterols from Plants

Sterol Lipid[a]	Formula [M]	$[M+Betainyl]^+$ (m/z)	Product Ion F_B (m/z)
Cholesterol	$C_{27}H_{46}O$	486.4311	118.0859
Cholestanol (I.S.)	$C_{27}H_{48}O$	488.4468	118.0859
Campesterol	$C_{28}H_{48}O$	500.4468	118.0859
Stigmasterol	$C_{29}H_{48}O$	512.4468	118.0859
Sitosterol	$C_{29}H_{50}O$	514.4624	118.0859
Stigmastanol (I.S.)	$C_{29}H_{52}O$	516.4781	118.0859

[a] In *Arabidopsis* stigmasterol and isofucosterol were not distinguished by Q-TOF measurements.
[b]I.S., internal standard

Table 7: Profiling of Sterol Esters from Plants

Sterol Ester Molecular Species[1]	Formula [M]	$[M+NH_4]^+$ (m/z)	Product Ion F_S (m/z)
16:3-Cholesterol	$C_{43}H_{70}O_2$	636.5714	369.3505
16:2-Cholesterol	$C_{43}H_{72}O_2$	638.5871	369.3505
16:1-Cholesterol (I.S.)	$C_{43}H_{74}O_2$	640.6027	369.3505
16:0-Cholesterol (I.S.)	$C_{43}H_{76}O_2$	642.6184	369.3505
16:3-Campesterol	$C_{44}H_{72}O_2$	650.5871	383.3662
16:2-Campesterol	$C_{44}H_{74}O_2$	652.6027	383.3662
16:1-Campesterol	$C_{44}H_{76}O_2$	654.6184	383.3662
16:0-Campesterol	$C_{44}H_{78}O_2$	656.6340	383.3662
16:3-Stigmasterol	$C_{45}H_{72}O_2$	662.5871	395.3662
16:2-Stigmasterol	$C_{45}H_{74}O_2$	664.6027	395.3662
16:3-Sitosterol	$C_{45}H_{74}O_2$	664.6027	397.3818
18:3-Cholesterol	$C_{45}H_{74}O_2$	664.6027	369.3505
16:1-Stigmasterol	$C_{45}H_{76}O_2$	666.6184	395.3662
16:2-Sitosterol	$C_{45}H_{76}O_2$	666.6184	397.3818
18:2-Cholesterol	$C_{45}H_{76}O_2$	666.6184	369.3505
16:0-Stigmasterol	$C_{45}H_{78}O_2$	668.6340	395.3662
16:1-Sitosterol	$C_{45}H_{78}O_2$	668.6340	397.3818
18:1-Cholesterol (I.S.)	$C_{45}H_{78}O_2$	668.6340	369.3505
16:0-Sitosterol	$C_{45}H_{80}O_2$	670.6497	397.3818
18:0-Cholesterol (I.S.)	$C_{45}H_{80}O_2$	670.6497	369.3505
18:3-Campesterol	$C_{46}H_{76}O_2$	678.6184	383.3662
18:2-Campesterol	$C_{46}H_{78}O_2$	680.6340	383.3662
18:1-Campesterol	$C_{46}H_{80}O_2$	682.6497	383.3662
18:0-Campesterol	$C_{46}H_{82}O_2$	684.6653	383.3662
18:3-Stigmasterol	$C_{47}H_{76}O_2$	690.6184	395.3662
18:3-Sitosterol	$C_{47}H_{78}O_2$	692.6340	397.3818
18:2-Stigmasterol	$C_{47}H_{78}O_2$	692.6340	395.3662
20:3-Cholesterol	$C_{47}H_{78}O_2$	692.6340	369.3505
18:2-Sitosterol	$C_{47}H_{80}O_2$	694.6497	397.3818
18:1-Stigmasterol	$C_{47}H_{80}O_2$	694.6497	395.3662
20:2-Cholesterol	$C_{47}H_{80}O_2$	694.6497	369.3505
18:0-Stigmasterol	$C_{47}H_{82}O_2$	696.6653	395.3662
18:1-Sitosterol	$C_{47}H_{82}O_2$	696.6653	397.3818

Table 7 (continued)			
20:1-Cholesterol	$C_{47}H_{82}O_2$	696.6653	369.3505
18:0-Sitosterol	$C_{47}H_{84}O_2$	698.6810	397.3818
20:0-Cholesterol	$C_{47}H_{84}O_2$	698.6810	369.3505
20:3-Campesterol	$C_{48}H_{80}O_2$	706.6497	383.3662
20:2-Campesterol	$C_{48}H_{82}O_2$	708.6653	383.3662
20:1-Campesterol	$C_{48}H_{84}O_2$	710.6810	383.3662
20:0-Campesterol	$C_{48}H_{86}O_2$	712.6966	383.3662
20:3-Stigmasterol	$C_{49}H_{80}O_2$	718.6497	395.3662
22:3-Cholesterol	$C_{49}H_{82}O_2$	720.5245	369.3505
20:2-Stigmasterol	$C_{49}H_{82}O_2$	720.6653	395.3662
20:3-Sitosterol	$C_{49}H_{82}O_2$	720.6653	397.3818
20:1-Stigmasterol	$C_{49}H_{84}O_2$	722.6810	395.3662
20:2-Sitosterol	$C_{49}H_{84}O_2$	722.6810	397.3818
22:2-Cholesterol	$C_{49}H_{84}O_2$	722.6810	369.3505
20:0-Stigmasterol	$C_{49}H_{86}O_2$	724.6966	395.3662
20:1-Sitosterol	$C_{49}H_{86}O_2$	724.6966	397.3818
22:1-Cholesterol	$C_{49}H_{86}O_2$	724.6966	369.3505
20:0-Sitosterol	$C_{49}H_{88}O_2$	726.7123	397.3818
22:0-Cholesterol	$C_{49}H_{88}O_2$	726.7123	369.3505
22:3-Campesterol	$C_{50}H_{84}O_2$	734.5401	383.3662
22:2-Campesterol	$C_{50}H_{86}O_2$	736.6966	383.3662
22:1-Campesterol	$C_{50}H_{88}O_2$	738.7123	383.3662
22:0-Campesterol	$C_{50}H_{90}O_2$	740.7279	383.3662
22:3-Stigmasterol	$C_{51}H_{84}O_2$	746.5401	395.3662
22:3-Sitosterol	$C_{51}H_{86}O_2$	748.5558	397.3818
22:2-Stigmasterol	$C_{51}H_{86}O_2$	748.6966	395.3662
22:1-Stigmasterol	$C_{51}H_{88}O_2$	750.7123	395.3662
22:2-Sitosterol	$C_{51}H_{88}O_2$	750.7123	397.3818
22:0-Stigmasterol	$C_{51}H_{90}O_2$	752.7279	395.3662
22:1-Sitosterol	$C_{51}H_{90}O_2$	752.7279	397.3818
22:0-Sitosterol	$C_{51}H_{92}O_2$	754.7436	397.3818

[a] In *Arabidopsis* stigmasterol and isofucosterol were not distinguished by Q-TOF measurements.
[b]I.S., internal standard

Table 8: Profiling of Sterol Glucosides from Plants

Sterol Glucoside Molecular Species[1]	Formula [M]	$[M+NH_4]^+$ (m/z)	Product Ion F_S (m/z)
Glc-Cholesterol	$C_{33}H_{56}O_6$	566.4415	369.3505
Glc-Cholestanol (I.S.)	$C_{33}H_{58}O_6$	568.4572	371.3662
Glc-Campesterol	$C_{34}H_{58}O_6$	580.4572	383.3662
Glc-Stigmasterol	$C_{35}H_{58}O_6$	592.4572	395.3662
Glc-Sitosterol	$C_{35}H_{60}O_6$	594.4728	397.3818
Glc-Stigmastanol (I.S.)	$C_{35}H_{62}O_6$	596.4885	399.3975

[a] In *Arabidopsis* stigmasterol and isofucosterol were not distinguished by Q-TOF measurements.
[b]I.S., internal standard

Table 9: Profiling of Acylated Sterol Glucosides from Plants

Acylated Sterol Glucoside Molecular Species[1]	Formula [M]	$[M+NH_4]^+$ (m/z)	Product Ion F_S (m/z)	Product Ion F_{AG} (m/z)
16:3-Glc-Cholesterol	$C_{49}H_{80}O_7$	798.6242	369.3505	395.2428
16:2 Glc-Cholesterol	$C_{49}H_{82}O_7$	800.6399	369.3505	397.2585
16:1-Glc-Cholesterol	$C_{49}H_{84}O_7$	802.6555	369.3505	399.2741
16:0-Glc-Cholesterol	$C_{49}H_{86}O_7$	804.6712	369.3505	401.2898
16:3-Glc-Campesterol	$C_{50}H_{82}O_7$	812.6399	383.3662	395.2428
16:2-Glc-Campesterol	$C_{50}H_{84}O_7$	814.6555	383.3662	397.2585
16:1-Glc-Campesterol	$C_{50}H_{86}O_7$	816.6712	383.3662	399.2741
16:0-Glc-Campesterol	$C_{50}H_{88}O_7$	818.6868	383.3662	401.2898
16:0-Glc-Campestanol (I.S.)	$C_{50}H_{90}O_7$	820.7025	385.3818	401.2898
16:3-Glc-Stigmasterol	$C_{51}H_{82}O_7$	824.6399	395.3662	395.2428
16:2-Glc-Stigmasterol	$C_{51}H_{84}O_7$	826.6555	395.3662	397.2585
16:3-Glc-Sitosterol	$C_{51}H_{84}O_7$	826.6555	397.3818	395.2428
18:3-Glc-Cholesterol	$C_{51}H_{84}O_7$	826.6555	369.3505	423.2741
16:1-Glc-Stigmasterol	$C_{51}H_{86}O_7$	828.6712	395.3662	399.2741
16:2-Glc-Sitosterol	$C_{51}H_{86}O_7$	828.6712	397.3818	397.2585
18:2 Glc-Cholesterol	$C_{51}H_{86}O_7$	828.6712	369.3505	425.2898
16:0-Glc-Stigmasterol	$C_{51}H_{88}O_7$	830.6868	395.3662	401.2898
16:1-Glc-Sitosterol	$C_{51}H_{88}O_7$	830.6868	397.3818	399.2741
18:1-Glc-Cholesterol	$C_{51}H_{88}O_7$	830.6868	369.3505	427.3054
16:0-Glc-Sitosterol	$C_{51}H_{90}O_7$	832.7025	397.3818	401.2898
18:0-Glc-Cholesterol	$C_{51}H_{90}O_7$	832.7025	369.3505	429.3211
16:0-Glc-Stigmastanol (I.S.)	$C_{51}H_{92}O_7$	834.7181	399. 3975	401.2898
18:3-Glc-Campesterol	$C_{52}H_{86}O_7$	840.6712	383.3662	423.2741
18:2-Glc-Campesterol	$C_52H_{88}O_7$	842.6868	383.3662	425.2898
18:1-Glc-Campesterol	$C_{52}H_{90}O_7$	844.7025	383.3662	427.3054
18:0-Glc-Campesterol	$C_{52}H_{92}O_7$	846.7181	383.3662	429.3211
18:0-Glc-Campestanol (I.S.)	$C_{52}H_{94}O_7$	848.7338	385.3818	429.3211
18:3-Glc-Stigmasterol	$C_{53}H_{86}O_7$	852.6712	395.3662	423.2741
18:3-Glc-Sitosterol	$C_{53}H_{88}O_7$	854.6868	397.3818	423.2741
18:2-Glc-Stigmasterol	$C_{53}H_{88}O_7$	854.6868	395.3662	425.2898
20:3-Glc-Cholesterol	$C_{53}H_{88}O_7$	854.6868	369.3505	451.3054
18:2-Glc-Sitosterol	$C_{53}H_{90}O_7$	856.7025	397.3818	425.2898
18:1-Glc-Stigmasterol	$C_{53}H_{90}O_7$	856.7025	395.3662	427.3054
20:2-Glc-Cholesterol	$C_{53}H_{90}O_7$	856.7025	369.3505	453.3211
18:0-Glc-Stigmasterol	$C_{53}H_{92}O_7$	858.7181	395.3662	429.3211
18:1-Glc-Sitosterol	$C_{53}H_{92}O_7$	858.7181	397.3818	427.3054
20:1-Glc-Cholesterol	$C_{53}H_{92}O_7$	858.7181	369.3505	455.3367
18:0-Glc-Sitosterol	$C_{53}H_{94}O_7$	860.7338	397.3818	429.3211
20:0-Glc-Cholesterol	$C_{53}H_{94}O_7$	860.7338	369.3505	457.3524
18:0-Glc-Stigmastanol (I.S.)	$C_{53}H_{96}O_7$	862.7494	399.3975	429.3211
20:3-Glc-Campesterol	$C_{54}H_{90}O_7$	868.7025	383.3662	451.3054
20:2-Glc-Campesterol	$C_54H_{92}O_7$	870.7181	383.3662	453.3211
20:1-Glc-Campesterol	$C_{54}H_{94}O_7$	872.7338	383.3662	455.3367
20:0-Glc-Campesterol	$C_{54}H_{96}O_7$	874.7494	383.3662	457.3524
20:3-Glc-Stigmasterol	$C_{55}H_{90}O_7$	880.7025	395.3662	451.3054
22:3-Glc-Cholesterol	$C_{55}H_{92}O_7$	882.5773	369.3505	479.3367
20:2-Glc-Stigmasterol	$C_{55}H_{92}O_7$	882.7181	395.3662	453.3211
20:3-Glc-Sitosterol	$C_5 5H_{92}O_7$	882.7181	397.3818	451.3054
20:1-Glc-Stigmasterol	$C_{55}H_{94}O_7$	884.7338	395.3662	455.3367
20:2-Glc-Sitosterol	$C_{55}H_{94}O_7$	884.7338	397.3818	453.3211
22:2-Glc-Cholesterol	$C_{55}H_{94}O_7$	884.7338	369.3505	481.3524

Table 9 (continued)				
20:0-Glc-Stigmasterol	$C_{55}H_{96}O_7$	886.7494	395.3662	457.3524
20:1-Glc-Sitosterol	$C_{55}H_{96}O_7$	886.7494	397.3818	455.3367
22:1-Glc-Cholesterol	$C_{55}H_{96}O_7$	886.7494	369.3505	483.3680
20:0-Glc-Sitosterol	$C_{55}H_{98}O_7$	888.7651	397.3818	457.3524
22:0-Glc-Cholesterol	$C_{55}H_{98}O_7$	888.7651	369.3505	485.3837
22:3-Glc-Campesterol	$C_{56}H_{94}O_7$	896.5929	383.3662	479.3367
22:2-Glc-Campesterol	$C_{56}H_{96}O_7$	898.7494	383.3662	481.3524
22:1-Glc-Campesterol	$C_{56}H_{98}O_7$	900.7651	383.3662	483.3680
22:0-Glc-Campesterol	$C_{56}H_{100}O_7$	902.7807	383.3662	485.3837
22:0-Glc-Campestanol (I.S.)	$C_{56}H_{102}O_7$	904.7964	385.3818	485.3837
22:3-Glc-Stigmasterol	$C_{57}H_{94}O_7$	908.5929	395.3662	479.3367
22:3-Glc-Sitosterol	$C_{57}H_{96}O_7$	910.6086	397.3818	479.3367
22:2-Glc-Stigmasterol	$C_{57}H_{96}O_7$	910.7494	395.3662	481.3524
22:1-Glc-Stigmasterol	$C_{57}H_{98}O_7$	912.7651	395.3662	483.3680
22:2-Glc-Sitosterol	$C_{57}H_{98}O_7$	912.7651	397.3818	481.3524
22:0-Glc-Stigmasterol	$C_{57}H_{100}O_7$	914.7807	395.3662	485.3837
22:1-Glc-Sitosterol	$C_{57}H_{100}O_7$	914.7807	397.3818	483.3680
22:0-Glc-Sitosterol	$C_{57}H_{102}O_7$	916.7964	397.3818	485.3837
22:0-Glc-Stigmastanol (I.S.)	$C_{57}H_{104}O_7$	918.8120	399.3975	485.3837

[a] In *Arabidopsis* stigmasterol and isofucosterol were not distinguished by Q-TOF measurements.
[b]I.S., internal standard

Table 10: Profiling of Glucosylceramides from Plants (*Fabaceae*)

GlcCer Molecular Species	Formula [M]	[M+H]+ (m/z)	Product Ion F_{Cer} (m/z)
Glc-d18:1-c12:0 (I.S.) [a]	$C_{36}H_{69}O_8N$	644.5460	464.4626
Glc-d18:2-h16:1	$C_{40}H_{73}O_9N$	712.5358	532.4724
Glc-d18:2-h16:0	$C_{40}H_{75}O_9N$	714.5515	534.4881
Glc-d18:1-h16:0	$C_{40}H_{77}O_9N$	716.5671	536.5037
Glc-d18:0-h16:0	$C_{40}H_{79}O_9N$	718.5828	538.5194
Glc-t18:1-h16:1	$C_{40}H_{75}O_{10}N$	730.5464	550.4830
Glc-t18:1-h16:0	$C_{40}H_{77}O_{10}N$	732.5620	552.4986
Glc-t18:0-h16:0	$C_{40}H_{79}O_9N$	734.5777	554.5143
Glc-d18:2-h18:1	$C_{40}H_{77}O_9N$	740.5671	560.5037
Glc-d18:2-h18:0	$C_{42}H_{79}O_9N$	742.5828	562.5194
Glc-d18:1-h18:0	$C_{42}H_{81}O_9N$	744.5984	564.5350
Glc-d18:0-h18:0	$C_{42}H_{83}O_9N$	746.6141	566.5507
Glc-t18:1-h18:1	$C_{42}H_{79}O_{10}N$	758.5777	578.5143
Glc-t18:1-h18:0	$C_{42}H_{81}O_{10}N$	760.5933	580.5299
Glc-t18:0-h18:0	$C_{42}H_{83}O_{10}N$	762.6090	582.5456
Glc-d18:2-h20:1	$C_{44}H_{81}O_9N$	768.5984	588.5350
Glc-d18:2-h20:0	$C_{44}H_{83}O_9N$	770.6141	590.5507
Glc-d18:1-h20:0	$C_{44}H_{85}O_9N$	772.6297	592.5663
Glc-d18:0-h20:0	$C_{44}H_{87}O_9N$	774.6454	594.5820
Glc-d18:2-h21:1	$C_{45}H_{83}O_9N$	782.6107	602.5473
Glc-d18:2-h21:0	$C_{45}H_{85}O_9N$	784.5933	604.5299
Glc-t18:1-h20:1	$C_{44}H_{83}O_{10}N$	786.6090	606.5456
Glc-t18:1-h20:0	$C_{44}H_{85}O_{10}N$	788.6246	608.5612
Glc-t18:0-h20:0	$C_{44}H_{87}O_{10}N$	790.6403	610.5769
Glc-d18:2-h22:1	$C_{46}H_{85}O_9N$	796.6297	616.5663
Glc-d18:2-h22:0	$C_{46}H_{87}O_9N$	798.6454	618.5820
Glc-d18:1-h22:0	$C_{46}H_{89}O_9N$	800.6610	620.5976
Glc-t18:1-h21:0	$C_{46}H_{91}O_9N$	802.6767	622.6133
Glc-t18:0-h21:0	$C_{45}H_{89}O_{10}N$	804.6525	624.5891

Table 10 (continued)			
Glc-d18:1-c24:1 (I.S.)	$C_{48}H_{91}O_8N$	810.6816	630.6812
Glc-d18:2-h23:0	$C_{47}H_{89}O_9N$	812.6576	632.5942
Glc-t18:1-h22:1	$C_{46}H_{87}O_{10}N$	814.6403	634.5769
Glc-t18:1-h22:0	$C_{46}H_{89}O_{10}N$	816.6559	636.5925
Glc-t18:0-h22:0	$C_{46}H_{91}O_{10}N$	818.6716	638.6082
Glc-d18:2-h24:1	$C_{48}H_{89}O_9N$	824.6610	644.5976
Glc-d18:2-h24:0	$C_{48}H_{91}O_9N$	826.6766	646.6132
Glc-d18:1-h24:0	$C_{48}H_{93}O_9N$	828.6923	648.6289
Glc-t18:1-h23:0	$C_{48}H_{95}O_9N$	830.7080	650.6446
Glc-t18:0-h23:0	$C_{47}H_{93}O_{10}N$	832.6838	652.6204
Glc-d18:2-h25:1	$C_{49}H_{91}O_9N$	838.6733	658.6099
Glc-d18:2-h25:0	$C_{49}H_{93}O_9N$	840.6889	660.6255
Glc-t18:1-h24:1	$C_{48}H_{91}O_{10}N$	842.6715	662.6081
Glc-t18:1-h24:0	$C_{48}H_{93}O_{10}N$	844.6872	664.6238
Glc-t18:0-h24:0	$C_{48}H_{95}O_{10}N$	846.7029	666.6395
Glc-d18:2-h26:1	$C_{50}H_{93}O_9N$	852.6923	672.6289
Glc-d18:2-h26:0	$C_{50}H_{95}O_9N$	854.7080	674.6446
Glc-d18:1-h26:0	$C_{50}H_{97}O_9N$	856.7236	676.6602
Glc-t18:1-h25:0	$C_50H_{99}O_9N$	858.7393	678.6759
Glc-t18:0-h25:0	$C_{49}H_{97}O_{10}N$	860.7151	680.6517
Glc-t18:1-h26:1	$C_{50}H_{95}O_{10}N$	870.7029	690.6395
Glc-t18:1-h26:0	$C_{50}H_{97}O_{10}N$	872.7185	692.6551
Glc-t18:0-h26:0	$C_{50}H_{99}O_{10}N$	874.7342	694.6708
Glc-d18:2-h28:1	$C_{52}H_{97}O_9N$	880.7566	700.6932
Glc-d18:2-h28:0	$C_{52}H_{101}O_9N$	882.7723	702.7089
Glc-d18:1-h28:0	$C_{52}H_{103}O_9N$	884.7879	704.7245
Glc-d18:0-h28:0	$C_{52}H_{103}O_9N$	886.8036	706.7402
Glc-t18:1-h28:1	$C_{52}H_{99}O_{10}N$	898.7672	718.7038
Glc-t18:1-h28:0	$C_{52}H_{101}O_{10}N$	900.7828	720.7194
Glc-t18:0-h28:0	$C_{52}H_{103}O_{10}N$	902.7985	722.7351

[a]I.S., internal standard.

Table 11: Profiling of Phospho- and Galactolipids from Plants

Molecular Species	Exact Molecular Mass (m/z)[a]	Molecular Species	Exact Molecular Mass (m/z)[a]
34:6 MGDG	764.5307	28:0 PS (I.S.)	680.4503
34:5 MGDG	766.5463	34:4 PS	756.4810
34:4 MGDG	768.5620	34:3 PS	758.4967
34:3 MGDG	770.5776	34:2 PS	760.5123
34:2 MGDG	772.5933	34:1 PS	762.5280
34:1 MGDG	774.6089	36:6 PS	780.4810
34:0 MGDG (I.S.) [b]	776.6246	36:5 PS	782.4967
36:6 MGDG	792.5620	36:4 PS	784.5123
36:5 MGDG	794.5776	36:3 PS	786.5280
36:4 MGDG	796.5933	36:2 PS	788.5436
36:3 MGDG	798.6089	36:1 PS	790.5593
36:2 MGDG	800.6246	38:6 PS	808.5123
36:1 MGDG	802.6402	38:5 PS	810.5280
36:0 MGDG (I.S.)	804.6559	38:4 PS	812.5436
38:6 MGDG	820.5933	38:3 PS	814.5593
38:5 MGDG	822.6089	38:2 PS	816.5749
38:4 MGDG	824.6246	38:1 PS	818.5906
38:3 MGDG	826.6402	40:4 PS	840.5749
34:6 DGDG	926.5835	40:3 PS	842.5906
34:5 DGDG	928.5992	40:2 PS	844.6062
34:4 DGDG	930.6148	40:1 PS	846.6219
34:3 DGDG	932.6305	40:0 PS (I.S.)	848.6375
34:2 DGDG	934.6461	42:4 PS	868.6062
34:1 DGDG	936.6618	42:3 PS	870.6219
34:0 DGDG (I.S.)	938.6775	42:2 PS	872.6375
36:6 DGDG	954.6148	42:1 PS	874.6532
36:5 DGDG	956.6305	34:4 PI	848.5283
36:4 DGDG	958.6461	34:3 PI 3	850.5440
36:3 DGDG	960.6618	34:2 PI 3	852.5597
36:2 DGDG	962.6774	34:1 PI 3	854.5753
36:1 DGDG	964.6931	34:0 PI 3 (I.S.)	856.5910
36:0 DGDG (I.S.)	966.7087	36:6 PI 3	872.5283
38:6 DGDG	982.6461	36:5 PI 3	874.5440
38:5 DGDG	984.6618	36:4 PI 3	876.5596
38:4 DGDG	986.6774	36:3 PI 3	878.5753
38:3 DGDG	988.6931	36:2 PI 3	880.5909
34:6 SGDG	828.4926	36:1 PI 3	882.6066
34:5 SGDG	830.5082	36:0 PI (I.S.)	884.6223
34:4 SGDG	832.5239	28:0 PE (I.S.)	636.4604
34:3 SGDG	834.5395	34:4 PE	712.4912
34:2 SGDG	836.5552	34:3 PE	714.5069
34:1 SGDG	838.5708	34:2 PE	716.5225
34:0 SQDG (I.S.)	840.5865	34:1 PE	718.5382
36:6 SGDG	856.5239	36:6 PE	736.4912
36:5 SGDG	858.5395	36:5 PE	738.5069
36:4 SGDG	860.5552	36:4 PE	740.5225
36:3 SGDG	862.5708	36:3 PE	742.5382
36:2 SGDG	864.5865	36:2 PE	744.5538
36:1 SGDG	866.6022	36:1 PE	746.5695
36:0 SQDG (I.S.)	868.6178	38:6 PE	764.5225
28:0 PA (I.S.)	610.4448	38:5 PE	766.5382
34:6 PA	682.4442	38:4 PE	768.5538

Table 11 (continued)

34:5 PA	684.4462	38:3 PE	770.5695
34:4 PA	686.4755	38:2 PE	772.5851
34:3 PA	688.4912	40:3 PE	798.6008
34:2 PA	690.5068	40:2 PE	800.6164
34:1 PA	692.5225	40:0 PE (I.S.)	804.6477
36:6 PA	710.4755	42:4 PE	824.6169
36:5 PA	712.4912	42:3 PE	826.6321
36:4 PA	714.5068	42:2 PE	828.6477
36:3 PA	716.5225	28:0 PG (I.S.)	684.4816
36:2 PA	718.5381	32:1 PG	738.5279
40:0 PA (I.S.)	778.6326	32:0 PG	740.5436
28:0 PS (I.S.)	680.4503	34:4 PG	760.5123
34:4 PS	756.4810	34:3 PG	762.5279
34:3 PS	758.4967	34:2 PG	764.5436
34:2 PS	760.5123	34:1 PG	766.5592
34:1 PS	762.5280	34:0 PG	768.5749
36:6 PS	780.4810	40:0 PG (I.S.)	852.6694
36:5 PS	782.4967	28:0 PC (I.S.)	678.5074
36:4 PS	784.5123	32:0 PC	734.5695
36:3 PS	786.5280	34:4 PC	754.5382
36:2 PS	788.5436	34:3 PC	756.5538
36:1 PS	790.5593	34:2 PC	758.5695
38:6 PS	808.5123	34:1 PC	760.5851
38:5 PS	810.5280	36:6 PC	778.5382
38:4 PS	812.5436	36:5 PC	780.5538
38:3 PS	814.5593	36:4 PC	782.5695
38:2 PS	816.5749	36:3 PC	784.5851
38:1 PS	818.5906	36:2 PC	786.6008
40:4 PS	840.5749	36:1 PC	788.6164
40:3 PS	842.5906	38:6 PC	806.5695
40:2 PS	844.6062	38:5 PC	808.5851
40:1 PS	846.6219	38:4 PC	810.6008
40:0 PS (I.S.)	848.6375	38:3 PC	812.6164
42:4 PS	868.6062	38:2 PC	814.6321
42:3 PS	870.6219	40:5 PC	836.6164
42:2 PS	872.6375	40:4 PC	838.6321
42:1 PS	874.6532	40:3 PC	840.6477
		40:2 PC	842.6634
		40:0 PC (I.S.)	846.6952

[a] Exact molecular masses correspond to NH_4^+ adducts (MGDG, DGDG, SQDG, PA, PI, PG) and H^+ adducts (PS, PE, PC).

[b] I.S., internal standard.

List of Publications

Parts of this thesis were published in:

Vera Wewer, Isabel Dombrink, Katharina vom Dorp and Peter Dörmann (2011) Quantification of sterol lipids in plants by quadrupole time-of-flight mass spectrometry. Journal of Lipid Research 52: 1039-1054

Additional publications:

Emanuel A Devers, Vera Wewer, Isabel Dombrink, Peter Dörmann and Georg Hölzl (2011) A processive glycosyltransferase involved in glycolipid synthesis during phosphate deprivation in *Mesorhizobium loti*. Journal of Bacteriology 193: 1377-1384

Felix Lippold, Katharina vom Dorp, Marion Abraham, Georg Hölzl, Vera Wewer, Jenny Lindberg Yilmaz, Ida Lager, Cyrille Montandon, Celine Besagni, Felix Kessler, Sten Stymne and Peter Dörmann (2012) Fatty acid phytyl ester synthesis in chloroplasts of *Arabidopsis.* Plant Cell 24: 2001-2014

Vera Wewer, Peter Dörmann and Georg Hölzl (2012) Analysis and quantification of plant membrane lipids by thin-layer chromatography and gas chromatography. In: Munnik T, Heilmann I, editors. Plant phosphoinositide signaling: methods and protocols. New York, Humana Press, New York (in press)

Michaela Kopischke, Lore Westphal, Korbinian Schneeberger, Richard Clark, Stephan Ossowski, Vera Wewer, Rene Fuchs, Jörn Landtag, Audrey Ah-Fong, Howard Judelson, Gerd Hause, Peter Dörmann, Volker Lipka, Detlef Weigel, Paul Schulze-Lefert, Dierk Scheel and Sabine Rosahl (2012) Impaired sterol ester synthesis alters the response of *Arabidopsis thaliana* to *Phytophthora infestans.* Plant Journal (submitted)

Nico de Storme, Joachim de Schrijver, Wim van Criekinge, Vera Wewer, Peter Dörmann, Danny Geelen (2012) Sexual polyploidization through pre-meiotic cytokinesis defects in a callose synthase and sterol biosynthesis mutants. Development (submitted)

Acknowledgements

First of all, I would like to thank Prof. Peter Dörmann for the opportunity to conduct the research for my PhD thesis in his group. I have benefitted greatly from his support and from his genuine interest in the progress of my work. Thank you very much for your confidence and the chance to indulge in many different interesting projects.

I am very grateful to Prof. Lukas Schreiber for agreeing to be the co-referee of my thesis. Furthermore, I want to thank the other members of my evaluation committee, Prof. Galinski and Prof. Goldbach.

This work was funded by the DFG as part of the Priority Program 1212 – Microbial Reprogramming of Plant Cell Development.

Dr. Thomas Ott and Prof. Martin Parniske from the Department of Genetics, LMU München, were very kind to share their experience of nodulation and mycorrhiza formation with me. I am also very grateful to the members of their group, especially to Joana Bittencourt Silvestre. Thank you very much for your hospitality!

I am very grateful to Dr. Dirk Warnecke from the University of Hamburg, who performed the heterologous expression experiments of *SGT1*, *SGT2* and *GCS* in *Pichia pastoris*.

Special thanks go also to the following people who contributed to this work: Helder Paiva cloned the RNAi constructs and the constructs for the heterologous expression in *Pichia pastoris*, and did a first transformation of *Lotus.* Dr. Isabel Dombrink introduced me to the secrets of mass spectrometry and set up Q-TOF MS/MS analysis of phospho- and galactolipids in our lab. Dr. Simone Zäuner started to establish GIPC analysis by Q-TOF MS/MS in *Arabidopsis*. Katharina vom Dorp established Glucosylceramide, DAG and TAG measurements by Q-TOF MS/MS in our lab. Meike Siebers was very helpful with photography and microscopy. Dr. Bettina Kriegs did the sequencing of *SGT1* and helped a lot with the TILLING plants.
I would also like to thank Dr. Nicole Gaude for laying the foundation for my project and for ongoing collaborations.

I was very lucky with my students; therefore I would like to acknowledge Josep Massana, Anna Moseler and Mathias Brands, who did their Bachelor theses in our lab. Thank you for your help!

I want to thank all the members of the IMBIO, you were great to work and live with!
I would especially like to thank Marlies Becker, for being a great help, especially in the final phase of my thesis; Brigitte Dresen-Scholz for helping me in many ways during the years; Ernst Peter Jonen, who can repair about everything; Abdou Fatihi for sharing good times and bad times from the beginning; Dr. Felix Lippold for help with data evaluation and for endless discussions about science and life in general; Helga Peisker for philosophical analysis of life and culture; Caro Hohn for her refreshing comments in every possible and impossible situation; Meike Siebers for her critical comments on artwork and for making life a bit nicer everyday; Katharina vom Dorp for always being there for me, you were my rock! Thank you also to Dr. Georg Hölzl, Dr. Ania Zbierzak, Tanja Fuchs, Barbara Kalisch, Veronika Behnen, Andreas Ahrends, Ellen Schulz and all other present or former members of our group.

The most exciting time of my project was certainly the time I spent with Dr. Isabel Dombrink, Katharina vom Dorp and Helga Peisker on the endless comedies and tragedies that came with the Q-TOF. Nobody could wish for a better team! I am also very grateful to Richard Heinz, our "knight in shining armor" on so many occasions, although the ladies fought many battles on their own.

I would like to thank my family for all the help and support during my studies and during the thesis. I am of course very grateful to Nora for luring me to Bonn. Who knows where else I might have ended up?

I owe a lot to my parents, and I do not mean mere genetics. They have given me the opportunity to do whatever I choose with my life and have provided me with just enough ambition to complete my thesis, but not too much to enjoy life.

Finally I want to thank Tobias, for being a constant source of joy, for supporting me in every imaginable way and for never, ever complaining about my work (except that one time…); and also for not taking things so seriously all the time.